Investigating the modulation of neonatal rat facial motoneurone excitability by monoamine neurotransmitters: Postsynaptic mechanisms and presynaptic modulation of glutamate release.

Emma Margaret Perkins

Thesis presented for degree of Doctor of Philosophy

The University of Edinburgh

2007

Declaration

I hereby declare that the work contained within this thesis was all my own.

Some of this work has been published and the reprint appears as an appendix.

Emma M. Perkins

May 2007

Acknowledgements

I would like to thank the Medical Research Council for their financial support that has enabled me to complete these studies and the Centre for Neuroscience Research for awarding me the studentship. I am also grateful for additional assistance I have received from the Edinburgh Alumni Fund, The Physiological Society and the BNA which has enabled me to attend several conferences during my studies. I am also very thankful that I had the opportunity to attend the Microelectrode Techniques course at the University of Plymouth (funded by the MRC).

I am grateful to everyone in the Division of Neuroscience not only for the huge amounts of technical assistance and academic advice they have given me during my studies but also for the great friendships I have made along the way. I would especially like to thank Dr Peter Kind for his assistance with the PLC-$\beta1^{-/-}$ mice and immunohistochemistry and Dr Thomas Wishart for providing the cultured cerebellar granule neurones.

Thanks also to my family and friends for their wonderful support, always being interested in my work (or pretending to at least) and for being there to cheer me up when things didn't go to plan.

Finally I would like to thank my supervisor, Dr Phil Larkman, without his fantastic advice and support over the years I would have been completely lost!

Abstract

The activity patterns of 5-HT-releasing neurons can be positively correlated with behavioural state and motor function and the central 5-HT system modulates motor activity at the cellular level. The rat facial motor nuclei are densely innervated by 5-HT releasing afferents and 5-HT-mediated modulation of ion channels on the soma and dendrites can markedly influence the excitability of facial motoneurones and their integration of excitatory postsynaptic potentials (EPSPs). 5-HT facilitates facial motoneuron excitation by inhibiting a 'leak' potassium (K^+) conductance (gK^+_{Leak}) and enhancing the hyperpolarisation-activated cation current, I_h. These actions of 5-HT have been confirmed using whole-cell voltage-clamp recordings from visually identified facial motoneurones in an acute brainstem slice preparation. Pharmacological approaches have been used to identify the receptors which mediate the actions of 5-HT in facial motoneurones. The inhibition of gK^+_{Leak} by 5-HT can be blocked by the 5-HT_{2A} receptor antagonist, R96544 (0.3 – 1μM) and the enhancement of I_h by 5-HT is sensitive to the 5-HT_7 receptor antagonist, SB269970 (0.3 – 10 μM).

Noradrenaline was also found to inhibit gK^+_{Leak}, via activation of α_1 adrenoceptors, and the molecular identity of the amine-sensitive 'leak' K^+ channels has been investigated. TASK-1 and TASK-3 are pH-sensitive two-pore domain K^+ channels that can be modulated by amines and provide 'leak' K^+ conductances in several central neurones. The mRNAs for these channels have been reported to be present in the rat facial motor nucleus. The gK^+_{Leak} in facial motoneurones is sensitive to changes in external pH and has a pK of ~7.1, which is intermediate between the

values for homomeric TASK-1 and TASK-3 channels (7.5 and 6.8 respectively). The TASK-1 selective inhibitor anandamide (10 μM), its stable analogue methanandamide (10 μM), the TASK-3 selective inhibitor ruthenium red (10 μM) and Zn^{2+} (100-300 μM) all failed to alter the actions of noradrenaline or changing external pH. These findings argue against principal contributions to gK_{Leak} by homomeric TASK-1 or TASK-3 channels. Isoflurane, a volatile anaesthetic that enhances heteromeric TASK-1 / TASK-3 currents, potentiated gK_{Leak} supporting a predominant role for heterodimeric TASK-1 / TASK-3 channels in the gK_{Leak} in facial motoneurones.

Evoked fast excitatory synaptic transmission in the facial motor nucleus has been characterised and NMDA and non-NMDA receptor-mediated components of this synaptic transmission have been identified. Through a combination of analysis of the paired pulse ratio, rate of failure to generate a response and the frequency and amplitude of miniature excitatory postsynaptic currents (mEPSCs) this study provides evidence to suggest that glutamate release from pre-synaptic terminals in the facial motor nucleus is depressed by 5-HT. This action of 5-HT is mediated by activation of presynaptic 5-HT_{1B} receptors as this effect is mimicked by the 5-HT_{1B} receptor agonist, CP93129 (10 μM) and can be blocked by the 5-HT_{1B} receptor antagonist, isamoltane (1 μM).

These studies indicate that the modulation of synaptic integration in the facial motor nucleus involves activation of distinct pre- and post-synaptic 5-HT receptor subtypes. These findings not only increase our understanding of the cellular mechanisms for

the 5-HT modulation of motor activity but may also be relevant to the role of 5-HT in the control of other central neurones.

Contents

Figure and Table List

Chapter 2

Chapter 3

Chapter 4

Chapter 5

Chapter 6

Abbreviations

4-AP	4-aminopyridine
5-HT	5-hydroxytryptamine
8-OH-DPAT	8-hydroxy-2-di-n-propylamino-tetralin
ACSF	artificial cerebrospinal fluid
AMPA	α-amino-3-hydroxy-5-methyl-4-isoxazolepropionic acid
AP-5	D-(-)-2-amino-5-phosphonopentanoic acid
ATFK	arachidonyl trifluoromethyl ketone
ATP	adenosine triphosphate
cAMP	cyclic adenosine monophosphate
CGN	cerebellar granule neurone
DAG	diacylglycerol
EPSC	excitatory postsynaptic current
EPSP	excitatory postsynaptic potential
FM	facial motoneurone
FMN	facial motor nucleus
gK^+	leak potassium conductance
GABA	γ-aminobutyric acid
G protein	GTP-binding protein
GDP	guanosine diphosphate
GTP	guanosine triphosphate
HCN	hyperpolarisation-activated cyclic nucleotide-gated
I_h	hyperpolarisation-activated cation current
IP_3	inositol triphosphate
IPSP	inhibitory postsynaptic potential
I/V	current / voltage
NA	noradrenaline
NBQX	2,3-Dioxo-6-nitro-1,2,3,4-tetrahydrobenzo[f]quinoxaline-7-sulfonamide
NMDA	*N*-methyl-D-aspartate
PE	phenylephrine
PIP_2	phosphatidylinositol bisphosphate
PKC	protein kinase C
PLC	phopholipase C
ppr	paired pulse ratio
RR	ruthenium red
TASK	TWIK-related acid-sensitive K^+
TEA	tetraethylammonium chloride
TWIK	two pore domain weakly inwardly rectifying K^+

Synopsis

This thesis addresses several aspects of rat facial motoneurone (FM) excitability in an attempt to further understanding of the mechanisms by which motoneurones process the thousands of inputs they receive to produce the functional output of muscle fibre contraction. The activity of central 5-HT and NA neurones show positive correlations with motor activity and both neurotransmitters modulate FM excitability. The ionic mechanisms by which this modulation is exerted are further investigated in this thesis and the findings are summarised here.

It has previously been determined that FMs possess ion channels (I_h and gK_{Leak}) in their membranes that control their intrinsic excitability. The modulation of I_h and gK_{Leak} underlies the excitatory actions of exogenously applied 5-HT and NA (Larkman and Kelly 1992; Larkman and Kelly 1997; Larkman and Kelly 1998).

The inhibition of gK_{Leak} in neonatal FMs by 5-HT and NA is confirmed in Chapter 3 and the molecular identity of the FM gK_{Leak} was further investigated. gK_{Leak} was found to be sensitive to changes in external pH suggesting the channel is a member of the TASK family of leak K^+ channels and the pH-sensitivity was found to be intermediate between the reported values for homomeric TASK-1 and TASK-3 channels (Talley, Lei et al. 2000; Karschin, Wischmeyer et al. 2001).

The pharmacology of gK_{Leak} was also investigated. Ruthenium red is known to block TASK-3 homomeric channels but was found to have no effect on the FM gK_{Leak} (Czirjak and Enyedi 2003). Human TASK-3 channels have also been shown to be blocked by Zn^{2+}, however, the gK_{Leak} in rat FMs was not found to be sensitive to Zn^{2+} (Leonoudakis, Gray et al. 1998; Clarke 2003). Anandamide has been reported

to block homomeric human TASK-1 channels at low micromolar concentrations (and homomeric TASK-3 channels at higher concentrations), however, it failed to block the FM gK_{Leak} (Maingret, Patel et al. 2001). Metabolic degradation of anandamide can occur in some *in vitro* preparations but this can be prevented with arachidonyl trifluoromethyl ketone (ATFK) (Barbuti, Ishii et al. 2002). Neither anandamide, in the presence of ATFK, or the metabolically stable analogue of anandamide, methanandamide, significantly blocked gK_{Leak} in FMs (Maingret, Patel et al. 2001). The pharmacological activity of ruthenium red and methanandamide was validated using cultured cerebellar granule neurones which have been shown to posses both TASK-1 and TASK-3 homomeric channels (Maingret, Patel et al. 2001; Han, Truell et al. 2002; Kang, Han et al. 2004). These pharmacological studies provided evidence against a homomeric TASK-1 or TASK-3 identity for the FM $gK_{Leak.}$

TASK-1 and TASK-3 subunits have also been shown to form functional heteromeric channels (Czirjak and Enyedi 2002; Talley and Bayliss 2002). The non-selective TASK-1 and TASK-3 channel inhibitor, bupivacaine, partially occluded the NA- and low pH-induced inhibition of the FM gK_{Leak} (Leonoudakis, Gray et al. 1998; Kim, Bang et al. 2000). The anaesthetic isoflurane inhibits currents mediated by homomeric TASK-1 channels and enhances currents carried by homomeric TASK-3 and heteromeric TASK-1 / TASK-3 channels (Berg, Talley et al. 2004). Isoflurane increased gK_{Leak} in four out of five FMs (it was inhibited in the remaining FM). The inhibition by bupivacaine, enhancement by isoflurane and the intermediate pH-sensitivity indicates that gK_{Leak} may be mediated by TASK-1/TASK-3 heteromeric channels. The observation that gK_{Leak} in one FM is inhibited by isoflurane suggests there may be heterogeneity of channel composition within the FM population.

Chapter 4 investigates the receptor subtypes that mediate the different actions of 5-HT in FMs (inhibition of gK_{Leak} and enhancement of I_h) and the adrenoceptor involved in the inhibition of gK_{Leak}. Earlier studies suggested that a 5-HT_2 receptor subtype mediated the inhibition of gK_{Leak} by 5-HT (Rasmussen and Aghajanian 1990). The 5-HT_{2A} receptor antagonist, R96544, significantly reduced the 5-HT-induced inhibition of gK_{Leak} supporting the involvement of this receptor subtype in the effects of 5-HT (Ogawa, Sugidachi et al. 2002). The enhancement of I_h by 5-HT has previously been shown to involve a direct action of cAMP on the channel, however, the receptor subtype that activates adenylate cyclase to produce the cAMP was unknown. 5-HT_7 receptors positively couple to adenylate cyclase activity and here it is shown that a recently developed 5-HT_7 receptor antagonist, SB269970, blocked the enhancement of I_h by 5-HT suggesting 5-HT_7 receptors mediate this excitatory action of 5-HT (Hagan, Price et al. 2000; Lovell, Bromidge et al. 2000). It is also determined that the inhibition of gK_{Leak} by NA was mimicked by the α-adrenoceptor agonist, phenylephrine, and blocked by the α_1-adrenoceptor antagonist, prazosin.

The mechanism by which receptor activation leads to closure of the channel carrying gK_{Leak} is also discussed in Chapter 4. 5-HT_{2A} and α_1-adrenoceptors couple to G_q proteins that stimulate phospholipase-C (PLC) activity, thereby increasing the hydrolysis of phosphatidylinositol biphosphate (PIP_2) in the membrane, however, altering the downstream pathways of PLC (increased Ca^{2+} from internal stores and protein kinase C activity) has no effect on FM gK_{Leak} (Alberts, Johnson et al. 2002). Mice lacking PLC-β1 showed a reduced NA-induced current, whereas the 5-HT-induced current was not significantly reduced. In addition, immunohistochemical

techniques were utilised to demonstrate the presence of PLC-β in the wild-type mouse FMN. Although PLC-β1 activity appears important for the action of NA in the FMN, the actions of NA appear not to be dependent on the transduction pathways that follow PLC activation (increased $[Ca^{2+}]_i$ and PKC activation, respectively) (Larkman and Kelly 1998; Larkman, Perkins et al 2003). Depletion of PIP_2 from the membrane has been proposed as a mechanism that underlies the inhibition of several two pore K-channels (including TASK-1 and TASK-3 channels) and KCNQ2/3 channels (Suh and Hille 2002; Zhang, Craciun et al. 2003; Lopes, Rohacs et al. 2005). It is possible that a similar mechanism underlies the inhibition of gK_{Leak} in rat FMs though a direct action of the G protein α subunits cannot be ruled out (Chen and Talley 2006).

How these postsynaptic actions of 5-HT and NA modulate synaptic transmission in FMs is of interest. Chapter 5 characterises fast synaptic inputs into FMs as the initial stage in understanding how 5-HT and NA modulates synaptic transmission in these neurones. Excitatory postsynaptic currents (EPSCs) were evoked by placing a stimulating electrode close to the dendrites of a FM. Minimal stimulation intensities were applied and evoked EPSCs that fluctuated in amplitude and occasionally failed to evoke a response. The AMPA/kainate glutamate receptor antagonist, NBQX, reduced the mean EPSC amplitude (Sheardown, Nielsen et al. 1990). An additional component of the EPSCs was revealed under conditions optimised for NMDA glutamate receptor activation and this component was reduced by the NMDA receptor antagonist, AP-5 (Olverman, Jones et al. 1984). These findings indicate that fast excitatory synaptic transmission in the FMN is mediated by the activation of non-NMDA and NMDA glutamate receptors. The identities of the receptor subtypes

involved were further investigated. The lack of inward rectification of the current-voltage relationship of the EPSCs indicates the involvement of AMPA receptors containing the GluR2 subunit (Sato, Kiyama et al. 1993). In addition, the NR1A/NR2B receptor antagonist, ifenprodil, reduced the NMDA-mediated EPSC confirming the involvement of this receptor subtype (Williams 1993).

The modulation of glutamate-mediated synaptic transmission by 5-HT is the focus of Chapter 6. The mean EPSC amplitude was found to be reduced in the presence of 5-HT. While postsynaptic 5-HT receptor activation could account for this effect on the EPSC, it is well established that 5-HT receptors can also function as heteroceptors to modulate the release of glutamate from the presynaptic terminal nucleus (Bobker and Williams 1989; Boeijinga and Boddeke 1996; Bouryi and Lewis 2003). Therefore, in Chapter 6, three techniques traditionally used to assess whether an effect is mediated presynaptically have been employed to address the synaptic location of this action of 5-HT (Stuart and Redman 1991). Analysis of the rate of failure to generate an EPSC (at a constant stimulus intensity) revealed that 5-HT receptor activation reduced the mean EPSC amplitude by increasing the failure rate. 5-HT application was also found to alter the amplitude ratio of two closely separated EPSCs (paired-pulse facilitation ratio) and alter the frequency but not the amplitude of miniature (spontaneous) EPSCs. These findings are consistent with a presynaptic location for the inhibitory action of 5-HT on glutamate-mediated EPSCs in the FMN.

Members of the 5-HT_1 receptor family mediate the majority of inhibitory actions of this neurotransmitter so the involvement of 5-HT_1 receptor subtypes in the reduction of EPSC amplitude was investigated. The reduction in EPSC amplitude and the

associated increase in failure rate at minimal stimulation intensities were mimicked by the 5-HT_{1B} receptor agonist, CP93129, and inhibited by the 5-HT_{1B} receptor antagonist, isamoltane (Waldmeier, Williams et al. 1988; Macor, Burkhart et al. 1990). Contrastingly, the 5-HT_{1A} agonist, 8-OH-DPAT, did not reduce the EPSC amplitude and the 5-HT-mediated reduction in amplitude was not altered in the presence of the 5-HT_{1A} receptor antagonist, WAY 100635 (Critchley, Childs et al. 1994). These findings indicate that 5-HT reduces EPSC amplitude through activation of 5-HT_{1B} receptors.

Chapter 1

1.1 Introduction

How does a neurone process the various inputs it receives to produce a functional output? This is a fundamental question in neuroscience and one that has prompted a great deal of investigation attempting to increase the understanding of how neurones function.

1.2 Neuronal signaling

During his studies of neuronal anatomy in the late nineteenth century Ramớn y Cajal proposed that the dendritic network (and soma) represents the input site of a neurone and that the axon represents the output site (Yuste and Tank 1996). Although some exceptions to this rule have emerged as our understanding of neuronal activity has advanced, Cajal's theory on the direction of signaling within a neurone remains valid.

In the 1950s Hodgkin, Huxley and Katz investigated the ionic basis of nerve conductance in the giant squid axon (Hodgkin and Huxley 1952). They determined that action potentials in this peripheral nerve are generated by a transient inward Na^+ current causing the axonal membrane to become less negatively charged (during the rising phase of the action potential or "spike") and that membrane repolarisation was mediated by a sustained outward K^+ current (Hodgkin and Huxley 1952). They also described the specific increase in Na^+ and K^+ permeability of the membrane during these periods, which has subsequently been identified as a result of the opening of voltage-dependent Na^+ and K^+ channels in the membrane (Hodgkin and Huxley

1952; Purves 2001). The axon potential flows down the axon due to an inactivation of the voltage-dependent Na^+ channels (Purves 2001). Recordings from mammalian spinal motoneurones provided evidence that central nerve fibres propagate action potentials by the same mechanism as peripheral nerves (discussed in (Llinas 1988)).

The mechanism underlying action potential initiation is now well understood. Neurotransmitters released from the presynaptic nerve terminal interact with specific ionotropic receptors on the postsynaptic membrane (Purves 2001). Binding of the neurotransmitter to the receptor induces a conformational change increasing the conductance of specific ion species through the receptor channel (Purves 2001). Neurotransmitters which result in conductance changes that result in membrane depolarisation (e.g. glutamate by increasing cation conductance) are excitatory and those that induce a membrane hyperpolarisation (e.g. GABA by increasing Cl^- conductance) are inhibitory (Kupfermann 1979; Purves 2001). These excitatory and inhibitory postsynaptic potentials (EPSPs and IPSPs, respectively) were first identified by intracellular electrophysiological recordings from spinal motoneurones and it was proposed that dendrites passively summate incoming EPSPs and IPSPs and the net change in somatic membrane potential could trigger action potential firing in the axon if it depolarised the membrane above the voltage-dependent Na^+ channel threshold (Coombs, Eccles et al. 1955; Coombs, Eccles et al. 1955; Whitehead and Rosenberg 1993; Yuste and Tank 1996; Purves 2001).

1.3 Dendrites as passive electrical cables

Dendrites were traditionally thought of as passive electrical cables and in 1959 Rall applied the cable theory to describe the passive flow of electric currents in dendritic networks (Rall 1959; Yuste and Tank 1996). Rall defined membrane resistance (R_m), membrane capacitance (C_m), internal (cytosolic) resistance (R_i), cable length (λ) and the dendritic-to-soma conductance ratio (ρ) and derived equations using these basic parameters to describe the flow of currents in model dendritic networks receiving distinct input patterns (Yuste and Tank 1996).

The majority of synaptic inputs occur in the dendritic network of neurones and the distance from the site of synaptic input to the soma can vary greatly within a single neurone. In theoretical neuronal models with only passive dendritic parameters inputs received in the distal dendrites are found to be attenuated in amplitude and have a longer time course when measured in the soma (Magee 2000; Williams and Stuart 2000). The high dendritic resistance causes a continuous voltage drop between the synapse and the soma, resulting in reduced EPSP amplitude (Magee 2000). The inputs received in the distal dendrites will appear smaller in amplitude compared to those received by more proximal dendrites due to increased amplitude filtering (Rall, Burke et al. 1967; Cook and Johnston 1999; Magee 2000). Thus in order for inputs received in distal dendrites to evoke a large enough change in the membrane potential at the site of action potential initiation several EPSPs would have to be evoked within a certain time period, this is termed temporal summation. Contrastingly, inputs received more proximal to the soma would appear to decay less before reaching the site of action potential initiation and would therefore be less

dependent on temporal summation (Rall, Burke et al. 1967). The kinetic decay of EPSPs is also subject to filtering and inputs received in distal dendrites have a prolonged time course at the soma (Magee 2000). This results in the inputs received in the distal dendrites (which would be lower in amplitude) having a prolonged time period for temporal summation to occur.

In this model of passive dendritic function the location of a synaptic input would strongly influence its effect on the postsynaptic cell, however, location-dependence of synaptic inputs is rarely observed experimentally (Magee 2000; Williams and Stuart 2000). Although dendrites do possess the basic cable properties described above and are capable of passive current flow it has become apparent that they also possess many dominant active properties that shape neuronal inputs and may remove the location variability of synaptic efficacy.

1.4 Active properties of dendrites

1.4.1 Dendritic potentials

Early evidence for active dendrites came from direct electrophysiological recordings of dendritic action potentials in cerebellar Purkinje neurones and cortical pyramidal neurones (Spencer and Kandel 1961; Llinás, Nicholson et al 1968; Takagi 2000). Purkinje neurones were found to produce Ca^{2+} spikes in the dendrites and Na^{+} spikes in the soma (Llinás and Sugimori 1980). This finding was supported by the discovery of voltage-sensitive Ca^{2+} channels in the Purkinje neurone dendrites by Ca^{2+} imaging techniques (Yuste and Tank 1996). Na^{+} and Ca^{2+} spikes were recorded from the dendrites of hippocampal and cortical pyramidal neurones of the

hippocampus and cortex and the presence of voltage-sensitive Ca^{2+} channels was also confirmed using Ca^{2+} imaging techniques (Yuste and Tank 1996).

The function of these active properties of the dendrites is not yet entirely clear but it has been proposed that due to the voltage-sensitive nature of these conductances they could increase the amplitude and duration of EPSPs (Yuste and Tank 1996). It has also been proposed that dendritic action potentials may play a role in long term plasticity of synapses by coincidence detection of the spike with incoming synaptic inputs (Yuste and Tank 1996).

1.4.2 The hyperpolarisation-activated current

The hyperpolarisation-activated cation current, I_h, has emerged as playing a crucial role in the integration of synaptic inputs in many types of neurones and its role in integration in neocortical and CA1 hippocampal pyramidal neurones has been particularly well documented (Magee 1998; Cook and Johnston 1999; Williams and Stuart 2000; Gulledge 2005). In these neurones I_h removes the location dependence of the time course of synaptic inputs (Magee 1999; Williams and Stuart 2000). When I_h is present there is an increase in membrane conductance due to the channels being activated at the resting membrane potential this increases the decay rate of EPSPs (Magee 1999; Williams and Stuart 2000). In addition, the voltage-dependent inactivation of I_h that occurs during EPSPs produces a net outward current which further prevents EPSP decay (Magee 1999; Williams and Stuart 2000). Expression of I_h channels was found to increase with distance from the soma (with high expression observed in the distal dendrites). This results in a location-independence of EPSP time course at the soma (Magee 1999; Williams and Stuart 2000). This is

directly supported by the finding that blocking I_h unmasks temporal summation similar to that predicted by passive neuronal models (Magee 1999; Williams and Stuart 2000).

1.5 Modulatory neuronal inputs

1.5.1 Neuromodulation by G protein-coupled receptors

In addition to inputs which evoke EPSPs and IPSPs many neurones receive modulatory inputs. Some of these inputs release neurotransmitters that can induce changes in neuronal excitability but do not directly cause action potential firing. However, these changes in neuronal membrane excitability can result in more or less fast synaptic input being required to evoke action potential firing. Several modulatory neurotransmitters mediate their effects through activation of membrane receptors that are coupled to intracellular signalling pathways through guanosine triphosphate (GTP) binding proteins (G proteins) (Purves 2001; Alberts, Johnson et al. 2002).

Ligand binding to a G protein coupled receptor induces a conformational change that leads to activation of the G protein causing it to release its bound GDP (guanosine diphosphate) allowing GTP to bind in its place (Alberts, Johnson et al. 2002). The GTP bound Gα subunit releases the Gβγ subunit complex activating both subunits allowing them to modulate their target proteins.

The vast diversity in G-protein coupled receptors, their intracellular signaling pathways and target effector proteins gives rise to several combinations for neuronal modulation and some of which are addressed in this thesis.

1.5.2 Presynaptic modulation of synaptic transmission

As described previously EPSPs and IPSPs occur as a result of neurotransmitters binding to postsynaptic receptors and opening an intrinsic ion channel (Kupfermann 1979; Purves 2001). The release of neurotransmitter from the presynaptic nerve terminal into the synaptic cleft requires the fusion of a vesicle filled with the neurotransmitter with the presynaptic membrane. Altering this release process is therefore a potential mechanism for neuromodulation.

The fusion of a neurotransmitter filled vesicle with the presynaptic membrane is dependent on Ca^{2+} entry into the nerve terminal (Purves 2001). When an action potential reaches the nerve terminal it depolarises the membrane and this potential change activates voltage-gated Ca^{2+} channels allowing Ca^{2+} entry into the terminal (Purves 2001). The increase in intracellular [Ca^{2+}] activates the vesicle's Ca^{2+}-dependent fusion machinery causing it to fuse with the membrane and release its contents into the synaptic cleft (Purves 2001). The Ca^{2+} entry into the terminal is crucial for neurotransmitter release therefore the activity of the voltage-gated Ca^{2+} channels represents a potential target for neuromodulation.

One mechanism for modulating Ca^{2+} entry into the terminal is to alter the activity of the voltage-gated Ca^{2+} channels. The first studies describing a G protein-mediated inhibition of Ca^{2+} currents were in dorsal root ganglion (DRG) neurones of embryonic chicks, however, it was also proposed that the Ca^{2+} current inhibition could occur at central nerve terminals where it would reduce neurotransmitter release (Dunlap and Fischbach 1978; Dunlap and Fischbach 1981). In the embryonic chick DRG neurones high voltage-activated (mainly N type) Ca^{2+} channels were found to

be inhibited following activation of G protein-coupled $GABA_B$, 5-HT and adrenergic receptors and it was subsequently determined that this inhibition was sensitive to pertussis toxins, implicating members of the G_i protein family (that are negatively coupled to adenylate cyclase) (Dunlap and Fischbach 1978; Dunlap and Fischbach 1981; Tedford and Zamponi 2006). It subsequently emerged that inhibition of Ca^{2+} channels occurred following activation of several types of G_i protein-coupled receptors (Mirotznik, Zheng et al. 2000; Tedford and Zamponi 2006). G_i protein-mediated inhibition did not appear to be dependent on changes in cAMP levels (cAMP is generated by adenylate cyclase activity) and in 1996 it was demonstrated that the $G_{\beta\gamma}$ subunit directly inhibits the channel (Herlitze, Garcia et al. 1996; Ikeda 1996).

As previously described, the Ca^{2+} entry into the nerve terminal is through voltage-gated Ca^{2+} channels, therefore an alternative mechanism for modulating presynaptic vesicle release is to prevent activation of these voltage-gated channels by altering the membrane potential. When an action potential reaches the nerve terminal it normally depolarises the membrane above the threshold for activation of the Ca^{2+} channels, however if the resting membrane potential of the terminal is sufficiently hyperpolarised the membrane may not reach the Ca^{2+} channel threshold. Membrane hyperpolarisation would occur as result of increased K^+ conductance and several K^+ channels have been identified as targets for G protein mediated modulation. K^+ conductances in the hippocampus were shown to be enhanced following 5-HT_1 receptor activation (Andrade, Malenka et al. 1986; Andrade and Nicoll 1987; Colino and Halliwell 1987). 5-HT_1 receptors are G_i protein coupled receptors and this increase in K^+ channel conductance was found to occur due to a direct interaction of

the $G_{\beta\gamma}$ subunit with the channels (Andrade, Malenka et al. 1986; Andrade and Nicoll 1987; Colino and Halliwell 1987). Similarly, activation of G_i protein-coupled muscarinic acetylcholine receptors in the heart result in the $G_{\beta\gamma}$ subunit activating G protein coupled inwardly rectifying K^+ (GIRK) channels (Logothetis, Kurachi et al. 1987; Reuveny, Slesinger et al. 1994).

It is interesting to note that while K^+ channels appear to be activated by $G_{\beta\gamma}$ subunits, the voltage-gated Ca^{2+} channels are inhibited by the $G_{\beta\gamma}$ subunit. Nevertheless, both mechanisms result in reduced Ca^{2+} entry into the terminal and the subsequent reduction in vesicle fusion causes a less neurotransmitter to be released into the synaptic cleft and an inhibition of synaptic transmission.

Modulation downstream of Ca^{2+} entry into the terminal has also been observed at the reticulospinal-motoneurone synapse in the lamprey (Blackmer, Larsen et al. 2001). At this synapse the $G_{\beta\gamma}$ subunits appear to interact directly with the fusion machinery to prevent vesicle fusion with the membrane and neurotransmitter release, however, this mechanism of inhibition has not yet been observed in the mammalian central nervous system (Blackmer, Larsen et al. 2001).

1.5.3 Postsynaptic modulation

Action potential initiation is dependent on the net potential change induced by incoming EPSPs and IPSPs depolarising the membrane above a certain threshold (for activation of the voltage-gated Na^+ channels), thus, altering the resting membrane potential will affect the net potential change and could have profound effects on the efficacy of synaptic transmission. Activation of G protein-coupled receptors which

target the ionic conductances that contribute to the neuronal resting membrane potential represents a postsynaptic mechanism for neuromodulation.

1.5.4 K^+ channel modulation

Several types of K^+ channels are important in the regulation of neuronal excitability and those that can be regulated by G protein activity are potential candidates for mediating neuromodulation.

Members of the twin-pore (2P) domain K^+ channel family provide 'leak' potassium conductances in several types of neurones (reviewed by (Goldstein, Bockenhauer et al. 2001; Patel and Honore 2001; Bayliss, Sirois et al. 2003)). 'Leak' potassium conductances (gK_{Leak}) are defined as having little or no voltage-dependence and hence contribute to the neuronal resting membrane potential (Goldstein, Bockenhauer et al. 2001; Patel and Honore 2001; Bayliss, Sirois et al. 2003). Several members of this family have been shown to be sensitive to G protein modulation.

In cerebellar granule neurones (CGNs) the mechano-gated TWIK-related K^+ (TREK) channels are inhibited by activation of group 1 metabotropic glutamate receptors (mGluRs) (Chemin, Girard et al. 2003). The Group 1 mGluRs are coupled to G_q proteins which stimulate phospholipase C activity (Alberts, Johnson et al. 2002; Chemin, Girard et al. 2003). Phospholipase C activity generates the intracellular messengers inositol trisphosphate (IP_3) and diacylglycerol (DAG) from phosphatidylinositol bisphosphate (PIP_2) (Alberts, Johnson et al. 2002). It appears that the diacylglycerol (DAG) directly inhibits TREK channels in CGNs (Chemin, Girard et al. 2003). It was also found that the TWIK-related acid-sensitive K^+

(TASK) channels members of the K_{2P} family are inhibited in CGNs following activation of the group 1 mGluRs (Bayliss, Sirois et al. 2003; Chemin, Girard et al. 2003). This inhibition did not appear to be dependent on the intracellular messenger molecules associated with G_q protein activation but rather due to a depletion of phospholipids from the membrane (Chemin, Girard et al. 2003). Inhibition of TASK channels has also been observed following activation of the M_3 muscarinic receptor which is also coupled to G_q proteins (Bayliss, Sirois et al. 2003).

G protein modulation of other K^+ channels can also regulate neuronal excitability. Members of the K_{ir} 2.0 (inwardly rectifying) family of K^+ channels such as Kir 2.1 (IRK1) have been found to be inhibited following activation of the M_1 muscarinic receptor by a mechanism involving the $G\alpha_q$ subunit (Firth and Jones 2001).

1.5.5 I_h modulation

In addition to its role in normalising temporal summation of EPSPs previously described, I_h, contributes to the resting membrane potentials in many neuronal types. Resting membrane potentials of neurons are typically between -50 mV to -100 mV and I_h is active within the range (Pape 1996). As I_h does not inactivate at hyperpolarised potentials, the sustained depolarising current helps set the resting membrane potential depolarised to the K^+ equilibrium potential (Pape 1996). Increasing the activity of I_h therefore represents a potential modulatory mechanism for increasing neuronal excitability.

I_h is carried by hyperpolarisation-activated cyclic nucleotide-gated cation channels (HCN1-4) (Ludwig, Zong et al. 1998; Santoro, Liu et al. 1998) and cAMP has been shown to modulate HCN channel activity in a variety of neurones including CA1

hippocampal neurons (Chen, Wang et al. 2001; Bickmeyer, Heine et al. 2002) neurones of the hypoglossal nuclei (Bobker and Williams 1989) and rat facial motoneurones (Larkman and Kelly 1992). This modulation of HCN channels is mediated by a direct action of cAMP on the channel and is not dependent on activation of protein kinase A and protein phosphorylation (Larkman and Kelly 1995; Kaupp and Seifert 2001).

cAMP is synthesised from ATP by adenylate cyclase and the activity of this enzyme can be stimulated the G_s protein and inhibited by G_i proteins (Alberts, Johnson et al. 2002). Neurotransmitters that activate G_s protein coupled receptors (such as 5-HT_4, 5-HT_6 and 5-HT_7 receptors and β-adrenoceptors) could potentially enhance I_h and increase neuronal excitability (IUPHAR 2000). In contrast those that activate G_i receptors (such as 5-HT_1 receptors) could suppress I_h and have an inhibitory effect on neuronal excitability.

In the hippocampus I_h can be enhanced by the activation of 5-HT_4 receptors and inhibited activation of 5-HT_{1A} receptors (Bickmeyer, Heine et al. 2002). Although this occurs in different neuronal compartments, it represents a system in which a neurotransmitter can modulate the same conductance via different G protein pathways to have opposing effects on neuronal excitability (Bickmeyer, Heine et al. 2002)

It has also been determined that 5-HT increases facial motoneurone excitability by enhancing I_h and although it was determined that this occurred as a result of a direct action of cAMP on the channel, the 5-HT receptor mediating this action has not yet

been identified and is addressed in Chapter 4 of this thesis (Larkman and Kelly 1992; Larkman and Kelly 1997; Larkman and Kelly 1998).

1.6 Motoneurones

1.6.1 Motoneurones as models for investigating input processing

The output of the CNS is manifested by motor behaviour and motoneurones provide the link between these two systems. Motoneurones signal the contraction of the muscle fibres they innervate, a functional output that is well understood and can be accurately measured. This relatively well-defined functional output of motoneurones and their suitability for electrophysiological recordings makes them useful models for investigating the mechanisms by which the thousands of inputs they receive are accurately processed.

1.6.2 Facial Motoneurones

The superficial and some deep muscles of the rat face are innervated by the seventh cranial nerve (VII) and the cell bodies of the motor component of this nerve are located in the facial motor nucleus (FMN, VII nucleus). The facial motor nuclei are organised into subnuclei within the lateral, intermediate and medial columns and the position of facial motoneurones (FMs) within the nuclei loosely represent the position of their target muscles on the face (Hinrichsen 1984; Friauf 1985; Paxinos 1985). For the purpose of this thesis FMs were not distinguished by location within the nucleus.

Exogenously applied 5-HT and NA have modulatory actions on FMs and *in vivo* the FMN is has been found to be densely innervated by 5-HT-releasing terminals

(Takeuchi, Kojima et al. 1983; Senba 1985; Larkman and Kelly 1992; Larkman and Kelly 1997; Larkman and Kelly 1998). These findings encouraged the investigations into the role of synaptic integration and neuromodualtion in the FMN described in this thesis.

Chapter 2 Methods

2.1 FM Electrophysiology

2.1.1 Animals

Male and female Wistar rats (or PLC-$\beta1^{-/-}$ mice and their littermate controls where stated) aged between postnatal days 4 and 16 (P4-P16) were used to prepare acute brainstem slices. All procedures were approved by the UK Animals (Scientific Procedures) Act 1986 and performed under UK Home Office License. Animals were obtained from an in house breeding colony maintained in a 12 hour light-dark cycle, in which breeding pairs were provided with food and water *ab libitum*.

2.1.2 Brainstem Slice Preparation

Motoneurones appear to be particularly sensitive to the lack of oxygen and mechanical damage that occurs during slice preparation. To increase the number of healthy neurones brainstem slices were cut in a modified artificial cerebrospinal fluid (ACSF) (Solution 2.1, Section 2.6) in which 50% of the NaCl was substituted with sucrose. This solution has the advantage of reducing the passive chloride entry into neurones that occurs during periods of hypoxia (Rothman 1985; Aghajanian and Rasmussen 1989). This passive chloride influx leads to cation and water entry which results in cell swelling and lysis (Rothman 1985). Lactate was included in the modified ACSF as there is evidence to suggest that it is the preferred substrate for energy production in hypoxic conditions (Schurr, West et al. 1988; Larrabee 1995; Magistretti 2005). 150 ml of the modified ACSF was cooled on ice to <4°C and oxygenated with a 95% O_2, 5% CO_2 gas mixture (BOC Gases, Manchester, UK).

Following cutting, slices were incubated in the modified ACSF with added Ca^{2+} (1 mM) as prolonged periods of reduced glutamate receptor activity can also reduce the viability of slices. A modified Gibb slice incubation chamber (Figure 2.1) was filled with 250 ml of the modified ACSF to which 1 mM $CaCl_2$ had been added and warmed to 30°C in a water bath (Edwards, Konnerth et al. 1989).

To support the brainstem during the slicing procedure a small block of agar (2%) was glued (cyanoacrylate adhesive, Fisher Scientific UK) close to the front edge of the cutting stage of a microslicer (DTK-100, Dosaka EM Co Ltd, Japan). A thin razor blade (Mackay and Lynn Ltd, Edinburgh, UK) was put into the blade holder of the microslicer and the chamber surrounding the cutting stage was filled with ice to keep the ACSF cold during slicing.

Animals were decapitated using UK Home Office approved procedures. The skull was exposed and carefully removed and the brain was bathed in ice-cold modified ACSF (Solution 2.1, Section 2.6) using a glass dropper made from a Pasteur pipette and a rubber teat. A thin razor blade was used to separate the midbrain and hindbrain at the level of the cerebellum (Figure 2.2). The hindbrain was gently eased away from the skull into a small beaker containing pre-oxygenated ice-cold modified ACSF. Cutting the cranial nerves on the underside of the brainstem as it is removed appeared to enhance motoneurone survival. The isolated hindbrain was left in the ice-cold modified ACSF for approximately 30 seconds to cool, this slowed metabolism in the tissue reducing cell death. This also had the added advantage of firming the tissue, which aided the slicing procedure. A small amount of cyanoacrylate adhesive was spread onto the cutting stage of the microslicer behind

the piece of agar. The hindbrain was removed from the beaker using a 5 ml plastic spoon and placed cut surface down on a piece of ACSF-soaked filter paper (Whatman International Ltd, Maidstone, UK) on an upturned Petri dish on ice. The cerebellum was dissected from the brainstem using a thin razor blade and removed using a small spatula. The isolated brainstem was then positioned on a spatula dorsal side up using a fine artist's paintbrush. Excess solution was removed using a small piece of filter paper and the brainstem stuck onto the cutting stage, cut edge down. The cutting stage was then put into the chamber of the microslicer and immediately filled with pre-oxygenated modified ACSF. The blade was locked at a cutting angle of 15° and moved into position in front of the brainstem at the level of the beginning of the facial nucleus.

Prior to cutting (and during if required) any blood vessels on the surface of the brainstem were dissected away using fine jewellers forceps (No. 5, A. Dumont & Fils, Switzerland) and microscissors (OC-498, Aesculap, Tuttlingen, Germany). Very dense connective tissue impedes light transmission through the slice and reduces the ability to visually identify facial motoneurones. Therefore, slice thickness (between 100 – 140 µm) was dependent on the age of the animal and the relative density of the connective tissue in the nucleus. Slices were cut at the lowest speed on the microslicer and the blade was set to oscillate at the highest frequency. After slices were cut they were immediately transferred to the incubation chamber.

The low Na^+ concentration in the modified ACSF is not suitable for electrophysiological studies thus recordings were made in normal ACSF (Solution 2.2, Section 2.6).

A

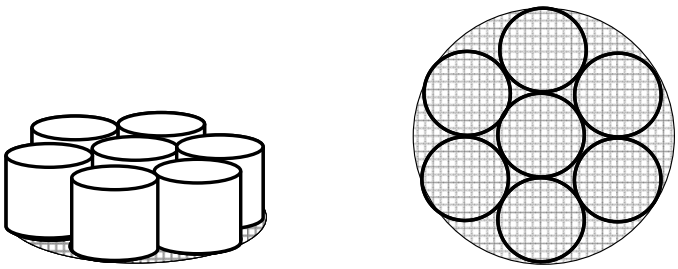

B

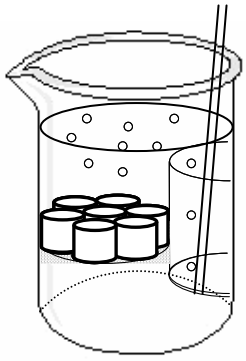

Figure 2.1. Modified Gibb incubation chamber (Edwards, Konnerth et al. 1989).

A. The slice holder was made from 1 cm segments of a 5 ml syringe glued together and a nylon grid attached to the bottom.

B. The slice holder was held in a 250 ml beaker with a segment cut from a 50 ml syringe. The solution was oxygenated with a 95% O_2, 5% CO_2 gas mixture through the syringe piece. The slices were held down in the slice holder by the bubbles rising to the surface through the syringe and pushing solution down on to the slices.

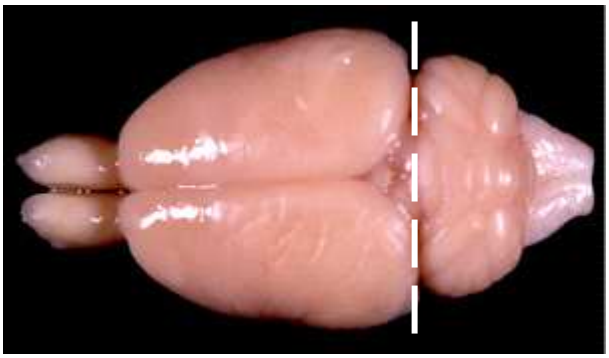

Figure 2.2. Position of cut to isolate brainstem.
Following removal of the skull-cap a razor blade was used to make a cut at the position of the dashed line and separating the hindbrain and the midbrain.

The viability of the slices seemed to be enhanced if the sucrose concentration was reduced gradually over the incubation period (following the protocol in Table 2.1) rather than immediately transferring them from a high sucrose to zero sucrose solution. At the end of the incubation period the slice chamber was removed from the water bath and maintained at room temperature. Slices were transferred to the recording chamber when required where they were held down by a nylon grid (Figure 2.3) (Edwards, Konnerth et al. 1989) and continuously perfused with oxygenated normal ACSF at a rate of 3 – 5 ml min^{-1}.

2.1.3 Patch-clamp Electrophysiology

The patch-clamp technique was developed by Neher and Sakmann and first utilised to resolve the single channel activity of acetylcholine-activated channels in cell-attached patches (Neher, Sakmann et al. 1978). The advantages of the patch-clamp technique over conventional intracellular recordings was that it allowed recordings to be made from cells that were too small to impale. The equipment and set up for patch clamp recordings was as described in Figure 2.4. Voltage protocols were generated by the PC, converted by the CED 1401 interface and the DAC output sent to the patch-clamp amplifier. The recording electrode was connected to the headstage of the amplifier which delivered the voltage commands to the recorded cell and recorded any current changes (when in the voltage clamp configuration). The patch-clamp amplifier was connected to pre-amplifiers to enable the output to be split and sent back to the computer (via the CED 1401 interface) and the oscilloscopes for real time monitoring of current changes (which was particularly useful for ensuring a GΩ seal was obtaining prior to going into the whole-cell

Time from decapitation (mins)	ACSF exchanged (% total volume)	Total sucrose (%)
0	0	50.00
30	10	45.00
45	12	39.60
60	12	34.85
75	14	29.96

Table 2.1. Protocol for sucrose exchange.

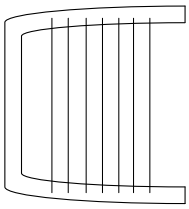

Figure 2.3. Nylon grid.
Slices were held in place in the recording chamber by U-shaped piece of platinum wire that was flattened in a vice and had a series of single nylon strands glued on to one side.

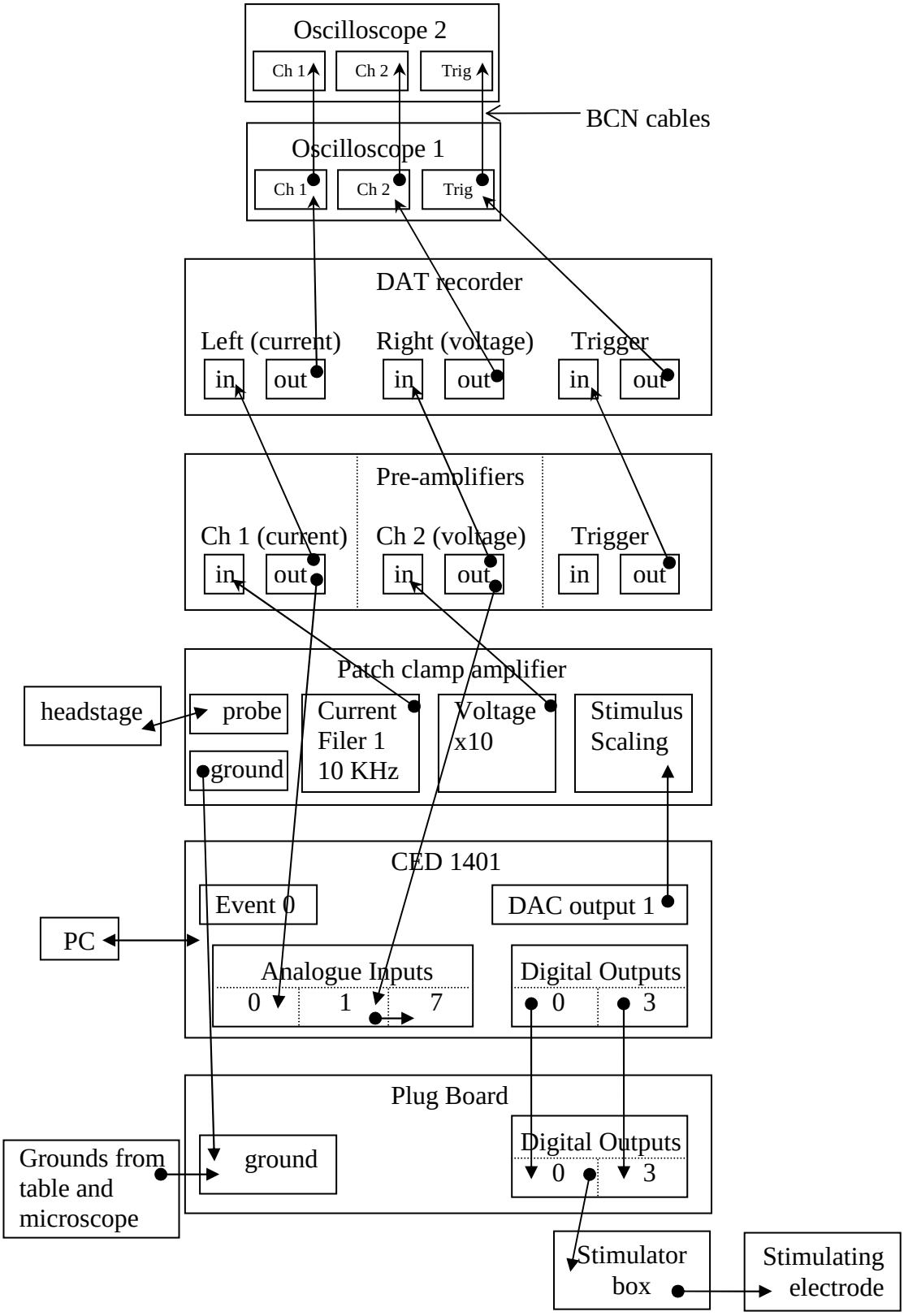

Figure 2.4. Equipment for patch-clamp electrophysiology.

Figure 2.4. Equipment for patch-clamp electrophysiology.

Oscilloscope (DSO) 400	Gould Electronics Ltd, Essex, UK.
Digital tape Recorder DTR-1404	Bio-logic Scientific Instruments.
Whole cell/patch clamp amplifier L/M-EPC 7B	List Medical, D-6100 Darmstadt, Germany.
1401 Interface	Cambridge Electronic Design, Cambridge, UK.
Isolated Stimulator DS2	Digitimer Ltd, Welwyn Garden, England.

configuration, see Section 2.1.5). The connections to the oscilloscopes were via the DAT recorder to ensure all data was recorded and could be played back at a different frequency if required for data analysis. All equipment and the anti-vibration table (on which all recordings were made) were connected to the ground on the patch-clamp amplifier.

The amplifier operating modes are detailed in Figure 2.5. The Vp-offset control was used to zero the potential difference that occurs between the bath and internal solutions (Section 2.1.5). The required holding potential was applied using the V-Hold command and the V-step function was rarely used as ramp and step changes were configured using the Signal software package (version 2.15, Cambridge Electronic Design (CED) Ltd, Cambridge, UK).

2.1.4 Cell Cleaning

The development of thin acute slices allows recordings to be made from visually identified motoneurones, significantly increasing the success rate of recordings. However, even in thin slices there is still a sufficient amount of connective tissue and cell debris in the facial nucleus to impede formation of high resistance seals without prior cleaning of the cell surface. Healthy cells are first identified using a x40 immersion objective on an Zeiss upright microscope and Nomarski differential optics.

Motoneurone cleaning was performed as described by (Edwards, Konnerth et al. 1989). A cleaning electrode was made from a glass electrode (GC120F-10, Harvard Apparatus Ltd, Kent, UK) pulled with a long thin shank using an upright electrode

Voltage clamp

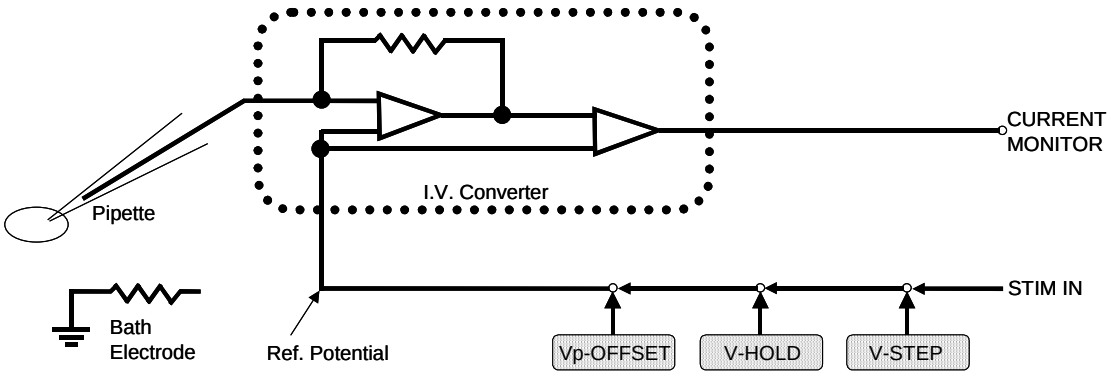

Current Clamp

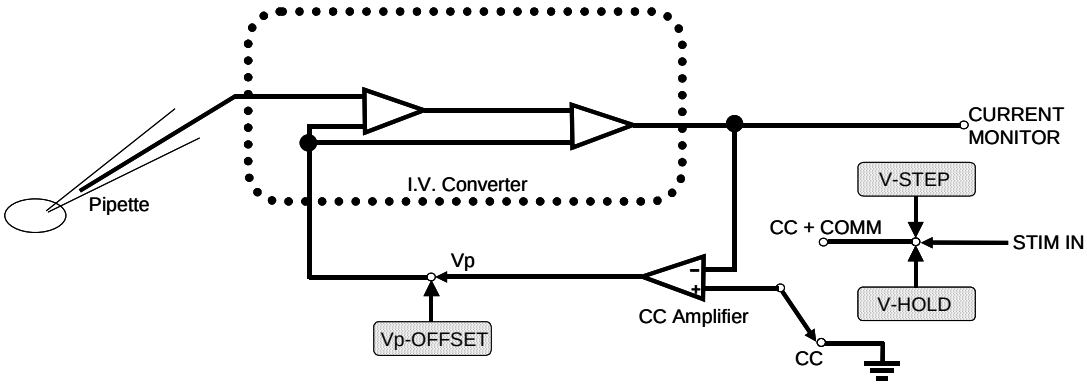

Figure 2.5. Amplifier operating modes.

puller (PP-83, Narishige Scientific Instruments, Tokyo, Japan). The tip of the electrode was then broken to 5 -10 µm in diameter using a micro forge (MF-830, Narishige Scientific Instruments, Tokyo, Japan). A suction line was connected to the end of the cleaning electrode and it was then positioned above the identified motoneurone using a fine manipulator (M0-103, Narishige Scientific Instruments, Tokyo, Japan). ACSF was then drawn into the tip of the cleaning electrode and the debris above the cell was loosened by blowing ACSF out of the cleaning electrode. Care was taken to avoid damaging the dendrites as this can result in death of the motoneurone (Edwards and Konnerth 1992). The debris was then removed by carefully sucking it into the cleaning electrode and the procedure repeated until the surface of the motoneurone was clear.

2.1.5 Whole-cell patch clamp recordings

Patch electrodes were pulled from borosilicate glass (7.5 cm segments of GC150TF-15, Harvard Apparatus Ltd, Kent, UK) to a resistance of 6 -12 MΩ when filled with standard internal solution and a tip diameter of approximately 0.5 – 1 µm. Prior to making electrodes the ends of the glass were fire-polished to prevent damaging the AgCl wire of the pipette holder. The glass was then cleaned in 100% ethanol, rinsed in distilled H_2O and dried in an oven to minimise the dust particles on the glass that could potentially block the tip of the electrode. Patch-pipettes were pulled using a Narishige patch-pipette puller (PP-83). The capacitance of the electrode that occurs when it is deeply immersed in the ACSF in the recording chamber is reduced by coating the shank of the electrode with Sylgard (Dow Corning Limited, Coventry, UK). The tip of the electrode was then heat polished using a micro forge (MF-830,

Narishige Scientific Instruments, Tokyo, Japan). Tip polishing smoothes the surface of the tip and can help remove small dust particles from the electrode. Electrodes were filled with internal solution (Solution 2.3, Section 2.6) using an electrode filler made from a 20 ml syringe, a 25 mm, 0.22 µm filter and a cannula (0.7 mm outside diameter) cut to the desired length. The internal solution was occasionally diluted to 90% to help maintain cell health during the recording period. Filling of electrodes was aided by the filament that runs the length of the glass. A small amount of internal solution was put on the end of the electrode and allowed to back fill the tip, this reduced the formation of air bubbles in the tip. The electrode was then 2/3 filled with the internal solution and any air bubbles in the electrode were dispersed by gentle flicking.

The filled electrode was put in the pipette holder attached to the headstage connected to the amplifier (EPC7B, List Medical, Darmstadt, Germany). Positive pressure was applied to the tip of the electrode by blowing through a suction line attached to the headstage and locked with a three-way valve. The electrode was then immersed in the ACSF in the recording chamber under the control of a fine manipulator (MX-1, Narishige Scientific Instruments, Tokyo, Japan). The reference point for the headstage was an AgCl pellet connected to the recording chamber by an agar bridge. Agar bridges were made by taking a small length of electrode glass (GC150TF-15, Harvard Apparatus Ltd, Kent, UK) and bending it to a 90º angle using a Bunsen burner. The glass was then filled with agar (2%) made up in normal ACSF. Using the bridge rather than putting the AgCl pellet directly prevented a junction potential arising at the AgCl and bath solution interface. It also allowed the composition of the bath solution to be changed slightly without generating a potential that would add

to the holding potential. The current output was zeroed using the offset control on the amplifier. Inputs commands were configured on a personal computer using the commercially available software package Signal (version 2.15, Cambridge Electronic Design (CED) Ltd, Cambridge, UK). Formation of a high resistance (GΩ) seal was monitored by measuring the current responses to a -10 mV, 10 ms step from the holding potential, performed in the voltage-clamp configuration. When the electrode was first put in the bath the current deflection observed gave a measure of the resistance of the electrode. The electrode was then manoeuvred to just above the visually identified cell and the electrode slowly lowered until it touched the cell soma. This was either monitored by looking down the objective or more routinely by observing a 10 – 20% increase in resistance (a decrease in the current deflection in response to the voltage command). The positive pressure was then removed resulting in a further increase in resistance. A GΩ seal was obtained by gently sucking on the suction line until there was no deflection on the current trace and the cell was in the cell-attached configuration. Any stray capacitance of the electrode was compensated for using the controls on the amplifier. The holding potential was then applied to the electrode using the amplifier. An 8 mV junction potential was routinely taken into consideration when calculating the holding potential to be applied (Neher 1992). The electrode was left in the cell-attached mode for a few seconds to enhance seal formation after which short sharp bursts of suction were applied to remove the piece of membrane in the tip of the electrode and break through into the whole-cell configuration. The current response to a -10 mV, 10 ms voltage step was measured to monitor the series resistance, which was compensated for by up to 70%. Gentle suction was applied and maintained throughout the

recording to help prevent any loose pieces of membrane or dust particles from blocking the tip.

2.2 Experimental Protocols

2.2.1 Modulation of I_h in FMs

FMs were voltage-clamped at -60 mV and changes in conductance mediated by I_h were measured using a voltage step to -100 mV (Figure 2.6A). This step was followed by a ramp to 0 mV to monitor any changes in gK_{Leak}. The step and ramp were preceded by a -10 mV, 10 ms step to monitor any changes in series resistance. Initial investigations into the receptor subtype that mediates the enhancement of I_h by 5-HT were performed in 12 K^+ ACSF (Solution 2.4, Section 2.6) in which the external [K^+] was increased to 12 mM. This solution resulted in a shift in the K^+ equilibrium potential to a more depolarised value. Under these conditions inhibition of gK_{Leak} by 5-HT was observed as an outward current whereas the enhancement of I_h was still observed as an inward current. The amplitude of I_h was also enhanced under these conditions. 5-HT was bath applied in the superfusing ACSF. A 15 sec application (flow rate = 3 – 5 ml min^{-1}) of 5-HT (10 µM) was routinely administered and the voltage command was applied when the observed inward current was maximal. After a control 5-HT response was obtained antagonists were bath applied for 10 mins. 5-HT was then co-applied in the presence of the antagonist. A voltage step protocol was occasionally used to monitor I_h activation and inactivation over a range of voltages (Figure 2.6B).

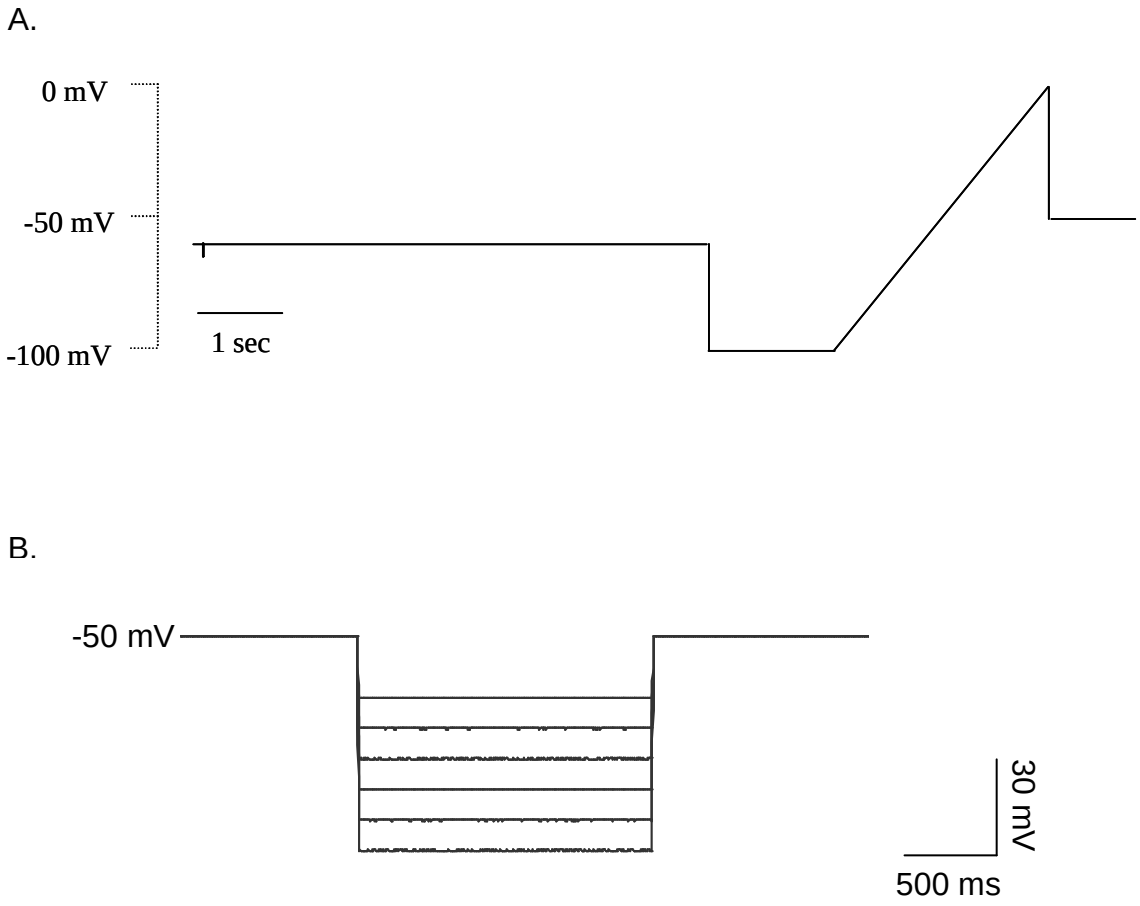

Figure 2.6. Voltage protocols to monitor changes in I_h in FMs.

A. Voltage ramp protocol
B. Voltage step command used to monitor changes in activation and inactivation of I_h at different potentials

2.2.2 Modulation of gK_{Leak} in FMs

Experiments designed to investigate the modulation of gK_{Leak} were performed on slices pre-incubated for a minimum of 30 mins with ZD-7288 (10 µM), to block I_h. ZD-7288 blocks the pore of I_h channels at an intracellular site, therefore, ZD-7288 (10 µM) was included in the internal solution to maintain an effective blocking concentration throughout the recording period (Shin, Rothberg et al. 2001). FMs were held at -50 mV and changes in conductance mediated by gK_{Leak} were measured using a voltage ramp from -100 mV to 0 mV (Figure 2.7). This ramp was preceded by a step to -100 mV to monitor the ZD-7288 mediated block of I_h. Series resistance monitored by a -10 mV, 10 ms step at the beginning of the sweep. 5-HT or NA was routinely applied in normal ACSF for 15 sec (flow rate = 3 – 5 ml min^{-1}) and the voltage command (Figure 2.7) applied when the response was maximal. External pH was modified using a pH ACSF (Solution 2.5, Section 2.6) titrated to the required pH with NaOH and oxygenated with 100% O_2 (BOC Gases, Manchester, UK) (Talley, Lei et al. 2000). pH-induced current changes were measured by applying a voltage ramp (Figure 2.7) when the current reached steady-state. Anandamide, bupivacaine, methanandamide and ruthenium red were all bath-applied through the superfusing ACSF (Section 2.7 for drug details). Slices were incubated in ATFK containing ACSF for a minimum of 10 mins prior to co-application with anandamide. Zn^{2+} was also applied through the ACSF, however, this ACSF did not contain any NaH_2PO_4 to prevent the Zn^{2+} precipitation.

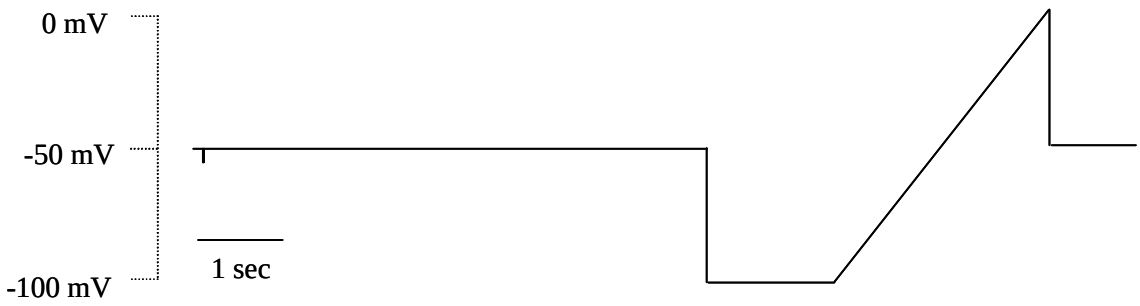

Figure 2.7. Voltage ramp protocol to monitor changes in gK_{Leak} in FMs.

External solutions containing isoflurane were prepared as previously reported (Simon, Hapfelmeier et al. 2001; Ranft, Kurz et al. 2004). Briefly, a saturated solution of isoflurane (15 mM, (Scheller, Bufler et al. 1997)) was prepared by adding an excess of anaesthetic to ACSF in a sealed glass bottle and stirring for 3 h at room temperature. Simon *et al*, 2001 found that dilutions between 1:30 to 1:7.5 of this stock solution resulted in a final aqueous concentration of 0.2 – 0.3 mM after bubbling with oxygen and delivery to the recording chamber. A 1:10 dilution was routinely used in the experiments described in this thesis

2.2.3 Evoked EPSCs and EPSPs

EPSCs and EPSPs were evoked using stimulating electrodes made from borosilicate glass (7.5 cm segments of GC150TF-15, Harvard Apparatus Ltd, Kent, UK) pulled to a resistance of 10 – 12 MΩ and had a tip diameter of 0.5 - 1 µm. The glass stimulating electrodes were filled with normal ACSF (Solution 2.2, Section 2.6) and attached to one piece of a bipolar stimulating wire on the headstage of a fine manipulator (MX-1, Narishige Scientific Instruments, Tokyo, Japan). The other part of the stimulating wire was put directly into the recording chamber to complete the circuit. Stimulation was applied using an isolated stimulator (DS2, Digitimer Ltd, Welwyn Garden, UK). Prior to making recordings from FMs the stimulating electrode was manoeuvred close to the surface of the slice to reduce the disruption to the seal caused by movement of the set up. EPSPs were evoked in the current-clamp configuration and series resistance was monitored using a 100 pA, 10 ms current step. The properties of the stimulating pulse were controlled by the isolated stimulator and were routinely 0.02 µs in duration and 3 – 10 V in intensity. For

initial searching of a response EPSCs were evoked at a frequency of 0.5 Hz and at an intensity of ~10 V. The stimulating electrode was lowered onto the surface of the slice at various positions until an EPSC was observed. Occasionally the recording electrode and stimulating electrode were filled with Lucifer Yellow (2 mg/ml) so the location of the stimulating electrode with reference to the FM could be visualised under fluorescence microscopy (Figure 2.8). The intensity of the stimulus was then reduced to 0 V and gradually increased until a response was observed. This type of minimal stimulation has previously been utilised to isolate single synapses (Lawrence, Grinspan et al. 2004). Once an appropriate stimulus intensity was selected EPSCs and EPSPs were evoked at a frequency of 0.05 Hz and a minimum of 10 sweeps were obtained under each condition. Two stimuli 50 ms apart were applied to monitor paired pulse facilitation/depression. Control responses were obtained in normal ACSF and 5-HT, 8-OH-DPAT, AP-5, CP93129, ifenprodil, isamoltane, NBQX and WAY 100635 were applied through the superfusing ACSF. The NMDA receptor-mediated response was revealed by blocking the AMPA receptor-mediated response with NBQX (20 µM) and removing the voltage dependent Mg^{2+} block by either depolarising to +20 mV or removing Mg^{2+} from the ACSF (Solution 2.6, Section 2.6). The Na^{+} channel blocker, QX314 (5 mM), was included in the internal solution when holding the FM at depolarised voltages was required.

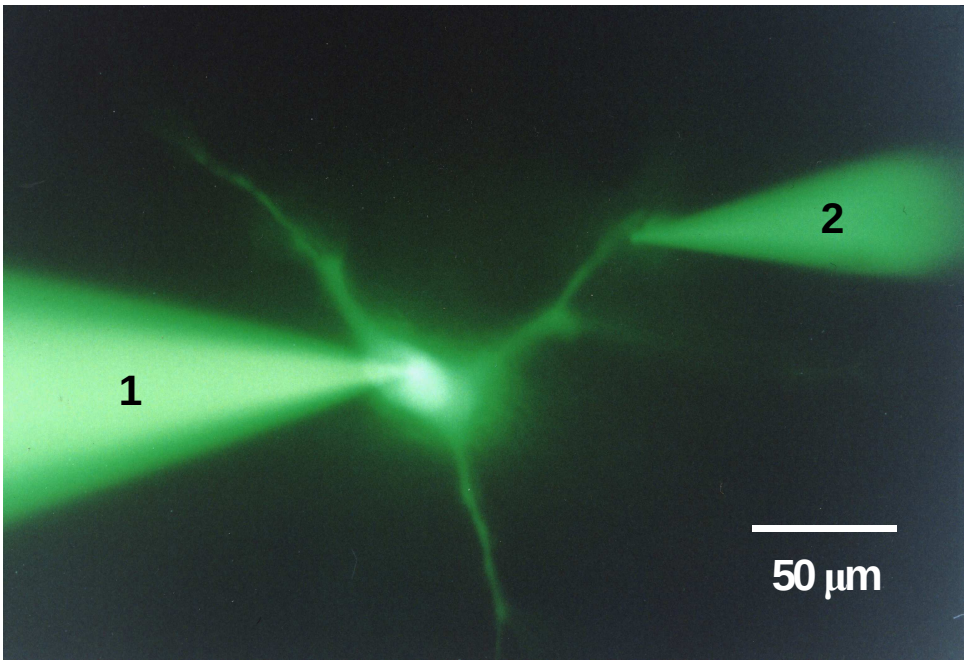

Figure 2.8 Positions of recording and stimulating electrodes.
The recording electrode (1) was filled with Lucifer Yellow (2 mg/ml) prior to making whole-cell recordings from the FM. The dye diffused into the FM and was visualised with fluorescence microscopy. The stimulating electrode (2) was also filled with Lucifer Yellow so it's position relative to the FMs dendrites could be observed.

2.2.4 Miniature EPSCs

FMs were held at -70 mV, action potential-dependent EPSCs were blocked by including tetrodotoxin (0.3 µM) and picrotoxin (50 µM) in the normal ACSF (Solution 2.2, Section 2.6) and the resulting 'mini' EPSCs represent spontaneous release of vesicles. A -10 mV, 10 ms voltage step was applied every minute to monitor series resistance and 5-HT and CP93129 were bath applied until the response reached steady-state.

2.2.5 PLC-β1$^{-/-}$ mice

Voltage-clamp recordings from FMs from PLC-β1$^{-/-}$ mice and their littermate controls were made using exactly the same procedure as for rat FMs (Section 2.1). The 5-HT- and NA-induced currents in these FMs measured following the protocol described in Section 2.2.3.

The non-selective PLC-β inhibitor, U73122, (10 µM) was applied to the superfusing ACSF following obtaining a control response to 5-HT or NA in PLC-β1$^{-/-}$ mice littermate controls.

2.3 Cerebellar Granule Neurone Electrophysiology

2.3.1 Cerebellar Granule Neurone Cultures

Cerebellar granule neurone (CGN) cultures were prepared by Mr Thomas Wishart from male and female Wistar rats aged P7 using UK Home Office approved procedures.

Dissociated granule cells were seeded on poly-D-lysine coated glass cover slips at a density of 7.5 x 10^5 cells cm^{-2}. The neurones were then cultured at 37ºC, 5% CO_2 in supplemented modified Eagle's medium (MEM, Gibco, Invitrogen, Paisley, UK) without Ca^{2+} and Mg^{2+} (Solution 2.7, Section 2.6). Cytosine-arabinoside (10 µM) was added after 24 hours to prevent glial cell growth. Electrophysiology was performed between 8 – 14 days *in vitro* (DIV).

Prior to making electrophysiological recordings the coverslips with the cultured CGNs were transferred to the recording chamber and perfused with the pH ACSF (Solution 5 titrated to pH 7.4) at a rate of 3 – 5 ml min^{-1}. Although the cultures can be maintained for several hours without oxygenation, the ACSF was oxygenated with 100% O_2 (BOC Gases, Manchester, UK) in order to maintain the experimental conditions used for slice experiments.

2.3.2 Perforated patch recordings from CGNs

The small size of CGNs can lead to fast dialysis of the cytoplasm and subsequent rundown in TASK-channel conductance when conventional whole-cell patch clamp recordings are made. To reduce this rundown the perforated-patch configuration was used to record from CGNs. Perforated-patch recordings were obtained by including the polyene antibiotic, amphotericin B, in the internal solution. The antibiotic forms small channels in lipid membranes that are only permeable to monovalent ions. This prevents movement of multivalent ions and dialysis of larger non-electrolytes such as glucose (Rae, Cooper et al. 1991). Perforated-patch recordings were made from CGNs at room temperature using the same set-up as for whole-cell recordings. Patch electrodes were made as for whole-cell recordings and the tip was filled with a

minimal amount of standard internal solution (Solution 2.3, Section 2.6). The electrode was then filled with standard internal solution with added amphotericin B (250 µg/ml). The amphotericin B containing internal solution was not filtered and was protected from light to maintain the efficacy of the antibiotic. The tip of the electrode was filled with standard internal solution as the amphotericin B prevented formation of a high resistance seal. The procedure for obtaining a GΩ seal with CGNs was identical as that described for FMs. Once in the cell-attached configuration a holding potential of -20 mV was applied and the cell left until the antibiotic formed sufficient channels in the membrane that the access resistance fell and stabilised. The time required for the change in access resistance to be observed depended on the volume of the standard solution in tip and the diffusion rate of the antibiotic (Rae, Cooper et al. 1991).

2.4 Experimental Protocol

2.4.1 Modulation of TASK channels in CGNs

CGNs were held at -20 mV and conductance changes were measured using voltage ramps from -20 to -110 mV, 900 milliseconds in duration (Figure 2.9). External pH was modified using a pH ACSF (Solution 2.5, Section 2.6) titrated to the required pH with NaOH and oxygenated with 100% O_2 (BOC Gases, Manchester, UK) (Talley, Lei et al. 2000). pH-induced current changes were measured by applying a voltage ramp (Figure 2.9) when the current reached steady-state. Anandamide and ruthenium red were bath-applied through the superfusing ACSF and voltage commands applied when the response was maximal.

Figure 2.9. Voltage ramp protocol to monitor changes in TASK conductances in CGNs.

2.5 Data Analysis

2.5.1 Data Acquisition

All current recordings were filtered by 10 kHz, 8-pole Bessel low-pass filter in the patch-clamp amplifier. The sampling frequency for data acquisition varied between configurations. Test pulses for obtaining GΩ seals were sampled at 3 kHz whereas all ramps were sampled at 200 Hz. The sampling rate for EPSCs and EPSPs was 10 kHz and continuous current records were sampled at 10 Hz. Signal files were saved to disc immediately following recordings being made. Outputs from the current and voltage channels were also recorded onto digital audio-tapes (DAT, Maxwell) through a digital tape recorder (DTR 1404, Bio-logic Scientific Instruments) to allow playback of data at different sampling frequencies and further offline analysis. Data was exported from Signal files as text files, which were then opened with Microsoft Excel (Microsoft Corporation) for further analysis.

2.5.2 Miniature EPSCs

Recordings were played back into the computer into an EDR file using John Dempster's Electrophysiology Data Recorder software (version 2.4.3, University of Strathclyde). The files were then converted to an ABF format using Justin Lee's ABF File Utility v2.1.74. ABF files were analysed using Justin Lee's Mini Analysis Program (version 6.0.7, Synaptosoft Inc.) in an EVT format. EPSCs were identified and checked individually to ensure a correct fit was obtained.

2.5.3 Equations

The Nernst equation was used to predict the K^+ equilibrium potential,

$E_K = RT / F \ln [K]_o / [K]_i$ (Equation 1)

where R is the gas constant, T is the temperature (Kelvin scale) and F is the Faraday constant.

Single exponential fits to the activation and deactivation of subtracted NA-sensitive current traces were performed using Signal software (v2.0, CED, Cambridge, UK) according to the equation,

$I_t = A + Be^{-t/\tau}$ (Equation 2)

where I_t is current amplitude at time t, A and B are constants and τ is the time constant.

The pH-sensitivity of FM membrane current could be described by a modified (4 parameter logistic) Hill Equation,

$y = y_{min} + (y_{max} - y_{min}) / [1 + (pH / pK)^b]$ (Equation 3)

where y is the holding current or input conductance, y_{max} the maximum response, y_{min} the minimum response and $b = -(b' * pK) / 0.434$ where b' is the Hill coefficient expressed as a function of H^+ concentration.

2.6 Solutions

Solution 2.1. Modified Artificial Cerebral Spinal Fluid.

Compound	Concentration (mM)
NaCl	56.5
Sucrose	113
$CaCl_2$	0
$MgSO_4$	5
KCl	3
NaH_2PO_4	1.25
$NaHCO_3$	26
Glucose	11
Lactate	4

pH = 7.4 when bubbled with 95% O_2, 5% CO_2

Solution 2.2. Normal Artificial Cerebral Spinal Fluid.

Compound	Concentration (mM)
NaCl	126
$CaCl_2$	2
$MgSO_4$	2
KCl	3
NaH_2PO_4	1.25
$NaHCO_3$	26
Glucose	11

pH = 7.4 when bubbled with 95% O_2 : 5% CO_2

Solution 2.3. Standard Internal Solution.

Compound	Concentration (mM)
KGluconate	122.5
KOH	17.5
Hepes	10
EGTA	0.2
NaCl	9
$MgCl_2$	1
MgATP	3
NaGTP	0.3

pH to 7.4 with KOH

Solution 2.4. 12 mM K^+ Artificial Cerebral Spinal Fluid.

Compound	Concentration (mM)
NaCl	117
$CaCl_2$	2
$MgSO_4$	2
KCl	12
NaH_2PO_4	1.25
$NaHCO_3$	26
Glucose	11

pH = 7.4 when bubbled with 95% O_2 : 5% CO_2

Solution 2.5. pH ACSF (Talley, Lei et al. 2000).

Compound	Concentration (mM)
NaCl	126
$CaCl_2$	2
$MgSO_4$	2
KCl	3
NaH_2PO_4	1.25
HEPES	10
Glucose	11

Titrated to the desired pH with NaOH and bubble with 100% O_2

Solution 2.6. Mg^{2+} free Artificial Cerebral Spinal Fluid.

Compound	Concentration (mM)
NaCl	126
$CaCl_2$	2
KCl	3
NaH_2PO_4	1.25
$NaHCO_3$	26
Glucose	11

pH = 7.4 when bubbled with 95% O_2 : 5% CO_2

Solution 2.7. Supplemented modified Eagle's medium (MEM, Gibco, Invitrogen, Paisley, UK).

Compound	Concentration
MEM	
Fetal calf serum	10%
Glucose	9.2 mM
Glutamine	0.56 mM
KCl	5.2 mM
Penicillin-streptomycin	1%

2.7 Drugs

Drug	**Supplier (cat. #)**	**Concentrations Used**
5-hydroxytryptamine creatine sulphate (5-HT)	Sigma (H7752)	10 µM
8-Hydroxy-DPAT hydrobromide (8-OH-DPAT)	Tocris (0529)	10 µM
amphotericin B solubilized	Sigma (A9528)	250 µg/ml in internal solution
anandamide (Arachidonylethanolamide)	Tocris (1339)	10 – 20 µM
AP-5 (AP-V or D-(-)-2-Amino-5-phosphonopentanoic acid)	Tocris (0106)	50 – 100 µM
Arachidonyl trifluoromethyl ketone (ATFK or AACOCF$_3$)	Tocris (1462)	10 µM
Bupivacaine hydrochloride	Sigma (B5274)	100 µM

Drug	**Supplier (cat. #)**	**Concentrations Used**
CP93129 dihydrochloride	Tocris (1032)	10 µM
Ifenprodil hemitartrate	Tocris (0545)	10 µM
Isoflurane		See Methods 2.2.3
Isamoltane hemifumarate	Tocris (0992)	1 µM
Lucifer Yellow	Sigma	2 mg/ml in internal solution
(*R*)-(+)-Methanandamide	Tocris (1121)	10 – 20 µM
NBQX (2,3-Dioxo-6-nitro-1,2,3,4-tetrahydrobenzo[f]quinoxaline-7-sulfonamide)	Tocris (0373)	20 µM
noradrenaline bitartrate (arterenol bitartrate)	Sigma (407453)	5 -10 µM

Drug	**Supplier (cat. #)**	**Concentrations Used**
Phenylephrine hydrocholride	Sigma (P6126)	30 µM
Prazosin	Tocris (0623)	0.5 µM
Propranolol	Tocris (0624)	10 µM
QX314	Tocris (1014)	5 mM
R96544	Tocris (1742)	0.3 – 1 µM
Ruthenium red	Sigma (R2751)	10 µM
SB29970A	Tocris (1612)	0.3 – 10 µM
Tetrodotoxin citrate	Tocris (1069)	0.3 µM

Drug	**Supplier (cat. #)**	**Concentrations Used**
U73122	Tocris (1268)	5 – 10 µM
WAY 100635 maleate salt	Sigma (W108)	1 µM
ZD-7288	Tocris (1000)	10 µM
Zinc chloride	Sigma (429430)	100 – 300 µM

2.8 PLC-β1 Immunohistochemistry

2.8.1 Tissue preparation

This work was performed in collaboration with Dr Peter Kind, The University of Edinburgh.

Wild type littermates of PLC-β1$^{-/-}$ mice were perfused with 4% paraformaldehyde using UK Home Office approved procedures. The brain was removed, the hindbrain isolated and kept overnight in 4% paraformaldehyde. The hindbrain was then transferred to 30% sucrose and left overnight or until the tissue sunk. 48 µm sections were cut on a freezing microtome and transferred to phosphate buffered saline (PBS).

2.8.2 Immunohistochemistry

Immunohistochemistry was performed using published procedures (Hannan, Kind et al. 1998).

Sections were blocked for 30 min with 5% (v/v) normal goat serum (NGS), 0.5% (v/v) Triton X-100, in PBS. The sections were then incubated overnight at 4°C with a primary antibody that specifically recognizes PLC-β1 (rabbit polyclonal; Santa Cruz Biotechnology, Santa Cruz, CA, USA), diluted (1 in 2000) in 1% NGS, 0.5% Triton X-100 in PBS. Sections were washed three times in 0.5% Triton X-100 in PBS for 10 min at room temperature with shaking. The sections were then incubated with biotin-conjugated secondary antibody (anti-rabbit, donkey derived, Vector Laboratories, Bretton, UK) at room temperature for 2 hours with shaking. After washing the sections 3 times as above they were incubated with Vectastain ABC Elite avidin detection reagent (Vector Laboratories, Bretton, UK) for 1 h. Following

a further three washes, colour detection was achieved by the addition of a solution containing 0.5 mg/ml 3,3′-diaminobenzidine (DAB, Sigma–Aldrich), 0.6% (w/v) Ni(NH4)(SO4) and 0.03% H2O2. The colour reaction was stopped with PBS, and sections were dehydrated and mounted under coverslips with DePeX (Merck, Lutterworth, UK).

Sections were examined and bright-field photomicrographs were prepared using a light microscope (Leica, Wetzlar, Germany).

Chapter 3

3.1 Introduction

The monoamine neurotransmitters 5-HT and NA are generally accepted to promote adult FM excitation by depolarising the postsynaptic membrane (VanderMaelen and Aghajanian 1980; Vandermaelen and Aghajanian 1982; Larkman, Penington et al. 1989; Larkman and Kelly 1992). The ionic mechanisms that underlie the membrane depolarisation by 5-HT have been previously determined as an enhancement of the hyperpolarisation activated cation current, I_h, and a decrease in a leak potassium (K^+) conductance (gK_{Leak}) (Larkman and Kelly 1992; Larkman and Kelly 1997; Larkman and Kelly 1998). In addition, NA promotes FM membrane excitation by inhibiting a potassium conductance but does not enhance I_h (Larkman and Kelly 1992). The primary aim of this study was to investigate the biophysical and pharmacological properties of the amine-sensitive gK_{Leak} in neonatal rat FMs. Some of this work has been published and a reprint of the manuscript appears in Appendix A (Larkman and Perkins 2005).

3.1.1 Leak K^+ conductances

'Leak' K^+ conductances (gK_{Leak}), characterised by no or weak voltage-dependence and fast kinetics, provide a major determinant in regulating excitability of many neuronal types. It has been widely suggested that members of the twin-pore (2P) domain K^+ channel family provide molecular correlates for physiologically identified "leak" K^+ conductances (reviewed by (Goldstein, Bockenhauer et al. 2001), (Patel and Honore 2001)). Unlike other K^+ channel subunits which have one pore domain and either two or six transmembrane domains, the K_{2P} channel subunits have 4

transmembrane segments and 2 pore-forming domains (Figure 3.1, (Lesage and Lazdunski 2000)). The K_{2P} subunits form functional channels as homomeric or heteromeric dimers (Lesage, Guillemare et al. 1996; Lesage and Lazdunski 2000; Berg, Talley et al. 2004). The 15 known members of this family can be grouped into six subfamilies: the two pore domain weakly inwardly rectifying K^+ (TWIK) channels (TWIK1, TWIK2 and KCNK7); TWIK-related K^+ (TREK) channels (TREK1, TREK2 and TRAAK); TWIK-related alkali-activated K^+ (TALK) channels (TALK1, TALK2 AND TASK2); the TWIK-related spinal cord K^+ (TRESK) channel and TWIK-related acid-sensitive K^+ (TASK) channels (TASK1, TASK3 and TASK5) (Bayliss, Sirois et al. 2003; Mathie 2007).

3.1.2 TASK channels

TASK-1 channels were the first K_{2P} molecular correlates of background or 'leak' K^+ conductances to be cloned (Duprat, Lesage et al. 1997; Leonoudakis, Gray et al. 1998). This was followed by the discoveries of four other members of this family (TASK 2-5) although TASK 2 and 4 have reclassified as members of the TALK subfamily (TASK4 is also named TALK2) (Kim, Bang et al. 2000; Ashmole, Goodwin et al. 2001; Decher, Maier et al. 2001; Gabriel, Abdallah et al. 2002).

In young rat hypoglossal motoneurons and adult turtle spinal motoneurons it has been proposed that members of the TASK group of 2P channels, underlie an amine-sensitive gK_{Leak} (Talley, Lei et al. 2000; Perrier, Alaburda et al. 2003). The presence of TASK-1 (KCNK3) and TASK-3 (KCNK9) mRNA has been demonstrated in the rat FMN, raising the possibility that TASK channels underlie the amine-sensitive

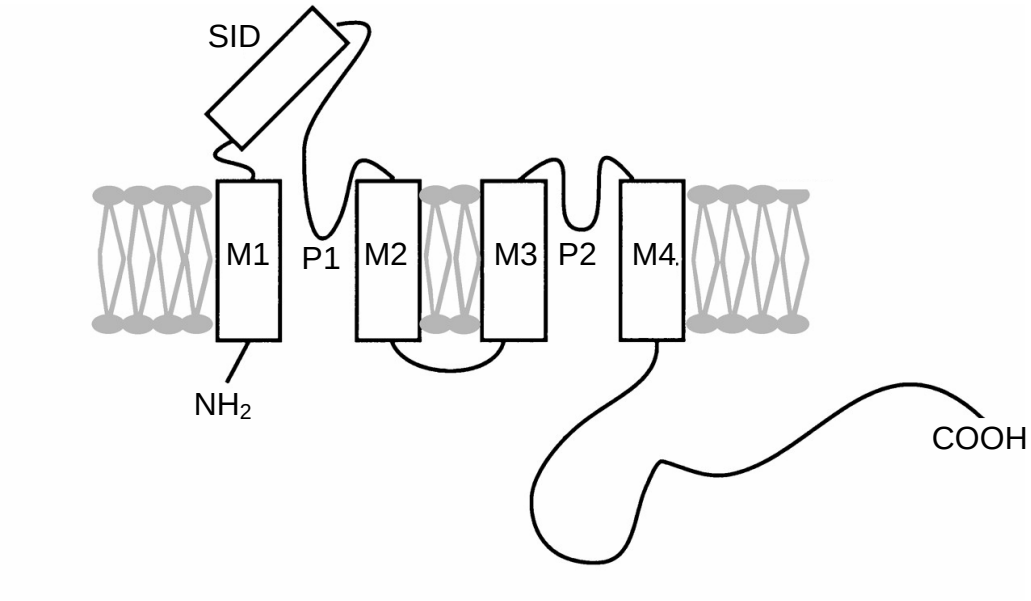

Figure 3.1. Structure of K2P receptor subunit.
The K_{2P} receptor contains four transmembrane segments (M1-4) and two pore forming loops (P1-2) and also has an extracellular self-interacting domain (SID). The subunits dimerize to form functional channels. Modified from (Lesage and Lazdunski 2000).

gK_{Leak} in FMs (Talley, Lei et al. 2000; Karschin, Wischmeyer et al. 2001; Vega-Saenz de Miera, Lau et al. 2001). Nevertheless, a motoneuron specific inwardly rectifying K^+ channel, Kir2.4, has also been proposed to underlie the amine-sensitive K^+ current in hypoglossal motoneurons and this may also be expressed by neonatal rat FMs (Karschin, Dissmann et al. 1996; Karschin and Karschin 1997; Topert, Doring et al. 1998).

TASK-1 and TASK-3 channels mediate openly rectifying currents with fast kinetics that can be distinguished by the pH at which they are half-maximally activated (pK) (Duprat, Lesage et al. 1997; Leonoudakis, Gray et al. 1998; Kim, Bang et al. 2000; Rajan, Wischmeyer et al. 2000). In addition, the endogenous cannabinoid, anandamide, preferentially blocks TASK-1 channels while the polycationic compound, ruthenium red (RR) selectively blocks TASK-3 channels (Maingret, Patel et al. 2001; Czirjak and Enyedi 2003). TASK-1 and TASK-3 also appear to form functional heterodimeric channels with emergent properties distinct from the respective homomeric channel (Czirjak and Enyedi 2002; Talley and Bayliss 2002; Kang, Han et al. 2004). In this respect, acetylcholine inhibits a gK_{Leak} in cultured rat cerebellar granule neurones with properties similar, but not identical, to TASK-1 (Watkins and Mathie 1996; Millar, Barratt et al. 2000). Single-channel studies have demonstrated the presence of homomeric TASK-1, homomeric TASK-3 and heteromeric TASK-1 / TASK-3 channels in these cells (Han, Truell et al. 2002; Kang, Han et al. 2004).

3.1.3 Hyperpolarisation-activated cation current

The channels which mediate I_h belong to the voltage-gated K^+ channel superfamily but I_h has the unique property of being a slowly developing inward current which is activated by membrane hyperpolarisation and not depolarisation like other members of this superfamily.

Four mammalian genes for the subunits which can form the hyperpolarisation-activated cyclic nucleotide-gated cation channel (HCN1-4) have been cloned (Ludwig, Zong et al. 1998; Santoro, Liu et al. 1998). HCN channels are tetrameric and each subunit has six transmembrane segments (S1-S6) with a pore-forming loop between S5 and S6 (Figure 3.2) (for reviews see (Kaupp and Seifert 2001; Accili, Proenza et al. 2002; Robinson and Siegelbaum 2003)). The GYG sequence motif that acts as a selectivity filter in K^+ channels is present in this loop region, however, the other amino acids in this region also allow for movement of Na^+ through the channel pore (Heginbotham, Lu et al. 1994; Pape 1996; Ludwig, Zong et al. 1998; Santoro and Tibbs 1999; Kaupp and Seifert 2001).

3.1.4 Voltage gating of HCN channels

Similar to other voltage-dependent channels, HCN channels have a voltage-sensor motif (Arg or Lys at every third position) in the fourth transmembrane segment (S4, Figure 3.2) (Ludwig, Zong et al. 1998). However, as HCN channels are activated by hyperpolarisation the mechanism by which this voltage-sensor activates the channel must differ from other voltage-dependent channels (which are activated by depolarisation). Potential mechanisms for this include coupling between the movement of the voltage sensor and the activation gate being reversed compared to

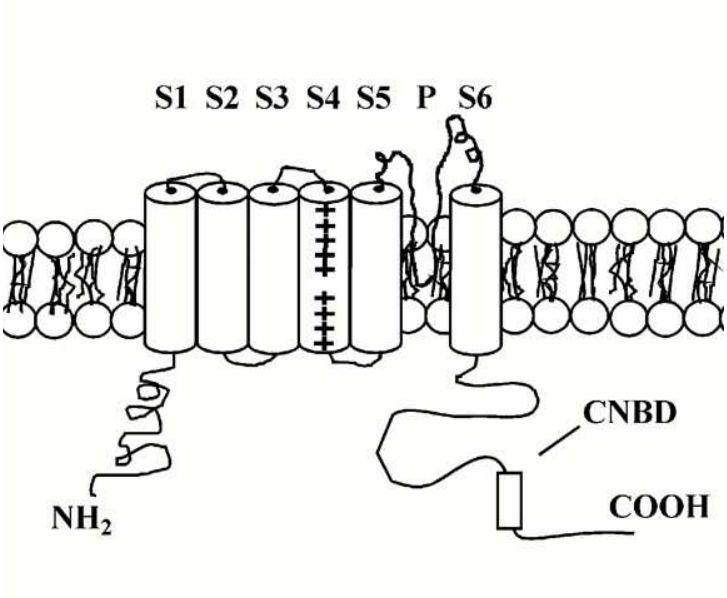

Figure 3.2. Structure of HCN subunit.

The subunit is comprised of six transmembrane segments (S1-S6) and a pore forming loop between S5 and S6. S4 contains the voltage sensor and the intracellular C-terminal region contains the cyclic nucleotide-binding domain (CNBD) (Modified from (Accili, Proenza et al. 2002)).

conventional voltage-gated channels, depolarisation of the membrane could stabilise the channel in the closed state or the channel could be inactivated at depolarised potentials and hyperpolarisation removes this inactivation (Kaupp and Seifert 2001; Rosenbaum and Gordon 2004).

3.1.6 Heterogeneity of I_h

There are four known genes encoding the I_h channel subunits (HCN1-4), which can form homomeric channels ((Ludwig, Zong et al. 1998; Santoro, Liu et al. 1998), for review see (Santoro, Chen et al. 2000)). There is also evidence for the existence of functional HCN1/2 heteromeric channels (Chen, Wang et al. 2001; Ulens and Tytgat 2001). Within the facial motor nucleus there are at least two classes of motoneurones that can be distinguished by the voltage-dependence of their I_h, suggesting more than one type of functional channel exists within this nucleus (Larkman and Kelly 1992)

3.1.7 HCN subunits in the facial motor nucleus

The distribution of the mammalian HCN channel subunits (HCN1-4) has been determined by *in situ* hybridization and Northern blotting (Ludwig, Zong et al. 1998; Santoro, Liu et al. 1998). HCN1 and HCN2 mRNA are highly expressed in the mouse brainstem motor nuclei including the facial motor nucleus, with a lower expression of HCN4 also being detected (Santoro, Chen et al. 2000). Immunohistochemical studies also indicate a high expression of HCN1 and HCN2 subunits in the facial motor nucleus with a lower expression of HCN3 and HCN4 subunits (Notom 2004).

3.1.8 Blockers of I_h

I_h is sensitive to block by caesium (Cs^+) ions, however Cs^+ also blocks inwardly rectifying K^+ channels (Larkman and Kelly 1997). The novel bradycardic agent, ZD 7288, acts by selectively blocking I_f in the heart and has also been shown to selectively block I_h in the central nervous system (BoSmith, Briggs et al. 1993; Harris and Constanti 1995). ZD 7288 has been utilised to investigate I_h in facial motoneurones and has been shown to block the channel at an intracellular site, in a voltage-independent manner (Harris and Constanti 1995; Larkman and Kelly 2001).

3.1.9 Aims

In addition to confirming the ionic mechanisms underlying the actions of 5-HT and NA in neonatal rat FMs the main aim of this chapter was to investigate the biophysical and pharmacological properties of the amine-sensitive gK_{Leak}. The pH-sensitivity of gK_{Leak} suggested the channel belonged to the TASK family of leak K^+ channels. Although the pharmacology of gK_{Leak} was inconsistent with homomeric TASK-1 or TASK-3 channels it did support a heteromeric TASK-1/TASK-3 channel identity.

3.2 Results

3.2.1 Effect of 5-HT on FMs

When a FM was voltage-clamped at a potential depolarised to the potassium equilibrium potential and close to its resting membrane potential (routinely between –50 and –70 mV) bath-application of 5-HT (10 µM) evoked an inward current (-57 ±

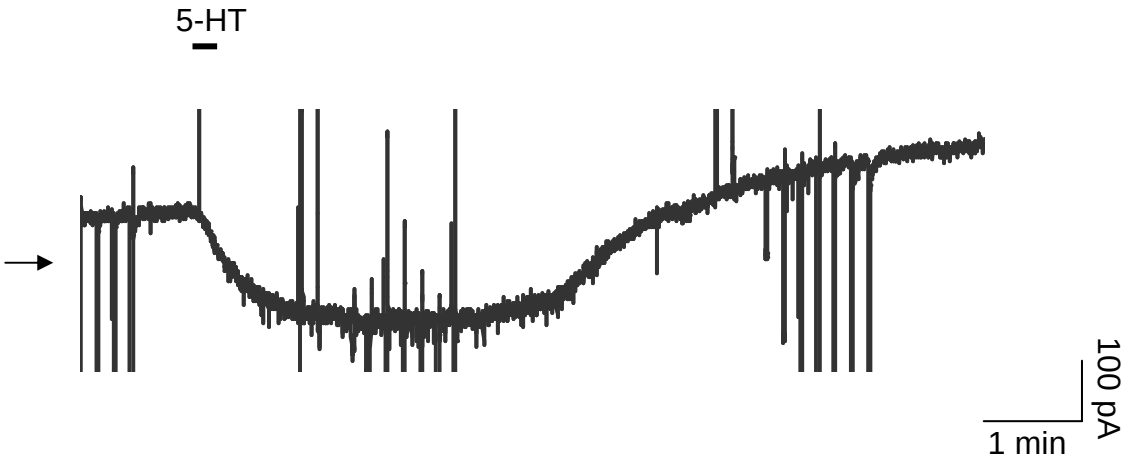

Figure 3.3. 5-HT evokes a large inward current.

Continuous current record obtained from a FM voltage-clamped at –50 mV in normal ACSF. Bath application of 5-HT (10 μM) evokes a large, reversible, inward current. The large vertical deflections represent current responses to voltage commands on a compressed time scale. The arrow indicates the zero current level.

20 pA at –50 mV, n = 6 under these conditions, example in Figure 3.3). This is the current that underlies the depolarisation of the FM membrane potential.

The current response to a hyperpolarising voltage step (from –50 to –100 mV) demonstrates that there are at least two distinct mechanisms underlying this inward current; an enhancement of I_h and a decrease in the instantaneous current (Figure 3.4).

3.2.2 5-HT enhances I_h

Stepping from –50 mV to –100 mV activated the slowly developing hyperpolarisation-activated cation current, I_h, and this current was significantly enhanced by 5-HT (increased by 29 ± 11%, n = 7, P = 0.0006, one sample t test, Figure 3.4. I_h amplitude was measured as the difference between the instantaneous and steady-state current in response to the voltage step). The tail currents that arise due to the slow deactivation of I_h were also larger in the presence of 5-HT, supporting the enhancement of I_h by 5-HT.

3.2.3 5-HT decreases the instantaneous current

In addition to enhancing I_h, 5-HT application resulted in a decrease in the instantaneous current response to a voltage step command. The availability of ZD7288, a selective blocker of I_h, allowed the 5-HT-mediated modulation of the instantaneous current to be investigated in isolation of the effects of 5-HT on I_h (BoSmith, Briggs et al. 1993; Larkman and Kelly 2001). The current responses to the hyperpolarising voltage steps demonstrate that in the presence of ZD 7288 (10 µM), I_h is abolished and is not increased in the presence of 5-HT (Figure 3.5C).

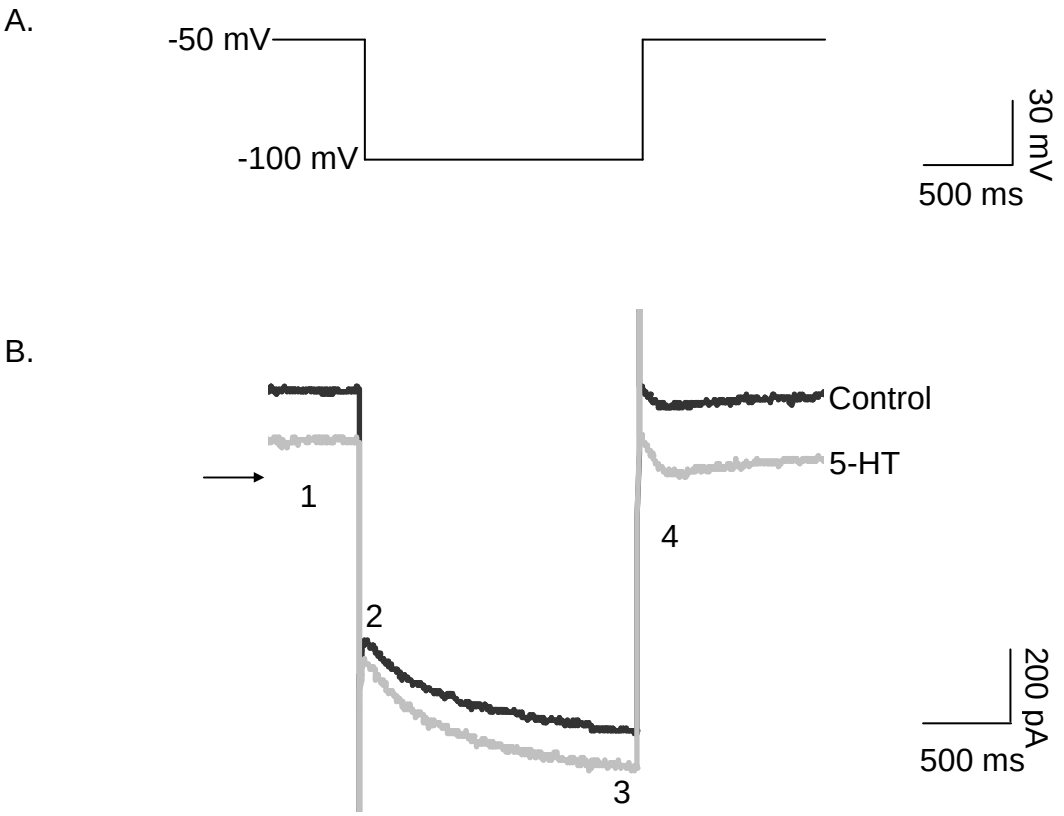

Figure 3.4. Multiple mechanisms underlie the 5-HT-evoked current.

A. Hyperpolarizing voltage step command used to monitor changes in conductance and I_h.

B. Current responses to hyperpolarizing voltage step (A) in control conditions (black) and following bath application of 5-HT (10 µM, grey). 5-HT evokes an inward current at the holding potential of –50 mV (1). There is a decrease in the instantaneous current (2) and an increase in I_h (3) following application of 5-HT. 5-HT also increases the tail current (4), which arises as I_h inactivates following removal of the hyperpolarizing voltage step. The arrow indicates the zero current level.

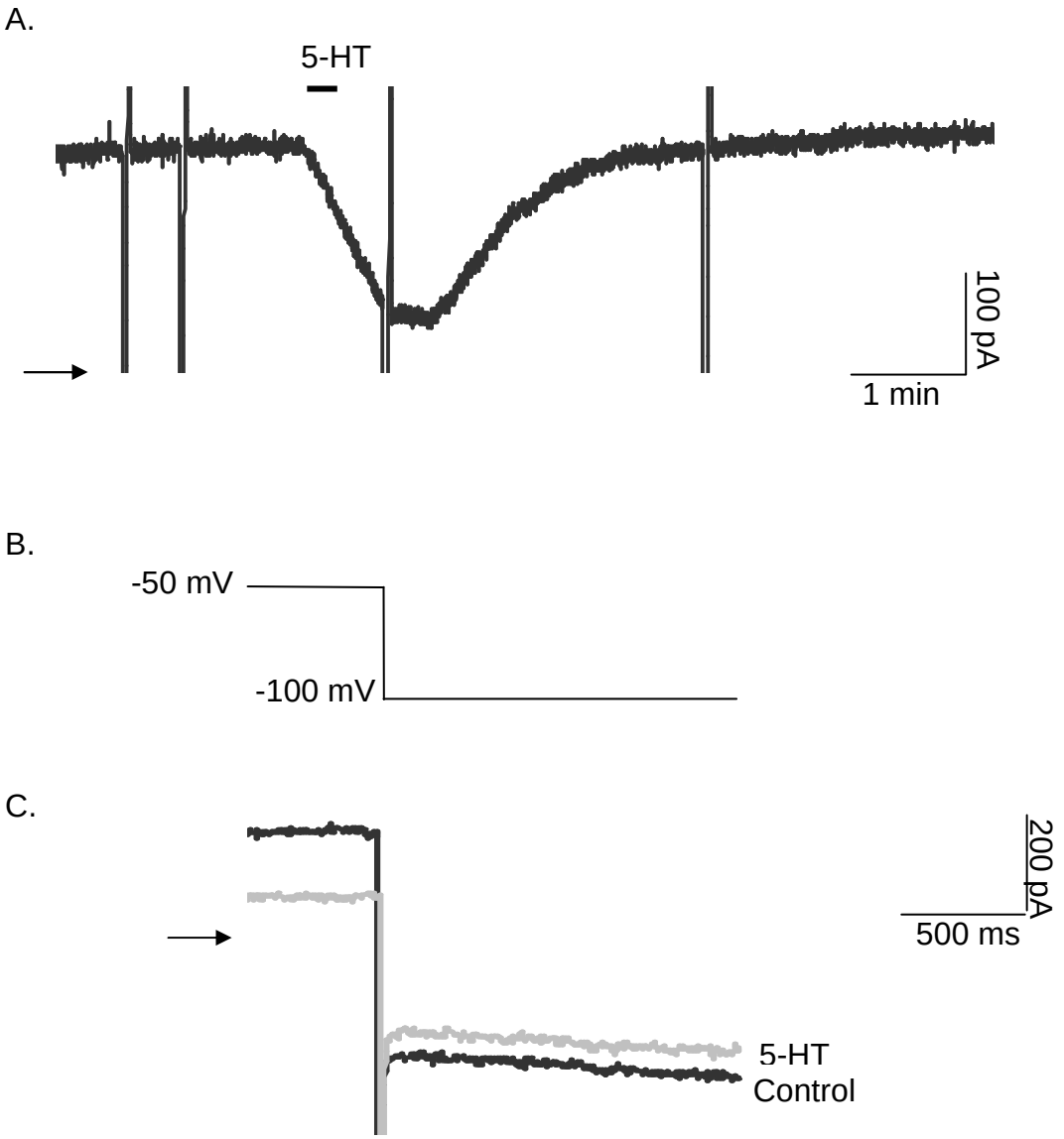

Figure 3.5. Actions of 5-HT in the presence of ZD7288, a blocker of I_h.

A. Continuous current record of a FM voltage-clamped at –50 mV in the presence of ZD7288 (10 μM). Bath application of 5-HT (10 μM) evokes a large inward current. The arrow indicates the zero current level and the large deflections represent attenuated current responses to voltage commands.

B. Hyperpolarizing voltage step command used to monitor changes in I_h.

C. Current responses to hyperpolarizing voltage step (B) in control conditions (black) and in the presence of 5-HT (10 μM, grey). In the presence of ZD7288 (10 μM) I_h is abolished. Under these conditions 5-HT decreases the current response. The arrow indicates the zero current level.

In the presence of ZD7288 (10 µM), 5-HT (10 µM) evoked an inward current when bath applied to FMs voltage-clamped at –50 mV (-64 ± 14 pA, n = 6, Figure 3.5A). 5-HT (10 µM) also decreased the current response to the hyperpolarising step compared to control when ZD 7288 (10 µM) was present (Figure 3.5C). Current-voltage (I/V) relationships were generated using the current response to a voltage ramp (Methods Figure 2.6). A reduction in the slope of an I/V plot indicates an increase in resistance / decrease in conductance. In Figure 3.6B the slope of the I/V relationship obtained from a FM in the presence of 5-HT (10 µM) was reduced compared to control, corresponding to a reduction in conductance from 12.3 nS to 8.9 nS (in the presence of ZD7288 (10 µM), conductance measurements were obtained from the slope of the I/V plot). In a representative sample of FMs 5-HT (10 µM) application resulted in a mean decrease in conductance from 8.0 ± 1.2 nS to 5.6 ± 0.9 nS (n = 6, P = 0.018, paired t test).

The 5-HT-induced current ($I_{5\text{-HT}}$) was obtained by subtraction of the control current response to the voltage ramp from the current response obtained in the presence of 5-HT and was plotted against voltage (Figure 3.6B). The 5-HT-induced current was approximately linear over the range measured. In the example shown in Figure 3.6 the point of intersection of the control I/V plot and the plots obtained in 5-HT is –84 mV. The mean point of intersection and hence reversal potential for this action of 5-HT was –85 ± 9 mV (n = 5), close to the E_K as predicted by the Nernst Equation (approximately –94 mV, Methods Equation 1). The difference in the reversal potential for the action of 5-HT and the predicted E_K may be due to a contribution of

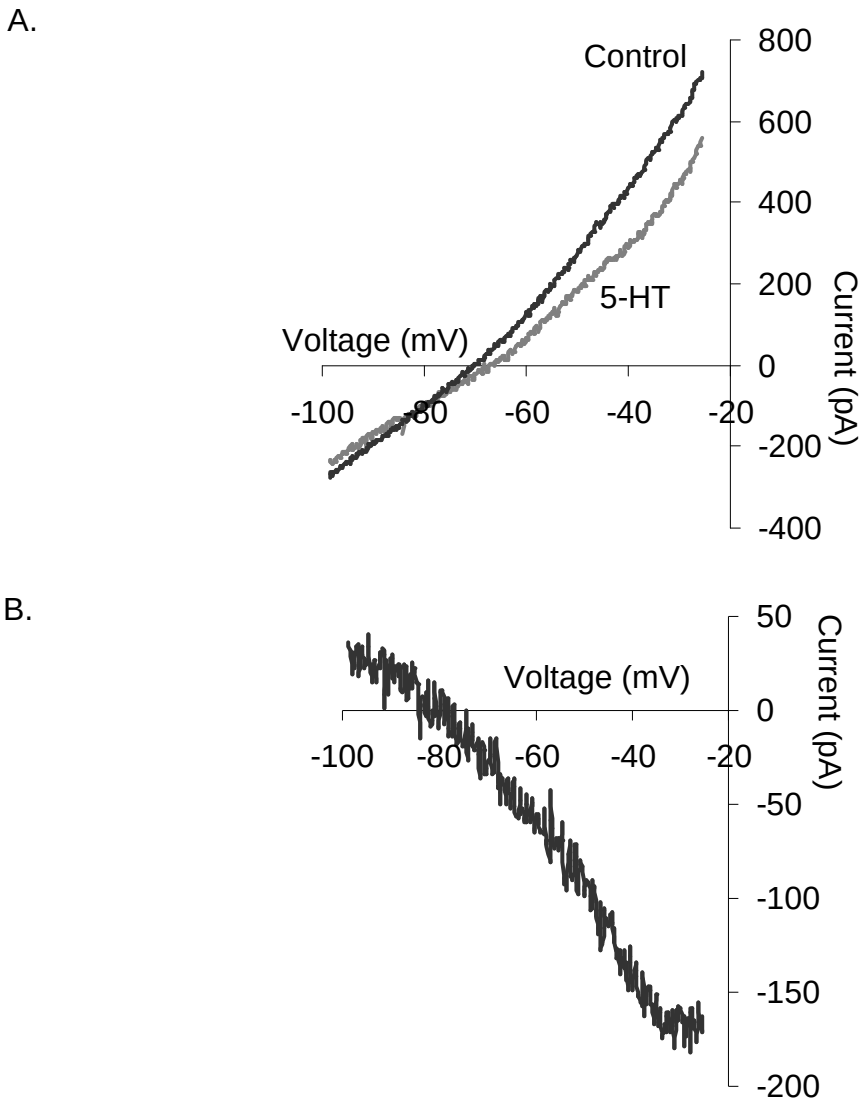

Figure 3.6. 5-HT inhibits a 'leak' potassium conductance (gK_{Leak}).

A. I/V relationships obtained from a FM in the presence (grey) and absence (black) of 5-HT (10 μM).

B. The 5-HT-induced current plot (obtained by subtraction of the control plot from the 5-HT plot shown in B). This current is approximately linear over the range measured and intersects with the x-axis at –84 mV, close to the E_K (as predicted by the Nernst Equation).

other ions or a slight underestimation of the junction potential, however, it is clear that a K^+ conductance plays a significant contribution. Taken together these findings suggest that one of the mechanisms by which 5-HT mediates FM depolarisation is through inhibition of a potassium conductance (*g*K). The approximate linearity of the $I_{5\text{-HT}}$ suggests a 'leak' *g*K (gK_{Leak}) (Goldstein, Bockenhauer et al. 2001; Patel and Honore 2001; Lesage 2003). These findings are consistent with other published studies (VanderMaelen and Aghajanian 1980; Vandermaelen and Aghajanian 1982; Larkman, Penington et al. 1989; Larkman and Kelly 1992).

3.2.4 NA inhibits a gK_{Leak}

NA had been shown to inhibit a conductance in adult rat FMs which is similar to the 5-HT-sensitive gK_{Leak} (Larkman and Kelly 1992). The presence of this NA-sensitive conductance in neonatal rat FMs has been further investigated Bath-application of NA induced an inward current in neonatal FMs voltage-clamped at -60 mV in standard ACSF containing 3 mM K^+ and ZD 7288 (10 μM) (Figure 3.7A). The I/V relationships in the presence and absence of NA indicated that the inward current was associated with a decrease in membrane conductance (Figure 3.7B). In a representative sample of FMs, NA (10 μM) induced an inward current of -58 ± 7 pA associated with a significant decrease in the mean conductance from 9.4 ± 0.8 nS to 7.3 ± 0.7 nS (n = 19, P = 0.02, paired t test). The NA-induced current (I_{NA}) appeared linear over the voltage range -40 to -90 mV (Figure 3.7C), however, some rectification was seen outwith these voltages (example in Figures 3.13B). I_{NA} reversed at -96 ± 3 mV (n = 19), -70 ± 2 mV, (n = 16) and -61 ± 2 mV (n = 14) when the ACSF contained 3, 7 or 12 mM K^+ respectively, in agreement with predictions

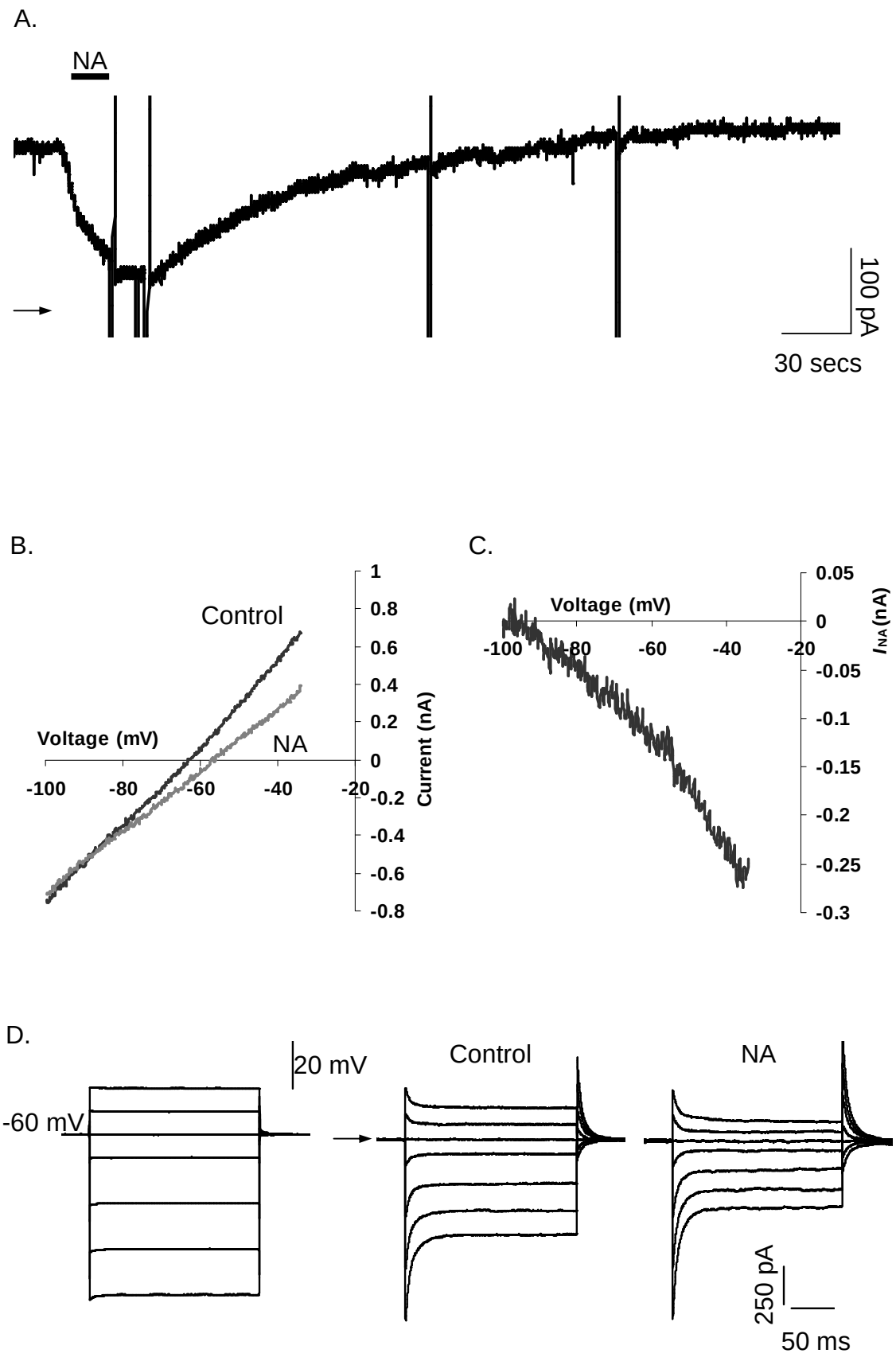
A.
NA
100 pA
30 secs
B.
Control
NA
Voltage (mV)
-100
-80
-60
-40
-20
1
0.8
0.6
0.4
0.2
0
-0.2
-0.4
-0.6
-0.8
Current (nA)
C.
Voltage (mV)
-100
-80
-60
-40
-20
0.05
0
-0.05
-0.1
-0.15
-0.2
-0.25
-0.3
I_{NA} (nA)
D.
20 mV
-60 mV
Control
NA
250 pA
50 ms

E.

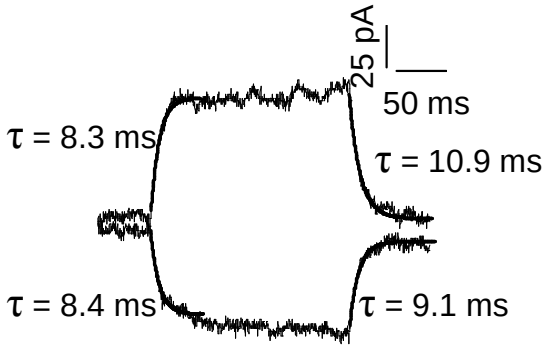

Figure 3.7. Noradrenaline inhibits a leak K^+ conductance in neonatal rat FMs.

A. Continuous current record of FM voltage-clamped at –50 mV demonstrating that bath application of NA (10 μM) evokes an inward current. Vertical deflections are attenuated current responses to voltage ramp commands and the arrow indicates the zero current level.

B. I/V relationships obtained from the same FM in the presence (grey) and absence (black) of NA (10 μM).

C. The NA-induced current (obtained by subtraction of plots shown in B) is approximately linear over the range measured and intersects with the x-axis at –94 mV, close to the E_K as predicted by the Nernst Equation (-97 mV, Methods Equation 1).

D. Voltage step commands of variable amplitude (left) and superimposed expanded current responses to the voltage step commands before (control, centre) and during (NA, right) application of NA (10 μM). ACSF contained 7 mM K^+ and the horizontal arrow indicates the zero current level for control and –150pA for NA trace.

E. Subtracted records of I_{NA} in response to –30 mV (upper trace) and +20 mV (lower trace) voltage steps. Single exponential curves with the time constants (τ) indicated (Methods Equation 2) have been superimposed on the activation and deactivation phases of the currents.

for the E_K obtained from the Nernst equation (Methods Equation 1). Subtracted current records (Figure 3.7D, E) indicated that the NA-sensitive gK_{Leak} displayed rapid, voltage-independent, activation and deactivation kinetics. Subtracted currents obtained after stepping from -60 mV to -40 mV displayed activation and deactivation time constants of 9 ± 1.6 ms (n = 7) and 6.6 ± 0.3 ms (n = 8), respectively. Stepping to –90 mV from –60 mV revealed activation and deactivation time constants of 6.9 ± 1.1 ms and 8.5 ± 0.7 ms (n = 8). These properties suggest that, in neonatal FMs, NA inhibits a gK^+ with properties very similar to the 5-HT-sensitive gK_{Leak}.

3.2.5 NA and 5-HT modulate the same gK_{Leak} in facial motoneurones

Application of a maximal concentration of NA (10 μM) in the continued presence of a maximal concentration of 5-HT (10 μM) failed to induce any further inward current (Figure 3.8A) suggesting that the two transmitters act on a shared population of leak K^+ channels. 5-HT (10 μM) or NA (10 μM) applied alone induced inward currents of -45 ± 4 pA (n = 5) and -34 ± 2 pA (n = 3), respectively (V_h = -50 mV, $[K^+]_o$ = 7 mM). Co-application of 5-HT and NA induced an inward current of -47 ± 8 pA. The transmitter-induced current over the range of voltage -30 to -90 mV possessed the same properties whether 5-HT or NA were applied together or separately (Figure 3.8B).

3.3 Identity of amine-sensitive gK_{Leak}

It has been widely suggested that members of the twin-pore (2P) domain K^+ channel family provide molecular correlates for physiologically identified "leak" K^+ conductances and the hypothesis that members of this family mediate gK_{Leak} in FMs

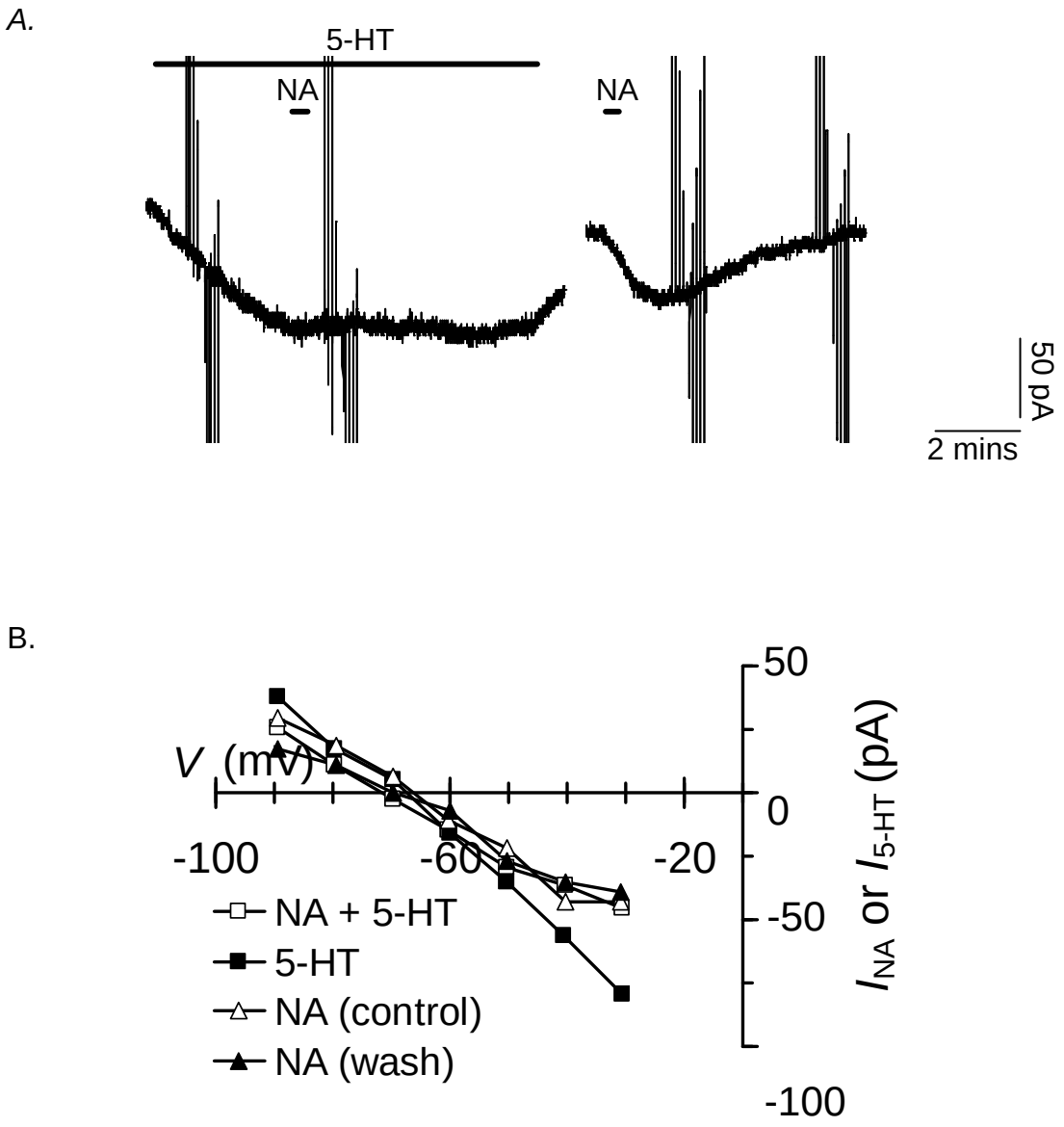

Figure 3.8. 5-HT and Noradrenaline inhibit the same leak K^+.

A. Continuous current records of membrane current from a FM voltage clamped at –60 mV demonstrating that the NA-induced inward current is occluded by the 5-HT-induced inward current. The large deflections represent current responses to voltage commands.

B. Plots of NA- and 5-HT-induced current (from the records shown in A) share the same biophysical properties and occlude over the voltage range tested. The NA (control) plot was obtained prior to application of 5-HT and the NA (wash) plot was obtained following washout of 5-HT.

has been investigated (reviewed by (Goldstein, Bockenhauer et al. 2001), (Patel and Honore 2001)).

3.3.1 External pH modulates a gK_{Leak}

Identification of mRNA for subunits belonging to the TASK and Kir2 families in the rat FMN and the knowledge that channels containing these subunits are sensitive to changes in external pH prompted us to investigate the functional expression of pH-sensitive K^+ channels in neonatal rat FMs (Topert, Doring et al. 1998; Talley, Lei et al. 2000; Talley, Solorzano et al. 2001). We evaluated the effects of changing the external pH on the resting membrane conductance under voltage-clamp conditions in the presence of ZD-7288 to prevent contamination by pH-sensitive I_h. Figure 3.9A illustrates I/V plots obtained in pH 8, 7 and 6 ACSF in the same FM. The I/V plots indicate that at a holding potential of –60 mV increasing the external $[H^+]$ induced an inward current associated with a decrease in membrane conductance. The current induced by changing external pH (I_{pH}), obtained by subtracting I/V plots obtained in each condition (Figure 3.9B), reversed close to the predicted E_K supporting the idea that at potentials depolarised to the E_K the net inward current reflects the inhibition of a resting outward K^+ current. I_{pH} appeared linear over the voltage range -40 to -90 mV however some rectification was seen out with this voltage range. These properties are characteristic of a pH-sensitive gK_{Leak}.

Results summarised from a population of FMs, voltage-clamped at -60 mV, indicate that switching from a standard physiological external pH of 7.4 to pH 6.0 induced an inward current of -46 ± 6 pA associated with a decrease in membrane conductance from 7.13 ± 0.77 nS to 5.29 ± 0.55 nS (n = 12).

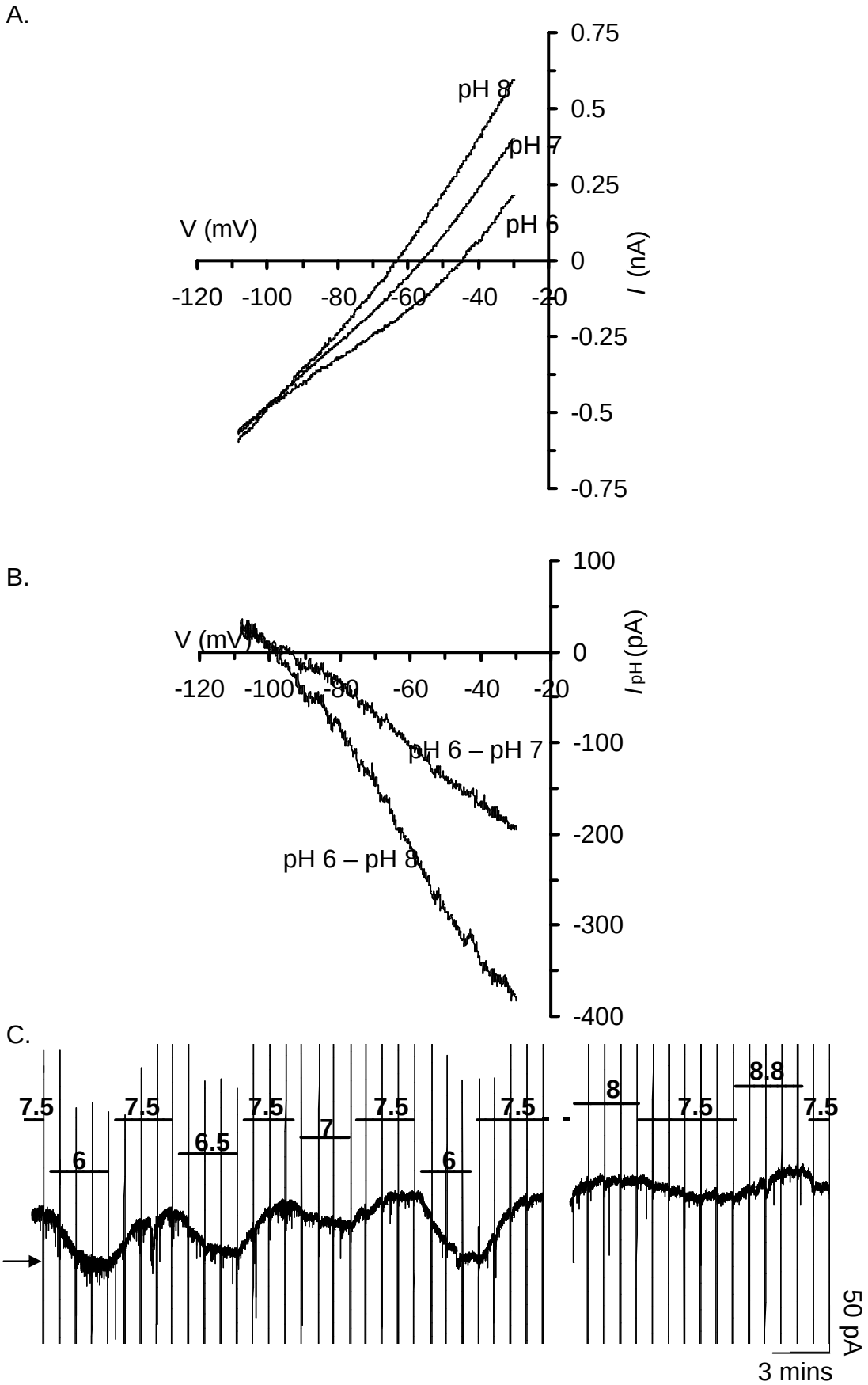
A.
0.75
pH 8
0.5
pH 7
0.25
V (mV)
pH 6
0
-120 -100 -80 -60 -40 -20
I (nA)
-0.25
-0.5
-0.75
B.
100
V (mV)
0
-120 -100 -80 -60 -40 -20
I pH (pA)
pH 6 – pH 7
-100
-200
pH 6 – pH 8
-300
-400
C.
7.5
7.5
7.5
7.5
7.5
8
8.8
7.5
7.5
6
6.5
7
6
50 pA
3 mins

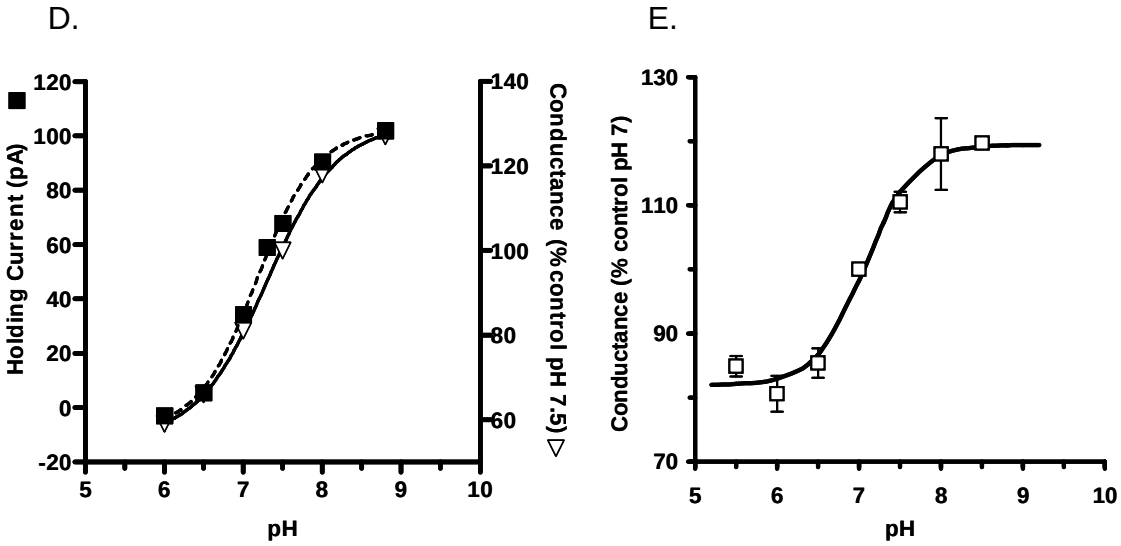

Figure 3.9. Altering external pH around the physiological range modulates a leak K^+ conductance in FMs.

A. Continuous current recording showing the effects of varying the pH of the ACSF on membrane current of a FM voltage clamped at -60 mV. The horizontal bars indicate the external pH and duration of application. Vertical deflections represent current responses to voltage commands not illustrated in this figure. The ACSF contained 3 mM K^+ and the horizontal arrow indicates the zero current level.

B. I/V relationships obtained using voltage ramp commands from a FM superfused with pH 6, pH 7 and pH 8 ACSF. Conductance decreases with increasing H^+ concentration.

C. Subtraction of the plots shown in A indicating that altering external pH modulates a leak K^+ conductance.

D. Plots of membrane current (left abscissa) and changes in membrane conductance, normalised to the conductance at pH 7.5 (right abscissa), at different external pH taken from the FM illustrated in C above. Conductance measurements were obtained by linear regression of the I/V relationship between –60 and –80 mV. The sensitivity of changes in membrane current and conductance to external pH could be described by a four-parameter logistic function (Methods, Equation 3). pK values of 7.2 and 7.3 and Hill slopes of 1.2 and 1 were obtained for current and conductance changes, respectively.

E. Averaged data (SEM, n = 8) showing the pH sensitivity of changes in membrane conductance normalised to the conductance at pH 7. The relationship could be described by a modified Hill equation (Methods, Equation 3) with a pK value of 7.1 ± 0.1 and a Hill slope of 1.5 ± 0.4 (R^2 = 0.9874).

Under the same conditions, switching from pH 7.4 to pH 8 resulted in an outward current (+22 ± 8 pA) and a conductance increase to 9.2 ± 1.5 nS (n = 4, membrane conductance at pH 7;4 for the same FMs was 8.3 ± 1.6 nS). Irrespective of the inward or outward nature of the change in membrane current, the reversal potential (V_{pH}) was close to the predicted E_K (pH 7.4 to pH 6, V_{pH} = -93 ± 1.4 mV; pH 7.4 to pH 8, V_{pH} = -89 ± 3 mV). Altering the external K^+ concentration ($[K^+]_o$) to 7 mM moved the V_{pH} to -66 ± 1.3 mV (n = 7) in close agreement with the change predicted by the Nernst equation.

The pH-sensitivity of gK_{Leak} was investigated further. Figure 3.9C shows a representative chart record of membrane current from a FM voltage clamped at -60 mV to which ACSF of varying pH was applied. The time required for the pH-induced current changes to reach a steady state varied from 2-5 minutes. We attribute this to the depth of the recorded FM in the slice, the relatively slow exchange of ACSF in the recording chamber and the H^+ buffering capacity of the slice. The amplitude of I_{pH} and the change in conductance over a range of external pH could be described by a modified Hill equation (Methods, Equation 3) (Figure 3.9D,E). As illustrated in Figure 3.9D, (for the FM shown in Figure 3.9C) measuring either parameter gave closely similar values for pH-sensitivity. Data taken from eight FMs, each of which was exposed to at least four changes in external pH, indicated a fit of the pH-evoked conductance with a pK value of 7.1 ± 0.1 and a Hill slope of 1.5 ± 0.4 (± SEM, R^2 = 0.9874). The pH-sensitive K^+ conductance was maximal at pH 8.2 while no further decrease in conductance was seen below pH 6. These data indicate that at physiological pH (~ 7.4) the resting pH-sensitive gK_{Leak} is approximately 70% of its maximal level.

3.3.2 NA and changes in external pH modulate the same gK_{Leak}

If NA and external pH (and 5-HT) alter FM excitability by modulating the same gK_{Leak} the effects of lowering external pH and transmitter application should occlude. The NA-induced inward current was examined in conditions designed to inhibit (pH 6.5) and activate (pH 7.7) I_{pH} (Figure 3.10A). When external pH was increased to 7.7, a maximal concentration of NA (10 μM) induced a robust inward current of -109 ± 19 pA (n = 5). Lowering external pH to 6.5 led to a dramatic reduction in I_{NA} to -34 ± 9 pA in the same FMs. In the example shown in Figure 3.10A the response to NA was almost completely occluded when the external pH was 6.5. Figure 3.10B shows that at pH 6.5, I_{NA} was occluded over the whole voltage range examined while at pH 7.7 the amplitude and the properties of I_{NA} were almost identical to those of the current induced by switching the external pH from 7.7 to 6.5. This supports the idea that both external pH and NA modulate the same gK_{Leak} and that both have an equivalent maximal level of inhibition.

3.4 The effects of TASK channel blockers on the pH- and NA-sensitive gK_{Leak}

3.4.1 Anandamide does not inhibit gK_{Leak}

The pH-sensitivity of gK_{Leak} suggested that TASK channels might contribute to this conductance. Low micromolar concentrations of the endogenous cannabinoid, anandamide, block homomeric human TASK-1 channels (Maingret, Patel et al. 2001). Homomeric TASK-3 channels are blocked by higher concentrations of anandamide. Bath-application of anandamide (10 - 20 μM) had no effect on FM membrane conductance at the holding potential (-50 mV) or over the voltage range

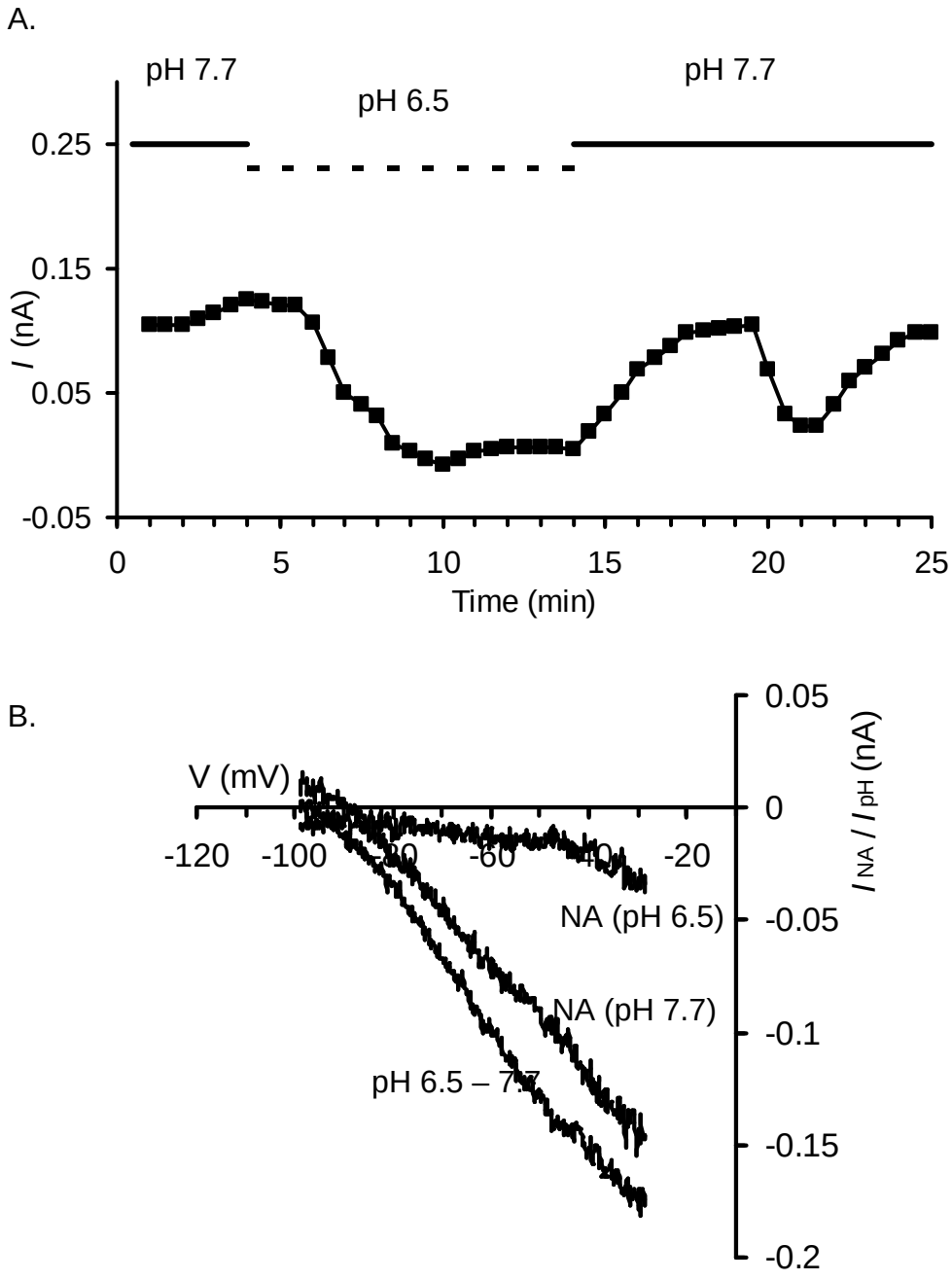

Figure 3.10. Inhibition of the leak K^+ conductance by lowering external pH occludes the effects of NA.

A. Plot of membrane current against time for a FM voltage-clamped at –60 mV. Solid and dashed horizontal bars indicate the times when the slice was superfused with pH 7.7 and pH 6.5 ACSF, respectively. Arrows indicate points at which NA (10 μM, 15 sec) was added to the ACSF. Note the almost complete occlusion of the NA-induced inward current in pH 6.5 ACSF.

B. Plots of the current induced by switching from pH 7.7 to pH 6.5 ACSF and the NA-induced current in both conditions from the same FM as A. Occlusion of the NA-induced current by pH 6.5 ACSF was independent of membrane potential.

tested in pH 7.4 ACSF (Figure 3.11A, B) or pH 6.0 (Figure 3.11A, C) (n = 4). Anandamide also had no effect on the decrease in current induced by either NA (10 μM) or lowering the external pH from 7.4 to 6 (Figure 3.11D). I_{NA} at a holding potential of -50 mV was -53 ± 3 pA in the absence of anandamide compared with -52 ± 3 pA in its presence (n = 3, 3 mM $[K^+]_o$).

3.4.2 Preventing metabolic degradation of anandamide

It has been reported that anandamide may be metabolically degraded in certain *in vitro* conditions and that this can be prevented by arachidonyl trifluoromethyl ketone (ATFK) (Barbuti, Ishii et al. 2002). When applied alone for up to 20 minutes ATFK (10 μM) had little effect on the holding membrane current when applied to two FMs. The holding current at –50 mV was 96 pA before and 120 pA after ATFK incubation for the first FM (Figure 3.12) and 110 pA before and 126 pA after ATFK for the second. The current induced by NA application was also unaffected in the presence of ATFK (-74 and –62 pA in the presence and absence of ATFK, respectfully for the first FM and –76 and -98 pA for the second FM).

Subsequent co-application of anandamide (10 μM) in the continued presence of ATFK did not induce a change in the resting membrane current (120 pA for the first FM and 126 pA for the second before application of anandamide and 109 pA for the first FM and 165 pA for the second FM after application of anandamide). In the continued presence of ATFK, anandamide also had no effect on the current induced by NA. In the first FM the NA-induced current was –62 pA and –64 pA before and

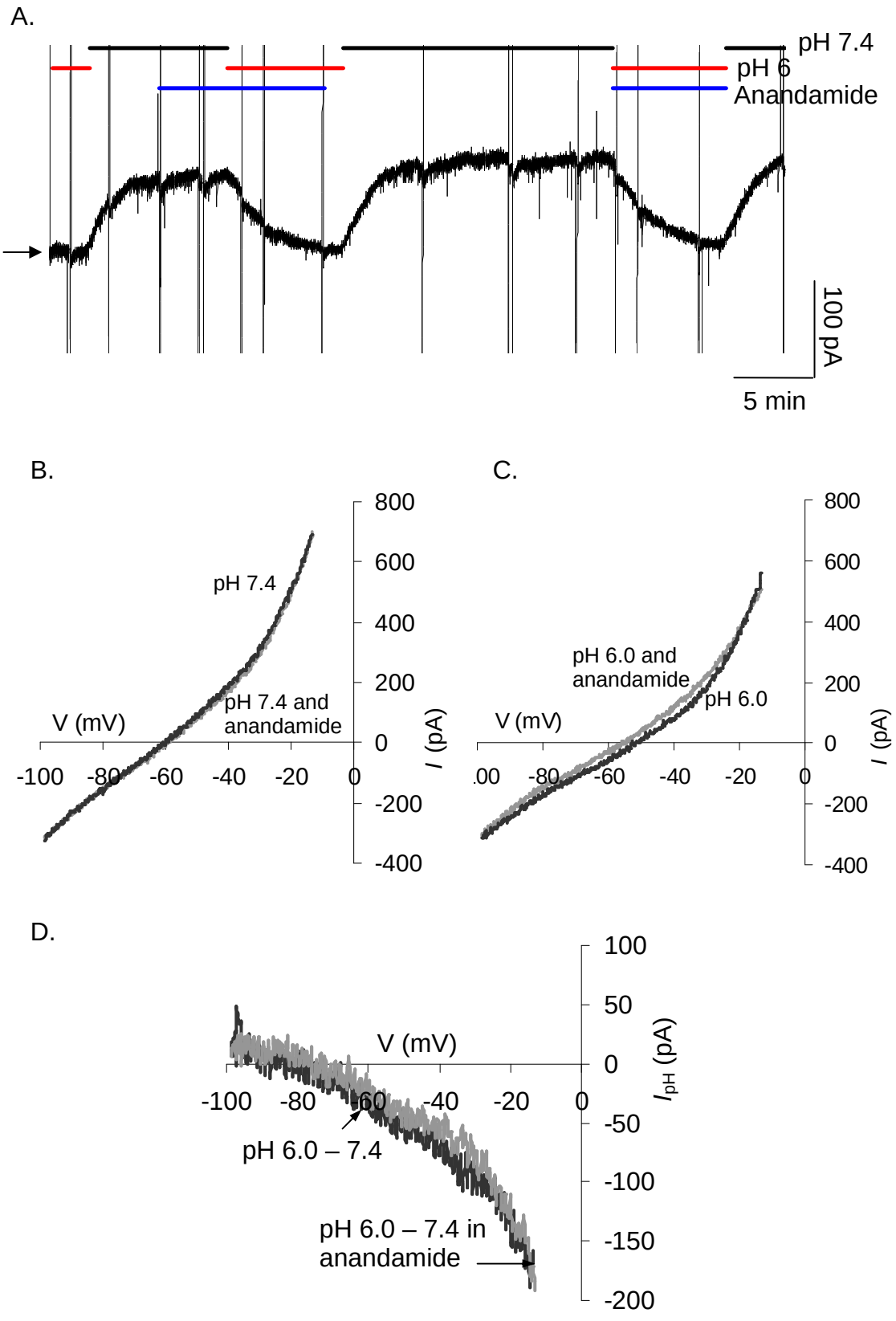
A.
pH 7.4
pH 6
Anandamide
100 pA
5 min
B.
800
600
400
200
0
-200
-400
pH 7.4
pH 7.4 and
anandamide
V (mV)
-100
-80
-60
-40
-20
0
I (pA)
C.
800
600
400
200
0
-200
-400
pH 6.0 and
anandamide
pH 6.0
V (mV)
-80
-60
-40
-20
0
I (pA)
D.
100
50
0
-50
-100
-150
-200
V (mV)
-100
-80
-60
-40
-20
0
I_pH (pA)
pH 6.0 – 7.4
pH 6.0 – 7.4 in
anandamide

Figure 3.11. Anandamide (10 μM) has no effect on the pH-sensitive gK_{Leak}.

A. Continuous current recording of membrane current against time for a FM voltage-clamped at -50 mV. Horizontal bars indicate the times when the slice was superfused with pH 7.4 ACSF, pH 6 ACSF and anandamide (10 μM). Vertical deflections are attenuated current responses to ramp voltage commands and the arrow indicates the zero current level. Anandamide failed to alter membrane current in pH 7.4 ACSF and had no effect on the amplitude or time course of the inward current induced by perfusion with pH 6 ACSF.

B. I/V relationships obtained from same FM as A in the presence (grey) and absence (black) of anandamide (10 μM) in pH 7.4 ACSF. Anandamide has no effect on the I/V relationship at pH 7.4.

C. I/V relationships obtained from same FM as A in the presence (grey) and absence (black) of anandamide (10 μM) in pH 6.0 ACSF. Anandamide has very little effect on the I/V relationship at pH 6.0.

D. Plot of the current induced by changing the pH from 7.4 to 6.0 (obtained by subtraction of plots in B and C) in the presence (grey) and absence (black) of anandamide (10 μM). Anandamide (10 μM) does not inhibit the current induced by changing pH.

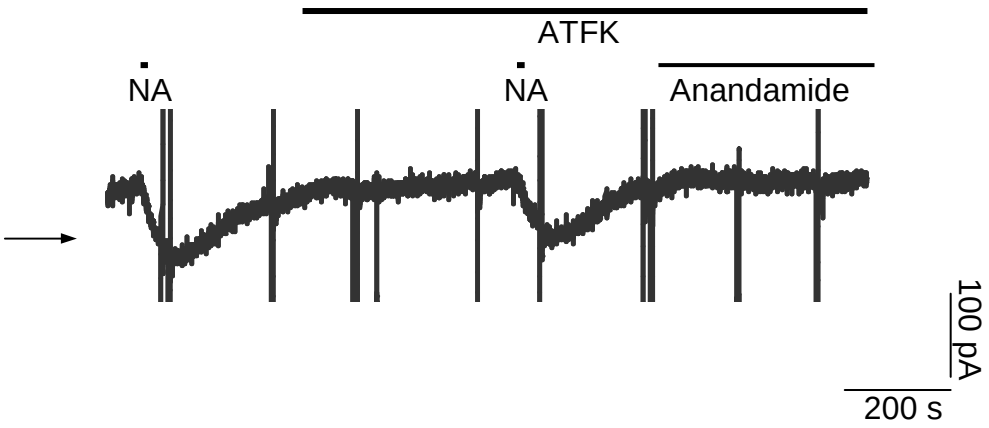

Figure 3.12. ATFK (10 μM) has no effect on the NA-sensitive gK_{Leak} and does not alter the efficacy of anandamide.

Continuous current recording from a FM voltage-clamped at -50 mV. Bath application of ATFK (10 μM) has no effect on the membrane current and co-application with NA (10 μM) evokes a large inward current, which is similar to the control response to NA. Subsequent application of anandamide (10 μM) with ATFK (10 μM) fails to induce an inward current. Vertical deflections are attenuated current responses to ramp voltage commands and the arrow indicates the zero current level.

after application of anandamide, respectively (and –98 pA before and –94 pA after anandamide application for the second FM).

3.4.3 Methanandamide does not inhibit gK_{Leak}

Methanandamide is a metabolically stable analogue of anandamide also shown to inhibit TASK-1 channels (Maingret, Patel et al. 2001). In the example shown in Figure 3.13 methanandamide (20 μM) failed to have any effect on the holding membrane current (210 pA and 236 pA in the presence and absence of methanandamide, respectively).

Under control conditions NA induced an inward current of -152 pA in the same FM, which was also unaffected by methanandamide (-147 pA following incubation with methanandamide, Figure 3.13). In a representative sample of FMs methanandamide was found to have little effect on the resting membrane current (126 ± 52 pA before and 157 ± 55 pA after methanandamide incubation, n = 3). In addition, I_{NA} was not altered in the presence and absence of methanandamide (-104 ± 48 pA and -102 ± 46 pA in the presence and absence of methanandamide, respectfully, n = 3).

3.4.4 Ruthenium red does not inhibit gK_{Leak}

Homomeric TASK-3, but not TASK-1, channels are inhibited by ruthenium red (RR) (Czirjak and Enyedi 2003). Application of RR (10 μM) to FMs had no effect on holding current at -50 mV or the inward current evoked by NA (n = 4, Figure 3.14A). The NA-induced current in the presence of RR (10 μM) was indistinguishable from the control response obtained in the absence of the TASK-3 blocker (Figure 3.14B). Thus, inward I_{NA} at a holding potential of -50 mV (3 mM $[K^+]_o$) was -50 ± 8 pA in

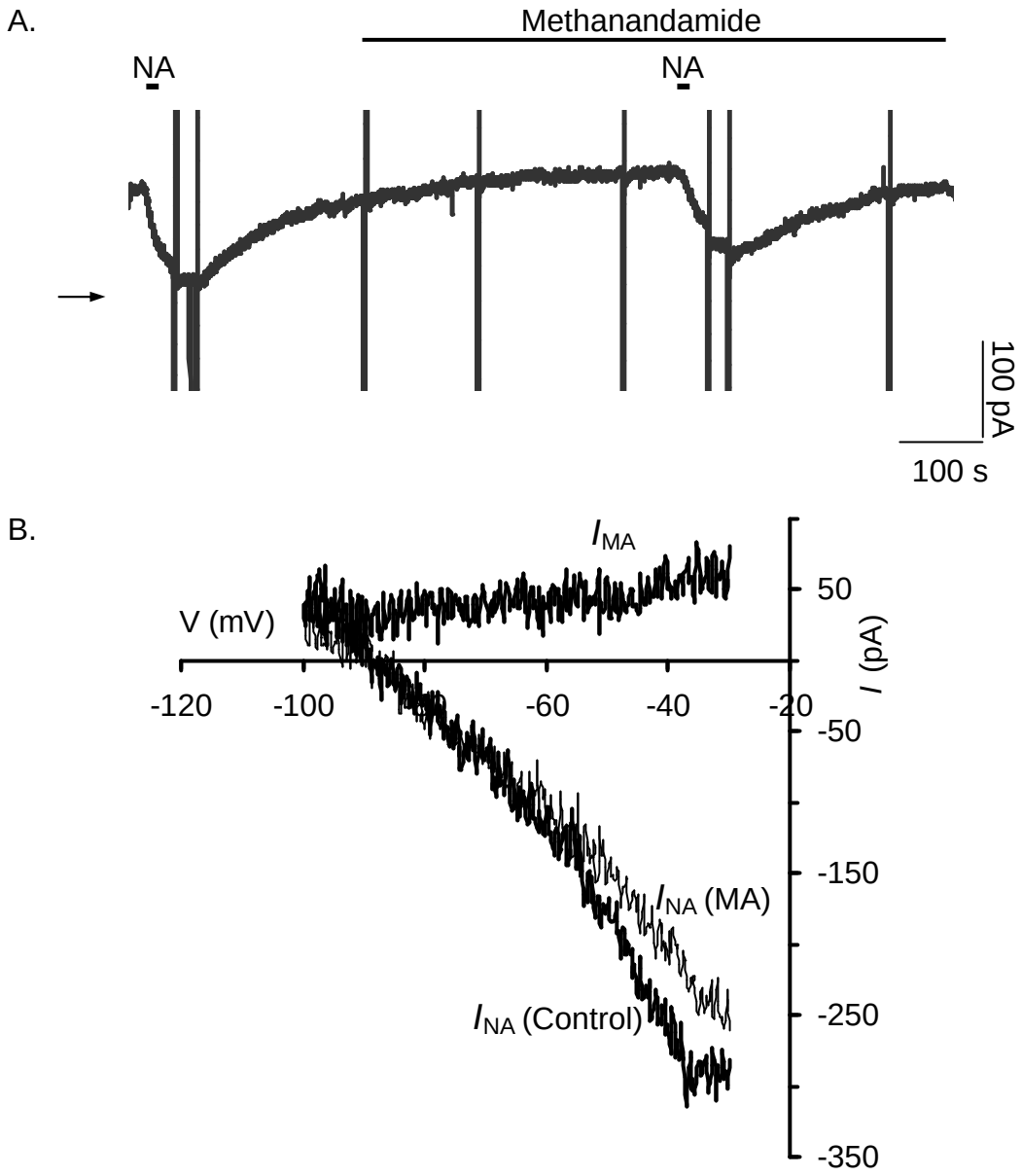

Figure 3.13. Methanandamide (20 μM) has no effect on the NA-sensitive gK_{Leak}.

A. Continuous current recording of membrane current against time for a FM voltage-clamped at -50 mV. Bath application of NA (10 μM) evokes a large inward current. The NA-induced current is not inhibited following incubation with methanandamide (20 μM, 11 minutes). Vertical deflections are attenuated current responses to ramp voltage commands and the arrow indicates the zero current level.

B. Plots of the methanandamide (20 μM)-induced current (I_{MA}) and the NA-induced current in the absence ($I_{NA(Control)}$) and presence ($I_{NA(MA)}$) of methanandamide. Methanandamide does not inhibit gK_{Leak} or I_{NA}.

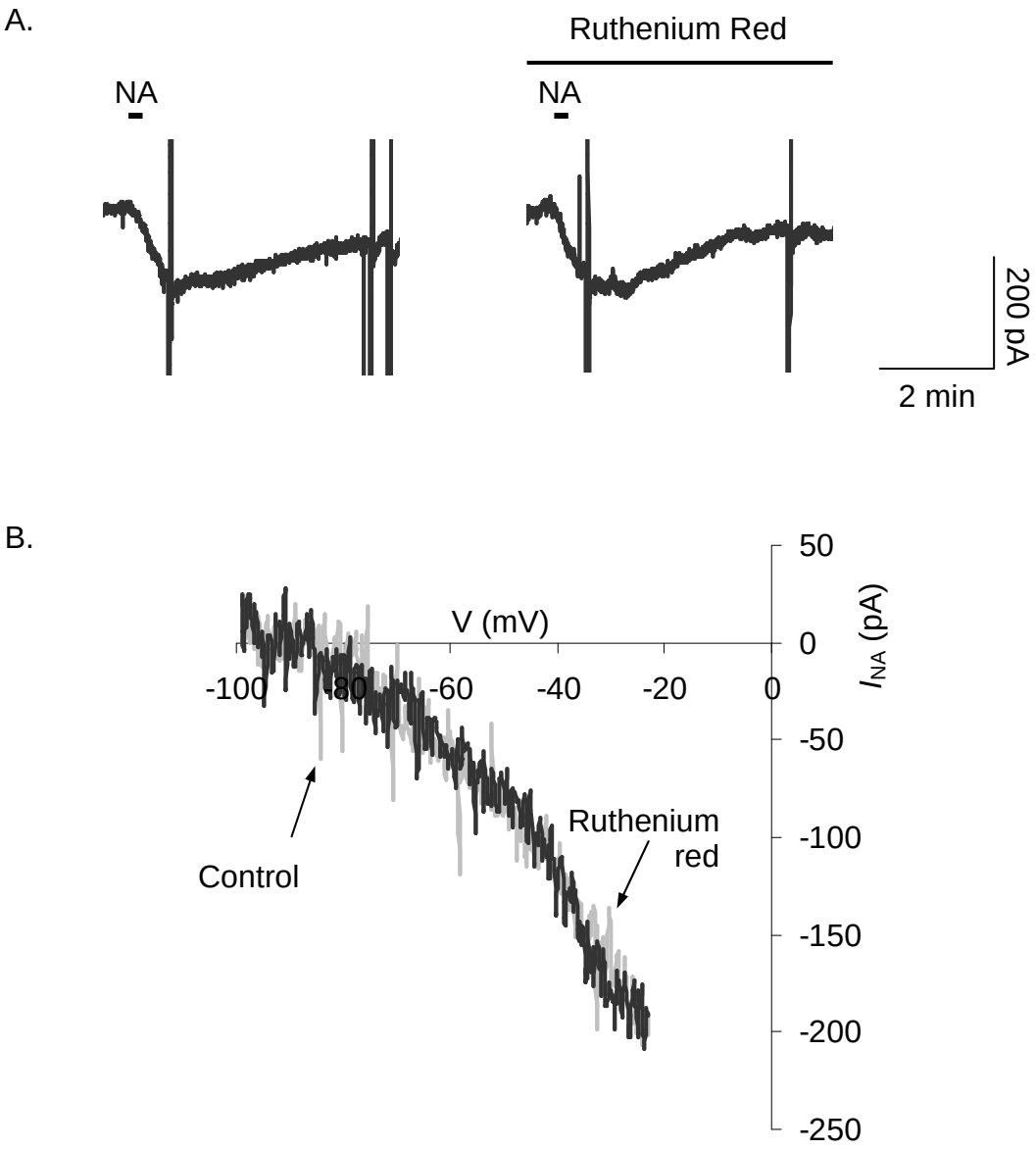

Figure 3.14. Ruthenium red (10 μM) has no effect on NA-induced inhibition of gK_{Leak}.

A. Current record of a FM voltage-clamped at –50 mV demonstrating inward current evoked under control conditions and following incubation with ruthenium red (10 μM, 10 minutes). Large deflections represent current responses to voltage commands.

B. Plots of NA-induced currents in the presence (grey) and absence (black) of ruthenium red (10 μM). Note that the currents superimpose indicating a lack of effect of ruthenium red.

the absence of RR compared with -59 ± 6 pA in its presence (n = 4). The V_{NA} was also unaffected by the presence of RR.

3.4.5 Zn^{2+} has no effect on the pH- and NA-sensitive gK_{Leak}

Homomeric human (h)TASK-1 channels, expressed in cell lines, display little sensitivity to Zn^{2+} (100 μM) while homomeric hTASK-3 channels are substantially (~70%) blocked at this concentration (Leonoudakis, Gray et al. 1998; Clarke 2003).

Bath-application of Zn^{2+} (100 - 300 μM) did not significantly affect FM membrane current (+3 ± 1.7 pA at -60 mV) or membrane slope conductance (5 ± 0.5 to 5.5 ± 0.5 nS in the presence of Zn^{2+} over the range -90 to -60 mV, n = 5) in pH 7.4 ACSF. In the same FMs, superfusion with pH 6 ACSF induced an inward current of -49 ± 11 pA and decreased membrane conductance to 3.6 ± 0.7 nS. I_{pH} obtained by changing external pH from 6 to 7.7 was unaffected by the presence of Zn^{2+}. Consistent with its lack of effect on I_{pH}, Zn^{2+} (100 – 300 μM) also failed to alter I_{NA} (Figure 3.15). Thus, inward I_{NA} at the holding potential (-52 mV, 7 mM $[K^+]_o$) was -51 ± 20 pA (n = 3) while outward I_{NA} at -102 mV was 92 ± 28 pA (n = 3). These values compared with -44 ± 13 pA and 88 ± 29 pA at -52 mV and -102 mV, respectively, in the presence of Zn^{2+} (300 μM). Despite this lack of effect on gK_{Leak}, in some FMs Zn^{2+} did inhibit a small NA-induced enhancement of a Ca^{2+} conductance (See arrowed inflection in Figure 3.15).

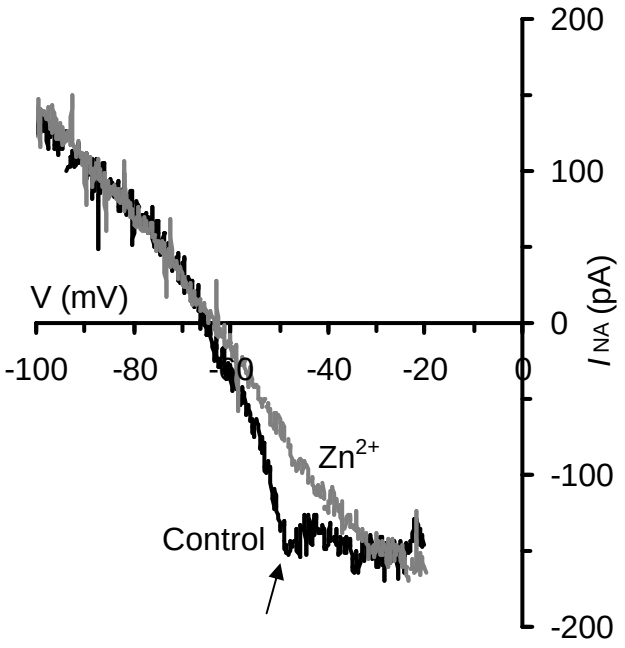

Figure 3.15. Zn^{2+} (300 μM) does not block the actions of NA on gK_{Leak}.

Plots of NA-induced currents, from a voltage-clamped FM, in the presence and absence of Zn^{2+} (300 μM). Zn^{2+} fails to block the actions of NA on gK_{Leak} but it does abolish an inflection attributable to enhanced gCa^{2+} (arrow).

3.4.6 Bupivacaine partially occludes the pH- and NA-sensitive gK_{Leak}

The local anaesthetic bupivacaine has been shown to non-selectively block TASK-1 and TASK-3 channels with IC_{50}'s around 100 μM (Leonoudakis, Gray et al. 1998; Kim, Bang et al. 2000). Bupivacaine (100 μM) induced an inward current in 4 FMs tested while in two further motoneurons bupivacaine (100 μM) failed to alter membrane current. At a holding potential of -50 mV (3 mM $[K^+]_o$) bupivacaine (100 μM) induced a current of -49 ± 12 pA (n = 4) which reversed at -87 ± 3 mV and displayed the linear I/V relationship characteristic of inhibition of gK_{Leak}. The NA-induced inward current was partially and reversibly occluded by bupivacaine gK_{Leak} (Figure 3.16). Thus, NA (10 μM) induced a current of -137 ± 33 pA and -94 ± 22 pA in the absence and presence of bupivacaine respectively, representing occlusion by 29 ± 8%.

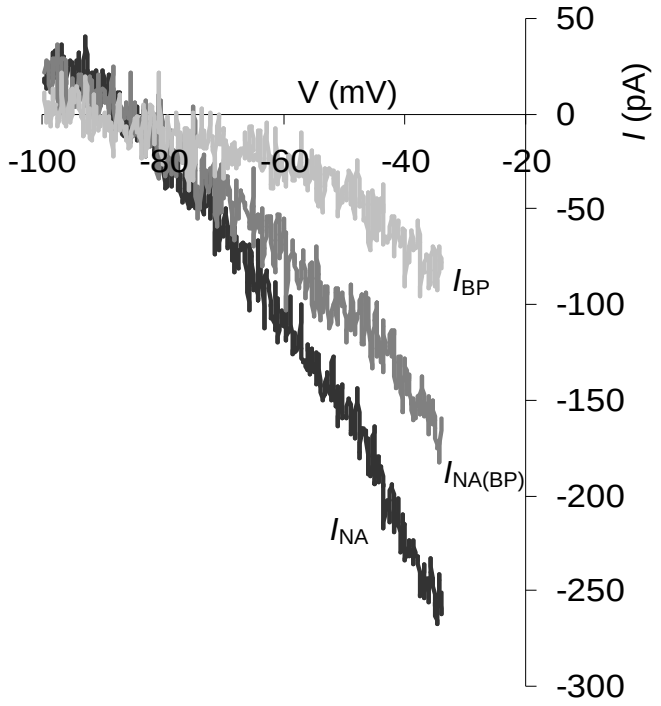

Figure 3.16. Bupivacaine (50 μM) partially occludes NA-induced inward current in FMs.

Plots of the current induced by bupivacaine (I_{BP}, 50 μM), NA (I_{NA}, 10 μM) and NA in the presence of bupivacaine ($I_{NA(BP)}$) demonstrating that bupivacaine (50 μM) partially occludes I_{NA} in FMs.

3.4.7 Isoflurane enhances gK_{Leak}

In a recent study of rat TASK channels the volatile anaesthetic isoflurane inhibited homomeric TASK-1 current but enhanced current carried by homomeric TASK-3 and heteromeric TASK-1 / TASK-3 channels (Berg, Talley et al. 2004). This enhancement was seen even when the current was optimally activated by external pH. We investigated the effects of isoflurane on FM gK_{Leak} when the conductance was optimally activated by an external solution of pH 8.

Bath-application of isoflurane (see Section 2.2.2 for solution preparation and concentration estimation) increased gK_{Leak} in four out of five facial FMs tested (V_{rev} = –63 ± 2 mV in ACSF containing 7 mM K^+, Figure 3.17). Expressed as a percentage of the maximal pH-sensitive current at –100 mV, obtained by exposing each FM sequentially to ACSF of pH 8 and pH 6, isoflurane enhanced the pH-sensitive current by 55 ± 6 % (n = 4). It is noteworthy that in the remaining FM isoflurane reversibly and reproducibly inhibited gK_{Leak}.

3.5 Validation of pharmacological activity of methanandamide and ruthenium red

The absence of any effects of anandamide, methanandamide and RR on FMs raised the possibility that these compounds were not active in the experimental set-up used. The ability of methanandamide and RR to inhibit putative TASK channel-mediated currents in cultured rat cerebellar granule neurones (CGNs) was tested (Maingret, Patel et al. 2001; Han, Truell et al. 2002; Kang, Han et al. 2004). Lowering pH to 6

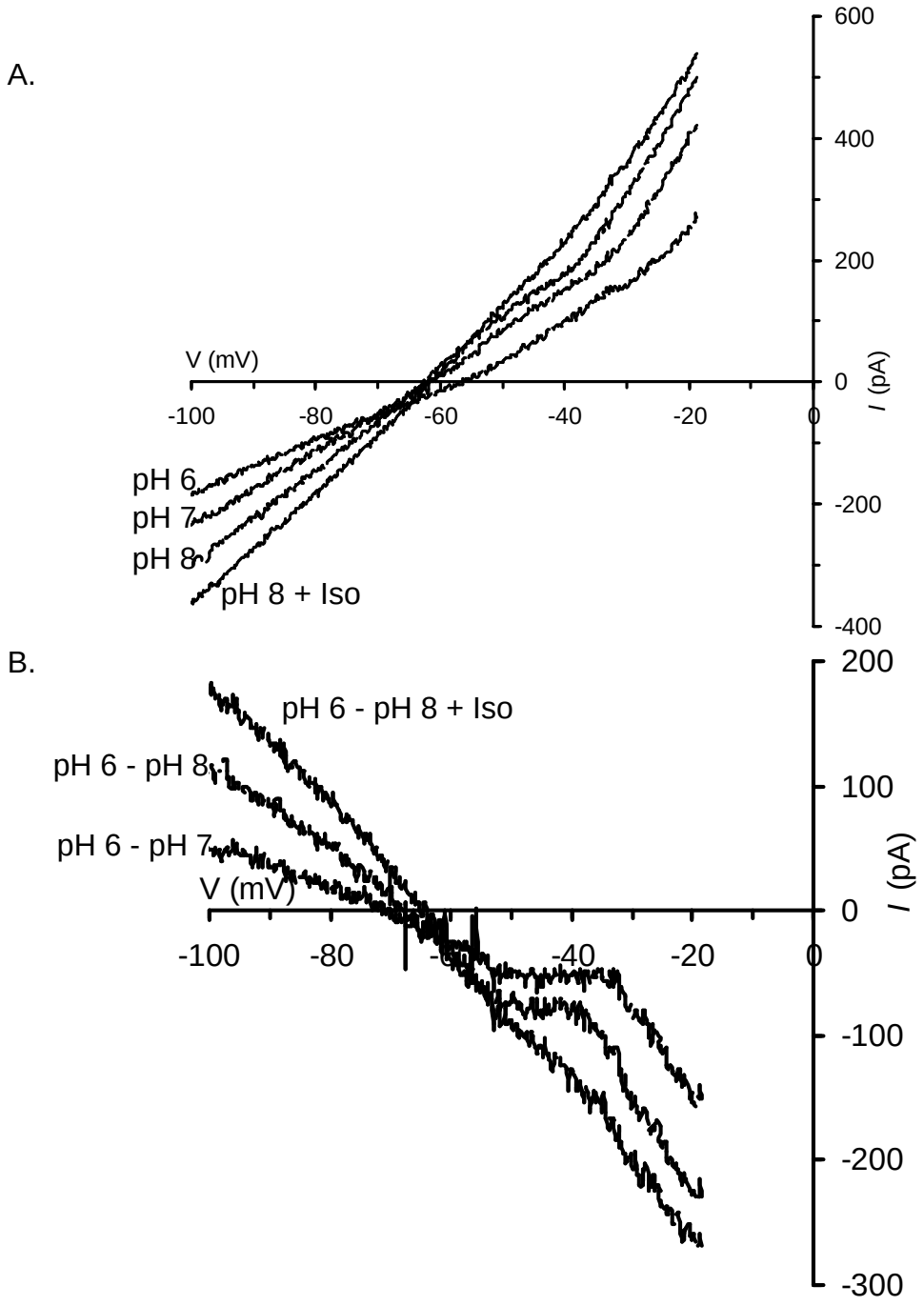

Figure 3.17. Isoflurane enhances the pH-sensitive gK_{Leak} in FMs.

A. I/V relationships from an FM superfused with pH 6, pH 7, pH 8 and pH 8 with isoflurane (concentration as indicated in Methods) ACSF. Isoflurane increases gK_{Leak} even when the conductance is maximally activated by pH 8 ACSF.

B. Subtraction of the plots shown in A indicating greater activation of the pH-sensitive gK_{Leak} in the presence of isoflurane (pH 6 – pH 8 + Iso) than in its absence (pH 6 – pH 8). The ACSF contained 7 mM K^+.

from 7.4 induced a current in CGNs with characteristics of a TASK-mediated leak K^+ conductance (Figure 3.18, 3.19).

3.5.1 Methanandamide inhibits TASK-like channels in cultured cerebellar granule neurones

In the example CGN shown in Figure 3.18 (voltage-clamped at -20 mV) lowering the pH from 7.4 to 6.0 induced a reversible current of -142 pA. The current induced by lowering pH from 6.0 to 7.4 at -50 mV was -58 pA (Figure 3.18). In a representative sample of CGNs lowering pH from 7.4 to 6.0 induced mean currents of -93 ± 52 pA and -46 ± 16 pA at holding potentials of -20 mV and -50 mV, respectively (n = 3). In the example in Figure 3.18 bath-application of methanandamide (20 μM) had a small effect on CGNs, inducing an inward current of -24 pA at -20 mV and -10 pA at -50 mV. This represents an inward current that was 17 % (at -20 mV) of the current induced by lowering pH. Methanandamide induced a mean inward current in a representative sample of CGNs that was 21 ± 5 % of the pH 6-induced current (n = 3). As can be seen from the I/V plots (Figure 3.18) lowering pH and methanadamide induced currents that were approximately linear over the range measured and had reversal potentials close to the predicted E_K, similar to the gK_{Leak} in FMs.

3.5.2 Ruthenium red inhibits TASK-like channels in cultured cerebellar granule neurones

In the example CGN shown in Figure 3.19, lowering pH induced an inward current of -149 pA at -20 mV (Figure 3.19). In the same CGN, RR (10 μM) induced an inward current of -79 pA (Figure 3.19). The currents induced by lowering pH and

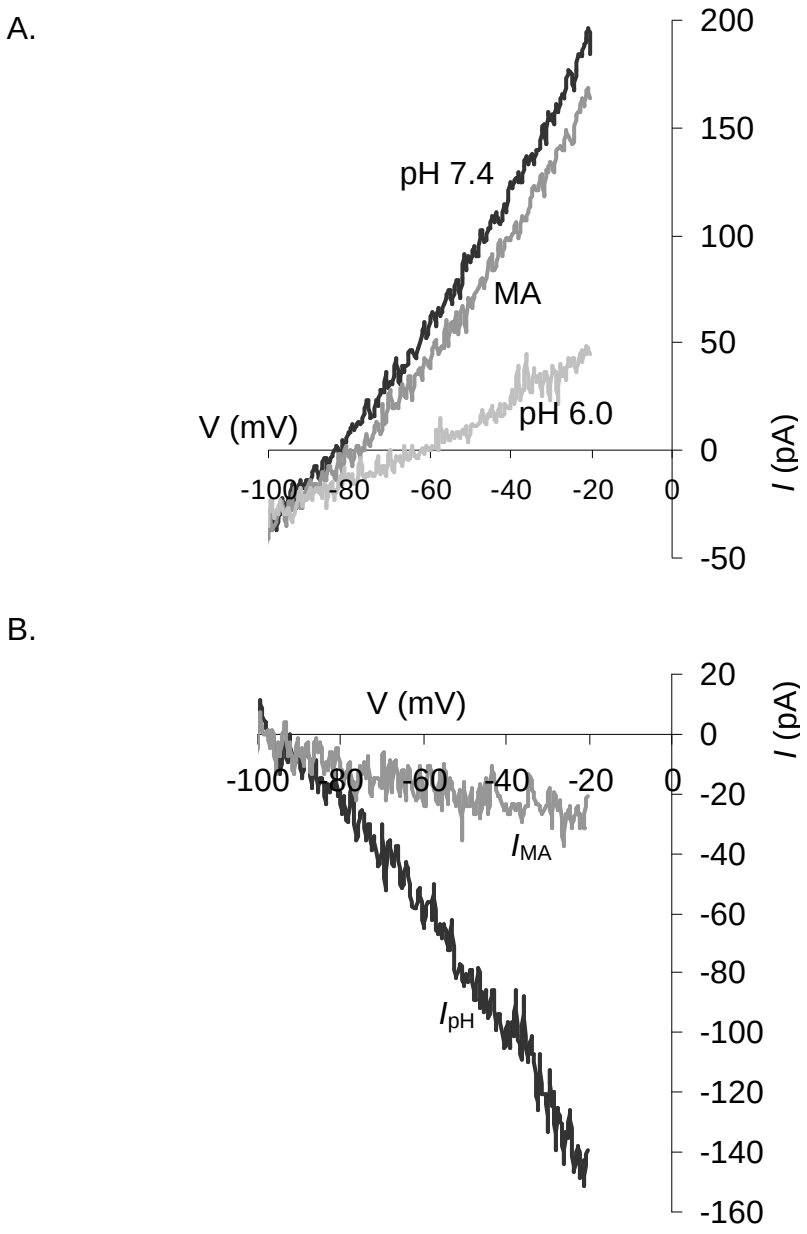

Figure 3.18. Methanandamide inhibits gK_{Leak} in CGNs

A. I/V plots obtained from a cultured CGN in pH 7.4 (black), pH 6.0 (light grey) and in the presence of methanandamide (10 μM, dark grey).

B. Currents induced by methanandamide (10 μM, I_{MA}) and changing from pH 6.0 to pH 7.4 (I_{pH}) obtained by subtraction of plots in A.

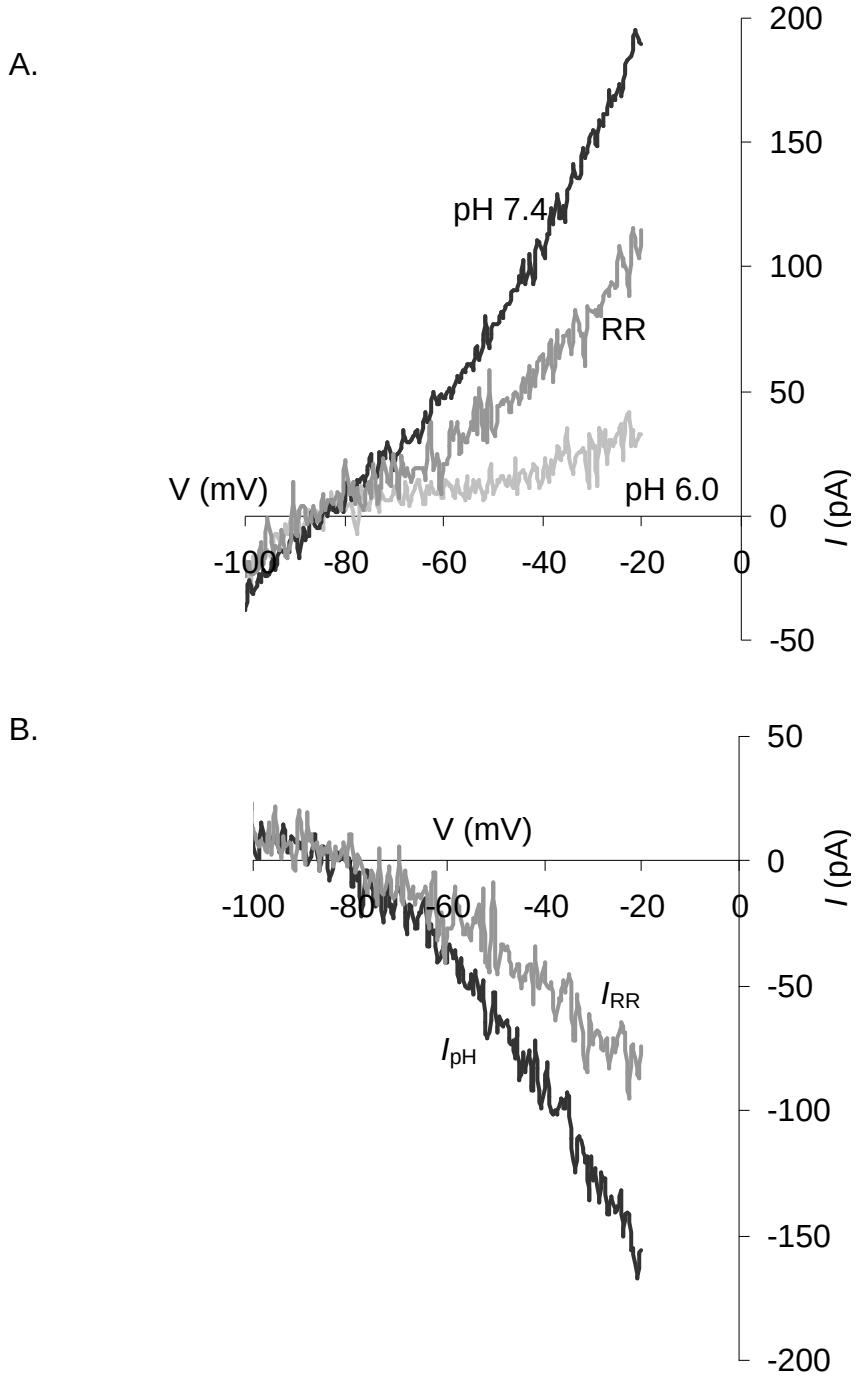

Figure 3.19. Ruthenium red inhibits gK_{Leak} in CGNs

A. I/V plots obtained from cultured CGN in pH 7.4 (black), pH 6.0 (light grey) and in the presence of ruthenium red (10 μM, dark grey).

B. Currents induced by ruthenium red (10 μM, I_{RR}) and changing from pH 6.0 to pH 7.4 (I_{pH}) obtained by subtraction of plots in A.

RR at -50 mV in this CGN were -60 pA and -32 pA, respectively. In a representative sample of CGNs RR (10 µM) induced an inward current that was 53 ± 2 % (n = 3) of the amplitude of the current induced by lowering pH.

These findings are consistent with reported effects of methanandamide and RR on TASK-1 and TASK-3 channels in cultured CGNs (Maingret, Patel et al. 2001; Han, Truell et al. 2002; Lauritzen, Zanzouri et al. 2003; Kang, Han et al. 2004).

3.6 Discussion

3.6.1 Excitatory effects of 5-HT and NA

5-HT and NA were found to have excitatory effects on neonatal rat FMs, consistent with previously reported excitatory effect of 5-HT on adult FMs (VanderMaelen and Aghajanian 1980; Vandermaelen and Aghajanian 1982; Larkman, Penington et al. 1989).

3.6.2 Ionic mechanisms mediating action of 5-HT and NA

5-HT was found to evoke an inward current in neonatal FMs voltage-clamped at potentials depolarised to the predicted E_K and the ionic mechanisms underlying this inward current were confirmed as an increase in I_h and decrease in a potassium conductance (gK_{Leak}). Additional properties of the 5-HT-sensitive potassium conductance were examined in the presence of the I_h blocker, ZD 7288 (BoSmith, Briggs et al. 1993). The current response to a hyperpolarising voltage step demonstrates that I_h is abolished in the presence of ZD 7288 and is no longer enhanced by 5-HT.

NA was found to evoke an inward current in neonatal FMs, mediated by an inhibition of a gK_{Leak} with similar properties to the 5-HT-sensitive gK_{Leak}. This is consistent with previous studies demonstrating that NA also promotes adult FM excitation through inhibition of a gK_{Leak} alone and not enhancement of I_h (Larkman and Kelly 1992). The inward current evoked by 5-HT occludes the NA-induced inward current suggesting these amines modulate the same conductance.

The I/V relationships obtained in the presence of 5-HT and NA provide evidence that these amines modulate a leak potassium conductance (gK_{Leak}). Firstly the slope of the I/V plot in the presence of 5-HT or NA are reduced compared to the slope of the control plots indicating that 5-HT and NA decrease conductance through closure of ion channels in the membrane. Secondly the point of intersection of the I/V plots in the presence and absence of 5-HT and NA and the point of intersection with the x-axis of $I_{5\text{-}HT}$ and I_{NA} are close to the predicted E_K, indicating 5-HT and NA decrease a gK. Thirdly, $I_{5\text{-}HT}$ and I_{NA} are approximately linear over the voltage range measured suggesting that the amine-sensitve gK shows little or no voltage-dependence, a characteristic property of gK_{Leak} (Goldstein, Bockenhauer et al. 2001).

3.6.3 I_h and gK_{Leak} contribute to the resting membrane potential

I_h and gK_{Leak} contribute to the resting membrane potential in a variety of central neurones (reviewed in (Pape 1996; Lesage and Lazdunski 2000)). The contribution of I_h to the membrane potential can be determined by recording current changes following application of ZD 7288. The effect of ZD 7288 application on FM holding current was not observed in the present study as slices were incubated with ZD 7288 prior to recordings being made, therefore the holding current in the absence of ZD

7288 was not measured. Previous studies demonstrate that when ZD 7288 was applied to FMs voltage-clamped close to the resting membrane potential it evoked an outward current that reversed at the predicted reversal potential for I_h (although not all FMs showed this response to ZD 7288) (Larkman and Kelly 2001). This supports a role for I_h in contributing to the resting membrane potential in FMs. gK_{Leak} is active at typical resting membrane potentials and the decrease in conductance observed when 5-HT and NA were applied in the presence of ZD 7288 supports a role for gK_{Leak} in setting the resting membrane potential in FMs. This is supported by recent findings that both I_h and a gK_{Leak} contribute to the resting membrane potential and control neocortical interneurone excitability (Gibson, Bartley et al. 2006).

3.7 Molecular identity of gK_{Leak} in FMs

3.7.1 5-HT, NA and external pH modulate the same gK_{Leak}

The results characterise a pH-sensitive conductance and several lines of evidence support the idea that pH and NA (and 5-HT) modulate the same gK_{Leak} in neonatal rat FMs. Firstly, NA and lowering external pH below the normal physiological level (pH 7.4) inhibited a current that displayed rapid kinetics, a small amount of rectification over the potential range -120 to -40 mV and a reversal potential at the predicted E_K. Secondly, lowering external pH occluded the actions of NA. Maximal concentrations of NA decreased membrane conductance to a level very close to the maximum level of inhibition obtained by lowering external pH. Thirdly, raising the external pH above pH 7.4 induced an outward current associated with an increase in membrane conductance and under these conditions the amplitude of the inward current induced by NA was increased. In addition, the pH- and NA-sensitive gK_{Leak}

displayed a common pharmacology to a wide range of K^+ channel blockers (Larkman and Perkins 2005). In combination, these results support a common target of modulation.

One possible explanation for the occlusion of the NA-mediated response by low external pH is a change in protein structure that disrupts agonist-receptor interactions. Reports suggest α_2- but not α_1-adrenoceptors display alterations in functional responses associated with changes in agonist binding affinity over the pH range 6 to 8 (Curro and Greenberg 1983; Nunnari, Repaske et al. 1987; Tateishi and Faber 1995). As the pharmacology of this action of NA indicates that an α_1-adrenoceptor mediates inhibition of gK_{Leak} in FMs (see Chapter 4) it is unlikely that occlusion of the NA-mediated modulation of gK_{Leak} by low external pH is due to altered agonist-receptor interactions.

3.7.2 pH-sensitivity of the amine-sensitive gK_{Leak}

The presence of mRNA for the pH-sensitive K^+ channels TASK-1 and TASK-3 in the FMN makes these channels potential candidates for gK_{Leak} (Talley, Lei et al. 2000; Karschin, Wischmeyer et al. 2001). TASK-1 and TASK-3 channels mediate openly rectifying, non-inactivating, whole-cell currents similar to the pH- and NA-sensitive gK_{Leak} in facial motoneurons (Duprat, Lesage et al. 1997; Leonoudakis, Gray et al. 1998; Kim, Bang et al. 2000; Rajan, Wischmeyer et al. 2000; Talley, Lei et al. 2000; Vega-Saenz de Miera, Lau et al. 2001). Activation and inactivation are described as "instantaneous". For example, TASK-3 channels expressed in *Xenopus* oocytes displayed time constants of around 4 ms, not very dissimilar from the values of 8 to 9 ms described here (Rajan, Wischmeyer et al. 2000). The sensitivity of

TASK-1 channels to external pH lies across the physiological range with a pK around 7.3 to 7.5(Duprat, Lesage et al. 1997; Talley, Lei et al. 2000). The pK for TASK-3 channels is approximately one pH unit lower in the range 6 to 6.7 (Kim, Bang et al. 2000; Rajan, Wischmeyer et al. 2000; Vega-Saenz de Miera, Lau et al. 2001) such that at physiological pH a TASK-3-mediated conductance should be maximally activated. The pH-sensitive gK_{Leak} of FMs has a pK close to 7.1, between the published ranges for either homomeric channel. At pH 7.4 it is activated to approximately 70% of its maximal level, suggesting against a homomeric TASK-3 identity. The pH-sensitivity of FM gK_{Leak} was determined in physiological external $[K^+]$ (3 mM) so the pK cannot be attributed to a previously described effect of high external $[K^+]$ on TASK-1 channels (Lopes, Gallagher et al. 2000; Lopes, Zilberberg et al. 2001).

Interestingly human Kir2.4 is inhibited by external H^+ over the range pH 6 to pH 8 with a pK of 7.1(Karschin, Dissmann et al. 1996; Topert, Doring et al. 1998; Hughes, Kumar et al. 2000). Kir2.4 mRNA, along with mRNA for Kir2.1 and Kir2.2, is expressed in some neonatal rat FMs. As such determining pH-sensitivity alone may not be sufficient to distinguish TASK and Kir2 channel types (Karschin and Karschin 1997; Topert, Doring et al. 1998). It has, however, been suggested that rat Kir2.4 channels are only slightly pH-sensitive (unpublished observations in (Talley, Lei et al. 2000)).

3.7.3 Pharmacology of the amine- and pH-sensitive gK_{Leak}

The lack of effect of methanandamide or anandamide, with or without pre-application of the metabolic inhibitor ATFK, suggests against a TASK-1 identity for

FM $gK_{Leak.}$ However, the insensitivity to anandamide of FM gK_{Leak} should not be overstated. A recent report suggests that unlike human TASK-1 and TASK-3 channels the rat homologues are not particularly sensitive to low concentrations of anandamide and that higher concentrations fail to discriminate the two channel types (Berg, Talley et al. 2004).

The inability of RR to block gK_{Leak} suggests against a TASK-3 identity. The expected effects of these ligands observed in cultured cerebellar granule cells indicate that the negative results cannot be attributed to factors that might affect the activity of these drugs or their delivery to the slices. Recently, Zn^{2+} has been used to discriminate between human TASK-1 and TASK-3 channels (Clarke 2003). Human TASK-1 is unaffected by Zn^{2+} (100 μM) whereas the same concentration blocks hTASK-3 by greater than 70% (IC_{50} = ~20 μM). While the insensitivity of the pH- and NA-sensitive gK_{Leak} to Zn^{2+} also argues against a TASK-3 channel identity there is a suggestion that rat TASK-3 channels are insensitive to Zn^{2+} (100 μM) (Leonoudakis, Gray et al. 1998; Kim, Bang et al. 2000). Recently though the gK_{Leak} in rat CG neurones has been shown to be substantially blocked by Zn^{2+} (100 μM) (Clarke, Veale et al. 2004).

It is of interest that the local anaesthetic bupivacaine inhibited a conductance that shared the properties of gK_{Leak} and at least partially occluded the actions of NA in some FMs. Bupivacaine inhibits both TASK-1 and TASK-3 channels with roughly equivalent potency (Leonoudakis, Gray et al. 1998; Kim, Bang et al. 2000) and its ability to block a pH-sensitive gK_{Leak} in thalamocortical neurones appears sufficient to ascribe this a TASK channel-mediated conductance (Meuth, Budde et al. 2003).

Nevertheless, bupivacaine also has actions on other channels including some voltage-gated K^+ channels (Gonzalez, Longobardo et al. 2001). Thus, while the current blocked by bupivacaine in FMs is consistent with a TASK-like gK_{Leak}, the additional block of other K^+ channels may also contribute to the overall effect of this drug.

3.7.4 Possible identities of FM gK_{Leak}: TASK-1 / TASK-3 heterodimers

Though the results described in this chapter suggest against homomeric TASK-1 or TASK-3 channels, evidence indicates TASK-1 and TASK-3 interact to form functional heterodimeric channels (Czirjak and Enyedi 2002; Talley and Bayliss 2002). Could FM gK_{Leak} be accounted for by heteromeric TASK-1 / TASK-3 channels? The pharmacologies of homomeric TASK-1, homomeric TASK-3 and heteromeric TASK-1 / TASK-3 currents expressed in various systems and FM gK_{Leak} are compared in Table 3.1. It has been suggested that heterodimer formation may be a favoured process when both TASK-1 and TASK-3 subunits are present, though recent studies on cultured cerebellar granule cells indicate both homomeric and heteromeric channels can also co-exist in the same cell (Czirjak and Enyedi 2002; Kang, Han et al. 2004). It has also been observed that isoflurane enhances current carried by heteromeric TASK-1 / TASK-3 and homomeric TASK-3 channels while inhibiting homomeric TASK-1 channels (Berg, Talley et al. 2004). Isoflurane enhances FM gK_{Leak} while ruthenium red the TASK-3 blocker has no effect. Heteromeric TASK-1 / TASK-3 channels are insensitive to ruthenium red because the channel subunits must provide symmetrical interaction sites for potency (Czirjak and Enyedi 2002; Kang, Han et al. 2004). These results are consistent with the

	TASK-1	TASK-3	TASK-1 / TASK-3	Rat FM gK_{Leak}
pK [1]	~ 7.5 (r)	~ 6.8 (r)	~ 7.3 (r)	~ 7.1
Isoflurane (0.3 mM) [1]	No effect (r)	~ +80% (r)	~ +50% (r)	~ +55%
Methanandamide (10 μM) [1]	~ -85% (r)	~ -64% (r)	~ -55% (r)	No Effect
Ruthenium red (5 μM) [3]	No Effect (r)	~ - 85% (r)	No Effect (r)	No Effect (10 μM)
Zn^{2+} (100 μM) [2, 7, 8]	~ -40% (r) No Effect (h)	No Effect (r) ~ -70% (h)	No Data ~ -20% (h)	No Effect
Bupivacaine (100 μM) [7, 8]	~ -60% (r)	~ -50% (r)	No Data	~ -30%
Ba^{2+} [7, 9]	IC_{50} ~ 400 μM (r)	IC_{50} ~ 300 μM (r)	No Data	~ -90 % (500 μM)
Cs^{+} [4, 7, 10]	~ -30% (100 μM, r)	~ -75% (3 mM, r) No Effect (10 mM, h)	No Data	No Effect (300 μM) ~ -85% (1 mM)
4-AP [5, 8]	~ -15% (10 mM, r)	No Data	No Data	~ -60% (4 mM)
TEA [5, 6, 7, 8]	~ -30 % (100 mM, r)	No Effect (1 mM, r)	No Data	No Effect (30 mM)

Table 3.1. Comparative pharmacology of TASK channels and rat FM gK_{Leak}.
Values indicated are % current increase (+) or decrease (-) in the presence of the drug indicated, except for the sensitivity of TASK-1 and TASK-3 homomers to Ba^{2+} for which the IC_{50} is given. Values for Ba^{2+} and Cs^{+} reflect optimal voltage-dependent blocker sensitivity. Species is either rat (r) or human (h). Where non-uniform drug concentrations are compared the concentrations are given in parentheses in the table. Data for TASK-1 / TASK-3 heterodimer refers to concatenated TASK-1 / TASK-3 construct. Data taken from [1](Berg, Talley et al. 2004) [2](Clarke, Veale et al. 2004) [3](Czirjak and Enyedi 2002a), [4](Czirjak and Enyedi 2002b), [5](Czirjak, Fischer et al. 2000), [6](Duprat, Lesage et al. 1997), [6](Kim, Bang et al. 2000), [7](Leonoudakis, Gray et al. 1998), [8](Lopes, Zilberberg et al. 2001) and [9](Meadows and Randall 2001).

suggestion that heteromeric TASK-1 / TASK-3 channels could account for FM gK_{Leak} The pK for heteromeric channels lies between the values for homomeric TASK-1 and TASK-3 channels but is nearer that of TASK-1 (Czirjak and Enyedi 2002; Talley and Bayliss 2002). The pK for FM gK_{Leak} is also consistent with a heteromeric channel. The pH-sensitivity of individual FMs did not differ significantly from the population average suggesting a single population of pH-sensitive K^+ channels predominates in these cells. Nevertheless, the observation in one FM that isoflurane inhibited gK_{Leak}, consistent with a TASK-1 channel identity (Berg, Talley et al. 2004), suggests gK_{Leak} may display some heterogeneity within the FM population.

Further evidence in favour of a heteromeric identity for FM gK_{Leak} is the observation that heteromeric channels share the Zn^{2+} insensitivity of TASK-1 homomers (Clarke, Veale et al. 2004). The insensitivity of gK_{Leak} to anandamide should be assessed in the light of the evidence that rat homomeric TASK-1 and TASK-3 channels expressed in HEK 293 cells show lower sensitivity to anandamide and methanandamide relative to human channels (Berg, Talley et al. 2004). In addition, these compounds show little selectivity between different rat channels. Anandamide (10 μM) blocks between 60 and 80% of the current flowing through homomeric channels and ~50% flowing through heteromeric channels. This latter observation is clearly at odds with the suggestion that a heteromeric channel mediates gK_{Leak} in FMs. However, distinct cellular environments may promote differences between endogenous channels and those expressed in cell lines. The sensitivity of the TASK-1 / TASK-3 heterodimer to bupivacaine is unknown. The lack of effect of the selective blockers of the homomeric channels precludes any quantification of the

relative contributions of channel isoforms within individual FMs similar to that performed elsewhere (Berg, Talley et al. 2004).

The gK_{Leak} in FMs displays properties of an amine-sensitive gK_{Leak} described in neonatal rat hypoglossal motoneurons (Talley, Lei et al. 2000). First described as TASK-1, hypoglossal motoneuron gK_{Leak} displays pharmacological differences to the cloned rat TASK-1 channel and is also enhanced by isoflurane leading to the suggestion that it may be a heteromeric channel (Talley, Lei et al. 2000; Talley and Bayliss 2002; Berg, Talley et al. 2004). It is of interest that the anandamide sensitivity of this gK_{Leak} has not been described (Berg, Talley et al. 2004).

3.7.5 Could other 2P K^+ channels underlie FM gK_{Leak}?

One study indicates protein for TASK-2 is found in the FMN (Gabriel, Abdallah et al. 2002). TASK-2 gives rise to outwardly rectifying currents with a pK around 7.8 suggesting activation at physiological pH. Outward current through TASK-2 channels is relatively insensitive to Ba^{2+} and Cs^+ and permeability to Rb^+ is less than for K^+, unlike TASK-1 (Reyes, Duprat et al. 1998; Niemeyer, Cid et al. 2001; Talley and Bayliss 2002). It has previously been determined that the FM gK_{Leak} is inhibited by Ba^{2+} (500 µM) and Cs^+ (1 mM) (Larkman and Perkins 2005). TASK-2 is also blocked by bupivacaine (Kindler, Paul et al. 2003). Nevertheless, alone this conductance could not account for the whole range of pH sensitivity or linearity of the gK_{Leak}. The CNS distribution of TASK-4 channels has not been established, however, they are activated by alkaline pH, show little activation at pH 7.5 and have slow activation kinetics which distinguishes them from gK_{Leak} in FMs (Decher, Maier et al. 2001). TASK-5 channels, either in homomeric or heteromeric (with

TASK-1) combinations, have so far eluded functional characterisation nevertheless mRNA does not appear to be present in FMs (Ashmole, Goodwin et al. 2001; Karschin, Wischmeyer et al. 2001).

3.7.6 Inwardly rectifying and voltage-gated K^+ channels

The absence of inward rectification in gK_{Leak} might be expected to preclude the involvement of Kir2.4 (and other Kir) channels. Nevertheless, block of the amine-sensitive gK_{Leak} by Ba^{2+} generates an inwardly rectifying I/V relationship (Larkman and Perkins 2005). This could represent either the voltage-dependent block of a single conductance or the block of an inwardly rectifying conductance that contributes to the overall properties of the gK_{Leak}. A characteristic of gK_{ir} is that the $V_{0.5}$ shifts with $[K^+]_o$ suggesting that the driving force on K^+ determines activation rather than voltage alone (Yamaguchi, Nakajima et al. 1990). Examination of the Ba^{2+}-sensitive component of gK_{Leak} in FMs indicated that $V_{0.5}$ was relatively independent of $[K^+]_o$ suggesting a predominantly voltage-dependent block, distinct from the properties of Kir channels (Larkman and Perkins 2005). Nevertheless, it is a possibility that Kir2 heterotetramers in association with accessory β subunits show emergent properties distinct from homomeric channels (Schram, Melnyk et al. 2002).

The NA- and pH-sensitive gK_{Leak} in FMs has also been shown to be blocked by 4-AP (4 mM) but not by TEA (30 mM) (Larkman and Perkins 2005). TASK-1 and TASK-3 channels are reported to be insensitive to both 4-AP and TEA (Duprat, Lesage et al. 1997; Leonoudakis, Gray et al. 1998; Czirjak, Fischer et al. 2000; Kim, Bang et al. 2000; Lopes, Gallagher et al. 2000; Meadows and Randall 2001; Vega-Saenz de Miera, Lau et al. 2001). It has previously been shown that 4-AP blocks fast and slow

transient outward K^+ currents in FMs though neither appear to contribute to the amine-sensitive gK_{Leak} (Larkman and Kelly 1998). Rapidly activating, slowly inactivating, 4-AP-sensitive, voltage-gated K^+ conductances have been characterised in cardiac muscle (Boyle and Nerbonne 1992). In particular, Kv1.5 has been suggested to contribute a sustained current at depolarised membrane potentials (reviewed in (Nerbonne 2000)). Kv1.5 channels are blocked by 4-AP, relatively TEA-insensitive, inhibited by acidosis, blocked by bupivacaine (EC_{50} ~10 μM) and while being sensitive to Zn^{2+} the EC_{50} is close to 800 μM (Clement-Chomienne, Ishii et al. 1999; Steidl and Yool 1999; Gonzalez, Longobardo et al. 2001; Kehl, Eduljee et al. 2002). The presence of Kv1.5 protein in FMs is unknown though it is present in motoneurons at all levels of the spinal cord (Matus-Leibovitch, Vogel et al. 1996). Nevertheless, a pK around 6.2 and a restricted voltage range for sustained current between, at best, -60 and 0 mV both suggest that alone these channels may not be sufficient to explain the properties of FM gK_{Leak}.

3.8 Concluding statement

This chapter confirms the enhancement of I_h by 5-HT and the inhibition of a gK_{Leak} by both 5-HT and NA as the ionic mechanisms that mediated the excitatory actions of these neurotransmitters in neonatal rat FMs (Larkman and Kelly 1992; Larkman and Kelly 1997; Larkman and Kelly 1998). This chapter also describes the pharmacological and biophysical properties of gK_{Leak} in FMs and provides evidence that the channel underlying this conductance is a TASK-1/TASK-3 heterodimeric channel. Confirming the action of 5-HT and NA and determining the molecular identity of gK_{Leak} and NA was necessary for the interpretation of functional

significance of the modulatory effect of 5-HT and NA on FM excitability. This modulation of $g\mathrm{K}_{\mathrm{Leak}}$ and I_{h} will also have consequences for synaptic integration in FMs.

Chapter 4

4.1 Introduction

5-HT and NA promote neonatal FM excitation by depolarising the postsynaptic membrane (see Chapter 3). The ionic mechanisms that underlie the membrane depolarisation have been confirmed as a decrease in gK_{Leak} (5-HT and NA) and an enhancement of the hyperpolarisation activated cation current, I_h, (5-HT only) (Larkman and Kelly 1992; Larkman and Kelly 1997; Larkman and Kelly 1998). However, the receptor subtypes that mediate these actions of 5-HT and NA have not yet been conclusively identified.

4.1.2 5-HT receptors

Advances in molecular biology techniques has vastly expanded the database on 5-HT receptors and there are currently 14 pharmacologically and structurally distinct subtypes of 5-HT receptors that are grouped into seven families ($5\text{-}HT_{1\text{-}7}$) by their signal transduction mechanism and structural similarities (Figure 4.1) (Barnes and Sharp 1999; IUPHAR 2000). The $5\text{-}HT_3$ receptor forms a ligand-gated ion channel and all the other 5-HT receptors are seven transmembrane spanning receptors that couple to intracellular membrane bound guanosine triphosphate (GTP) binding proteins (G proteins) that can activate various intracellular signalling pathways.

The chapter focuses on the roles of $5\text{-}HT_2$ and $5\text{-}HT_7$ receptors in the excitatory effects of 5-HT.

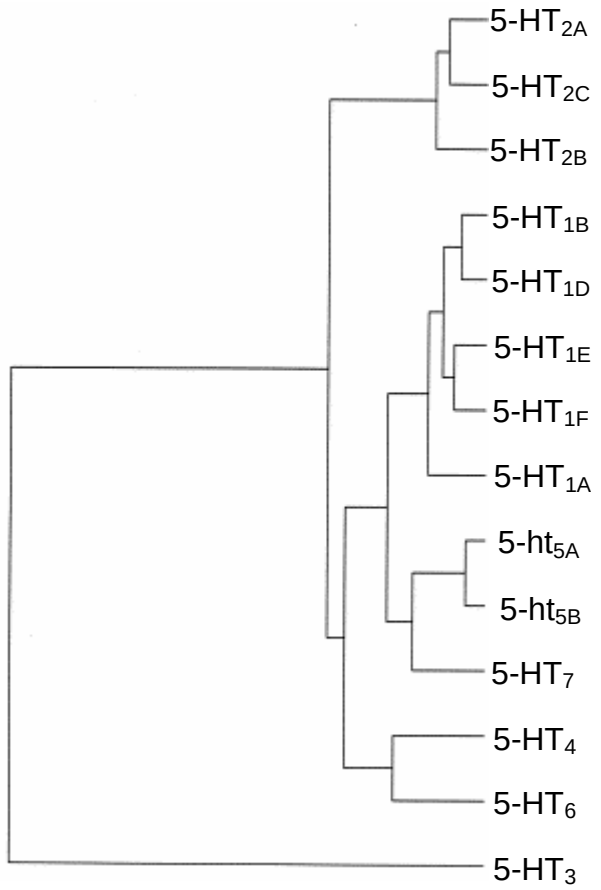

Figure 4.1. Dendrogram of 5-HT receptors.
Dendrogram depicting relationship between the known 5-HT receptors. Modified from (Barnes and Sharp 1999).

4.1.3 5-HT_2 receptors

All 5-HT_2 receptors are positively coupled to phospholipase C (PLC) through G_q proteins. Phospholipase C activity increases the hydrolysis of phosphatidylinositol bisphosphate (PIP_2) producing the intracellular messengers inositol triphosphate (IP_3) and diacylglycerol (DAG) (Alberts, Johnson et al. 2002). IP_3 is released into the cytosol and is free to bind to IP_3 receptors on the endoplasmic reticulum membrane resulting in the opening of calcium channels formed by the IP_3 receptors, releasing calcium from these intracellular stores (Alberts, Johnson et al. 2002). DAG remains membrane bound and activates protein kinase C, leading to phosphorylation of target proteins. Evidence supporting this transduction mechanism following activation of 5-HT_2 receptors is reviewed in Boess *et al* (1994). Expression of 5-HT_{2A} or 5-HT_{2C} receptors in mouse fibroblasts was found to activate PLC and raise intracellular [Ca^{2+}] ([$Ca^{2+}]_i$) (Julius, Huang et al. 1990). When expressed in AV-12 cells both the human and rat 5-HT_{2B} receptors were found to couple positively to phosphatidylinositol hydrolysis (Kursar, Nelson et al. 1992; Kursar, Nelson et al. 1994). It was also found that when the cloned 5-HT_2 receptor subtypes were expressed in *Xenopus laevis* oocytes, application of 5-HT resulted in an opening of Ca^{2+}-sensitive Cl^- channels, indicating an increase in $[Ca^{2+}]_i$ (reviewed in (Boess and Martin 1994)).

4.1.4 5-HT_2 receptors in the facial nucleus

Autoradiographical studies using the 5-HT_{2A} receptor antagonist, [^{3}H]-MDL-100907, identified 5-HT_{2A} binding sites in some of the brainstem nuclei including the trigeminal and facial motor nuclei (Lopez-Gimenez, Mengod et al. 1997). This

presence of 5-HT_{2A} receptors in facial motoneurones is supported by both immunohistochemical and *in situ* hybridisation studies (Pompeiano, Palacios et al. 1994; Cornea-Hébert 1999; Fonseca, Ni et al. 2001; Volgin, Fay et al. 2003). However, not all immunohistochemical studies detected 5-HT_{2A} receptors in the facial motor nucleus (Morilak, Garlow et al. 1993).

5-HT_{2B} receptors in the rat have been identified in peripheral tissue, particularly in the stomach fundus (Kursar, Nelson et al. 1992). Although mRNA for the 5-HT_{2B} receptor has been detected in the human brain, several early studies failed to detect 5-HT_{2B} receptors in the rat brain (Kursar, Nelson et al. 1994; Pompeiano, Palacios et al. 1994). Subsequently 5-HT_{2B} receptor protein has been detected in the frontal cortex, cerebellum, hypothalamus, medial amygdala and spinal cord of the rat but its presence in the facial nucleus has not been reported (Duxon, Flanigan et al. 1997).

5-HT_{2C} mRNA was has been detected in regions of the brainstem and spinal cord including cranial motor nuclei such as the facial motor nuclei, however, the protein distribution of this receptor in the brainstem has not been reported (Pompeiano, Palacios et al. 1994).

4.1.6 Do 5-HT_2 receptor mediate inhibition of FM gK_{Leak}?

The excitatory responses to 5-HT_{2A} and 5-HT_{2C} receptor activation in the rat perform cortex, nucleus accumbens and cortical pyramidal neurones are all mediated by an inhibition of K^+ conductances raising the possibility that these receptors may be involved in the inhibition of gK_{Leak} in FMs (North and Uchimura 1989; Araneda and Andrade 1991; Sheldon 1991; Aghajanian and Marek 1997). In addition, non-selective 5-HT_2 receptor activation has been shown to have excitatory effects on rat

hypoglossal motoneurones and facial motoneurones (Rasmussen and Aghajanian 1990; Bouryi and Lewis 2003). The development of subtype selective antagonists including the 5-HT_{2A}-selective antagonist, R-96544, has enabled this issue to be addressed (Ogawa, Sugidachi et al. 2002).

4.1.7 Increase in intracellular cAMP mediates enhancement of I_h by 5-HT

It has previously been determined that the enhancement of I_h by 5-HT in FMs is mediated by an increase in intracellular cyclic AMP (cAMP) (Larkman and Kelly 1997). The cAMP binds to an intracellular region of the channel shifting its activation range to more depolarised potentials (Larkman and Kelly 1992; Larkman, Kelly et al. 1995).

5-HT receptor subtypes that couple positively to adenylate cyclase (via G_s proteins) to increase intracellular cAMP levels belong to the 5-HT_4, 5-HT_6 and 5-HT_7 receptor subfamilies (Barnes and Sharp 1999; IUPHAR 2000; Alberts, Johnson et al. 2002). However, previous pharmacological investigations using the 5-HT_4 receptor-selective antagonist, GR-113808A, and the 5-HT_6 and 5-HT_7 antagonist, clozapine, failed to implicate these receptors in the enhancement of I_h in FMs (Larkman and Kelly 1997). The role of the 5-HT_7 receptor subtype has been re-examined in this chapter due to the emergence of the high affinity 5-HT_7 receptor selective antagonist, SB269970 (Hagan, Price et al. 2000; Lovell, Bromidge et al. 2000).

4.1.8 5-HT_7 receptors in FMs

Although, 5-HT_7 receptor mRNA and protein has been detected in the cortex, hippocampus, thalamus, hypothalamus and tenia tecta, the expression of 5-HT_7

receptors in the brainstem nuclei has not yet been reported.(Neumaier, Sexton et al. 2001).

4.1.9 Adrenoceptors mediating inhibition of gK_{Leak} in FMs

The receptors that are activated by noradrenaline (adrenoceptors) are the α_1-, α_2- and β-adrenoceptors (Docherty 1998). The α_1-adrenoceptors are G_q protein coupled receptors that activate the PLC pathway (see 5-HT_2 receptor section) and mediate the excitatory effects of NA, whereas the α_2-adrenoceptors inhibit cAMP formation (Docherty 1998). The β-adrenoceptors are coupled to adenylate cyclase activity (IUPHAR 2000).

α_1-adrenoceptor mRNA has been detected in the facial motor nucleus, suggesting this receptor subtype mediates the inhibition of gK_{Leak} by NA in FMs (VanderMaelen and Aghajanian 1980; Larkman and Kelly 1992; Pieribone, Nicholas et al. 1994). This issue has been addressed using the α_1-adrenoceptor selective agonist, phenylephrine, and antagonist, prazosin (IUPHAR 2000).

4.1.10 Aims

The ionic mechanisms that underlie the membrane depolarisation by 5-HT have been confirmed as an enhancement of the hyperpolarisation activated cation current, I_h, and decrease in a potassium conductance (see Chapter 3) (Larkman and Kelly 1992; Larkman and Kelly 1997; Larkman and Kelly 1998). In addition, NA promotes FM membrane excitation by inhibiting a potassium conductance but does not enhance I_h (Larkman and Kelly 1992).

In this chapter pharmacological approaches have been utilised to identify the receptor subtypes underlying 5-HT- and NA-mediated depolarisation of FMs. The findings suggest that inhibition of gK_{Leak} is mediated by activation of 5-HT_{2A} and α_1-adrenoceptor activation and the enhancement of I_h is mediated by 5-HT_7 receptor activation. The mechanism by which receptor activation leads to inhibition of gK_{leak} is also addressed in this chapter. The results suggest a role for PIP_2 hydrolysis in NA-induced channel closure but the evidence is less conclusive for a similar involvement in the actions of 5-HT on these channels.

4.2 Results

4.2.1 5-HT Receptor subtype mediating inhibition of gK_{Leak}

Preliminary studies indicated that non-selective 5-HT_2 antagonists block the action of 5-HT on gK_{Leak} and the presence of 5-HT_{2A} and 5-HT_{2C} receptors in the rat FMN prompted an investigation into whether this receptor-subtype mediates this action of 5-HT (Pompeiano, Palacios et al. 1994; Wright, Seroogy et al. 1995).

In the example shown in Figure 4.2, 5-HT (10 μM) evoked an inward current of –252 pA when applied to a FM voltage-clamped at –50 mV (in the presence of ZD7288, 10 μM). This inward current was associated with a reduction in membrane conductance from 9.9 nS to 5.0 nS. The mean inward current at the holding potential (-50 mV) and reduction in membrane conductance evoked by 5-HT was –123 ± 65 pA and from 8.2 ± 0.9 nS to 5.2 ± 0.4 nS (P = 0.017, paired *t* test), respectively (n = 3). The 5-HT_{2A} receptor antagonist, R96544 (0.3 μM), was applied for a minimum of 10 minutes and had no effect on membrane current (77 ± 84 pA before, and 105 ± 68 pA after incubation with R96544, n = 3) (Ogawa, Sugidachi et al. 2002). 5-HT

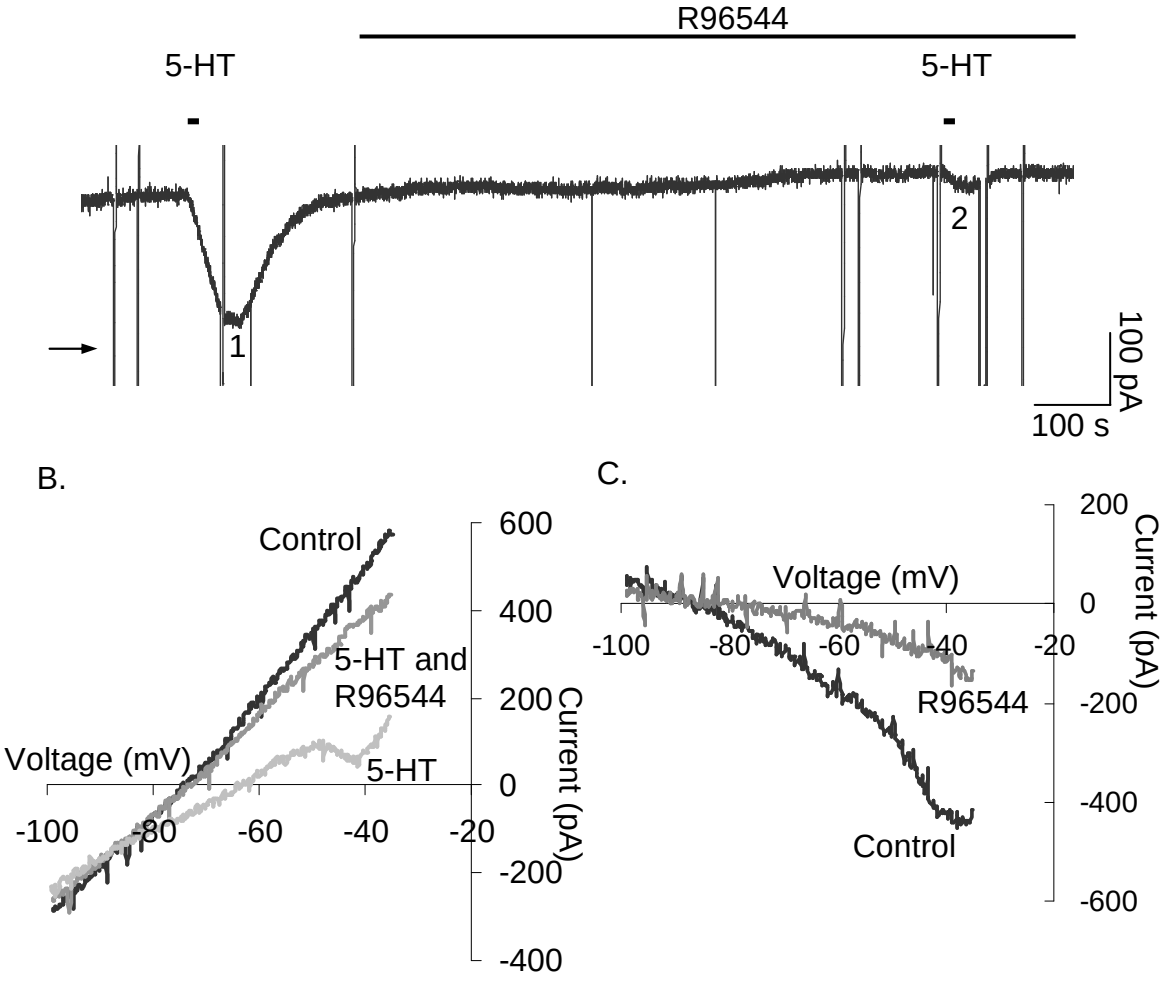

Figure 4.2. The 5-HT$_{2A}$ receptor antagonist (R96544, 0.3 μM) partially blocks inhibition of *g*K$_{Leak}$ by 5-HT.

A. Continuous current record of facial motoneuron voltage-clamped at –50 mV in the presence of ZD7288 (10 μM). Bath application of 5-HT (10 μM) evokes a large inward current (1). Following incubation with the 5-HT$_{2A}$ receptor antagonist, R96544 (0.3 μM, 10 minutes), bath application of 5-HT (10 μM) in the continued presence of the antagonist evokes a smaller inward current. The arrow indicates the zero current level.

B. I/V relationships obtained from a facial motoneuron in the presence (light grey) and absence (black) of 5-HT (10 μM). 5-HT only has a small effect on the I/V relationship when applied in the presence of R96544 (0.3 μM, dark grey).

C. Plot of the 5-HT-induced current (obtained by subtraction of plots shown in B) indicate that R96544 (0.3 μM) reduces the 5-HT-induced current (grey) compared to control (black).

was then co-applied with the antagonist. In the example in Figure 4.2, incubation with R96544 (0.3 μM) reduced the inward current evoked by 5-HT to –56 pA (22 % of control response) and reduced the change in conductance (12.8 nS to 10.6 nS in presence of 5-HT). Incubation with R96544 (0.3 μM) caused a reduction in the mean inward current evoked by 5-HT at the holding potential to –30 ± 18 pA (n = 3, Figure 4.2A), representing a significant reduction to 28 ± 14 % of control (n = 3, P = 0.04, one sample *t* test, Figure 4.4). In the presence of R96544 (0.3 μM), the 5-HT-mediated inhibition of gK_{Leak} is reduced over the entire voltage range and 5-HT no longer significantly reduces the mean FM membrane conductance (10.6 ± 1.2 nS to 9.2 ± 0.8 nS, P = 0.07, paired *t* test, Figure 4.2B, C). Conductance measurements were calculated from the slope of the I/V plot. The time limitations of voltage-clamp recordings from FMs did not allow for the reversibility of this antagonist to be investigated.

A similar experiment was carried out on separate group of FMs where the concentration of R96544 was increased to 1 μM. R96544 (1 μM) had no effect on membrane current at the holding potential (-50 mV, 147 ± 60 pA before and 182 ± 65 pA after incubation with R96544, n = 3). Figure 4.3A demonstrates the current evoked by 5-HT (10 μM) following incubation with R96544 (1 μM) is reduced compared to control (-18 pA in the presence of R96544 (1 μM) compared to –85 pA under control conditions). The mean 5-HT induced current (measured at –50 mV) was reduced from –50 ± 18 pA to –8 ± 5 pA in the presence of R96544 (1 μM). This represents a significant reduction in inward current evoked by 5-HT (10 μM) to 15 ± 5% of control (P = 0.003, one sample *t* test, n = 3, Figure 4.4). R96544 (1 μM) reduces the inhibition of gK_{Leak} by 5-HT over the whole voltage range tested (Figure

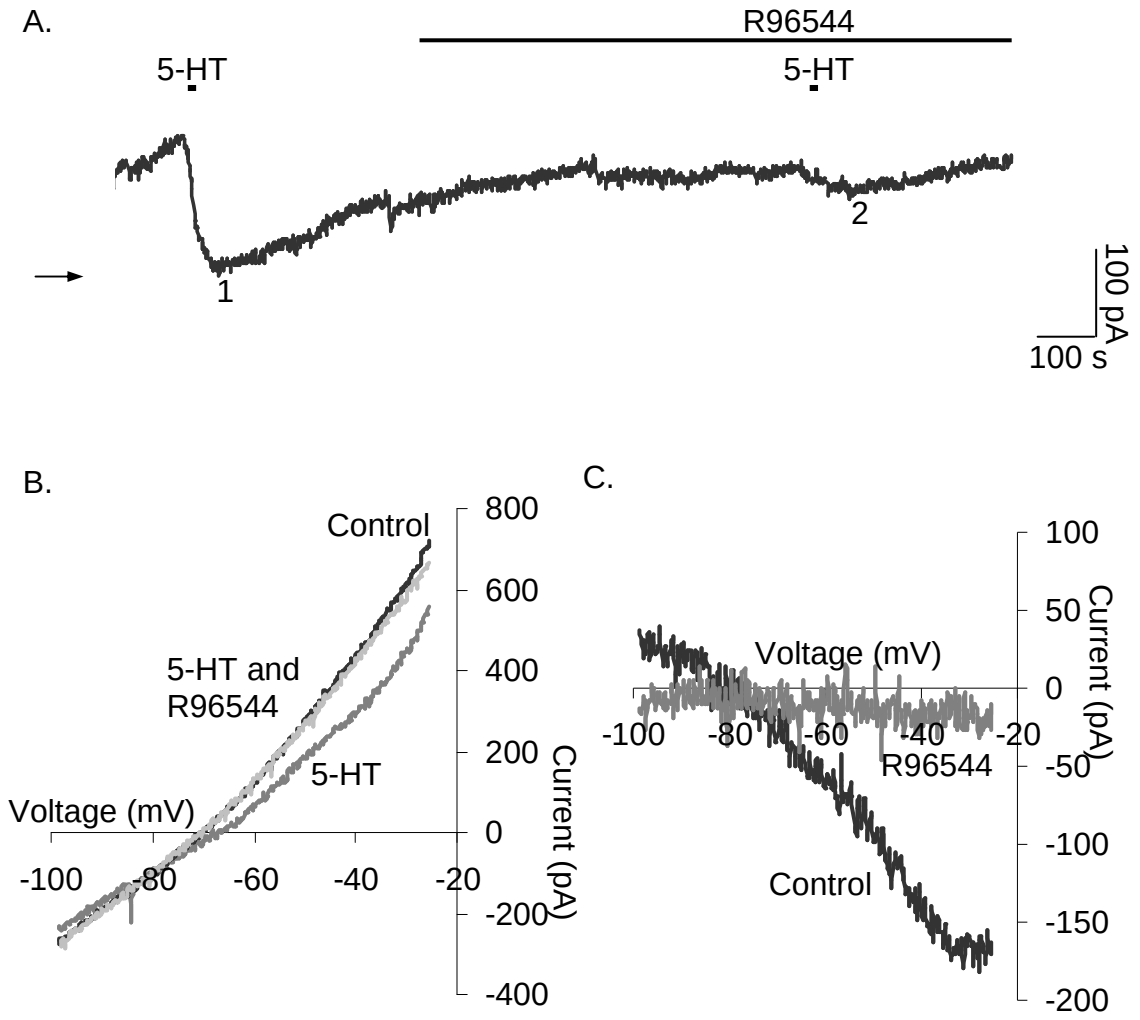

Figure 4.3. The 5-HT$_{2A}$ receptor antagonist (R96544, 1 μM) blocks inhibition of *g*K$_{Leak}$ by 5-HT.

A. Continuous current record of FM voltage-clamped at –50 mV in the presence of ZD7288 (10 μM). Bath application of 5-HT (10 μM) evokes a large inward current (1). Following incubation with the 5-HT$_{2A}$ receptor antagonist, R96544 (1 μM, 10 minutes), bath application of 5-HT (10 μM) in the continued presence of the antagonist evokes an inward current that is reduced compared to control (2). The arrow indicates the +150 pA level.

B. I/V relationships obtained from a facial motoneuron in the presence (dark grey) and absence (black) of 5-HT (10 μM). 5-HT has no effect on the I/V relationship when applied in the presence of R96544 (1 μM, light grey).

C. Plots of the 5-HT-induced current (obtained by subtraction of plots shown in B) indicate that R96544 (0.3 μM) abolishes the 5-HT-induced current (grey) compared to control (black).

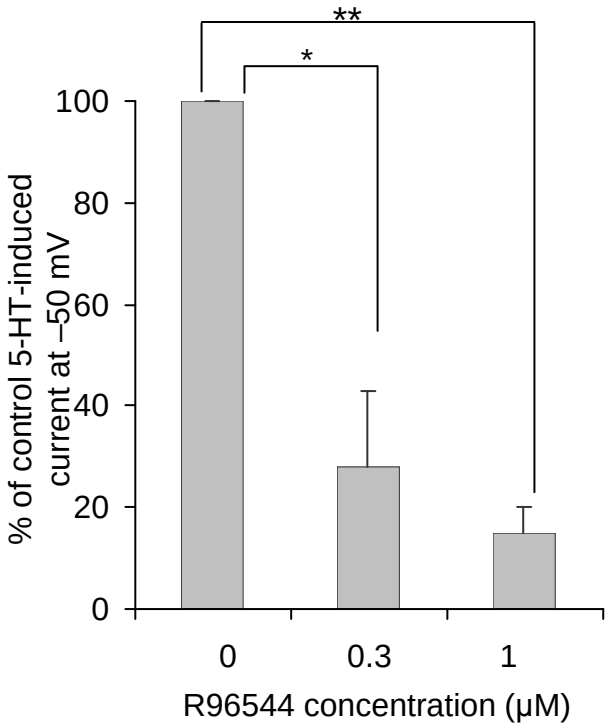

Figure 4.4. Summary of effects of R96544 on 5-HT-induced current.
The 5-HT_{2A} receptor antagonist, R96544, reduces the 5-HT-induced current compared to control. The 5-HT-induced current was measured at –50 mV and is expressed as the mean percentage of the control 5-HT-induced current and error bars represent the SEM (n = 3 for each antagonist concentration). 0.3 μM of the antagonist significantly reduced the 5-HT-induced current (* P= 0.04). Increasing the concentration of the antagonist to 1 μM results in a greater reduction in the 5-HT-induced current (** P = 0.003). Statistical significance was assessed by one sample *t* test.

4.4B, C). In the example shown in Figure 4.3, the conductance change induced by 5-HT (10 μM) under control conditions was from 12.3 nS to 8.9 nS. In the same FM and in the presence of R96544 (1 μM), 5-HT no longer altered membrane conductance (11.6 nS and 11.7 nS in the presence and absence of 5-HT). Under control conditions 5-HT application resulted in a mean reduction in conductance from 7.8 ± 2.5 nS to 6.0 ± 2.0 nS (n =3) and this was inhibited by R96544 (1 μM) (7.7 ± 2.4 nS to 7.5 ± 2.3 nS in the presence of 5-HT for the same FMs). These data indicate 5-HT_{2A} receptor activation mediates the inhibition of gK_{Leak} by 5-HT in FMs.

4.2.2 Mechanism of enhancement of I_h by 5-HT

As previously established 5-HT enhances I_h by shifting the steady-state activation curve to more depolarised potentials and increasing the rate of activation (Larkman and Kelly 1992). These effects of 5-HT have been confirmed here (Figure 4.5). In Figure 4.5B the current responses in the presence of 5-HT were shifted so the peak of the instantaneous current was the same as the control, thereby clearly illustrating the enhancement of I_h over the activation range (enabling the effect on I_h to be detected visually). In the example shown in Figure 4.5 the enhancement of the amplitude and rate of activation of I_h by 5-HT is apparent between –90 mV and –120 mV. This is consistent with the previous findings that intracellular cAMP shift the activation range of I_h to more depolarised potentials (Larkman and Kelly 1997).

4.2.3 Optimising conditions for investigating I_h modulation

Prior to establishing the identity of the receptor that mediates the inhibition of gK_{Leak}, the modulation of I_h could not be isolated pharmacologically. An alternative

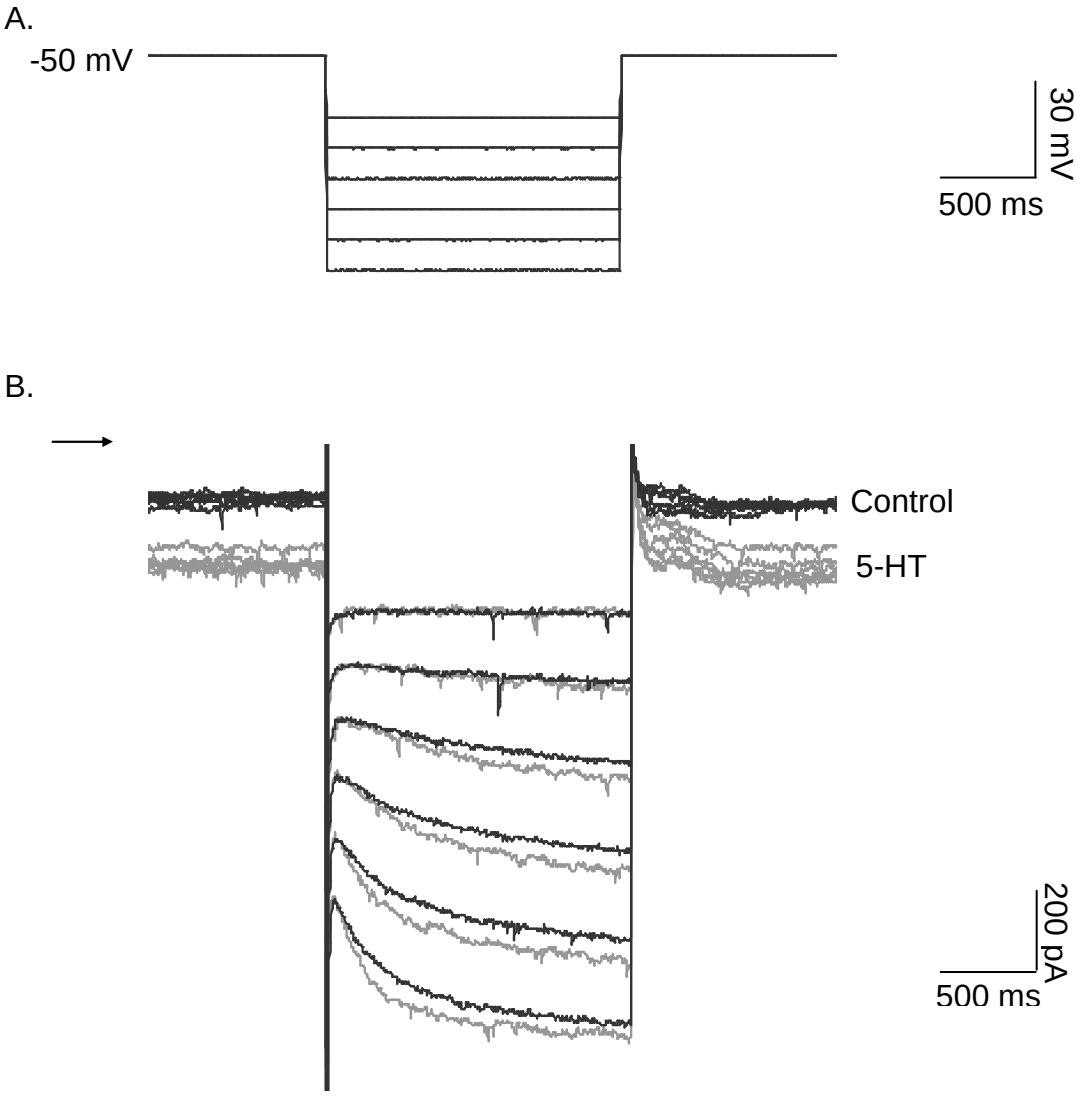

Figure 4.5. 5-HT shifts the threshold for activation of hyperpolarisation-activated cation current, I_h.

A. Voltage command (10 mV steps) used to monitor changes in I_h.

B. Current responses to hyperpolarizing voltage steps (A) in control conditions (black) and following bath application of 5-HT (10 µM, grey). The 5-HT responses were shifted so the peak of the instantaneous current was the same as the control value, this enables the effect on I_h to be observed The arrow indicates the zero current level.

approach to studying the 5-HT actions on I_h is to optimise I_h and minimise contribution of gK_{Leak} to the overall 5-HT response. The external potassium concentration was increased from 3 mM to 12 mM, which shifted the E_K to approximately –59 mV (as predicted by the Nernst Equation, Methods Equation 1). Under these conditions in a FM voltage-clamped around –59 mV inhibition of gK_{Leak} would not evoke any significant net current change and in cells voltage-clamped below -59 mV inhibition of gK_{Leak} would be observed as an outward current. H-channels are mixed cation channels with a higher selectivity for K^+ over Na^+ and the increased driving force that arises by increasing the external K^+ concentration results in a larger I_h being measured. When 5-HT was applied to a FM voltage-clamped at –60 mV in 12 mM K^+ ACSF (Methods Solution 2.4) an inward current was observed (-47 ± 8 pA, n =10, Figure 4.6A). Previous studies have shown this inward current to be abolished by ZD-7288 (Larkman & Kelly, 1998). Under these conditions I_h was significantly enhanced by 5-HT application (increased by 31 ± 6 pA, n = 8, $P < 0.0001$, one sample *t* test, Figure 4.6B).

4.2.4 5-HT receptor subtype mediating enhancement of I_h

It has previously been determined that the mechanism for the enhancement of I_h by 5-HT involves a phosphorylation-independent action of cAMP on the channel, however, the 5-HT receptor subtype mediating this effect has not previously been identified (Larkman, Kelly et al. 1995; Larkman and Kelly 1997). cAMP is produced by adenylate cyclase and members of 5-$HT_{4, 6}$ and $_7$ receptor families are known to couple to G-proteins that promote adenylate cyclase activity. Prior incubation with the 5-HT_4 receptor antagonist, GR-113808A, or the 5-$HT_{6/7}$ receptor

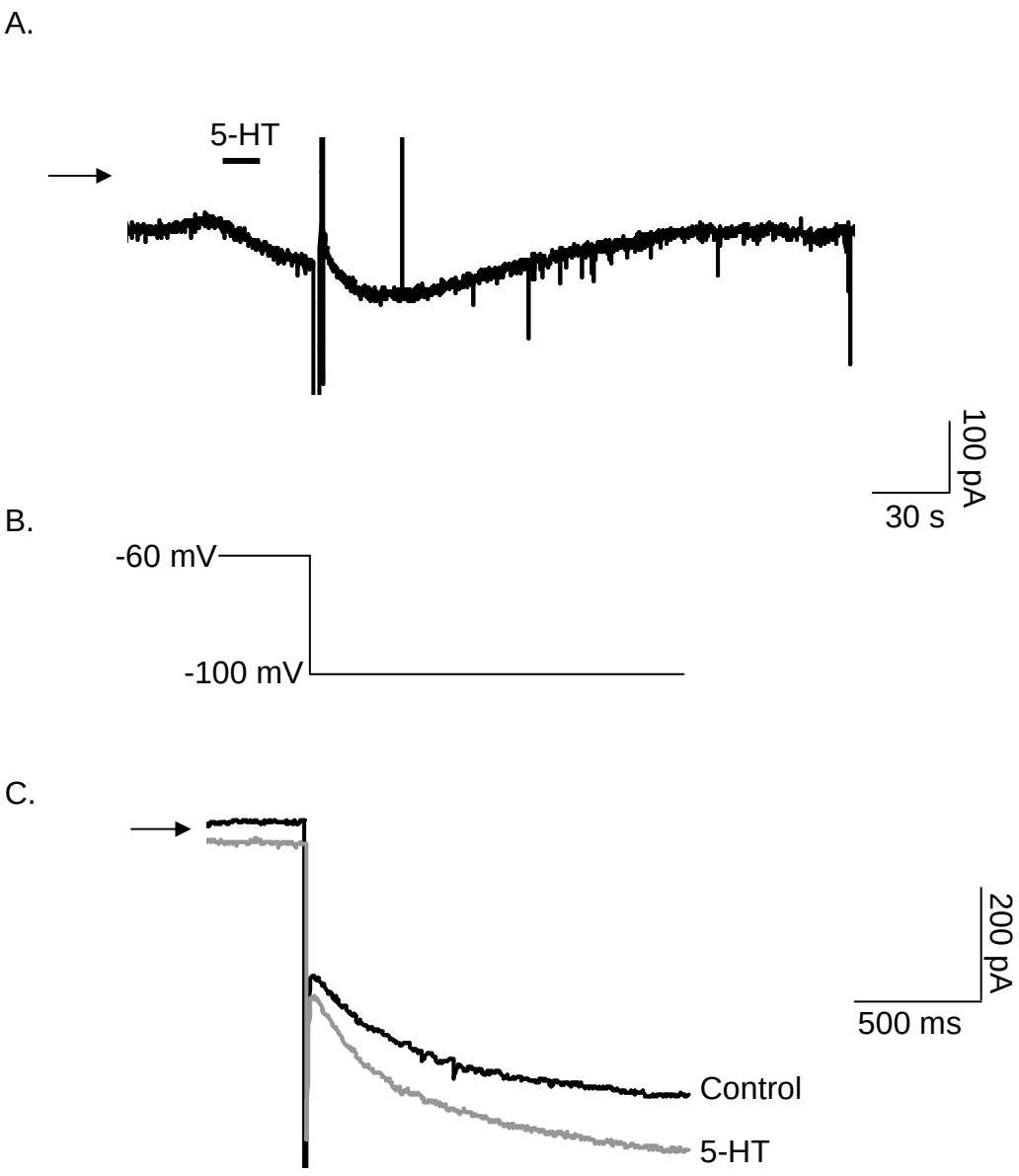

Figure 4.6. In 12 mM $[K^+]_o$ 5-HT enhances I_h.

A. Continuous current record of a facial motoneuron voltage-clamped at – 60mV in 12 mM K^+ ACSF. 5-HT evokes an inward current and the large deflections represent current responses to voltage commands. The arrow indicates the – 200 pA level.

B. Voltage command used to monitor changes in I_h.

C. Current responses to hyperpolarizing voltage steps (B) in control conditions (black) and following bath application of 5-HT (10 µM, grey). The arrow indicates the –300 pA current level.

antagonist, clozapine, did not block the enhancement of I_h by 5-HT (Larkman and Kelly 1997). However, the development of the selective 5-HT_7 receptor antagonist, SB269970, has allowed the contribution of this receptor to the enhancement of I_h by 5-HT to be further investigated (Hagan, Price et al. 2000; Lovell, Bromidge et al. 2000).

Figure 4.7A demonstrates that bath-application 5-HT (10 μM) to a FM voltage-clamped at –60 mV evokes a control inward current of –68 pA. This inward current was replicated following a second application of 5-HT (Figure 4.7A). The mean 5-HT-evoked inward current under these conditions was –60 ± 4 pA (n = 4). The 5-HT_7 receptor antagonist, SB269970 (10 μM), was applied for a minimum of 10 minutes prior to co-application of 5-HT with the antagonist and had no effect on the membrane current at the holding potential (-140 ± 50 pA under control conditions and -124 ± 46 pA following incubation with SB269970, P = 0.07, paired *t* test, n = 4). In the example in shown in Figure 4.7B, in the presence of SB269970 (10 μM) the inward current evoked by 5-HT was reduced from –68 pA to -8 pA. The mean inward current evoked by 5-HT in the presence of SB269970 (10 μM) was 14 ± 3 pA, representing a significant reduction compared to control (P = 0.01, paired *t* test, n = 4). The small outward current observed is due to the inhibition of gK_{Leak} by 5-HT (Figure 4.7B). In the same FM as Figure 4.7, the current response to a hyperpolarising voltage step demonstrates that 5-HT (10 μM) enhances steady-state I_h by 162 pA (21 %, Figure 4.8B). The mean enhancement of I_h by 5-HT was 101 ± 21 pA, representing an increase of 22 ± 1 % (n = 4). Following prior incubation with SB269970 (10 μM) the enhancement of I_h by 5-HT, in the example shown in Figure 4.8, was reduced to 101 pA (17 %, Figure 4.8C). The mean enhancement of I_h by

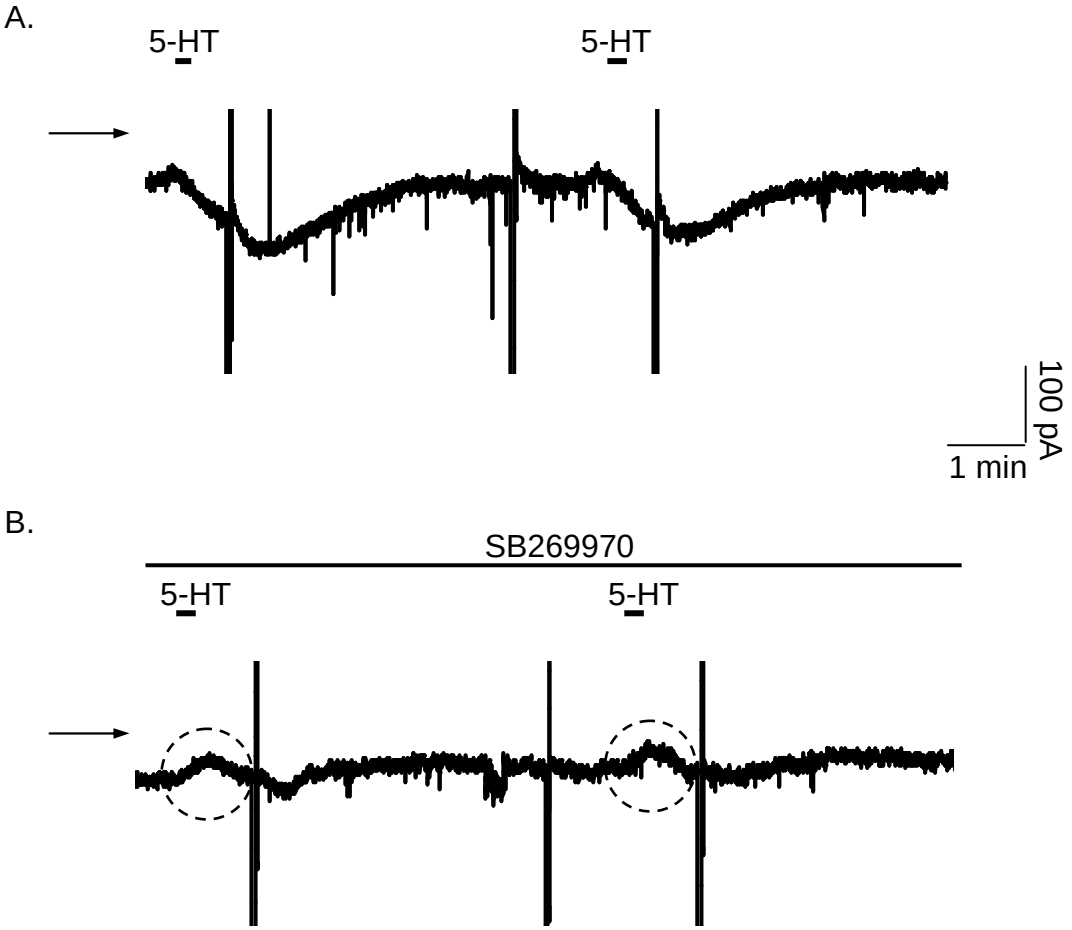

Figure 4.7. SB269970 (10 μM) reduces the 5-HT-evoked inward.

A. Continuous current record from a facial motoneuron voltage-clamped at –60 mV in 12 mM K^+ ACSF. 5-HT (10 μM) evokes a large, reversible inward current, which is reproducible. The large deflections on the current trace represent current responses to voltage commands on a compressed time scale and the arrow indicates the –200 pA level.

B. Continuous current record from the same facial motoneuron voltage-clamped at –60 mV in the presence of the 5-HT_7 receptor antagonist, SB269970 (10 μM), in 12 mM K^+ ASCF, following incubation with the antagonist for 10 mins. The inward current evoked by 5-HT (10 μM) is reduced compared to control. Note the outward currents that arise due to inhibition of gK_{Leak} by 5-HT (highlighted by the dashed circles). The arrow indicates the –200 pA level.

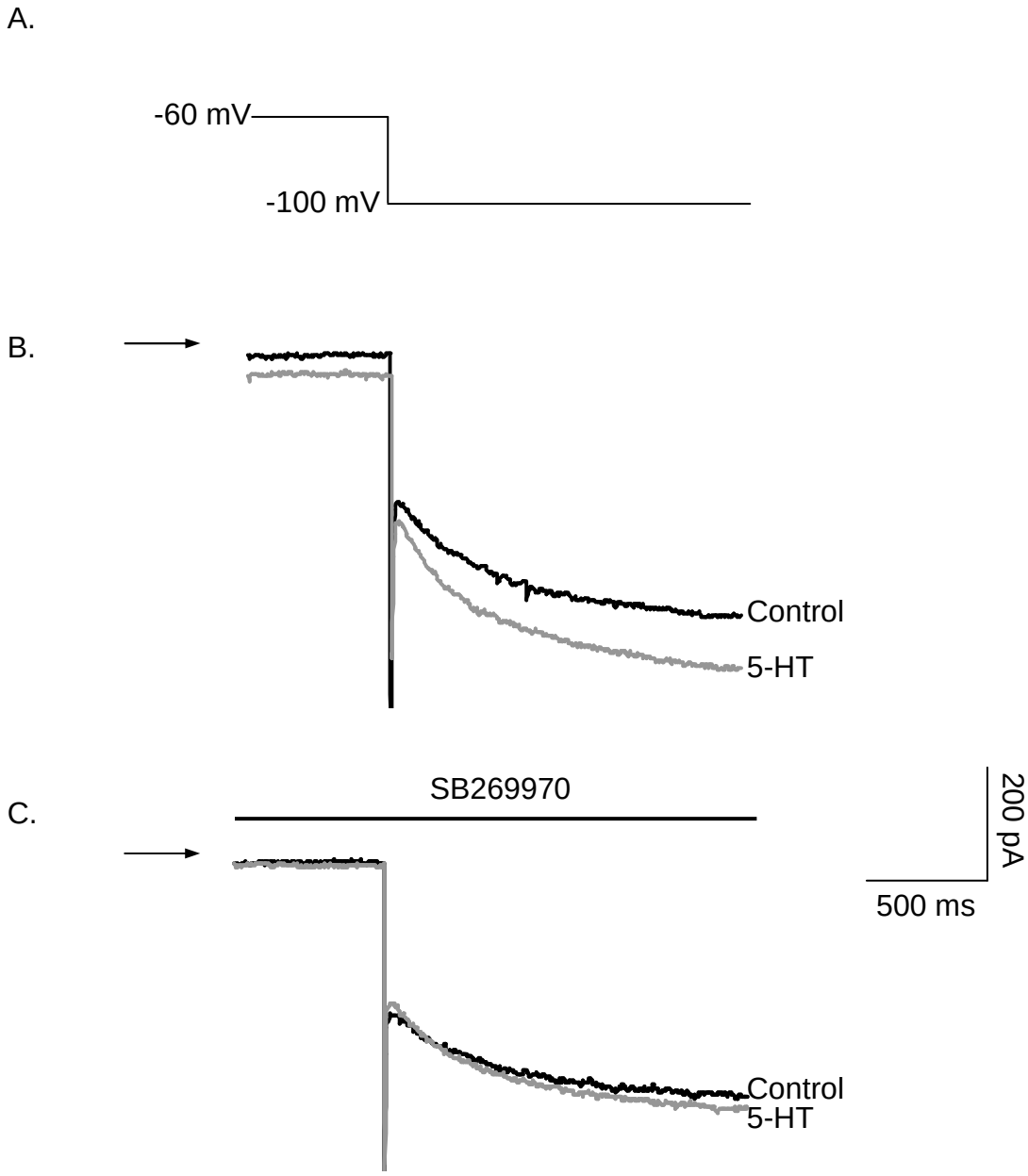

Figure 4.8. SB269970 (10 μM) reduces the enhancement of I_h by 5-HT.

A. Hyperpolarizing current command used to monitor changes in I_h.

B. Current responses to hyperpolarizing voltage (A) from a facial motoneuron in 12 mM K^+ ACSF in the presence (grey) and absence (black) of 5-HT (10 μM). The arrow indicates the –200 pA level.

C. Current responses to hyperpolarizing voltage (A) from a facial motoneuron in 12 mM K^+ ACSF in the presence (grey) and absence (black) of 5-HT (10 μM), following incubation with the 5-HT_7 receptor antagonist, SB269970 (10 μM) for 10 minutes. The enhancement of I_h by 5-HT is reduced compared to control. The arrow indicates the –200 pA level.

5-HT in the presence of SB269970 (10 μM) was 59 ± 14 pA, representing an increase of 15 ± 2 % (n = 4). Thus the enhancement of I_h in the presence of SB269970 (10 μM) was significantly reduced to 58 ± 5 % of control (P = 0.004, one sample *t* test, n = 4).

The high antagonist concentration used in the above experiment raised the possibility that other receptor subtypes were being affected by the antagonist, thus the experiment was repeated using a lower concentration. 5-HT (10 μM) was bath-applied to a FM voltage-clamped at –60 mV and the current response to a hyperpolarising voltage step demonstrates that, in this example, 5-HT enhances I_h by approximately 129 pA (Figure 4.9B). Bath application of SB269970 (0.3 μM) for a minimum of 10 minutes to the recorded FM had no effect on the membrane current (-237 ± 132 pA under control conditions and -254 ± 141 pA in SB269970, P = 0.22, paired *t* test, n = 3). Figure 4.9C demonstrates that when 5-HT (10 μM) was co-applied with the antagonist the enhancement of I_h by 5-HT was reduced to 2 pA. The mean enhancement of I_h by 5-HT was reduced to 29 ± 14% of control in the presence of SB269970 (0.3 μM) (n = 3, P = 0.04, one sample *t* test, Figure 4.9C).

The enhancement of I_h by 5-HT was significantly reduced by both 0.3 μM and 10 μM of SB269970 and the effects of these two antagonist concentrations were not significantly different from each other (P = 0.1, unpaired *t* test). These data indicate that activation of 5-HT_7 receptors mediates the enhancement of I_h by 5-HT in FMs.

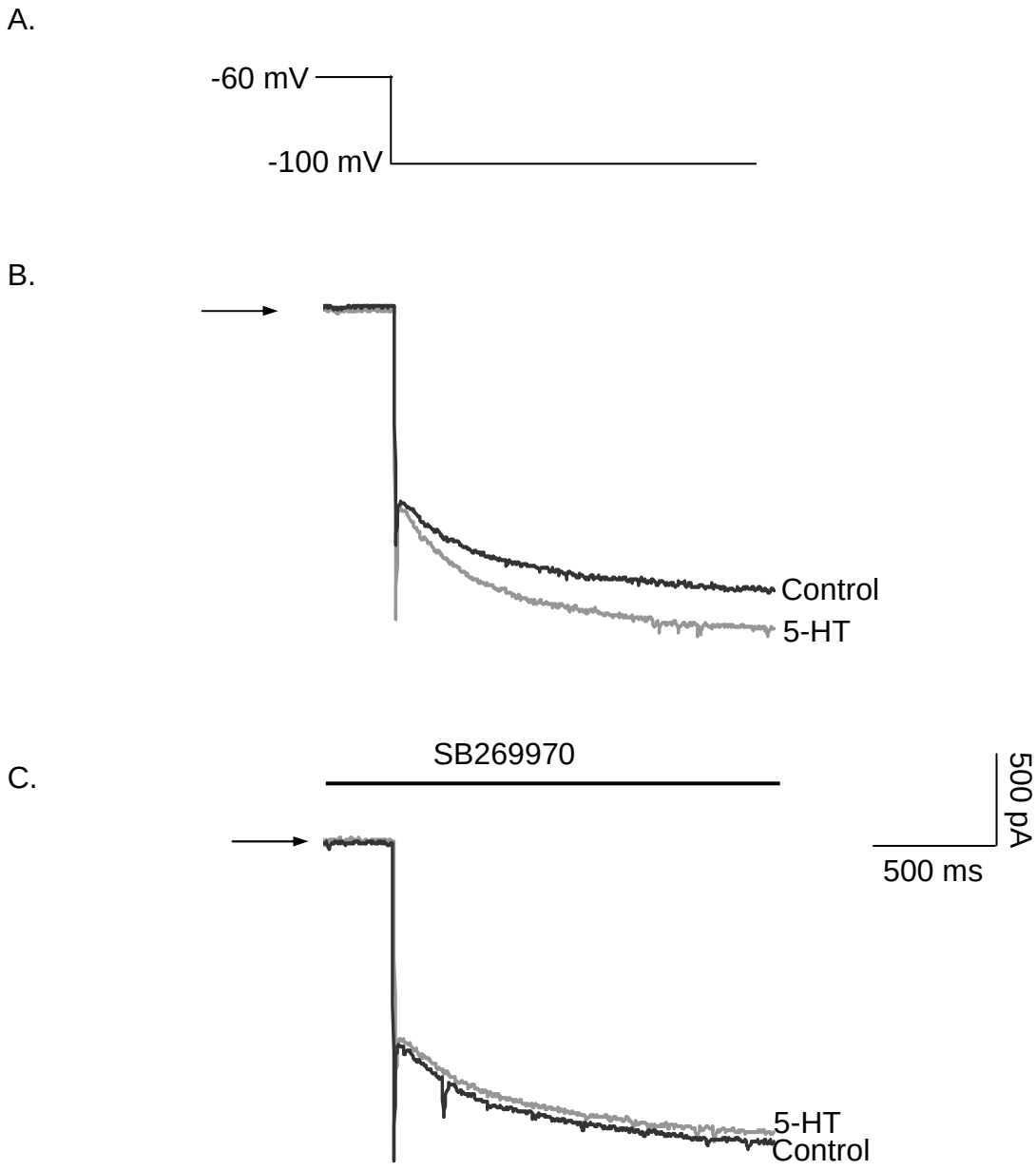

Figure 4.9. SB269970 (0.3 μM) reduces the enhancement of I_h by 5-HT.

A. Hyperpolarizing current command used to monitor changes in I_h.

B. Current responses to hyperpolarizing voltage (A) from a facial motoneuron in 12 mM K^+ ACSF in the presence (grey) and absence (black) of 5-HT (10 μM). The arrow indicates the -500 pA level.

C. Current responses to hyperpolarizing voltage (A) from the same facial motoneuron in 12 mM K^+ ACSF in the presence (grey) and absence (black) of 5-HT (10 μM), following incubation with the 5-HT_7 receptor antagonist, SB269970 (0.3 μM) for 10 minutes. The enhancement of I_h by 5-HT is reduced compared to control (B). The arrow indicates the –500 pA level.

4.2.5 α_1-adrenoceptors mediate inhibition of gK_{leak} in FMs.

NA also promotes FM excitability by inhibiting gK_{Leak} in FMs (Chapter 3) and the adrenoceptor subtype mediating this action of NA has been investigated. The α-adrenoceptor agonist, phenylephrine (PE), mimicked the ability of NA to inhibit gK_{Leak} with an EC_{50} of ~1 μM (n = 12, Figure 4.10). The β-adrenergic receptor agonist isoproterenol (5 - 100 μM) had no effect on gK_{Leak} (n = 3). NA- and PE-induced inhibition of gK_{Leak} could be abolished by bath-application of the α_1-adrenergic receptor antagonists, prazosin (0.5 – 1 μM, n = 5) (Figure 4.10A, B). Modulation of gK_{Leak} by NA and PE was not blocked by the β-adrenergic receptor antagonist propranolol (10 μM; n = 3, Figure 4.10D).

Chapter 3 described the identification of gK_{Leak} based on its pH-sensitivity and it is known that lowering external pH has been shown to alter agonist receptor interactions for some adrenoceptors. It was therefore important to confirm the identity of the adrenoceptor mediating these actions in FMs as the α_1-adrenoceptor as this subtype is not sensitive to changes in external pH (Curro and Greenberg 1983; Nunnari, Repaske et al. 1987; Tateishi and Faber 1995).

4.3 Mechanism for inhibition of gK_{Leak}

The receptors that mediate the inhibition of gK_{Leak} (5-HT_{2A} and α_1-adrenoceptors) are both coupled to G_q proteins. The G_q pathway stimulates phospholipase-C activity which in turn increases the hydrolysis of phosphatidylinositol biphosphate (PIP_2) in the membrane (Alberts, Johnson et al. 2002). This results in the generation of the intracellular messengers inositol triphosphate (IP_3) and diacylglycerol (DAG)

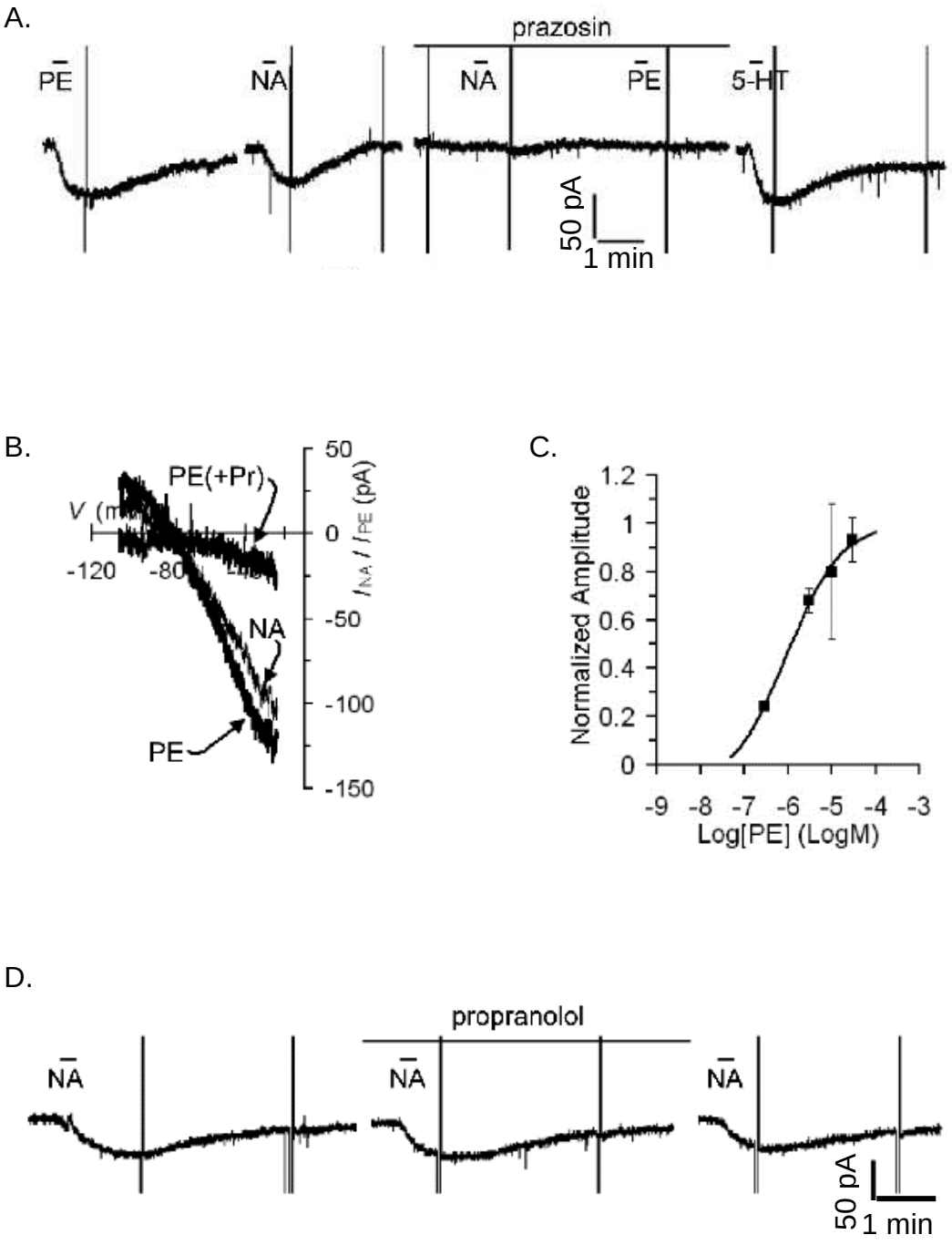
A.
prazosin
PE
NA
NA
PE
5-HT
50 pA
1 min
B.
PE(+Pr)
V (m
-120
-80
NA
PE
50
0
-50
-100
-150
I_NA / I_PE (pA)
C.
Normalized Amplitude
1.2
1
0.8
0.6
0.4
0.2
0
-9 -8 -7 -6 -5 -4 -3
Log[PE] (LogM)
D.
propranolol
NA
NA
NA
50 pA
1 min

Figure 4.10. Noradrenaline inhibits gK_{Leak} through activation of α_1 adrenoceptors.

A. Continuous current records from an FM voltage-clamped at -60 mV showing that the inward currents evoked by bath-application of phenylephrine (PE, 30 μM) and NA (5 μM) were inhibited by the α_1 receptor antagonist, prazosin (0.5 μM). The response to 5-HT (10 μM) was unaffected by this antagonist.

B. The NA- and PE-induced currents, obtained by subtraction of current responses to voltage ramps, share the same biophysical properties and are blocked over the whole voltage range by prazosin.

C. Dose response curve for PE. Response amplitude was normalised to the response to 5-HT (10 μM). Data points represent mean ± SEM for 5 different FMs. The solid line represents a fit of the data to (Methods Equation 3) with an EC_{50} of 1 μM and a Hill slope of 0.71.

D. Continuous current records from an FM voltage-clamped at -60 mV showing a lack of effect of the β-adrenergic receptor antagonist, propranolol (10 μM), on the currents induced by NA (5 μM).

(Alberts, Johnson et al. 2002). However, initial studies have determined that the downstream effects of these molecules (increased $[Ca^{2+}]_i$ and PKC activation, respectively) are not involved in the inhibition of gK_{Leak} (Larkman and Kelly 1998; Larkman, Perkins et al 2003). More recently it has been determined that the excitatory effects of activation of 5-HT_2 receptors can occur without the involvement of DAG or IP_3 signalling (Czirjak, Petheo et al. 2001; Lopes, Rohacs et al. 2005). Instead it appears that PIP_2 depletion from the membrane underlies an agonist-induced inhibition of K_{2P} and M channels (Czirjak, Petheo et al. 2001; Lopes, Rohacs et al. 2005). This mechanism for inhibition of gK_{Leak} in FMs has been further investigated.

4.3.1 PLC-β1 is present in the facial nucleus

Figure 4.11 shows a representative sample section (48 µm thick) from a wild type mouse (8 days old) stained with an antibody to PLC-β1 (1 in 2000 dilution). The facial nucleus displays low, but distinct, levels of immunoreactivity for PLC-β1 indicating that this enzyme is present in FMs. Although the presence of PLC-β1 in the FMN supports a role of this enzyme in the agonist-induced inhibition of gK_{Leak} other G_q coupled-receptors may be present in FMs which may also require PLC-β activity.

The functional contribution of PLC-β1 to the 5-HT- and NA-induced inhibition of gK_{Leak} was assessed using mice in which PLC-β1 had been knocked out. Table 4.1 summarises the data from 3 PLC-$\beta1^{-/-}$ mice and 6 littermate controls. Neither the amplitude nor density of the current induced by 5-HT were significantly different in the PLC-$\beta1^{-/-}$ mice (Table 4.1). However, both the amplitude and the density of

A.

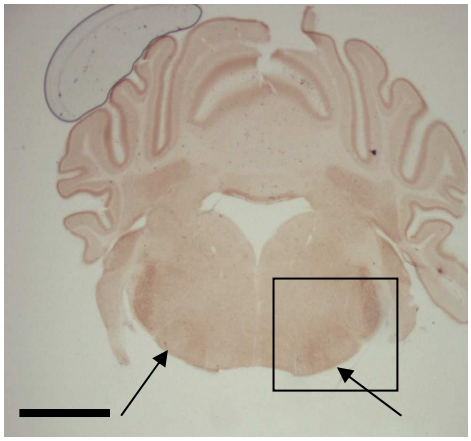

B.

Figure 4.11. PLC-β is present in the facial nucleus.

A. Representative section from a P8 wildtype mouse demonstrates immunoreactivity for PLC-β1 in the facial nucleus (arrows). The scale bar represents 1.5 mm.

B. Higher magnification of section highlighted by the box in A. The presence of PLC-β1 in the FMN can be clearly seen (arrow). The scale bar represents 400 µm.

	Control / PLC-β1$^{-/+}$ (N = 6)	**PLC-β1$^{-/-}$ (N = 3)**
$I_{5\text{-}HT}$ Amplitude (pA)	-54.5 ± 11.6 (n = 10)	-60.7 ± 13.5 (n = 6)
$I_{5\text{-}HT}$ Density (pA/pF)	-1.96 ± 0.44 (n = 10)	-1.87 ± 0.57 (n = 6)
I_{NA} Amplitude (pA)	-44.3 ± 9.7 (n = 7)	**-9.8 ± 5.1 (n = 6)***
I_{NA} Density (pA/pF)	-1.72 ± .047 (n = 7)	**-0.34 ± 0.57 (n = 6)****

Table 4.1. PLC-β1$^{-/-}$ mice show significantly reduced NA-induced current.
Current amplitude was measured at a holding potential of -58 mV. Statistical significance was assessed by Student's *t* test ($^{*}P < 0.01$, $^{**}P < 0.001$, N = number of animals, n = number of recordings).

the current induced by NA were significantly lower in the PLC-β1$^{-/-}$ mice compared to their littermate controls (Table 4.1). $I_{5\text{-HT}}$ might not be reduced in the PLC-β1$^{-/-}$ mice for several reasons. Firstly, our sample size may be too small, secondly 5-HT$_2$ receptors may couple to a different isoform of PLC-β or thirdly PLC-β might not be involved.

The contribution of other isoforms was investigated using the non-specific PLC-β inhibitor, U73122 (Bleasdale, Bundy et al. 1989). The mean control 5-HT-induced current at -50 mV was -103 ± 38 pA. Following incubation in ACSF containing U73122 (10 μM) the 5-HT-induced current was -97 ± 30 pA (n = 3). The lack of effect of the inhibitor suggested that PLC activity is not required for this action of 5-HT. However, one possibility is that the incubation time in these acute application experiments is not long enough to allow U73122 to enter the FMs at a high enough concentration to inhibit PLC-β isoforms. In an attempt to address this an alternative experimental approach was taken and U73122 was included in the internal solution. Responses to 5-HT obtained from FMs when U73122 was included in the pipette were compared with control responses to 5-HT obtained from FMs in the same slices using patch pipettes that did not contain the inhibitor. A control 5-HT-induced current of -26 ± 5 pA (at -50 mV) was obtained from three applications of 5-HT. In another FM from the same slice in which U73122 (5 μM) was included in the internal solution, the 5-HT-induced current were +21 and +13 pA (2 applications of 5-HT). From this limited data the indications are that an isoform of PLC may be required for the 5-HT-induced inhibition of gK_{Leak}. However, more extensive studies will be needed to confirm these initial observations.

4.4 Discussion

4.4.1 5-HT_2 receptor activation inhibits gK_{Leak}

Activation of 5-HT_2 receptors mediates the excitatory action of 5-HT by decreasing potassium conductances in several types of neurons including rat nucleus accumbens neurons and pyramidal neurons in the piriform cortex (North and Uchimura 1989; Sheldon 1991). 5-HT_{2A} receptor protein and mRNA for both the 5-HT_{2A} and 5-HT_{2C} receptors have been detected in the FMN (Pompeiano, Palacios et al. 1994; Cornea-Hébert 1999; Fonseca, Ni et al. 2001; Volgin, Fay et al. 2003). The 5-$HT_{2A/2C}$ selective agonist, 1-[2,5-demethoxy-4-methylphenyl]-2-aminopropane (DOM), has previously been shown to have excitatory effects on FMs (Rasmussen and Aghajanian 1990). These findings suggested that 5-HT_{2A} or 5-HT_{2C} receptor activation could mediate the inhibition of gK_{Leak} and this was investigated further.

Application of the 5-HT_{2A} receptor antagonist, R96544 (0.3 μM or 1 μM) had no effect on FM membrane current but did significantly block the 5-HT-mediated inhibition of gK_{Leak}.

4.4.2 Selectivity of R96544

R96544 has 100-fold lower affinity for 5-HT_{1A}, 5-HT_{1B}, 5-HT_{1D}, 5-ht_{5A}, 5-HT_6 and 5-HT_7 receptors and was found to be ineffective at modulating 5-HT_3- or 5-HT_{2B}-mediated actions of 5-HT (Ogawa, Sugidachi et al. 2002). However, R96544 does display relatively high affinity for 5-HT_{2C} receptors (although 4-fold less than 5-HT_{2A} receptors), therefore the action of this antagonist in FMs does not rule out the involvement of 5-HT_{2C} receptors in the 5-HT-mediated modulation of gK_{Leak}

(Ogawa, Sugidachi et al. 2002). A similar set of experiments performed using RS-101221, which has 100-fold selectivity for 5-HT_{2C} receptors over 5-HT_{2A} receptors would conclusively determine the contribution of 5-HT_{2A} and/or 5-HT_{2C} receptors to the 5-HT-mediated excitation of FMs (Bonhaus, Weinhardt et al. 1997).

4.4.3 Developmental changes in 5-HT_2 receptor expression

It is worthwhile noting that the experiments with R96544 were performed on neonatal rats aged between postnatal days 4 and 16 and one study has documented the postnatal development of 5-HT_2 receptors in hypoglossal motoneurones (Volgin, Fay et al. 2003). In hypoglossal motoneurones the expression of 5-HT_{2A} mRNA was higher compared to 5-HT_{2C} mRNA expression in rats aged 3-14 days old (Volgin, Fay et al. 2003). The percentage of motoneurones expressing 5-HT_{2C} mRNA increased with age, however, expression of 5-HT_{2C} mRNA alone was never observed (Volgin, Fay et al. 2003). This study also describes the increase in 5-HT_{2A} immunoreactivity in the FMN postnatal days 5 and 19 (Volgin, Fay et al. 2003). If a similar change in 5-HT_{2C} receptor expression occurs in the FMN this could significantly affect any further studies into the role of 5-HT_{2A} and 5-HT_{2C} receptors in this nucleus and should, therefore, be investigated further by immunohistochemical analysis of receptor expression between postnatal days 4 and 16.

4.4.4 5-HT_7 receptor activation enhances I_h

5-HT enhances I_h through a direct action of cAMP on the channel and previous investigations failed to identify the receptor subtype mediating this effect of 5-HT (Larkman and Kelly 1997). 5-HT_4, 5-HT_6 and 5-HT_7 receptors are all coupled

positively to adenylate cyclase and enhance cAMP production, therefore, representing potential candidates for the receptor mediating the enhancement of I_h in FMs. The 5-HT_4 receptor antagonist, GR-113808A, and the 5-$HT_{6/7}$ receptor antagonist, clozapine, had no effect on the enhancement of I_h by 5-HT (Larkman and Kelly 1997). 5-HT_7 receptors have been implicated in the 5-HT-mediated enhancement of I_h in CA1 hippocampal neurons, in the anterodorsal thalamus and in dorsal root ganglion neurons (Cardenas, Del Mar et al. 1999; Chapin and Andrade 2001; Bickmeyer, Heine et al. 2002). The potential role of this receptor subtype was further investigated in FMs using the highly selective 5-HT_7 receptor antagonist, SB 269970, (100-fold higher affinity for 5-HT_7 over other 5-HT receptors) (Lovell, Bromidge et al. 2000). SB 269970 significantly decreased the enhancement of I_h by 5-HT indicating 5-HT_7 receptors mediate this action of 5-HT. The 5-HT_7 receptors are the most recently identified members of the 5-HT receptor family and their action in FMs provides evidence for novel functional role in the modulation of motor activity.

4.4.5 α_1-adrenoceptors mediate NA-induced inhibition of gK_{Leak}

The pharmacology of the NA-induced inhibition of gK_{Leak} was investigated in FMs and suggested a α_1-adrenoceptor subtype. This is consistent with the signal transduction mechanism of α_1-adrenoceptors (increased PLC-β activity via G_q protein activity) being the same as that of 5-HT_2 receptors which were found to mediate the 5-HT induced inhibition of gK_{Leak} (Alberts, Johnson et al. 2002).

This finding also suggests that occlusion of the NA-mediated modulation of gK_{Leak} by low external pH (Chapter 3) is not due to altered agonist-receptor interactions as

α_2- but not α_1-adrenoceptors show altered functional responses associated with changes in agonist binding affinity over the pH range 6 to 8 (Curro and Greenberg 1983; Nunnari, Repaske et al. 1987; Tateishi and Faber 1995).

4.4.6 Agonist and antagonist concentrations used in slices

The concentrations of the agonists and antagonists used in these experiments are much higher than the EC_{50} or IC_{50} values reported in the literature for *in vitro* assays. This is common for slice electrophysiology as the dense extracellular matrix in slices can reduce access of the drug to the cell that is being studied. In addition, uptake or metabolism of some compounds may also occur, reducing the actual concentration around the recorded cell. For example, the reported affinities for 5-HT at 5-HT_2 and 5-HT_7 receptors are 1 – 17 nM (K_i or K_d values) whereas 10 µM 5-HT is required to routinely produce a maximal response in FMs (Peroutka and Snyder 1979; Ruat, Traiffort et al. 1993). R96544 has a reported IC_{50} of 2.2 nM, however, 0.3 µM R96544 only partially blocked the 5-HT-induced inhibition of gK_{Leak} and 10 µM fully blocked this response to 5-HT (Ogawa, Sugidachi et al. 2002). These concentrations are unlikely to effect most other 5-HT receptor subtypes due to the high selectivity of this compound for the 5-HT_{2A} receptor (Ogawa, Sugidachi et al. 2002). However, these concentrations may also block 5-HT_{2C} receptors and the contribution of this subtype should be further investigated (see section 4.4.2). The reported K_d values for SB269970 binding to 5-HT_7 receptor-expressing HEK293 cells and guinea pig cortex membranes are 1.25 ± 0.3 nM and 1.7 ± 0.3 nM, respectively (Thomas, Atkinson, et al. 2000). In this study 0.3 – 10 µM SB269970 was used, however, due to the high selectivity of this antagonist for 5-HT_7 receptors

over the other subtypes it is unlikely that even at these concentrations other 5-HT receptors were blocked (Lovell, Bromidge et al. 2000).

4.4.7 Mechanism for receptor activation leading to inhibition of gK_{Leak}

Inhibition of FM gK_{Leak} by 5-HT involves activation of 5-HT_2 receptors and α_1 adrenoceptors mediate the similar actions of NA. Both receptor subtypes couple through G_q proteins to phospholipase C (PLC)-mediated hydrolysis of phosphatidyl-4,5-inositol-bisphosphate (PIP_2). The detection of PLC-β1 in the FMN by immunohistochemistry raises the possibility that modulation of gK_{Leak} by these neurotransmitters may involve activation of this enzyme. This is supported by the finding that in PLC-$\beta1^{-/-}$ mice the NA-induced current is significantly altered. However, previous studies have demonstrated that altering the downstream pathways of PLC (increased $[Ca^{2+}]_I$ and PKC signaling) did not affect gK_{Leak} (Larkman 2003).

G_q-coupled muscarinic M_1 and group 1 metabotropic glutamate receptors, but not G_i-coupled muscarinic M_2 receptors, inhibit co-expressed human TASK-1 and TASK-3 channels through a PIP_2 hydrolysis-dependent pathway (Czirjak, Petheo et al. 2001; Chemin, Girard et al. 2003). The PLC inhibitor, U73122, did reduce the inhibition of TASK-1 following M_1 receptor activation, however, the downstream signals of phospholipase C (Ca^{2+} and DAG) did not appear to be involved (Czirjak, Petheo et al. 2001). Externally applied U73122 did not effect the 5-HT-mediated reduction in gK_{Leak} and although inclusion of U73122 in the internal solution did appear to prevent the inhibition of gK_{Leak} this experiment did lack a direct control response to 5-HT.

PIP_2 has been shown to directly activate several K_{2P} channels and it is proposed that PIP_2 depletion from the membrane underlies the agonist-induced inhibition of these channels (Lopes, Rohacs et al. 2005). Modulation of the activity of membrane ion channels is emerging as a common role for PIP_2. KCNQ2/3 channels (which underlie the M current) can be activated by PIP_2 application and recovery from agonist-induced inhibition of the channel is dependent on PIP_2 synthesis (Suh and Hille 2002; Zhang, Craciun et al. 2003). Additionally, G protein-gated inwardly rectifying K^+ channels, inwardly rectifying background K^+ channels, human *ether-a-go-go*–related gene (HERG) K^+ channels and N-type Ca^{2+} channels have all been shown to be regulated by PIP_2 (Huang, Feng et al. 1998; Bian, Cui et al. 2001; Gamper, Reznikov et al. 2004; Cho, Lee et al. 2005).

Although the PLC-mediated hydrolysis of PIP_2 has been shown to modulate the activity of several ion channels, one study suggests that inhibition of TASK-1 and TASK-3 channels is through a direct action of the Gα subunit and is independent of PLC and PIP_2 (Chen, Talley et al. 2006).

4.5 Concluding statement

This chapter has investigated the receptor subtypes which mediate the excitatory actions of 5-HT and NA in neonatal FMs. The inhibition of gK_{Leak} by 5-HT and NA was mediated by activation of 5-HT_{2A} receptors (and possibly 5-HT_{2C} receptors) and α_1-adrenoceptors, respectively. The enhancement of I_h was found to be a result of activation of 5-HT_7 receptors providing a novel functional role for this receptor subtype.

In addition, the mechanism by which 5-HT_2 receptor and α_1-adrenoceptor activation leads to inhibition of gK_{Leak} was investigated. The detection of PLC-β1 in the FMN and the finding that PLC-$\beta1^{-/-}$ mice show reduced NA-induced current supports a role for this enzyme in the inhibition of gK_{Leak}. However, the mechanism by which this occurs does not appear to be via the conventional signaling pathways of this enzyme. One possibility is that PIP_2 in the membrane support the channel in its open state and its PLC-mediated hydrolysis results in channel closure.

Chapter 5

5.1 Introduction

5.1.1 Excitatory synaptic transmission

Glutamate is the principal excitatory neurotransmitter within the mammalian CNS and preliminary studies indicate glutamate has excitatory actions on FMs (VanderMaelen and Aghajanian 1980). Fast synaptic responses to glutamate are mediated by three subtypes of ionotropic receptors characterized by the selective agonists that activate them: *N*-methyl-D-aspartate (NMDA), α-amino-3-hydroxy-5-methyl-4-isoxazolepropionic acid (AMPA) and kainate (Figure 5.1).

5.1.2 Glutamate receptors

Glutamate receptors form ion channels that are permeable to Na^+ and K^+. Additionally, NMDA and some AMPA receptors (those lacking the GluR2 subunit) are permeable to Ca^{2+} (Dingledine, Borges et al. 1999). The net effect of the movement Na^+, Ca^{2+} and K^+ ions through the channels mediates a depolarisation of the postsynaptic membrane, if a sufficient depolarization occurs at the cell soma an action potential will be triggered in the postsynaptic neurone. Ca^{2+} influx into the postsynaptic terminal also triggers biochemical effects that can be important for synaptic plasticity (reviewed in (Soderling, Tan et al. 1994; Dingledine, Borges et al. 1999)).

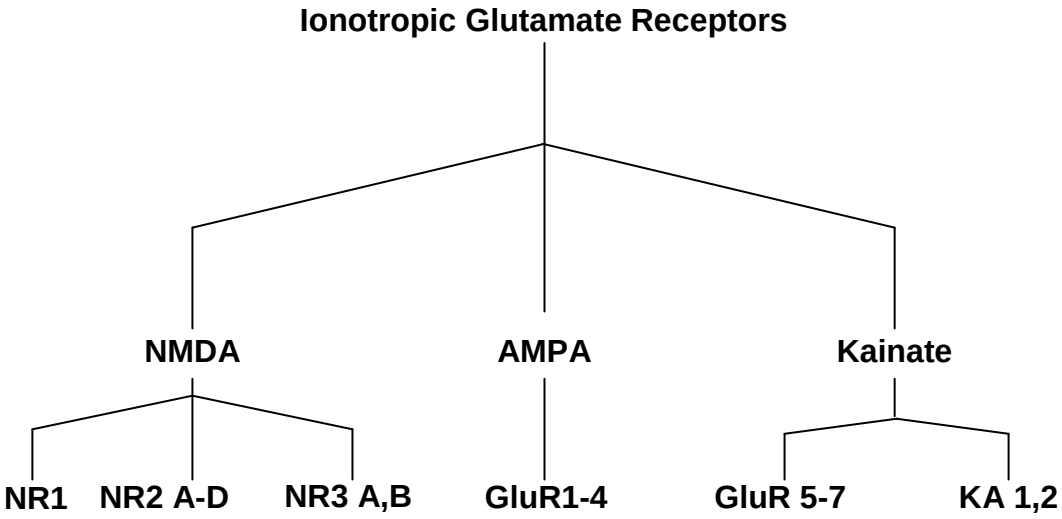

Figure 5.1. Classification of ionotropic glutamate receptors.
Ionotrophic glutamate receptors are classified according to the selective agonists which activate them.

NMDA and non-NMDA glutamate receptors co-localize at many central synapses and are activated by glutamate with differing time courses (O'Brien, Isaacson et al. 1997; Ozawa, Kamiya et al. 1998). AMPA glutamate receptors have fast kinetics, their permeability to Ca^{2+} is dependent on subunit composition and they are not blocked by extracellular Mg^{2+}. Conversely NMDA receptors have intrinsically slow kinetics, are highly permeable to Ca^{2+} and show a voltage-dependent block by Mg^{2+} (Mayer, Westbrook et al. 1984). Removal of the Mg^{2+} block of NMDA receptors (and their subsequent activation by glutamate) occurs following the depolarization of the membrane which occurs when non-NMDA glutamate receptors are activated (Mayer, Westbrook et al. 1984).

Originally, glutamate receptors were thought to exist as pentamers, however, evidence now exists supporting a tetrameric structure from studies on NMDA and GluR2 receptors (Schorge and Colquhoun 2003; Tichelaar, Safferling et al. 2004). Functional NMDA glutamate receptor requires both the NR1 and an NR2 subunit. This is due to the glutamate binding site being located on the NR2 subunit and the binding site for the obligatory co-agonist, glycine, on the NR1 subunit (Kleckner and Dingledine 1988; Dingledine, Borges et al. 1999).

5.1.3 Glutamate receptors in the FMN

Glutamate receptors are widely expressed throughout the mammalian CNS and immunohistochemistry and *in situ* hybridisation studies have identified AMPA, NMDA and kainate receptor subunits in the FMN. All four of the known AMPA receptor subunits are present in the FMN, with GluR2, 3 and 4 showing higher expression than the GluR1 subunit (Martin, Blackstone et al. 1993; Sato, Kiyama et

al. 1993). The expression patterns of kainate receptors subunits (GluR 5-7, KA1-2) has been less well examined and only moderate staining with GluR6/7 and KA2 specific antibodies has been reported in the FMN (Petralia, Wang et al. 1994).

All NMDA receptors are believed to contain at least one NR1 subunit, this subunit contains the binding site for the obligatory co-agonist, glycine. NR1 is highly expressed in most central neurones, including FMs (Petralia, Yokotani et al. 1994). The glutamate-binding site for NMDA receptors is located on the NR2 subunit, of which there are four known subtypes (NR2A-D). Immunohistochemistry using an antibody that recognizes both NR2A and NR2B subunits shows positive staining in the FMN, however, it has been well reported that NMDA receptor subunit composition changes during development (Petralia, Wang et al. 1994). Members of a third class of NMDA receptor (NR3A-B) have also been cloned although the role of this subunit is not fully understood. NR3 subunits are insensitive to glutamate and can be expressed with NR1 subunits to form excitatory glycine receptors that are relatively Ca^{2+}-impermeable and insensitive to block by extracellular Mg^{2+} (Chatterton, Awobuluyi et al. 2002). When co-expressed with NR1 and NR2 subunits, members of the NR3 class reduce the glutamate-induced current in a dominant-negative manner (Nishi, Hinds et al. 2001; Chatterton, Awobuluyi et al. 2002). Interestingly, NR3 subunits are found predominantly in motoneurones including those of the FMN (Nishi, Hinds et al. 2001).

5.1.4 Aims

The aim of this chapter was to characterise excitatory synaptic transmission in neonatal rat facial motor neurones. The interpretation of any effects of 5-HT on synaptic integration would be simplified if single synapses were being activated so minimal stimulation protocols were used to attempt to stimulate single synapses. Minimal stimulation intensities were applied close to the FM dendrites and evoke excitatory postsynaptic currents (EPSCs) and potentials (EPSPs) that fluctuated in amplitude. Whether these fluctuations in amplitude represented quantal release from a single synapse or stimulation of more than one synapse was further investigated using paired pulse analysis.

The identity of the postsynaptic receptors which mediate EPSCs in FMs was also investigated to provide further insight into synaptic transmission in the facial nucleus. A pharmacological approach was used to identify a non-NMDA and NMDA glutamate receptor component to EPSCs in FMs and the subunit composition of these receptors.

5.2 Results

5.2.1 Evoked EPSCs in facial motoneurones

EPSCs were evoked by positioning a stimulating electrode close to the dendrites of the FM and applying minimal stimulation (see Methods). In a representative FM, voltage-clamped at –70 mV, stimulating close to the dendrites evokes a fast EPSC with mean amplitude of –92 pA (Figure 5.2A, mean of 21 EPSCs including failures).

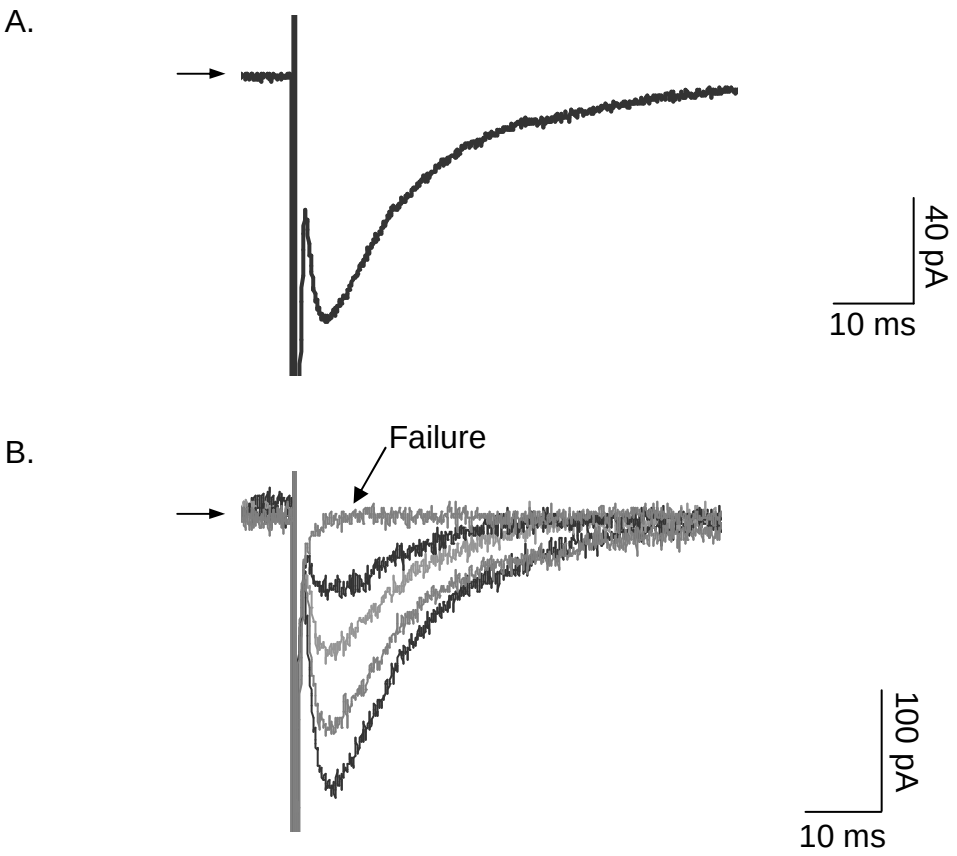

Figure 5.2. Stimulating close to the dendrites of a FM evokes EPSCs.

A. Mean of 21 events (including failures) recorded from a FM voltage-clamped at –70 mV. The arrow indicates the zero current level and the large deflection before the EPSC represents the stimulus artifact.

B. Representative traces from the same FM as A, demonstrating that a constant stimulus intensity occasionally fails to generate a response (failure) and evokes EPSCs that fluctuate in amplitude. The horizontal arrow indicates the zero current level and EPSC were evoked at a frequency of 0.05 Hz.

Figure 5.2B shows example individual traces from the same FM indicating that EPSCs showed discrete amplitude fluctuations and that stimulation occasionally failed to generate an EPSC (a criteria for minimal stimulation). The individual example EPSCs shown in Figure 5.2B had peak amplitudes of 56, 113, 169 and 219 pA. EPSCs evoked using minimal stimulation intensities, at a holding potential of –70 mV, had mean amplitude of –80 ± 3 pA and rise and decay time constants of 1.8 ± 0.6 and 11.1 ± 3.0 ms, respectively (n = 15, Table 5.1).

The fluctuations in EPSC amplitude could occur as a result of release of one or more vesicles from a single synapse or activation of multiple synapses. As the stimulation intensity was increased the rate of failure to evoke an EPSC decreased and eventually more synapses were recruited and the mean EPSC amplitude significantly increased.

5.2.2 Evoked EPSPs in facial motoneurones

After an EPSC was evoked as described above, the recording mode was switched to current-clamp and an excitatory postsynaptic potential (EPSP) recorded. Figure 5.3A shows an example of a mean EPSP, 2.2 mV in amplitude, recorded from a FM at its resting membrane potential (-72.5 mV, mean of 34 events including failures). Individual traces from the same FM demonstrate that EPSPs showed discrete amplitude fluctuations and that stimulation occasionally failed to generate an EPSP (Figure 5.2B). The example EPSPs shown in Figure 5.3B are 0.9, 1.8 and 2.7 mV in amplitude. Figure 5.3B also demonstrates that when the same FM was voltage-clamped at –70 mV, an identical stimulation evoked EPSCs that demonstrated fluctuations in amplitude similar

	EPSC	EPSP
Amplitude	-80 ± 3 pA	1.8 ± 1.3 mV
Rise time constant	1.8 ± 0.6 ms	2.5 ± 1.3 ms
Decay time constant	11.1 ± 3.0 ms	31.7 ± 10.0 ms

Table 5.1. Properties of averaged synaptic events from FMs.

EPSCs were evoked in FMs voltage-clamped at –70 mV (n = 15) using minimal stimulus intensities. EPSPs were measured at the resting membrane potential (-67 ± 3 mV) and evoked using minimal stimulus intensities that generated EPSCs, in the same FMs, with a mean amplitude of –26 ± 10 pA (n = 3).

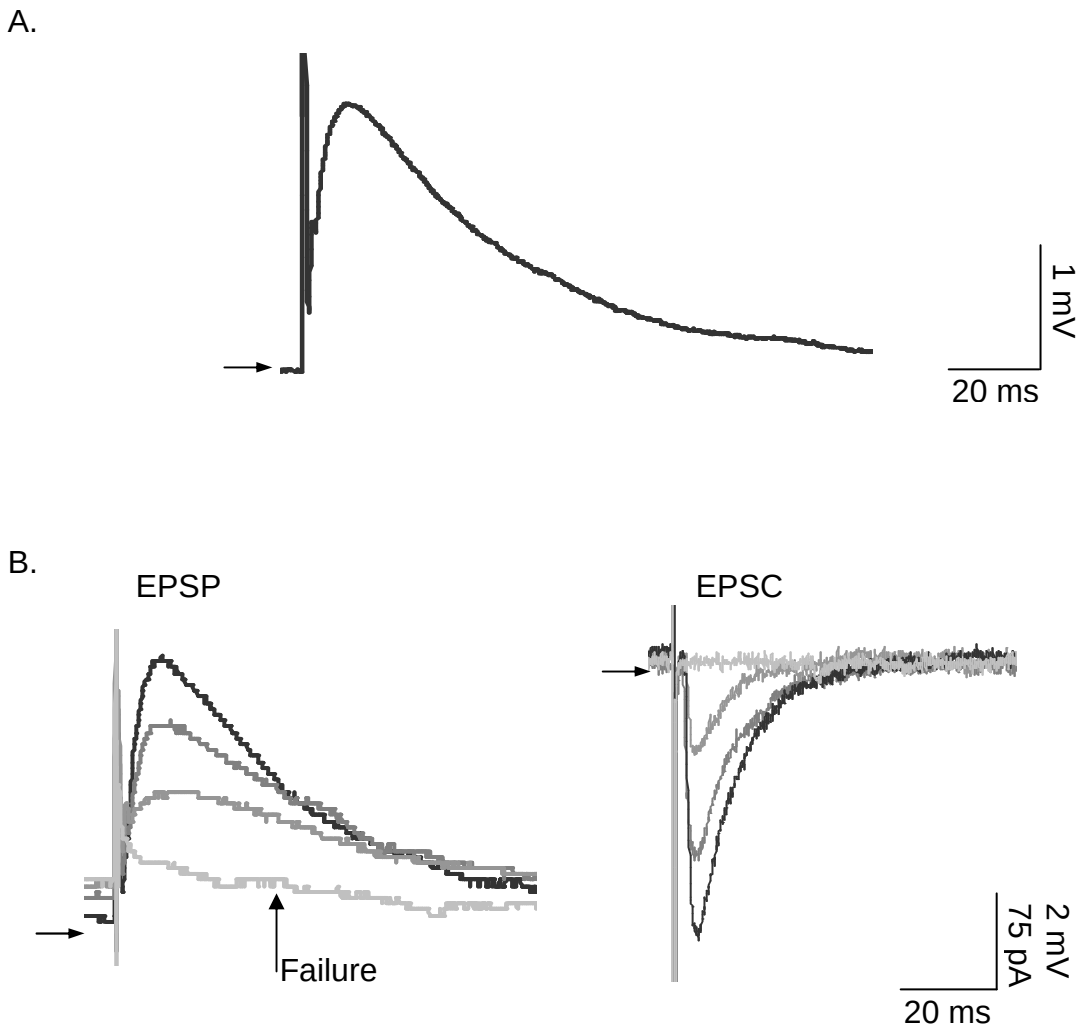

Figure 5.3. Stimulating close to the dendrites of a FM evokes EPSPs.

A. Mean of 34 events (including failures) recorded from a current-clamped FM at the resting membrane potential (-72.5 mV, as indicated by arrow). The large deflection before the EPSP represents the stimulus artifact.

B. Representative traces from the same FM as A, demonstrating that a constant stimulus intensity occasionally failed to generate a response (as indicated) and evoked EPSPs that fluctuate in amplitude. When the same motoneuron was voltage-clamped at –70 mV, an identical stimulation evoked EPSCs with fluctuations in amplitude that corresponded with the EPSPs. The horizontal arrows indicate the –72 mV and the –100 pA levels. Stimulation was applied at a frequency of 0.05 Hz.

to that of the EPSPs (approximately 98, 195 and 285 pA). EPSPs evoked at the resting membrane potential (-68 ± 3 mV), using minimal stimulation intensities that evoked EPSCs with a mean amplitude of –26 ± 10 pA, had mean amplitude of 1.8 ± 1.3 mV and rise and decay time constants of 2.5 ± 1.3 and 31.7 ± 10.0 ms, respectively (n = 3, Table 5.1).

5.2.3 Current-voltage relationship of EPSC amplitude

Current-voltage (I/V) relationships of EPSC amplitude can indicate the ions which pass through the open receptor channel and also provide insight into receptor subunit composition. The I/V plot shown in Figure 5.4A was generated from an average of a minimum of 10 EPSCs from 4-7 FMs for each potential (any failures were omitted from the average). EPSCs from a representative FM demonstrate that the amplitude of individual EPSCs change proportionally with voltage (Figure 5.4B). This I/V relationship had a reversal potential of –17 ± 4 mV (n = 4-7) and was found to be outwardly rectifying (ratio of 2.6, see Methods). This outward rectification occurs as a result of an NMDA glutamate receptor component (see section 5.3) being revealed at potentials where the receptor block by Mg^{2+} is removed (Nowak, Bregestovski et al. 1984). The failure rate did not appear to change when the holding potential was altered suggesting that the probability of vesicle release was not dependent on the postsynaptic membrane potential.

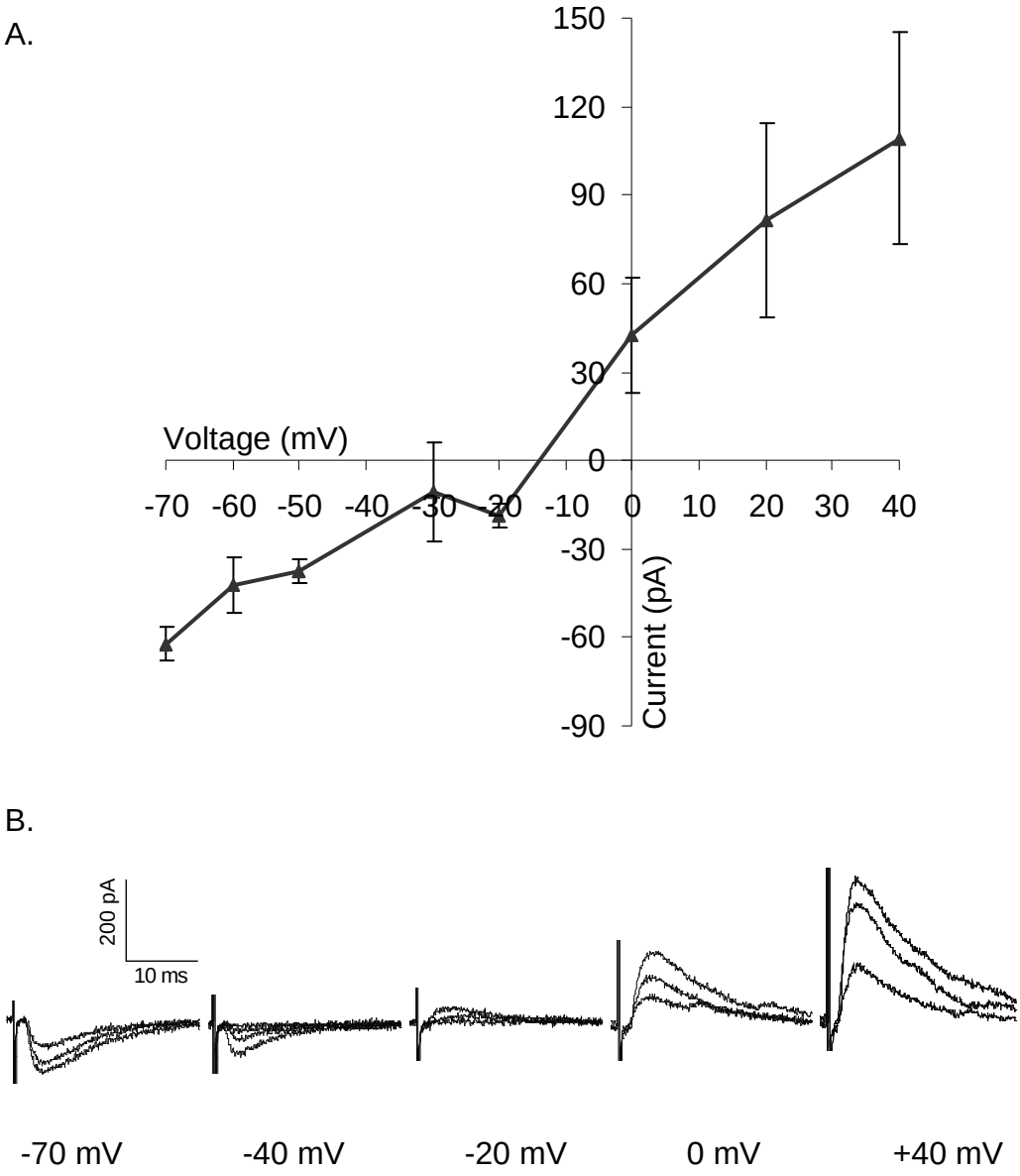

Figure 5.4. Current-voltage relationship of mean EPSC amplitude in FMs.

A. I/V relationship generated from the mean EPSC amplitude (without failures) at each potential (n = 4-7 facial motoneurones, with an average of a minimum of 10 EPSCs at each potential in each cell)

B. Example traces from a representative facial motoneurones demonstrating that the amplitude of individual EPSCs varies relative to the holding potential.

5.2.4 Paired pulse facilitation

Vesicular release of neurotransmitter is dependent on Ca^{2+} influx into the presynaptic terminal. When two identical stimulation pulses are applied close together the residual Ca^{2+} in the presynaptic terminal after the first pulse can increase the probability of release following the second pulse, resulting in the second of a pair of mean EPSCs being larger in amplitude than the first (reviewed in (Zucker 1989)). Minimal stimulation intensities were used to target a minimum number of synapses and occasionally only single synapses were stimulated. Analysis of the paired pulse ratio of two EPSCs evoked close together was used to assess whether single synapses could be stimulated in FMs

Figure 5.5 shows the mean EPSCs evoked by paired stimuli (50 ms apart) in a FM voltage-clamped at –70 mV (including failures). The amplitude of the first mean EPSC in this FM was –25 pA and the amplitude of the second EPSC was –39 pA (including failures, Figure 5.5A). This represents a paired pulse ratio of 1.6 (mean amplitude of EPSC 2/mean amplitude of EPSC 1). When the EPSCs from this FM were averaged excluding the failures, the first EPSC was –37 pA in amplitude and the second EPSC was –36 pA (Figure 5.5B). The lack of paired pulse facilitation when failures were excluded indicates that the EPSCs in this FM were generated by activation of a single synapse (Stevens and Wang 1995). The EPSCs at this putative single synapse show amplitude fluctuations providing evidence supporting quantal release at a central synapse.

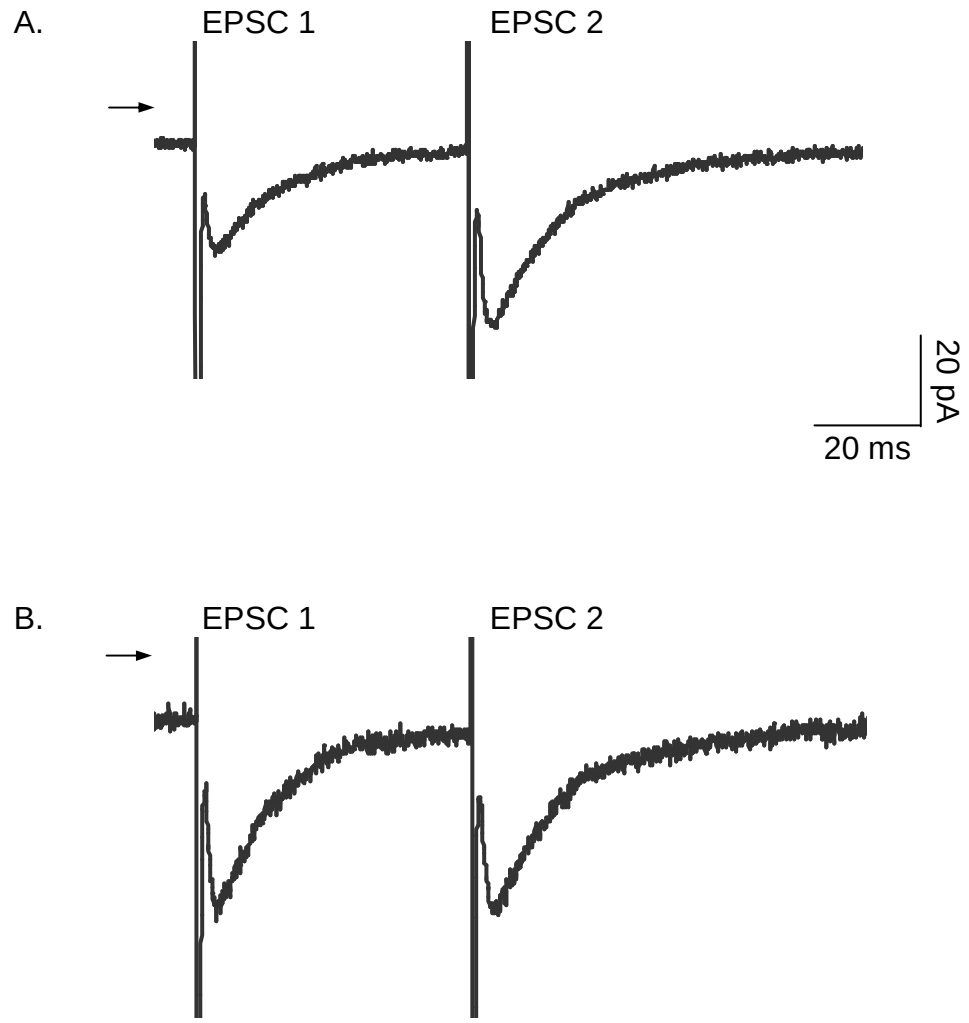

Figure 5.5. Paired pulse facilitation at single synapses.

A. Mean EPSCs (including failures) evoked by paired stimuli (50 ms apart) in a FM voltage-clamped at –70 mV. Note that EPSC 2 is larger than EPSC 1. The arrow indicates the –160 pA level.

B. Mean EPSCs from the same FM as A with failures excluded. Note that now EPSC 1 and 2 are of similar amplitude. The arrow indicates the –160 pA level.

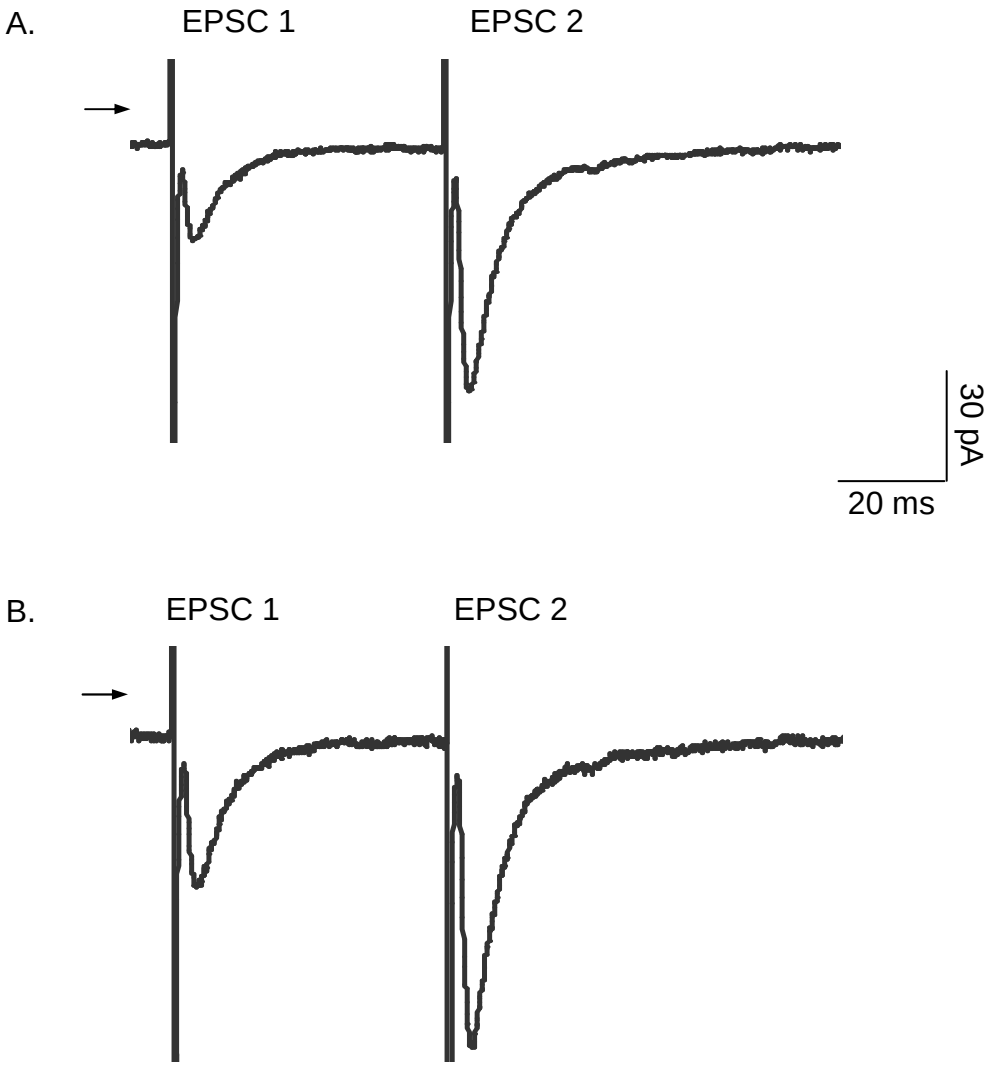

Figure 5.6. Paired pulse facilitation at multiple synapses.

A. Mean EPSCs (including failures) evoked by paired stimuli (50 ms apart) in a FM voltage-clamped at –70 mV. Note that EPSC 2 is larger than EPSC 1. The arrow indicates the –160 pA level.

B. Mean EPSCs from the same FM as A with failures excluded. Note that EPSC 2 is still much larger than EPSC 1. The arrow indicates the –160 pA level.

Figure 5.6A demonstrates paired pulse facilitation in another FM voltage-clamped at -70 mV. When failures were included the first EPSC was –27 pA in amplitude and the second was -73 pA representing a paired pulse ratio of 2.7. When failures were excluded from the mean EPSC in this FM the amplitude of the first EPSC was -40 pA and the amplitude of the second was -83 pA (Figure 5.6B). The paired pulse ratio for this FM was now 2.1. When mean EPSCs still show paired pulse facilitation when failures are excluded (as in this example) it is an indication that the EPSCs are generated by activation of multiple synapses (Stevens and Wang 1995).

An alternative method for assessing the number of synapses activated was also applied to EPSCs evoked in FMs. Cumulative amplitude histograms can be generated by plotting the number of EPSCs in each amplitude bin against amplitude. Clear peaks in these histograms are indicative of quantal amplitudes, however, the accuracy of this analysis method is dependent on having a large sample size. As EPSCs were only evoked every 20 seconds in all recordings insufficient numbers of EPSCs were evoked during the recording period to enable accurate histograms to be generated. Figure 5.7 is a typical example of a cumulative probability histogram of EPSC amplitude from a representative FM. Arrows indicate potential peaks in the histogram but the sample size is insufficient to permit a statistically significant analysis.

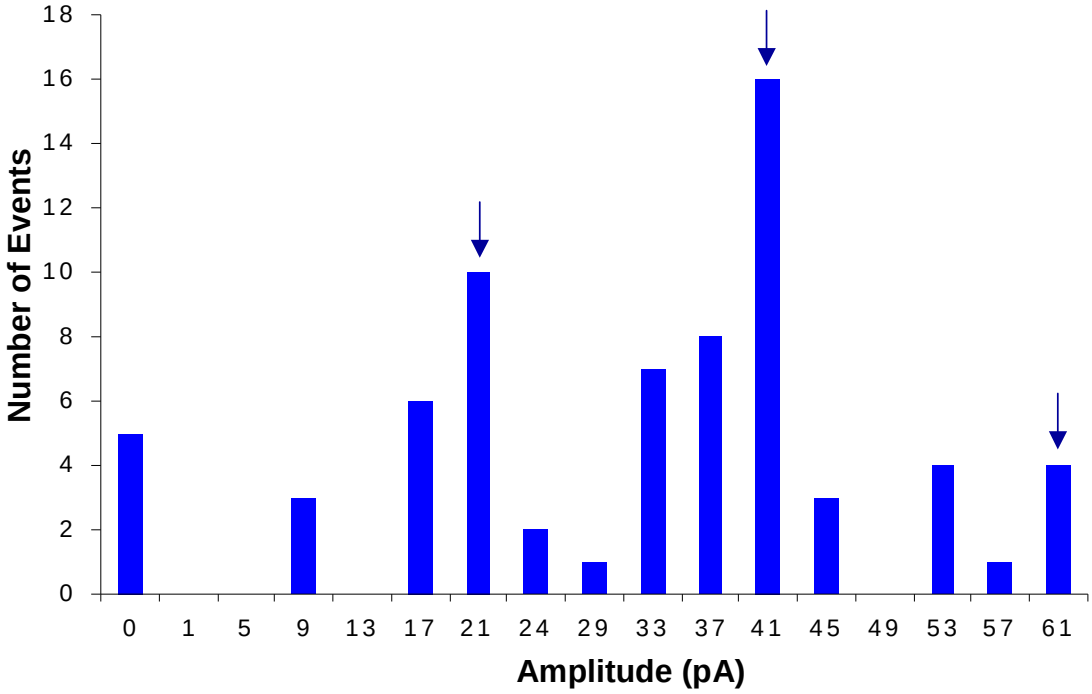

Figure 5.7. Probability histogram of evoked EPSC amplitude.

In this example FM the distribution of individual equally spaced EPSC amplitudes suggests there are three peak amplitudes (indicated by arrows). This could potentially be interpreted as a result of activation of up to three synapses or quantal release from a single synapse.

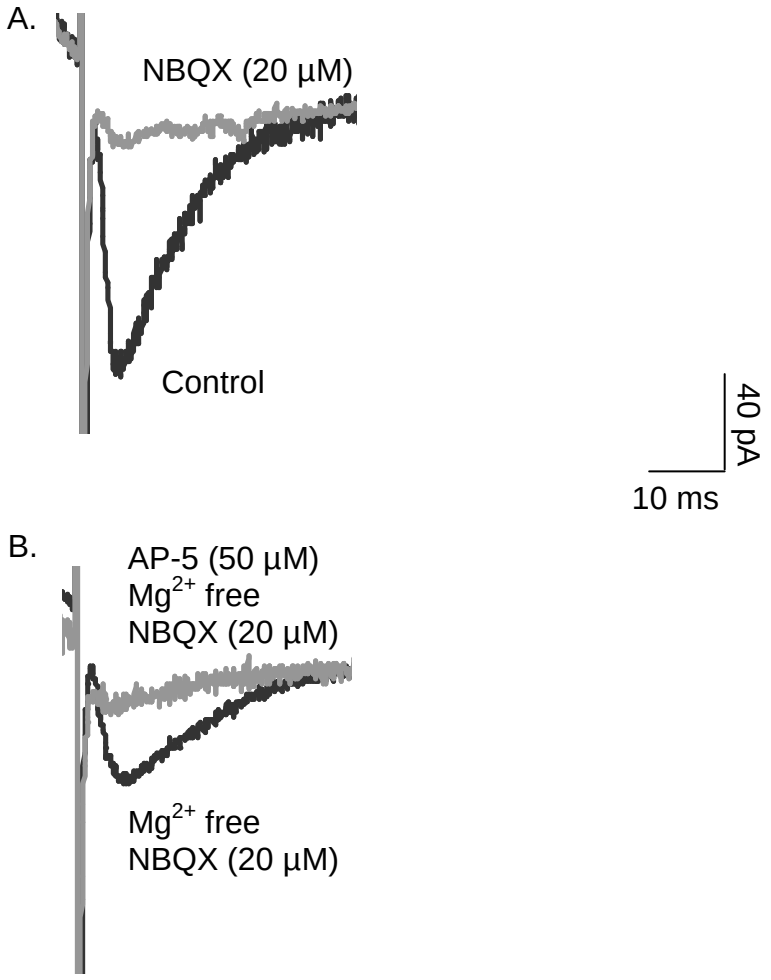

Figure 5.8. Effect of NBQX, AP-5 and removing external Mg^{2+} on EPSC amplitude in FMs.

A. Representative mean EPSCs obtained from a FM voltage-clamped at -70 mV demonstrating that the mean EPSC amplitude is reduced in the presence of NBQX (20 µM, grey) compared to control (black).

B. Representative mean EPSCs obtained from the same FM voltage-clamped at -70 mV demonstrating that in the presence of NBQX (20 µM), removal of external Mg^{2+} reveals an EPSC. The amplitude of this EPSC is reduced in the presence of AP-5 (50 µM, grey) compared to control (black).

5.3 Receptors mediating excitatory synaptic transmission

5.3.1 Glutamatergic receptor contribution to EPSCs

The nature of the neurotransmitter and receptors involved in generating EPSCs in FMs was investigated using pharmacological and physiological techniques. Figure 5.8A demonstrates that the mean EPSC amplitude from a representative FM was reduced following application of the AMPA/kainate glutamate receptor antagonist, NBQX (20 μM) (Sheardown, Nielsen et al. 1990). In this example, NBQX (20 μM), reduced the mean EPSC amplitude from -122 pA to -17 pA (response to a minimum of 10 stimuli was recorded under each condition). NBQX inhibited the EPSC amplitude in every FM tested and amplitude of the mean EPSC from 12 FMs was reduced from –80 ± 8 pA to -12 ± 2 pA in the presence of NBQX (20 μM, n = 12, P < 0.0001, paired *t* test, Figure 5.9). This represents a significant reduction in EPSC amplitude to 16 ± 3 % of control (n = 12, P < 0.0001, one sample *t* test).

NMDA glutamate receptors are blocked by Mg^{2+} at hyperpolarised potentials so in order to determine whether they contribute to EPSCs in FMs the Mg^{2+} block had to be removed (Nowak, Bregestovski et al. 1984). After observing a reduction in EPSC amplitude by NBQX (20 μM), the external solution was switched to Mg^{2+}-free ACSF (also containing NBQX, 20 μM). As the Mg^{2+} concentration in the bath solution was lowered an EPSC was revealed. In the example shown in Figure 5.8B, the low concentration of external Mg^{2+} allowed an EPSC with a mean amplitude of -54 pA (average of 17 traces including failures) to be recorded. The mean EPSC amplitude from a representative sample of FMs under these conditions was significantly increased to -48 ± 7 pA (n = 6, P = 0.006, paired *t* test).

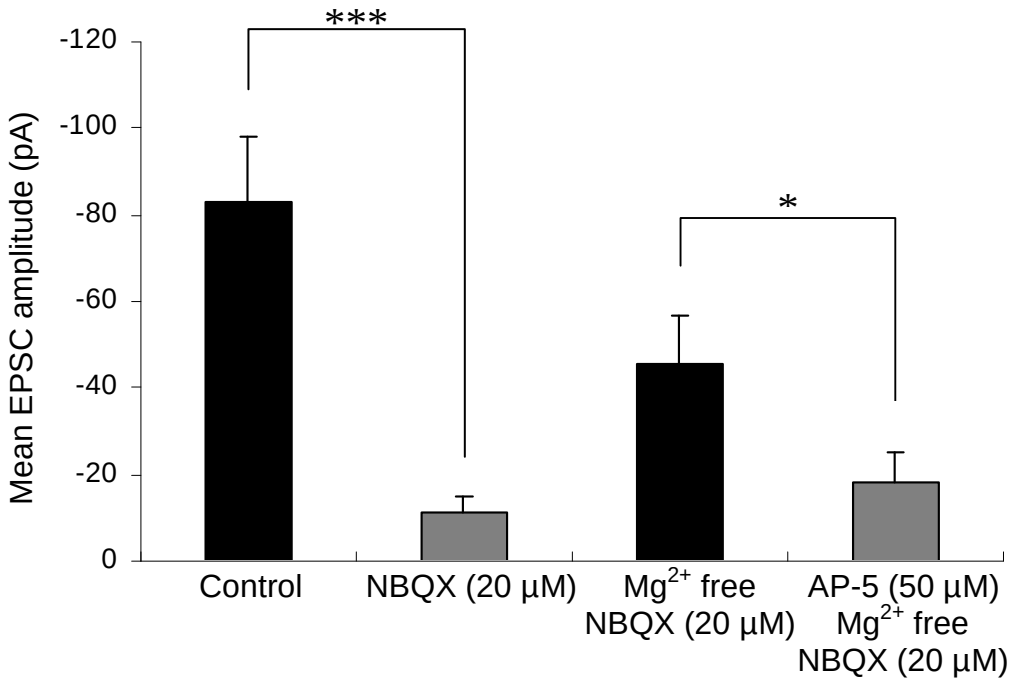

Figure 5.9. Summary of effect of NBQX, AP-5 and removing external Mg^{2+} on EPSC amplitude.

NBQX (20 µM) significantly reduces the mean EPSC amplitude compared to control (n = 12, *** P < 0.001). Removal of external Mg^{2+} reveals an EPSC which is significantly reduced in the presence of AP-5 (50 µM, n = 6, P = 0.03). A minimum of 10 EPSCs were obtained from each FM under each condition and statistical significance was assessed by an unpaired *t* test.

The mean rise and decay times of this EPSC were 3.0 ± 1.7 and 17.9 ± 13.9 ms, respectively (n = 6). This increase in the rise time of the EPSC (compared to 1.6 ± 0.8 ms for the control EPSC) was consistent with a contribution of NMDA receptors (Mayer, Westbrook et al. 1984). In order to confirm that these EPSCs were mediated by NMDA glutamate receptor activation their sensitivity to the NMDA glutamate receptor antagonist, AP-5, was tested (Olverman, Jones et al. 1984). As demonstrated in Figure 5.8B, bath-application of AP-5 (50 μM) reduced the mean EPSC in this FM to –25 pA. The mean EPSC amplitude from the sample FMs was significantly reduced to –20 ± 5 pA (n = 4, P = 0.03, paired *t* test, Figure 5.9). Thus in the presence of NBQX and low external Mg^{2+}, application of AP-5 (50 μM) significantly reduced the mean EPSC amplitude to 39 ± 9 % of control (n = 4, P = 0.0067, one sample *t* test).

An alternative method used for removing the voltage-dependent Mg^{2+} block of NMDA glutamate receptors was to voltage-clamp the FM at a depolarised potential. Figure 5.10A shows the block of non-NMDA glutamate receptor-mediated EPSCs by NBQX (20 μM) at –70 mV, as described earlier. In the continued presence of NBQX (20 μM), the FM was depolarised to +20 mV. This removes the voltage-dependent Mg^{2+} block of NMDA receptors and reveals EPSCs which were observed as outward currents. Figure 5.10B shows the mean EPSC from a representative FM under these conditions and the amplitude of this EPSC is +112 pA. Individual EPSCs from this FM are shown in Figure 5.10C. The mean EPSC amplitude at +20 mV in the presence of NBQX (20 μM) was +83 ± 20 pA (n = 4).

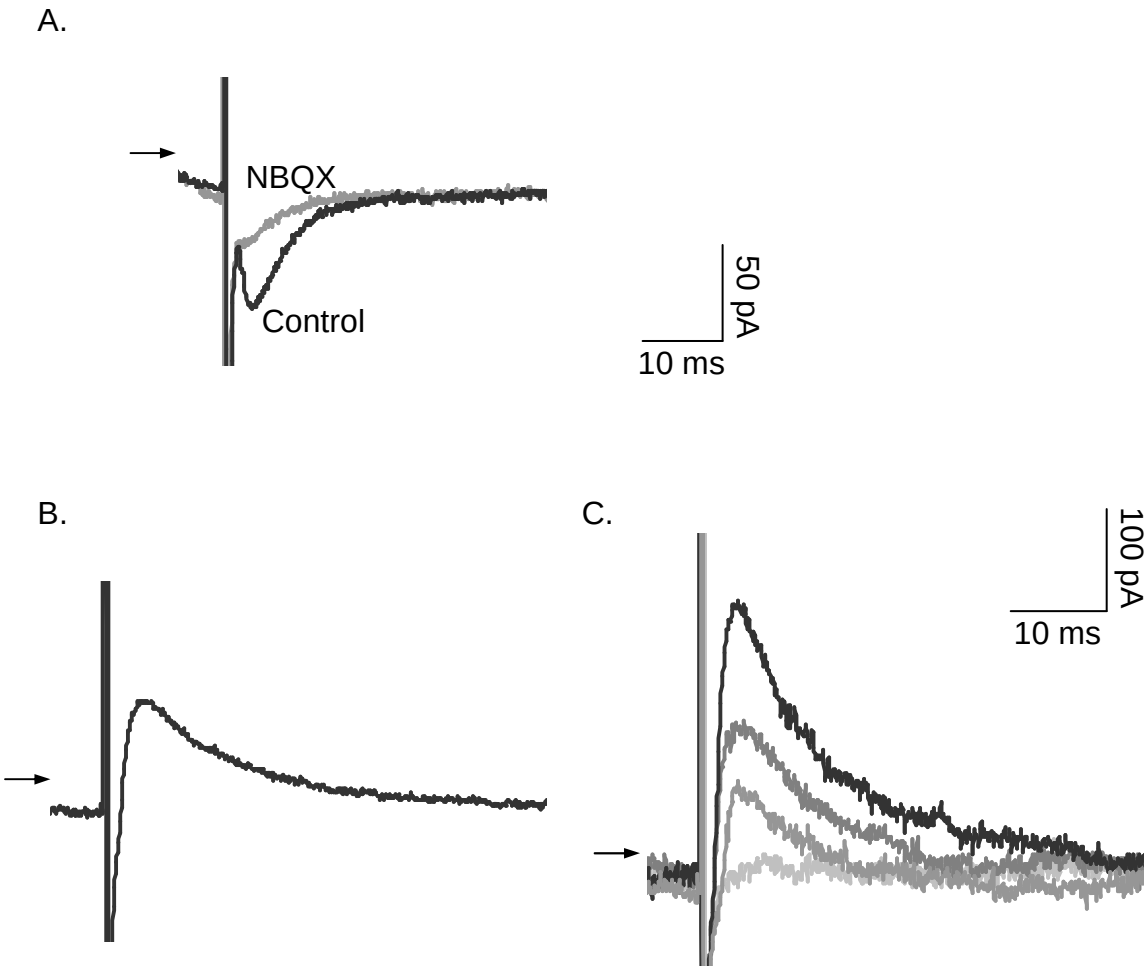

Figure 5.10. Effect of depolarizing FM on EPSC amplitude in the presence of NBQX.

A. Representative mean EPSCs obtained from a FM voltage-clamped at -70 mV in the presence (grey) and absence of NBQX (20 μM, black) demonstrating that AMPA/kainate glutamate receptor-mediated responses are blocked. The arrow represents the -150 pA level.

B. Mean EPSC obtained from the same FM voltage-clamped at +20 mV, demonstrating that in the continued presence of NBQX (20 μM) removal of the voltage-dependent Mg^{2+} block reveals an EPSC. The arrow represents the 700 pA level.

C. Representative EPSCs obtained from the same FM voltage-clamped at +20 mV, demonstrating that in the continued presence of NBQX (20 μM) removal of the voltage-dependent Mg^{2+} block reveals EPSCs that fluctuate in amplitude. The arrow represents the 700 pA level.

In the example shown in Figure 5.10 the non-NMDA component is not entirely blocked by NBQX, therefore the EPSC at +20mV may be partially mediated by non-NMDA receptor activation.

5.3.2 Identification of glutamate receptor subunits

Having identified an AMPA/kainate and NMDA glutamate receptor contribution to EPSCs in FMs, the receptor subtypes involved were further investigated. The lack of subtype selective AMPA or kainate glutamate receptor antagonists prevented the use of a pharmacological approach to determine which subtypes contribute to EPSCs in FMs, however, it has been established that the I/V relationship of GluR2-lacking AMPA receptors show a high degree of inward rectification (Sato, Kiyama et al. 1993). Figure 5.11A shows a control EPSC recorded from a FM voltage-clamped at +40 mV. In this example, bath application of AP-5 (100 μM) reduced the EPSC amplitude from +234 pA to +97 pA, representing a reduction by 59 %. The mean EPSC amplitude recorded at +40 mV was +142 ± 38 pA and this was reduced to +73 ± 25 pA following application of AP-5 (100 μM, n = 4). Having blocked NMDA glutamate receptors with AP-5 (100 μM), I/V relationships of EPSC amplitude were generated from a minimum of 10 EPSCs (with failures omitted) for each potential (n = 4, Figure 5.11B). This I/V relationship had a reversal potential of –17 ± 4 mV (n = 4-7) and was found to show outward rectification (ratio of 2.0, see Methods) suggesting the GluR2 subunit was present at the synapses tested.

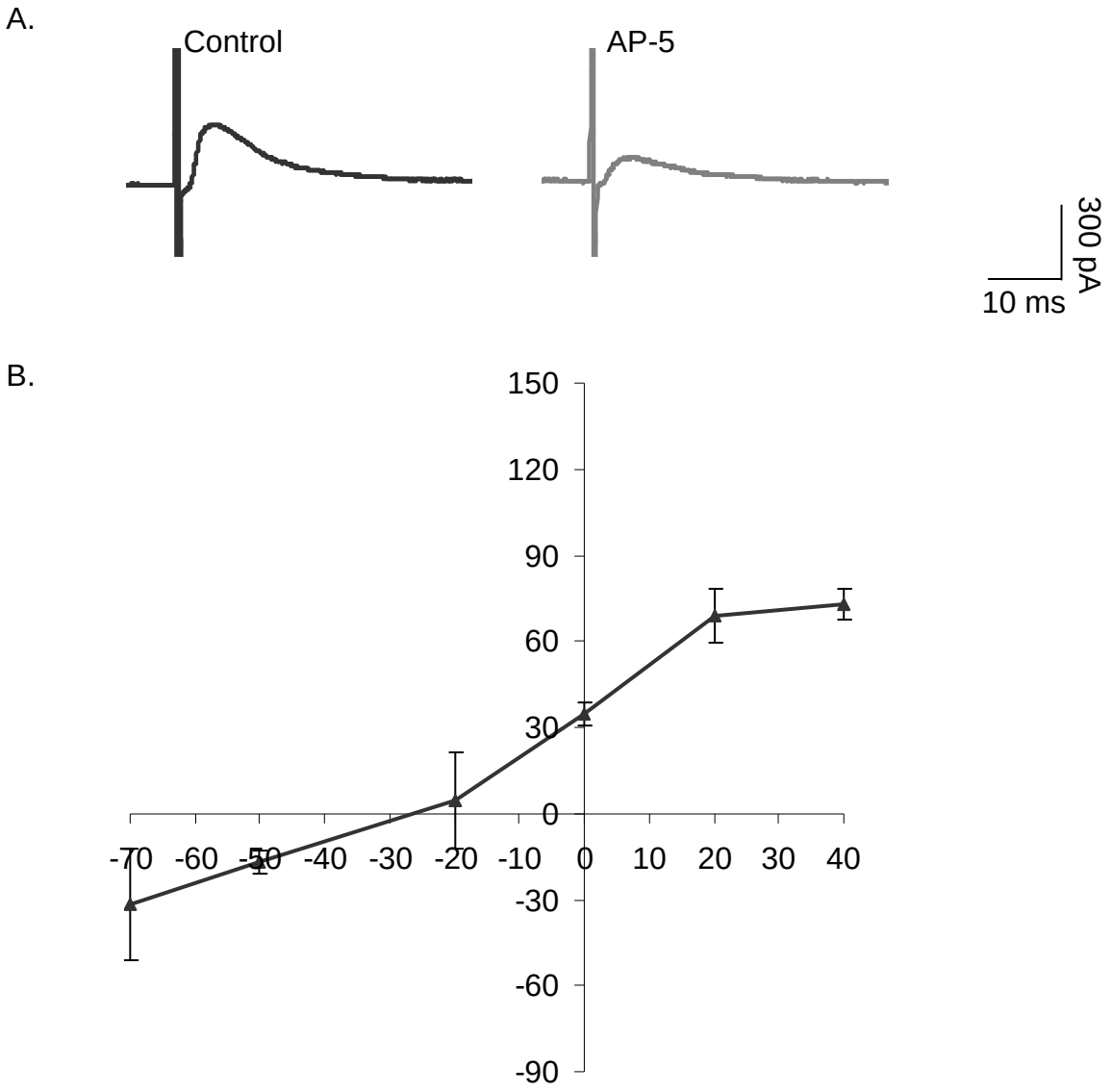

Figure 5.11. Current-voltage relationship of mean EPSC amplitude in FMs in the presence of AP-5.

A. Traces from a representative FM demonstrating that the amplitude of the mean EPSC at +40 mV is reduced in the presence of AP-5 (100 μM, grey) compared to control (black).

B. I/V relationship in the presence of AP-5 (100 μM) generated from the mean EPSC amplitude (without failures) at each potential (n = 4 FMs, with an average of a minimum of 10 EPSCs at each potential in each cell).

Ifenprodil is an NMDA glutamate receptor antagonist that has approximately 400-fold higher affinity for NR1A/NR2B than NR1A/NR2A receptors in Xenopus oocytes (Williams 1993). Ifenprodil was used to assess the contribution of NR1A/NR2B receptors to EPSCs in FMs. Figure 5.12A shows a control mean EPSC recorded from a FM voltage-clamped at –70 mV and the mean EPSC in the presence of NBQX (20 μM). In the example shown NBQX (20 μM) causes a reduction in EPSC amplitude from –58 pA to –28 pA, a reduction of 52 %. The mean control EPSC amplitude from 5 representative FMs at –70 mV was –48 ± 6 pA and this was reduced to –12 ± 6 pA in the presence of NBQX (20 μM, P = 0.0014, n = 5, paired t test). This represents a significant reduction by 76 ± 10 % (P = 0.0015, n = 5, one sample t test).

Having blocked AMPA/kainate glutamate receptors with NBQX (20 μM), Mg^{2+}-free ACSF was applied to remove the Mg^{2+} block of NMDA glutamate receptors. In the FM shown in Figure 5.12B, removal of external Mg^{2+} revealed an EPSC with an amplitude of –47 pA which was reduced to –19 pA in the presence of ifenprodil (10 μM). The mean EPSC amplitude recorded in Mg^{2+}-free external solution, in the presence of NBQX (20 μM) at –70 mV was significantly increased to –30 ± 5 pA (P = 0.0057, n =5, paired *t* test). This was reduced to –12 ± 3 pA in the presence of ifenprodil (10 μM), representing a significant reduction in EPSC amplitude by 57 ± 8 % (P = 0.0022, n = 5, one sample *t* test). These data indicate that NR1A/NR2B receptors make a significant contribution to synaptic transmission in FMs at the synapses tested.

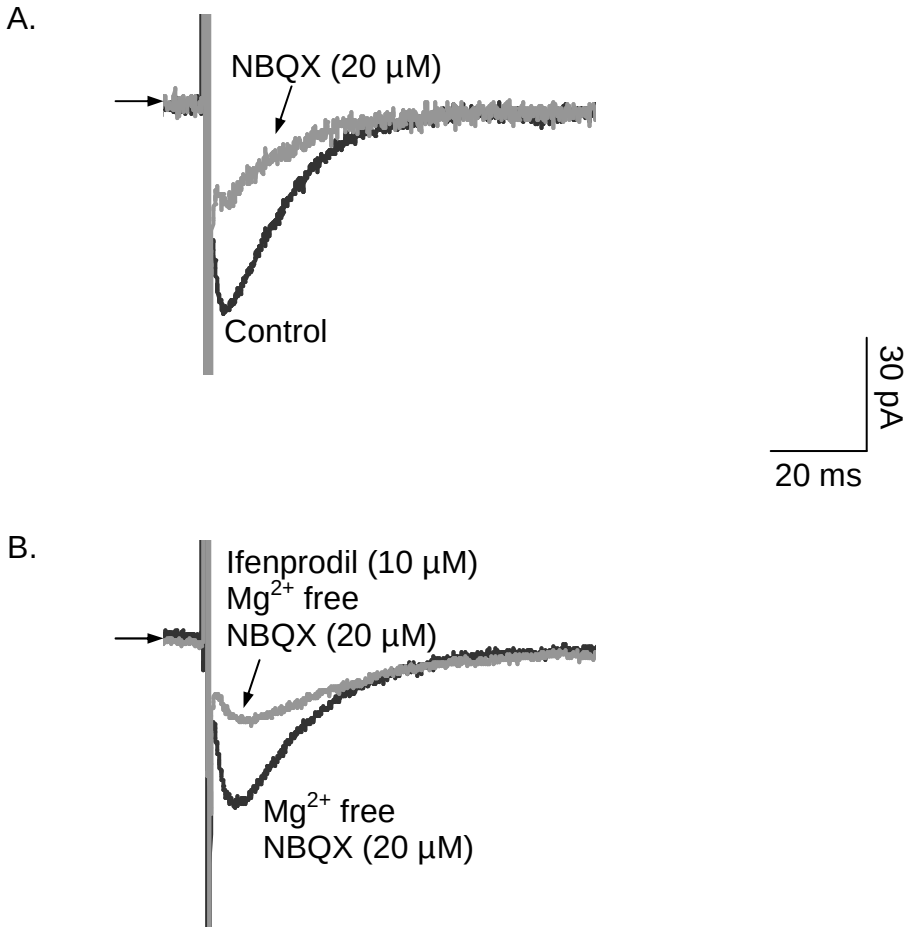

Figure 5.12. Effect of ifenprodil on EPSC amplitude in FMs in Mg^{2+}-free ACSF and in the presence of NBQX.

A. Representative mean EPSCs obtained from a FM voltage-clamped at -70 mV demonstrating that the mean EPSC amplitude is reduced in the presence of NBQX (20 µM, grey) compared to control (black). The arrow indicates the –120 pA level.

B. Representative mean EPSCs obtained from the same FM voltage-clamped at -70 mV demonstrating that in the presence of NBQX (20 µM), removal of external Mg^{2+} reveals an EPSC. The amplitude of this EPSC is reduced in the presence of ifenprodil (10 µM, grey) compared to control (black). The arrow indicates the –100 pA level.

5.4 Discussion

5.4.1 Excitatory synaptic transmission in the facial nucleus

Stimulation close to the dendrites of a FM voltage-clamped at -70 mV evoked inward currents with fast kinetics consistent with activation of postsynaptic glutamatergic receptors and previous findings that glutamate has excitatory actions on FMs (VanderMaelen and Aghajanian 1980). It was also possible to evoke EPSPs when the FM was held in the current-clamp configuration, however, the subsequent characterisation of these synapses was performed in the voltage-clamp configuration.

5.4.2 Number of release sites activated

Stimulation evoked EPSCs that showed amplitude fluctuations and whether these fluctuations occurred as a result of quantal release at one synapse or activation of multiple synapses was investigated further. EPSCs in FMs were evoked by a stimulation paradigm based on minimal stimulation (Raastad, Storm et al. 1992). The original criteria for minimal stimulation was that release failed at a rate of approximately 50 % and that the EPSC amplitude remained constant at a range of stimulus intensities (until it was increased over the threshold for minimal stimulation), however, this has been modified so that the stimulus intensity applied results in the lowest possible failure rate without a subsequent increase in mean EPSC amplitude above that observed with a 50 % failure rate (Raastad, Storm et al. 1992; Lawrence, Grinspan et al. 2004). In FMs the stimulus intensity was determined by first identifying a functional synapse with a relatively high stimulus, the stimulus was then turned to its lowest setting and gradually increased until an

EPSC was observed. The stimulus intensity was then increased until the failure rate was at its minimum (approximately 25 %) without observing an increase in the mean EPSC amplitude (Lawrence, Grinspan et al. 2004). At these intensities EPSCs were evoked with discrete amplitude reminiscent of quantal release at the neuromuscular junction and some central synapses (for reviews see (Kuno 1971; Tremblay, Laurie et al. 1983)). Traditionally, cumulative probability histograms of EPSC amplitude would be generated to analyse whether quantal release from a single release site (or several identical sites) is occurring or whether release is from several sites with different quantal contents. However, in the experiments described here the stimulation was only applied once every 20 seconds to ensure no synaptic plasticity occurred and the cumulative probability histograms generated from the number of events recorded could not be used to reliably predict the number of release sites.

Paired pulse analysis can be a useful tool in determining whether minimal stimulation is only activating one synapse if the assumption is made that each synapse has only a single release site (Stevens and Wang 1995). At a single synapse paired pulse facilitation of mean EPSCs occurs as a result of release probability of the second stimulation being greater than the first (thought to be due to the residual Ca^{2+} in the terminal). As the same amount of neurotransmitter is release following both these stimuli the lower mean amplitude of the first EPSC is only due to the higher failure rate. Thus, at a single synapse, removal of failures results in the first and second mean EPSCs being of equal amplitude (Stevens and Wang 1995). If multiple synapses are being stimulated then the amplitude of the second pulse (even in the absence of failures) will be greater than the first. This occurs as a result of the

probability of release following the second pulse being high (due to the residual Ca^{2+}) in a larger proportion of the synapses (Stevens and Wang 1995).

In the FMs tested, some demonstrated the paired pulse properties of single synapses whereas in others more than one synapse was clearly being stimulated. Identical stimulation paradigms were used in all FMs suggesting that where multiple synapse involvement was demonstrated it is likely that only a few synapses would be activated.

The EPSCs recorded at the single synapses identified by paired pulse analysis showed amplitude fluctations providing evidence supporting the release of multiple quanta at a single central synapse (Sastry and Bhagavatula 1996; Auger and Marty 2000; Stevens 2003).

5.4.3 AMPA/kainate receptors contribute to EPSCs

Control EPSCs were sensitive to block by NBQX indicating a role for non-NMDA glutamate receptors in fast excitatory synaptic transmission in FMs. Several non-NMDA antagonists have affinity for both kainate and AMPA glutamate receptors and cannot be used to distinguish between the two types of receptors. NBQX is more potent at AMPA receptors (IC_{50} = 0.15 μM assessed by rat cortical membrane radioligand binding assays) than at kainate receptors (IC_{50} = 4.8 μM) (Sheardown, Nielsen et al. 1990), however, at the concentration used in these experiments (20 μM) it is likely that kainate receptors would also be significantly blocked and could also contribute to EPSC in FMs.

5.4.4 GluR2 receptor contribution to EPSCs

GluR2 receptors are the most abundantly expressed AMPA glutamate receptors and are highly expressed in all cranial motonuclei (Martin, Blackstone et al. 1993). The lack of inward rectification of the I/V relationship obtained in the presence of AP-5 (to block the NMDA receptor contribution) indicates that receptors containing the edited form of the GluR2 receptor subunit contribute to EPSCs in FMs (Sato, Kiyama et al. 1993). However, the inward rectification of non-GluR2 containing AMPA glutamate receptors is dependent on a block by intracellular polyamines (such as spermine and spermidine) (Donevan and Rogawski 1995). As polyamines were not added to the intracellular solution, the dialysis of intracellular polyamines during whole cell recordings cannot be ruled out as a factor in the lack of inward rectification.

5.4.5 NMDA receptors are present in FMs

The contribution of NMDA receptors to EPSCs in FMs was investigated. NMDA receptors are blocked by extracellular Mg^{2+} at typical resting membrane potentials (and more hyperpolarised potentials). When Mg^{2+} was removed from the ACSF or the FM was voltage-clamped at depolarised potentials, the Mg^{2+} block was reduced and an EPSC was revealed. This EPSC was sensitive to block by the selective NMDA receptor antagonist, AP-5. Activation of non-NMDA receptors can depolarise the postsynaptic membrane sufficiently to remove the Mg^{2+} block of NMDA receptors *in vivo* and the data obtained here indicates the presence of NMDA receptors at all the synapses tested. Both NMDA and non-NMDA glutamate receptor subtypes are expressed in FMs and the data provided here further supports

the involvement of both NMDA and non-NMDA receptors at excitatory synapses in the FMN.

NMDA and non-NMDA glutamate receptor activation is involved in the majority of fast excitatory synaptic transmission in the mammalian CNS and has been shown to mediate synaptic transmission in several motor nuclei (reviewed in (Rekling, Funk et al. 2000)). NMDA and non-NMDA glutamate receptors have been shown to co-localise at synapses in hypoglossal motoneurones (O'Brien, Isaacson et al. 1997). However, one characterisation of glutamatergic inputs into hypoglossal motoneurones concluded that only non-NMDA glutamate receptors mediate EPSCs in these cells (Bouryi and Lewis 2003). It is worth noting that the contribution of NMDA receptors was only assessed in motoneurones voltage-clamped at –70 mV (Bouryi and Lewis 2003). At this potential NMDA glutamate receptors would be blocked by extracellular Mg^{2+}, therefore AP-5 would not be expected to reduce the EPSC amplitude.

5.4.6 NR2B receptor contribution to EPSCs

The NMDA glutamate receptor mediated EPSC in FMs was partially blocked by ifenprodil. Ifenprodil has 400-fold higher affinity for NR1/NR2B receptors over NR1/NR2A receptors and at the concentration used here (1 μM) selectively blocks NR2B containing receptors (Reynolds and Miller 1989; Williams 1993). The presence of NR1/NR2B receptors in neonatal rat FM is consistent with the developmental pattern of NMDA receptors (Wenzel, Fritschy et al. 1997). In neonatal rats the predominant NMDA receptor subunits are NR1, NR2B and to a lesser extent, NR2D (Wenzel, Fritschy et al. 1997). In juvenile and adult rat

brainstem the predominant subunits are NR1, NR2A and NR2D (Wenzel, Fritschy et al. 1997). The data presented here confirms the contribution of NR2B subunits and it is proposed that the residual current that is not blocked by ifenprodil is mediated by NR1/NR2D receptors. A developmental change in NMDA glutamate receptor composition is also demonstrated in the trigeminal motor nucleus where the number of NR2B expressing neurones decreases between postnatal days 3-4 and 11, however, NR2D expression was not assessed in this nucleus (Turman JE 2002).

5.5 Concluding statement

This chapter provides a characterisation of excitatory synaptic transmission in neonatal rat FMs, the nature of which was previously unknown. Transmission at the synapses tested involved the activation of both non-NMDA and NMDA glutamate receptors. In addition, the minimal stimulation protocol utilised in this chapter enabled both single and multiple synapses to be recorded and identified using paired pulse analysis. The findings of this chapter will assist the interpretation of subsequent investigations into synaptic integration in the FMN and its modulation by monoamines.

Chapter 6

6.1 Introduction

6.1.1 Effects of 5-HT on synaptic transmission

5-HT is generally accepted to promote FM excitability through postsynaptic actions and Chapters 3 and 4 of this thesis investigate the mechanisms underlying this excitability and the receptors that mediate these effects of 5-HT (VanderMaelen and Aghajanian 1980; Vandermaelen and Aghajanian 1982; Larkman, Penington et al. 1989). However, the effect of 5-HT on fast excitatory synaptic transmission has not previously been investigated. Pre-synaptic effects of 5-HT are the focus of this chapter.

6.1.2 Direct inhibitory effect of 5-HT

The inhibitory actions of 5-HT are mediated by activation members of the 5-HT_1 subfamily (5-$HT_{1A,B,D,E\ and\ F}$). The 5-HT_1 receptors are negatively coupled to adenylate cyclase through G_i proteins, however, it has become apparent that the hyperpolarisation induced by 5-HT_{1A} receptor activation in central neurones involves a direct action of Gβγ subunits on inwardly rectifying potassium (K^+) channels (Andrade, Malenka et al. 1986; Colino and Halliwell 1987).

6.1.3 Inhibition of neurotransmitter release by 5-HT

In addition to a postsynaptic hyperpolarisation, several 5-HT_1 receptor subtypes can also modulate neurotransmitter release through presynaptic mechanisms. 5-HT_{1A}, 5-HT_{1B} and 5-HT_{1D} presynaptic autoreceptors have been shown to inhibit the release of 5-HT from the nerve terminal (Barnes and Sharp 1999).

Some regions which have high levels of 5-HT_{1B} binding sites do not express 5-HT_{1B} receptor mRNA (such as the substanita nigra and globus pallidus) suggesting that the receptors are located presynaptically in these regions and function as heteroreceptors to modulate release of other neurotransmitters from the nerve terminal (Bruinvels, Landwehrmeyer et al. 1994; Barnes and Sharp 1999). Indeed, 5-HT_{1B} heteroreceptors inhibit glutamate release from the presynaptic terminal in the subiculum, cingulate cortex and hypoglossal motor nucleus (Bobker and Williams 1989; Tanaka and North 1993; Boeijinga and Boddeke 1996; Bouryi and Lewis 2003).

The identification of 5-HT_{1A} receptor mRNA in the facial nucleus and the evidence for functional 5-HT_{1A} and 5-HT_{1B} heteroreceptors in the hypoglossal motor nucleus prompted an investigation into the role of these receptor subtypes in the inhibitory actions of 5-HT in the facial nucleus using subtype selective agonists and antagonists (Pompeiano, Palacios et al. 1992; Bouryi and Lewis 2003).

6.1.3 Aims

The aim of this chapter was to investigate the effect of 5-HT on synaptic transmission. The initial experiments revealed that 5-HT application resulted in a decrease in the mean evoked EPSC amplitude. This inhibitory action of 5-HT was in contrast to the known excitatory postsynaptic actions of 5-HT on FMs (see Chapters 3 and 4) and was therefore investigated further. A pharmacological approach was used to determine that 5-HT_{1B} receptors mediate this inhibitory action of 5-HT and analysis of the failure rate, paired pulse ratio and frequency of spontaneous release was used to determined that this action occurs presynaptically. Thus it was

determined that 5-HT reduces glutamate release from the presynaptic terminal through activation of 5-HT_{1B} receptors.

6.2 Results

6.2.1 5-HT reduces EPSC amplitude

Application of 5-HT (10 μM) reduced the mean EPSC amplitude in a representative FM from –31 pA to –4 pA (Figure 6.1). This reduction in EPSC amplitude was coupled with a change in the holding current of –73 pA mediated by the postsynaptic effects of 5-HT (Chapter 3 and 4). The mean control EPSC from a sample of 16 FMs was –40 ± 5 pA and this was reduced to –13 ± 2 pA in the presence of 5-HT (10 μM). This represents a significant reduction to 36 ± 7 % of the control (n = 16, $P < 0.0001$, one sample *t* test, Figure 6.4). The average inward current evoked by 5-HT (10 μM) in these FMs was –117 ± 20 pA (n = 16). In the majority of neurones tested this inhibition of EPSC amplitude by 5-HT was reversible and further pharmacological experiments were only performed on FMs in which the EPSC fully recovered from 5-HT inhibition.

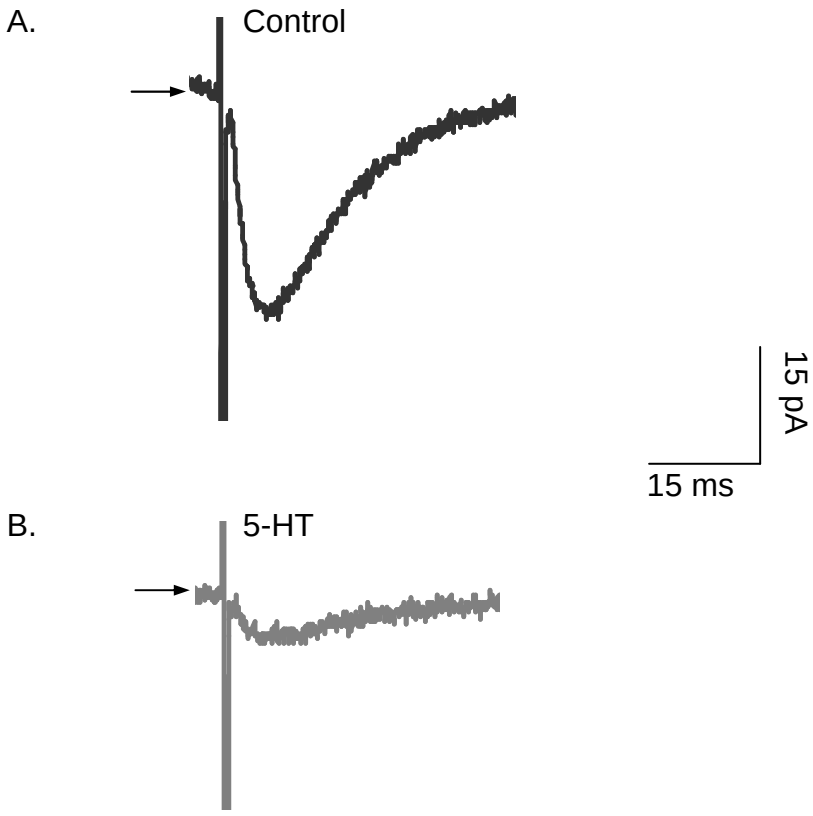

Figure 6.1. 5-HT reduces EPSC amplitude in facial motoneurones.

A. Mean control EPSC (average of 18 EPSCs including failures) from a facial motoneuron voltage-clamped at –70 mV. The arrow indicates the –130 pA level.

B. Mean EPSC (average of 24 EPSCs including failures), demonstrating that 5-HT (10 μM) reduces the mean EPSC amplitude compared to control (A). The arrow indicates the –200 pA level.

6.2.2 5-HT receptor subtypes mediating reduction in EPSC amplitude

The 5-HT receptor subtype that mediates the reduction in EPSC amplitude was investigated using receptor subtype selective agonists and antagonists. The 5-HT_{1A} and 5-HT_{1B} receptors were focussed on due to their inhibitory nature and the finding that activation of these receptors mediates a reduction in EPSC amplitude in rat hypoglossal motoneurones (Bouryi and Lewis 2003).

6.2.3 Subtype selective 5-HT_{1B} receptor agonist reduces EPSC amplitude

In a FM in which 5-HT (10 μM) reduced the mean EPSC amplitude from –34 pA to –7 pA (reduced to 21 % of control), bath-application of the 5-HT_{1B} receptor selective agonist, CP93129 (10 μM) (Macor, Burkhart et al. 1990), reduced the EPSC amplitude from –34 pA to –9 pA (reduced to 26 % of control, Figure 6.2). In a sample group of FMs CP93129 (10 μM) application resulted in a reduction in EPSC amplitude from –22 ± 5 pA to –4 ± 2 pA (n = 6). This represents a significant reduction to 20 ± 6 % of the control (n = 6, $P < 0.0001$, one sample *t* test, Figure 6.4). In the same FMs the mean control EPSC was –30 ± 17 pA and this was reduced to –16 ± 9 pA in the presence of 5-HT (10 μM), representing a significant reduction to 33 ± 9 % of control (n = 6, $P = 0.017$, one sample *t* test). The reduction in EPSC amplitude by CP93129 (10 μM) was not significantly different to the reduction in amplitude observed following 5-HT (10 μM) application ($P = 0.27$, unpaired *t* test). Partial recovery (to 44 ± 15 % of control EPSC amplitude) was observed in 4 of the neurones tested, however this may have been increased if a longer period of wash out had been allowed.

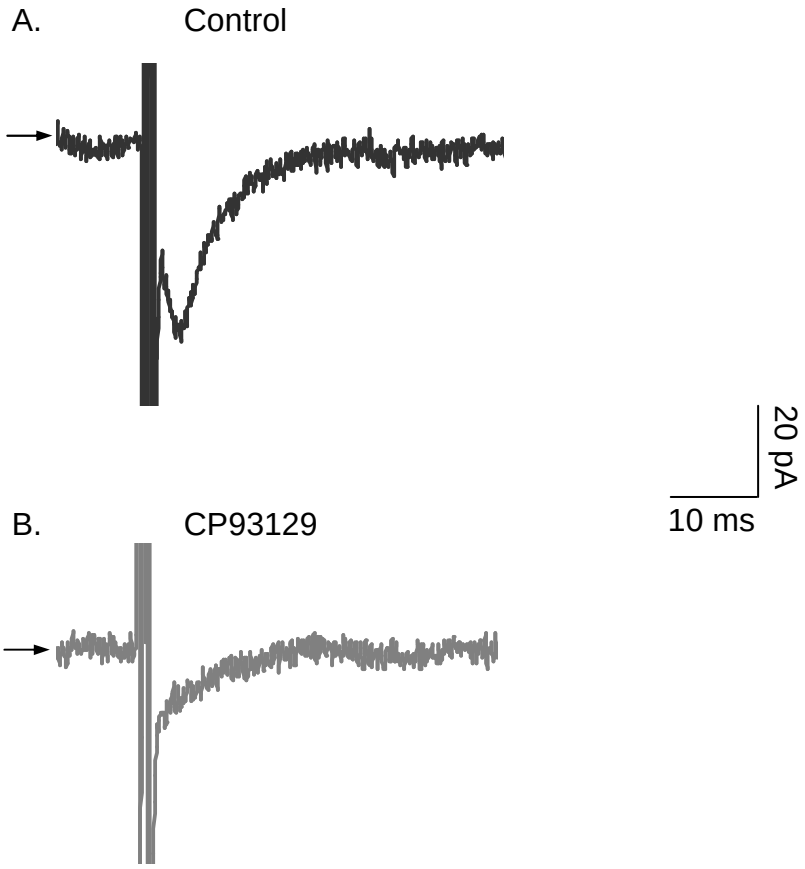

Figure 6.2. CP93129 reduces EPSC amplitude in facial motoneurones.

A. Mean control EPSC (average of 10 EPSCs including failures) from a FM voltage-clamped at –70 mV. The arrow indicates the –120 pA level.

B. Mean EPSC (average of 10 EPSCs including failures) demonstrating that the 5-HT_{1B} receptor agonist, CP93129 (10 μM), reduces the mean EPSC amplitude compared to control (A). The arrow indicates the –120 pA level.

As expected the reduction in EPSC amplitude observed in the presence of CP93129 (10 μM) was not coupled with a large postsynaptic inward current (-7 ± 16 pA, n = 6), whereas 5-HT (10 μM) evoked an inward current of –107 ± 19 pA in the same FMs (n = 6, P = 0.0076, paired *t* test).

Application of the 5-HT_{1A} receptor selective agonist, 8-OH-DPAT (10 μM) (Arvidsson, Hacksell et al. 1981; Peroutka 1985), had no effect of EPSC amplitude in the FM shown in Figure 6.3 (-23 pA and –24 pA in absence and presence of 8-OH-DPAT, respectfully). In the same FM, 5-HT (10 μM) reduced the EPSC amplitude from –44 pA to –13 pA (reduced to 30 % of control). In a sample group of FMs 8-OH-DPAT (10 μM) caused only a very small reduction in EPSC amplitude from –25 ± 1 pA to –21 ± 2 pA (n = 3). This represents a non-significant reduction to 85 ± 9 % of the control (n = 3, P = 0.23, one sample *t* test, Figure 6.4). In the same FMs the mean control EPSC was –47 ± 10 pA and this was reduced to –16 ± 8 pA in the presence of 5-HT (10 μM), representing a significant reduction to 30 ± 11 % of control (n = 3, P = 0.02, one sample *t* test). The reduction in EPSC amplitude mediated by 5-HT was significantly greater than that observed following 8-OH-DPAT application (n = 3, P = 0.018, paired *t* test). In addition, 8-OH-DPAT (10 μM) did not evoke a large inward current (-10 ± 22 pA, n = 3), whereas 5-HT (10 μM) evoked an inward current of –77 ± 42 pA in the same FMs. The 5-HT_{1B} receptor agonist, CP93129 (10 μM), but not the 5-HT_{1A} receptor agonist, 8-OH-DPAT (10 μM), reduced EPSC amplitude to a similar degree as 5-HT (10 μM).

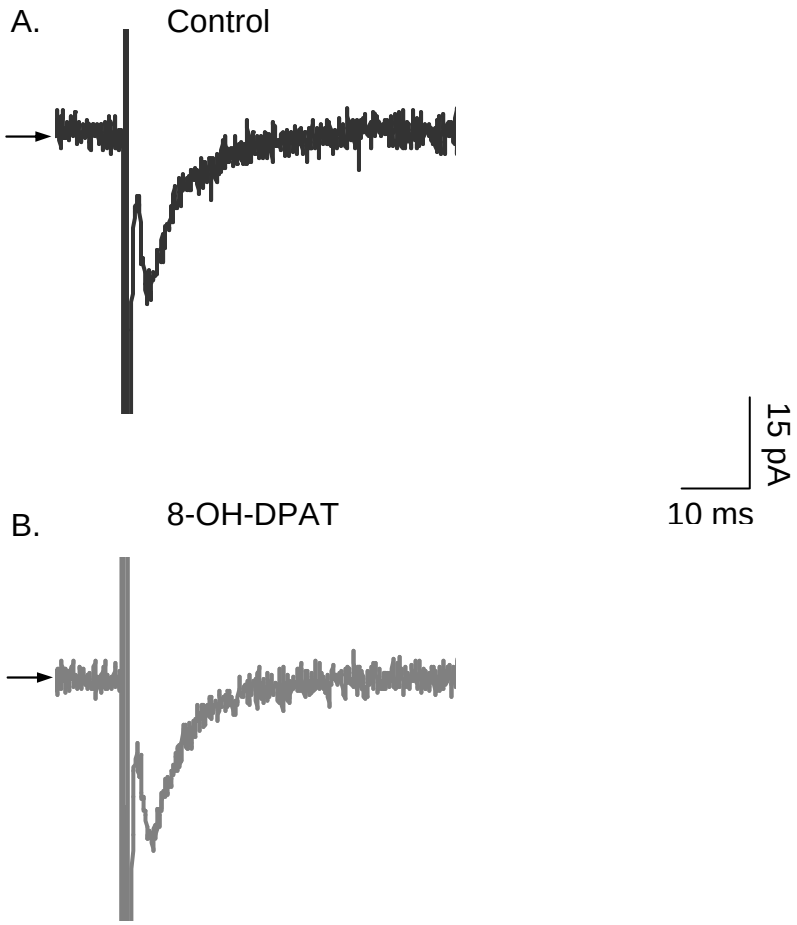

Figure 6.3. 8-OH-DPAT does not affect EPSC amplitude in facial motoneurones.

A. Mean control EPSC (average of 10 EPSCs including failures) from a FM voltage-clamped at –70 mV. The arrow indicates the –70 pA level.

B. Mean EPSC (average of 10 EPSCs including failures) demonstrating that the 5-HT_{1A} receptor agonist, 8-OH-DPAT (10 μM), has no effect on the mean EPSC amplitude. The arrow indicates the –73 pA level.

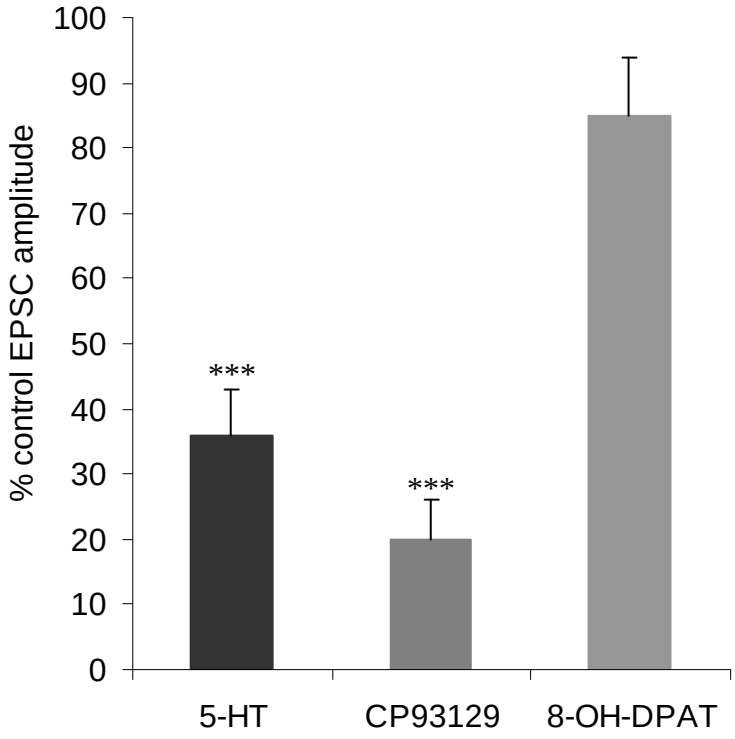

Figure 6.4. Summary of effects of 5-HT$_1$ receptor selective agonists on EPSC amplitude.

Bar chart summarising the reduction in EPSC amplitude in the presence of 5-HT (10 μM, n = 16), the 5-HT$_{1B}$ selective agonist, CP93129 (10 μM, n = 6) and the 5-HT$_{1A}$ selective agonist, 8-OH-DPAT (10 μM, n =3). A minimum of 10 EPSCs were obtained from each FM under control conditions and in the presence of the agonist. Statistical significance was assessed by a one sample *t* test (*** P<0.0001).

6.2.4 Subtype selective 5-HT$_{1B}$ receptor antagonist blocks reduction in EPSC amplitude

Figure 6.5 demonstrates the effects of the 5-HT$_{1B}$ receptor antagonist, isamoltane (1 μM) (Waldmeier, Williams et al. 1988). In an example FM voltage-clamped at –70 mV, 5-HT (10 μM) reduced the mean EPSC amplitude from –66 pA to –24 pA under control conditions, corresponding to a reduction to 36 % of control. Following incubation with isamoltane (1 μM), co-application of 5-HT (10 μM) with the antagonist reduced the ESPC from –34 pA to –26 pA. This represents a reduction to only 76 % of control. In a representative group of FMs, 5-HT (10 μM) reduced the EPSC amplitude from –41 ± 11 pA to –14 ± 4 pA (n = 5). Thus, in these FMs, 5-HT (10 μM) causes a significant reduction in EPSC amplitude to 30 ± 10 % of control (n =5, P = 0.0023, one sample *t* test). The mean EPSC following recovery from 5-HT was –38 ± 12 pA in amplitude and was not significantly altered by incubation with isamoltane (–33 ± 13 pA, n = 5, P = 0.24, paired *t* test). In the continued presence of the antagonist, 5-HT (10 μM) reduced the EPSC amplitude from –33 ± 13 pA to –20 ± 7 pA (n = 5). This represents a reduction in EPSC amplitude to 64 ± 10 % of control (n =5) and although this still represents a significant reduction by 5-HT (P = 0.024, one sample t test), it is significantly less than the reduction observed under control conditions (n = 5, P = 0.0058, paired *t* test, Figure 6.5).

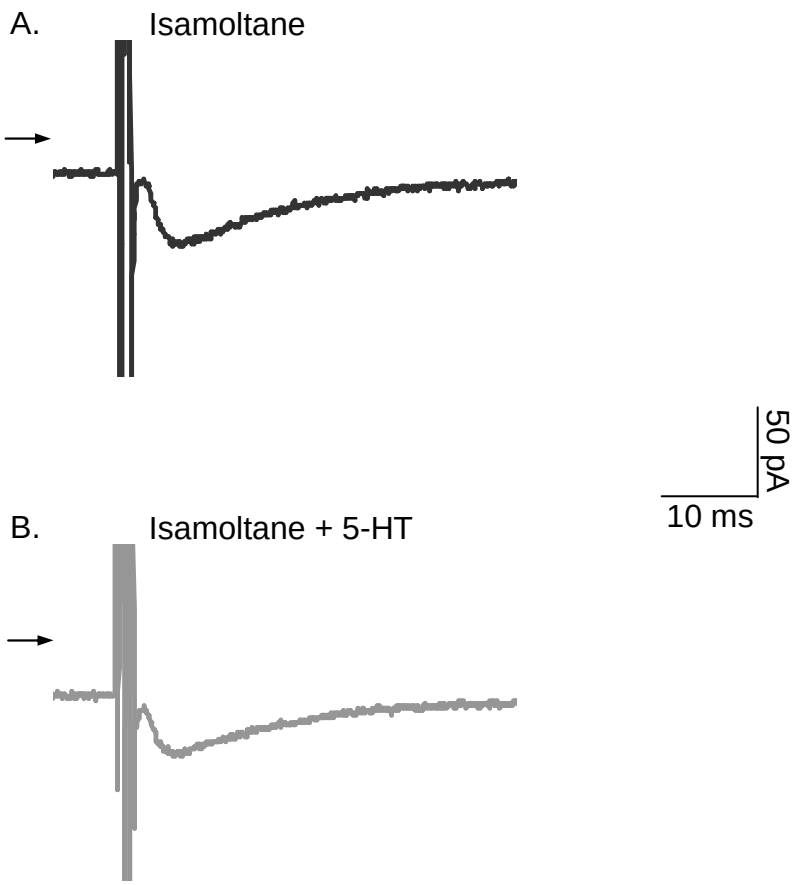

Figure 6.5. Isamoltane blocks the reduction in EPSC amplitude by 5-HT in facial motoneurones.

A. Mean EPSC (average of 10 EPSCs including failures) in the presence of the 5-HT_{1B} receptor antagonist, isamoltane (1 μM) from a FM voltage-clamped at –70 mV. The arrow indicates the –300 pA level.

B. Mean EPSC (average of 12 EPSCs including failures) in the presence of isamoltane (1 μM) and 5-HT (10 μM) from the same motoneurone as (A). Note that the arrow indicates the –400 pA level so the inward current evoked by 5-HT is not blocked.

In the presence of isamoltane (1 μM), 5-HT (10 μM) evoked a postsynaptic inward current of -71 ± 14 pA which was not significantly different from the inward current of -77 ± 26 pA evoked by 5-HT under control conditions (n = 5, P = 0.57, paired *t* test).

Figure 6.6 demonstrates the lack of effect of the 5-HT_{1A} receptor antagonist, WAY 100635 (1 μM) (Critchley, Childs et al. 1994). In an example FM voltage-clamped at –70 mV, 5-HT (10 μM) reduced the mean EPSC amplitude from –28 pA to –10 pA under control conditions, corresponding to a reduction to 36 % of control. Following incubation with WAY 100635 (1 μM), co-application of 5-HT (10 μM) with the antagonist reduced the ESPC from –22 pA to –4 pA. This represents a reduction to 18 % of control, which is similar to the control response. In a sample group of FMs, 5-HT (10 μM) reduced the EPSC amplitude from –31 ± 5 pA to –9 ± 0.4 pA (n = 3). Thus, in these FMs, 5-HT (10 μM) causes a significant reduction in EPSC amplitude to 31 ± 5 % of control (n =3, P = 0.0046, one sample *t* test). The same group of FMs were then incubated with WAY 100635 (1 μM), following which 5-HT (10 μM) was co-applied with the antagonist. The mean EPSC amplitude before and after incubation with WAY 100635 (1 μM) was –24 ± 4 pA and –18 ± 2 pA, respectively (n = 3, not significantly different, P = 0.20, paired *t* test). In the presence of WAY 100635 (1 μM) 5-HT (10 μM) reduced the EPSC to –4 ± 2 pA (n = 3). This represents a significant reduction in EPSC amplitude to 20 ± 8 % of control (n = 3, P = 0.0092, one sample *t* test) which is also not significantly different to the reduction observed under control conditions (n = 3, P = 0.14, paired *t* test, Figure 6.6).

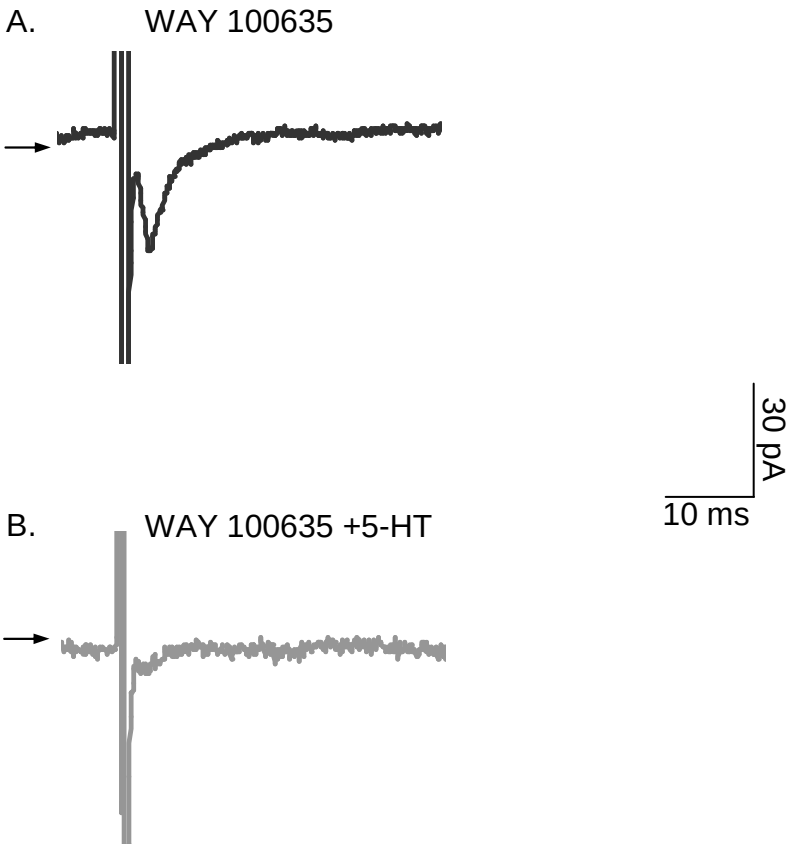

Figure 6.6. WAY 100635 has no effect on the reduction in EPSC amplitude by 5-HT in facial motoneurones.

A. Mean EPSC (average of 10 EPSCs including failures) in the presence of the 5-HT_{1A} receptor antagonist, WAY 100635 (1 μM), from a FM voltage-clamped at –70 mV. The arrow indicates the –40 pA level.

B. Mean EPSC (average of 12 EPSCs including failures) in the presence of WAY 100635 (1 μM) and 5-HT (10 μM) from the same motoneurone as (A). Note that the arrow indicates the –140 pA level so the inward current evoked by 5-HT is not blocked.

Under control conditions 5-HT (10 μM) evoked a postsynaptic inward current of -102 ± 8 pA which was not significantly different from the inward current of -109 ± 19 pA evoked by 5-HT in the presence of WAY 100635 (1 μM, n = 3, P = 0.81, paired *t* test).

6.3 Mechanism for reduction in EPSC amplitude

5-HT_{1B} receptors can function as heteroceptors to modulate the release of glutamate from the presynaptic terminal, however 5-HT_{1B} receptors can also act at the postsynaptic membrane (Bobker and Williams 1989; Boeijinga and Boddeke 1993; Boeijinga and Boddeke 1996). The finding that the 5-HT_{1B} agonist does not evoke any postsynaptic responses suggests the receptor mediates its effect through presynaptic mechanism and this possible location of 5-HT_{1B} receptors in the FMN was investigated using three different techniques.

6.3.1 Activation of 5-HT_{1B} receptors increases failure rate

Analysis of the rate of failure to generate an EPSC in response to minimal stimulation under control conditions and in the presence of 5-HT receptor agonists was performed. The response to a minimum of ten stimuli were obtained from each FM under control conditions and in the presence of each agonist. In the absence of 5-HT, stimulation failed to produce an EPSC at a rate of 25 ± 5 % in each neurone (n = 18, Figure 6.7). In the presence of 5-HT (10 μM) this failure rate was significantly increased to 65 ± 7 % (n = 16, P < 0.0001, unpaired *t* test, Figure 6.7). Similarly, following application of the 5-HT_{1B} receptor subtype selective agonist, CP93129

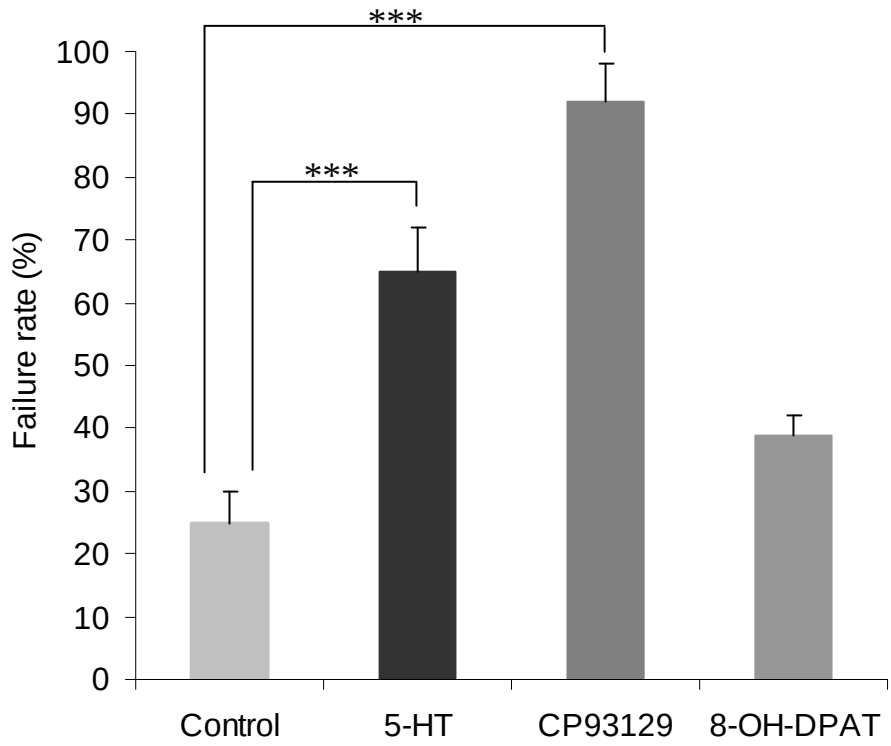

Figure 6.7. Summary of effects of 5-HT_1 receptor selective agonists on EPSC failure rate.

Bar chart summarising the rate of failure to evoke an EPSC under control conditions and in the presence of 5-HT (10 μM, n = 16), the 5-HT_{1B} selective agonist, CP93129 (10 μM, n = 6) and the 5-HT_{1A} selective agonist, 8-OH-DPAT (10 μM, n =3). Minimums of 10 stimuli were applied to each FM under control conditions or in the presence of the agonists. The failure rates in the presence of 5-HT (10 μM) and CP93129 (10 μM) were significantly higher than under control conditions. Statistical significance was assessed by an unpaired *t* test (*** $P<0.0001$).

(10 μM), the failure rate was significantly increased to 92 ± 6 % (n = 6, P < 0.0001, unpaired *t* test, Figure 6.7).

The increase in failure rate mediated by CP93129 was not significantly different from the increase in failures observed following 5-HT application (P = 0.07, unpaired *t* test). In contrast the 5-HT_{1A} receptor subtype selective agonist, 8-OH-DPAT (10 μM), did not significantly increase the failure rate (39 ± 3 %, n = 3, P = 0.23, unpaired *t* test, Figure 6.7).

6.3.2 5-HT_{1B} receptor activation changes the paired pulse ratio

The ratio between two EPSCs evoked close together can also provide insight into whether modulation of the EPSC is due to a pre- or post-synaptic effect. As described in Chapter 5 when two EPSCs are evoked 50 ms apart in FMs, the second EPSC is larger in amplitude than the first (termed paired pulse facilitation). The ratio between the amplitude of these two EPSCs is the paired pulse ratio (ppr = EPSC 2/EPSC 1). It is widely accepted that changes in the paired pulse ratio are indicative of a presynaptic mechanism (Stuart and Redman 1991). The effect of 5-HT on the ppr for glutamatergic EPSCs in FMs was investigated. Figure 6.8A shows the mean control EPSC (with failures) recorded from a representative FM voltage-clamped at –70 mV. The paired pulse ratio under these conditions was 1.6. Figure 6.8A also demonstrates that application of 5-HT reduces the mean amplitude of both EPSCs. Under control conditions the amplitude of EPSC 1 was -33 pA and in the presence of 5-HT (10 μM) it was reduced to –5 pA (a reduction to 15 % of control). The amplitude of EPSC 2 was -52 pA and was reduced to –15 pA in the presence of 5-HT (10 μM, a reduction to 29 % of control).

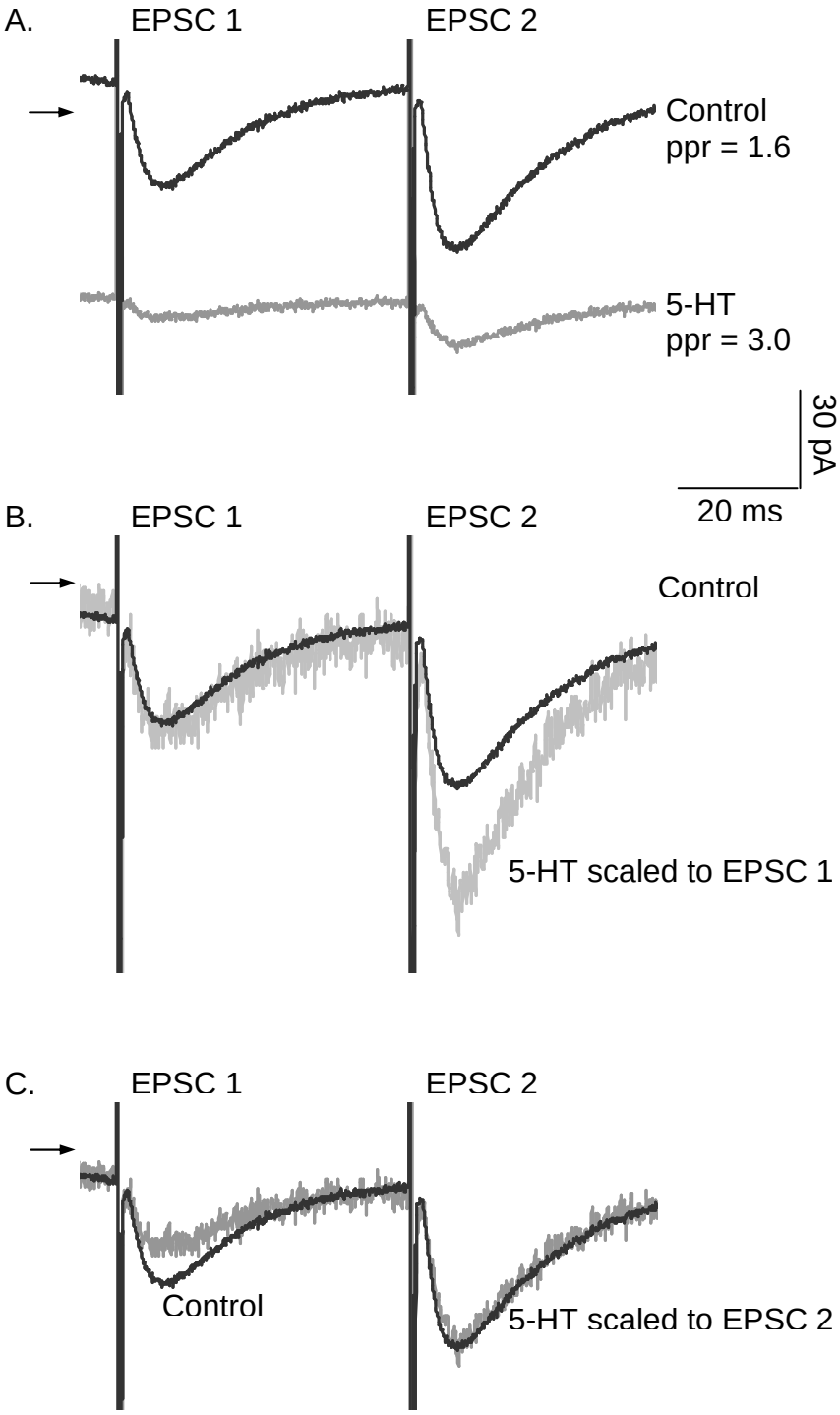
A.
EPSC 1
EPSC 2
Control
ppr = 1.6
5-HT
ppr = 3.0
30 pA
20 ms
B.
EPSC 1
EPSC 2
Control
5-HT scaled to EPSC 1
C.
EPSC 1
EPSC 2
Control
5-HT scaled to EPSC 2

Figure 6.8. Effect of 5-HT on paired pulse ratio in facial motoneurones.

A. Mean EPSCs (minimum of 10 EPSCs with failures) recorded from a facial motoneuron voltage-clamped at –70 mV under control conditions (black) demonstrating that when two stimuli are evoked close together (50 ms apart) the second mean EPSC is larger in amplitude than the first. In the presence of 5-HT (10 μM, grey) both mean EPSCs are reduced in amplitude, however the paired pulse ratio (ppr) is increased. The arrow indicates the –140 pA level.

B. Identical mean EPSCs as (A) except that the trace obtained in the presence of 5-HT (10 μM, grey) has been scaled up so that the first EPSCs under each condition are equal in amplitude. Note that the second EPSC is relatively larger in the presence of 5-HT. The arrow indicates the –120 pA level for the control response. The baseline for the scaled 5-HT response has been compensated for comparison.

C. Identical mean EPSCs as (A) except that the trace obtained in the presence of 5-HT (10 μM, grey) has been scaled up so that the second EPSCs under each condition are equal in amplitude. Note that the first EPSC is relatively smaller in the presence of 5-HT. The arrow indicates the –120 pA level for the control response. The baseline for the scaled 5-HT response has been compensated for comparison.

In the presence of 5-HT (10 μM) the paired pulse ratio was increased to 3.0. This was coupled with an inward current of –58 pA due to the previously characterized postsynaptic effects of 5-HT (Chapters 3 and 4). In order to demonstrate this change in paired pulse ratio the amplitude of the 1st EPSC obtained in the presence of 5-HT was scaled up to the same amplitude as the 1st control EPSC. Note that the holding current for the scaled up traces in the presence of 5-HT were compensated for so that they were approximately equal to the control holding current. Figure 6.8B shows that when this was done the second mean EPSC in the presence of 5-HT is larger than control. The scaled up traces also illustrate that 5-HT does not alter the kinetics of the EPSC. Similarly, Figure 6.8C demonstrates that when the EPSCs in the presence of 5-HT (10 μM) are scaled up so that the second mean EPSCs are equal in amplitude, the first mean EPSC in the presence of 5-HT is smaller than control. The mean paired pulse ratio under control conditions was 1.5 ± 0.1 and this was significantly increased to 2.3 ± 0.2 in the presence of 5-HT (10 μM, n = 8, P = 0.0081, paired *t* test). These data and Figure 6.8 demonstrate that application of 5-HT (10 μM) changes the paired pulse ratio supporting the suggestion that 5-HT has a presynaptic action in the FMs tested.

Figure 6.9A shows the mean EPSCs from another FM voltage-clamped at –70 mV. The paired pulse ratio under control conditions was 2.8. As shown previously, application of the 5-HT$_{1B}$ receptor agonist, CP93129 (10 μM), reduces the mean amplitude of both EPSCs. Under control conditions the amplitude of EPSC 1 was -33 pA and in the presence of CP93129 (10 μM) it was reduced to –9 pA (a reduction to 27 % of control).

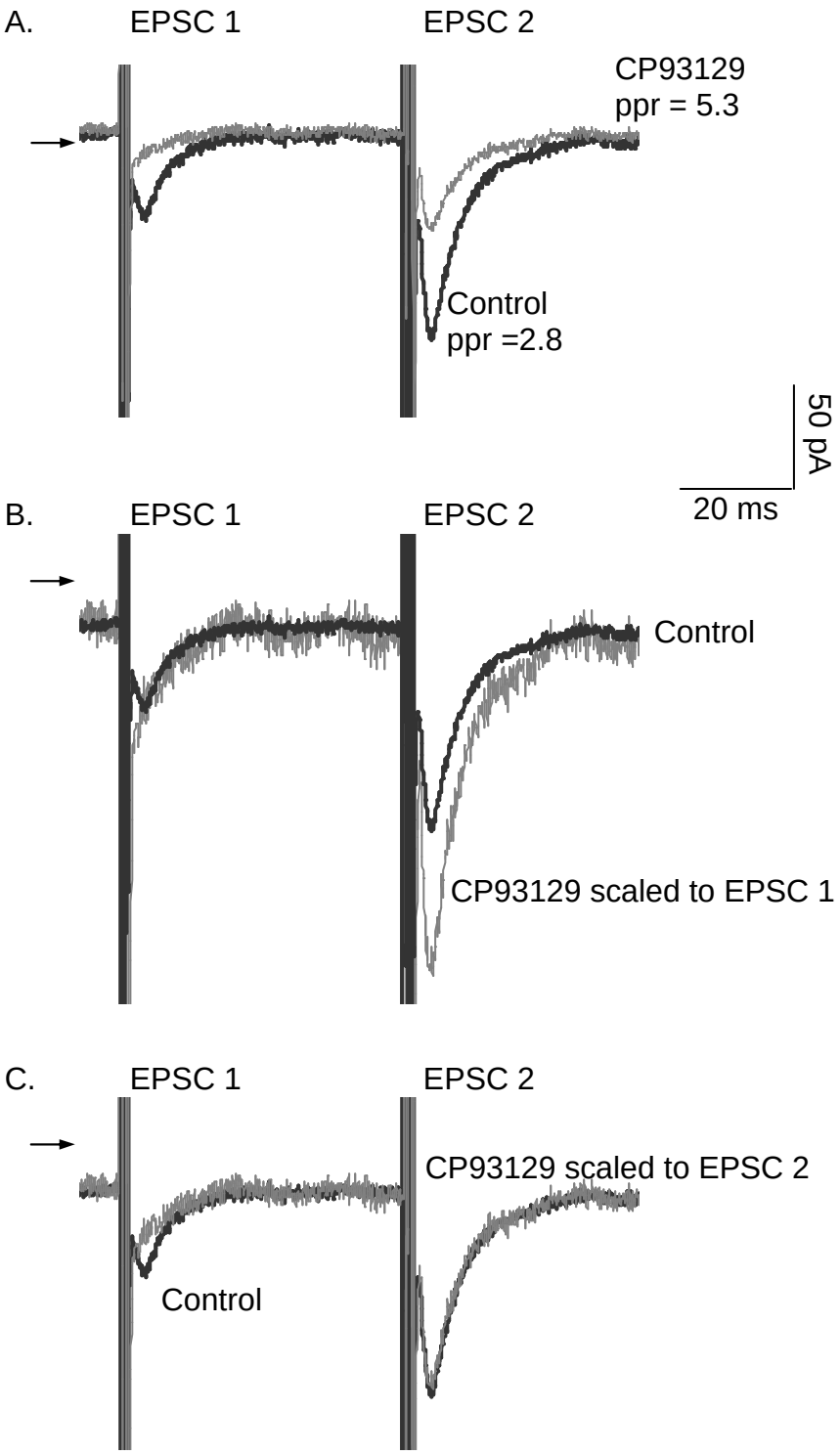
A.
EPSC 1
EPSC 2
CP93129
ppr = 5.3
Control
ppr =2.8
50 pA
20 ms
B.
EPSC 1
EPSC 2
Control
CP93129 scaled to EPSC 1
C.
EPSC 1
EPSC 2
CP93129 scaled to EPSC 2
Control

Figure 6.9. Effect of CP93129 on paired pulse ratio in facial motoneurones.

A. Mean EPSCs recorded from a facial motoneuron voltage-clamped at –70 mV under control conditions (black) demonstrating that when two stimuli are evoked close together (50 ms apart) the second mean EPSC is larger in amplitude than the first. In the presence of CP93129 (10 μM, grey) both mean EPSCs are reduced in amplitude. The arrow indicates the –125 pA level.

B. Identical mean EPSCs as (A) except that the trace obtained in the presence of CP93129 (10 μM, grey) has been scaled up so that the peak of the first EPSCs under each condition are equal in amplitude. Note that the second EPSC is relatively larger in the presence of CP93129. The arrow indicates the –100 pA level for the control response. The baseline for the scaled CP93129 response has been compensated for comparison.

C. Identical mean EPSCs as (A) except that the trace obtained in the presence of CP93129 (10 μM, grey) has been scaled up so that the second EPSCs under each condition are equal in amplitude. Note that the first EPSC is relatively smaller in the presence of CP93129. The arrow indicates the –100 pA level for the control response. The baseline for the scaled CP93129 response has been compensated for comparison.

The amplitude of EPSC 2 was -94 pA and was reduced to –47 pA in the presence of CP93129 (10 μM, a reduction to 50 % of control). In the presence of 5-HT (10 μM) the paired pulse ratio was increased to 5.3. CP93129 (10 μM) did not alter the holding current (-129 pA and –122 pA in the absence and presence of CP93129, respectively). As for the 5-HT response, the traces obtained in the presence of CP93129 (10 μM) were scaled up so that the mean EPSCs were equal in amplitude. Figure 6.9B demonstrates that when the EPSCs in the presence of CP93129 (10 μM) are scaled up so that the first mean EPSCs are equal in amplitude, the second mean EPSC in the presence of CP93129 is larger than control. Similarly, Figure 6.9C demonstrates that when the EPSCs in the presence of 5-HT (10 μM) are scaled up so that the second mean EPSCs are equal in amplitude, the first mean EPSC in the presence of CP93129 is smaller than control. The mean paired pulse ratio under control conditions was 2.2 ± 0.2 and in the presence of CP93129 it was 5.2 ± 2.1 (n = 6). Although there is an increase in the paired pulse ratio in the presence of CP93129 the data is not significantly different (P = 0.14, paired *t* test), and it is speculated that this may be due to the large variation in the paired pulse ratio within this group of FMs.

As discussed previously, the 5-HT_{1A} receptor agonist, 8-OH-DAPT (10 μM), does not alter the amplitude of the first EPSC. In a representative FM the first EPSC was -23 pA and –24 pA in amplitude in absence and presence of 8-OH-DAPT (10 μM), respectively (Figure 6.10). The amplitude of the second EPSC under control conditions was –37 pA and –38 pA in the presence of 8-OH-DPAT (10 μM, Figure 6.10).

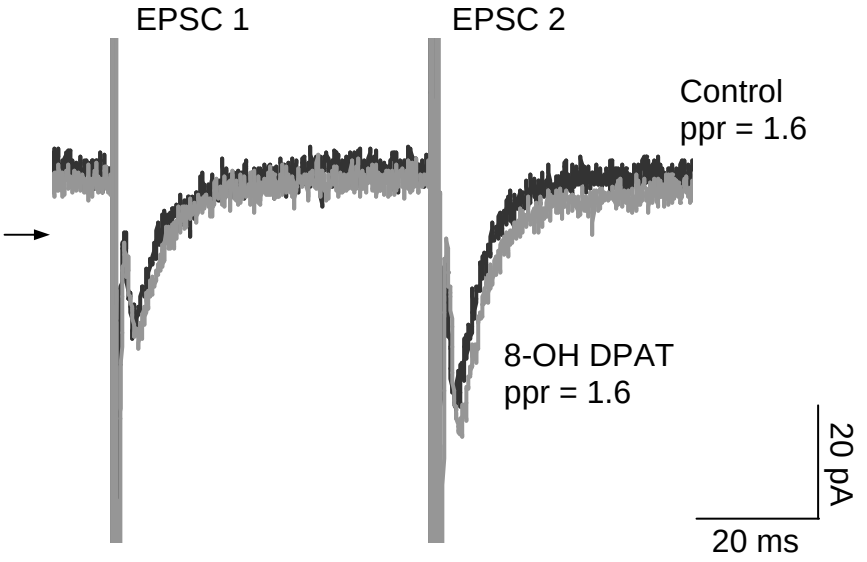

Figure 6.10. Effect of 8-OH DPAT on paired pulse ratio in facial motoneurones.
Mean EPSCs recorded from a FM voltage-clamped at –70 mV under control conditions (black) demonstrating that when two stimuli are evoked close together (50 ms apart) the second mean EPSC is larger in amplitude than the first. In the presence of 8-OH-DPAT (10 μM, grey) both mean EPSCs are similar in amplitude to control. The arrow indicates the –80 pA level.

Thus, the paired pulse ratio was unchanged in the presence of 8-OH-DPAT (10 μM, 1.6 in both the presence and absence of agonist, Figure 6.10). The mean control paired pulse ratio was 1.5 ± 0.1 and was 1.4 ± 0.1 in the presence of 8-OH-DPAT (10 μM) (n = 3, P = 0.24, paired *t* test).

6.3.3 Activation of 5-HT$_{1B}$ receptors alter spontaneous release frequency

Analysis of the frequency and amplitude of spontaneous EPSCs can also be used to determine whether an effect occurs through a pre- or post-synaptic mechanism. Spontaneous or miniature (mini) EPSCs were recorded from FMs in the presence of tetrodotoxin (TTX 0.3 μM) to block action potential dependent-transmitter release. Thus mini EPSCs are mediated by spontaneous release of neurotransmitter from the presynaptic terminal. A change in mini EPSC amplitude is thought to be due to a postsynaptic effect, whereas a change in the frequency at which these spontaneous events occur is due to a presynaptic mechanism. Figure 6.11 shows sample traces from a representative FM demonstrating that frequency of mini EPSCs are reduced in the presence of 5-HT (10 μM). Figure 6.12A shows a cumulative probability histogram of inter-event interval, which corresponds to mini EPSC frequency. In this FM the control frequency was 4.7 events s^{-1} and this was reduced to 3.2 events s^{-1} in the presence of 5-HT (10 μM). This represents a significant reduction in frequency (P = 0.01, assessed by the Kolmogorov-Smirnov two sample test). Figure 6.12B shows the cumulative probability histogram of mini EPSC amplitude. In this FM the control amplitude was –89 ± 2 pA (n = 1397 events) and the amplitude

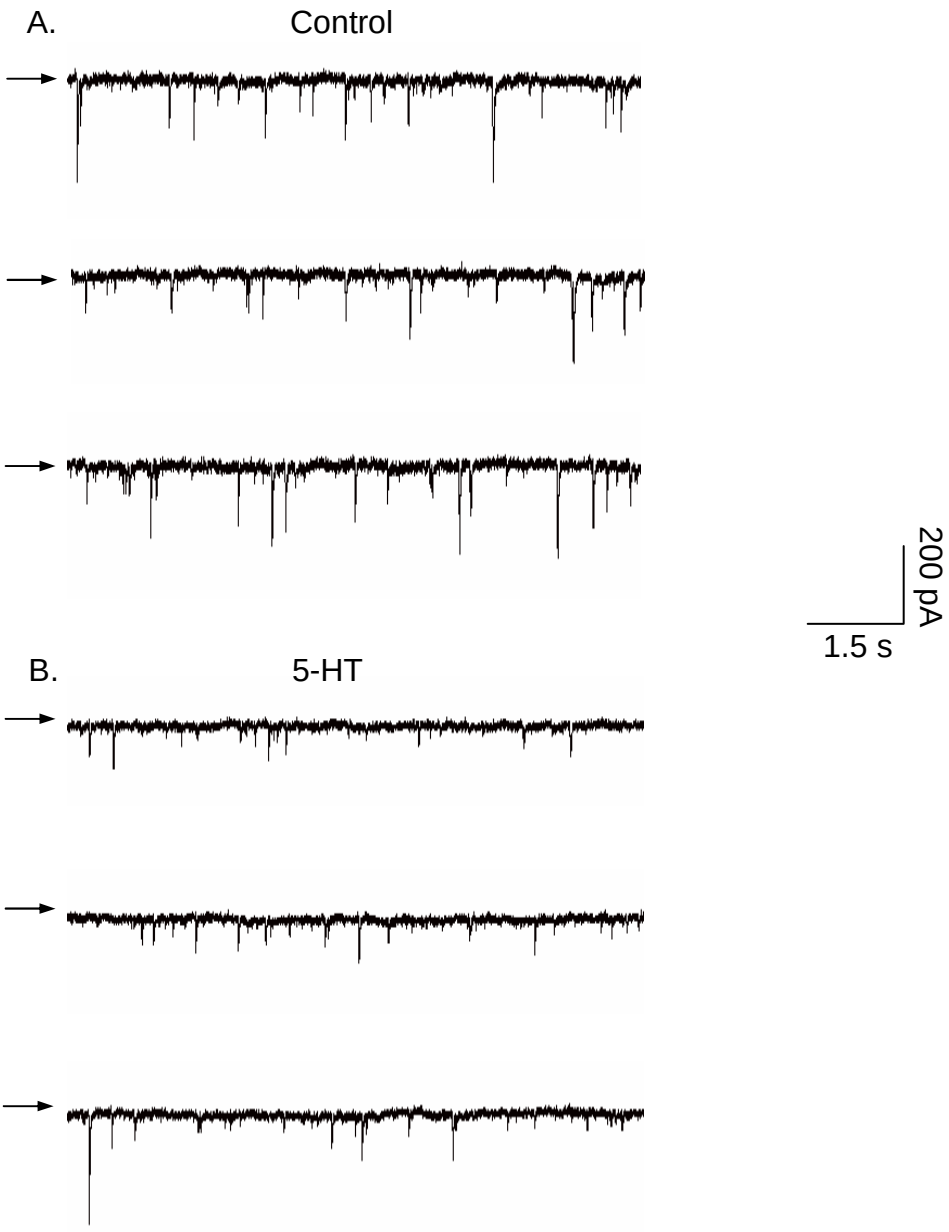

Figure 6.11. 5-HT reduces the frequency of miniature EPSCs in facial motoneurones.

A. Control recording from a representative motoneuron voltage-clamped at –70 mV in the presence of TTX (0.3 μM). The downward deflections are miniature EPSCs. The arrows indicate the –43 pA level.

B. Recording from the same motoneuron as A following application of 5-HT (10 μM). The frequency of miniature EPSCs is reduced. The arrows indicate the –150 pA level.

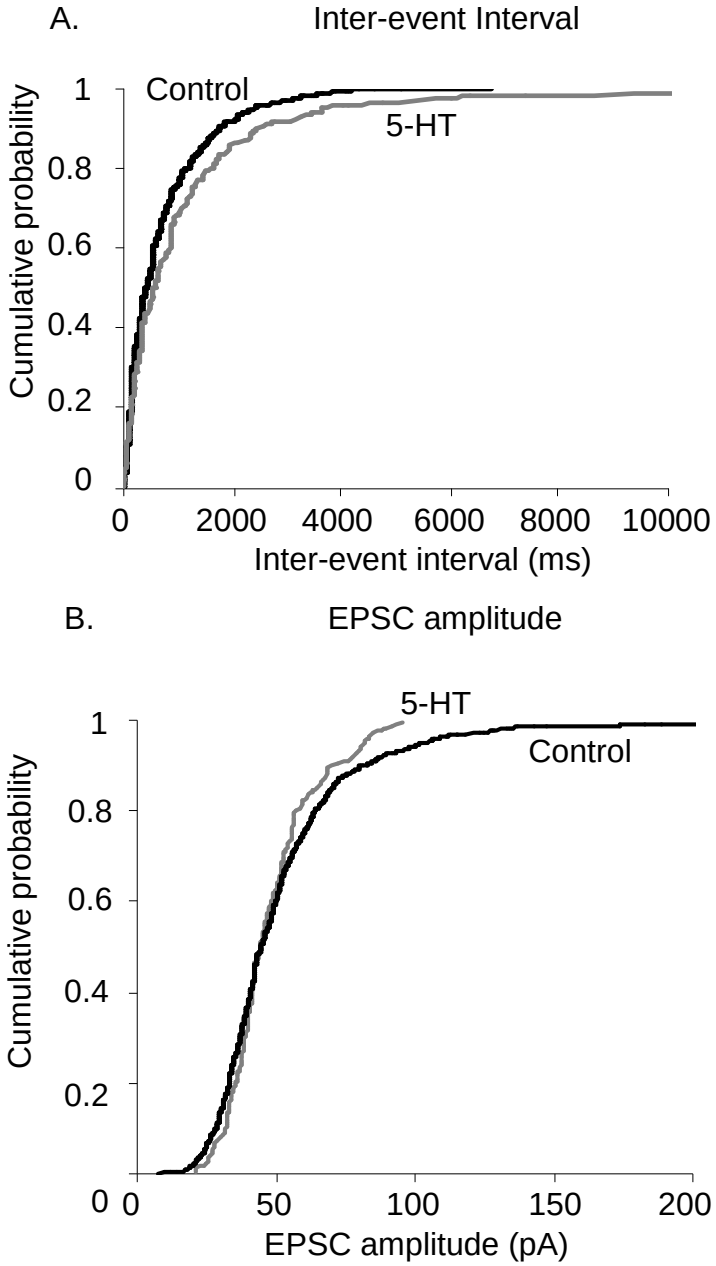

Figure 6.12. Cumulative probability histograms of EPSC frequency and amplitude in facial motoneurones.

A. Cumulative probability histogram of the inter-event interval (corresponding to frequency) of miniature EPSCs from a representative motoneuron (sample traces shown in Figure 6.11). The EPSC frequency is significantly lower in the presence of 5-HT (10 μM, grey, P = 0.01, Kolmogorov-Smirnov two sample test).

B. Cumulative probability histogram of miniature EPSC amplitude from a representative motoneuron (sample traces shown in Figure 6.11) voltage-clamped at –70 mV. The EPSC amplitude is not significantly changed in the presence of 5-HT (10 μM, grey, P = 0.26, Kolmogorov-Smirnov two sample test).

following 5-HT (10 μM) application was not significantly different at -67 ± 2 pA (n = 730 events, P = 0.26, Kolmogorov-Smirnov two sample test). As shown previously, bath application of 5-HT (10 μM) also evoked an inward current of –107 pA due to its postsynaptic mechanisms. In a sample group of FMs the frequency of mini EPSCs was significantly reduced from 3.1 ± 0.9 events s^{-1} under control conditions to 2.0 ± 0.7 events s^{-1} in the presence of 5-HT (10 μM, n = 3, P = 0.02, paired *t* test). In the sample group of FMs the amplitude of mini EPSCs was 69 ± 11 pA under control conditions and 55 ± 6 pA in the presence of 5-HT (10 μM), representing a non-significant effect (n = 3, P = 0.06, paired *t* test). The rise times for mini EPSCs were not significantly altered by 5-HT (10 μM) and were 4.5 ± 0.2 ms and 5.5 ± 0.4 ms, in absence and presence of 5-HT, respectively (n = 3, P = 0.12, paired *t* test). In addition, the decay times for mini EPSCs were also not significantly affected by 5-HT (10 μM) and were 19.0 ± 1.3 ms and 19.4 ± 1.8 ms, in absence and presence of 5-HT, respectively (n = 3, P = 0.31, paired *t* test). Thus, 5-HT (10 μM) significantly reduces the frequency of mini EPSCs but has no effect on their amplitude or rise and decay times indicating that 5-HT evokes a presynaptic effect.

6.4 Discussion

6.4.1 5-HT inhibits synaptic transmission

In addition to evoking an inward current as described earlier (Chapters 3 and 4), 5-HT was found to significantly inhibit the mean amplitude of evoked excitatory synaptic transmission in FMs.

6.4.2 5-HT_{1B} receptor activation reduces EPSC amplitude

The pharmacology of this inhibitory action of 5-HT indicates the involvement of 5-HT_{1B} but not 5-HT_{1A} receptors. CP93129 is highly selective for 5-HT_{1B} receptors (EC_{50} = 56 ± 5 nM) over other 5-HT receptors (> 150 times lower affinity at 5-HT_{1A} and 5-HT_{1D} receptors) and this study has demonstrated that CP93129 mimics the 5-HT inhibition of EPSC amplitude but does not evoke any of the postsynaptic excitatory actions of 5-HT (Macor, Burkhart et al. 1990). The 5-HT_{1A} receptor agonist, 8-OH-DPAT, does not inhibit EPSC amplitude nor was it found to evoke any of the excitatory actions of 5-HT. The lack of an excitatory effect of 8-OH-DPAT might seem as 8-OH-DPAT has been described as a partial agonist at 5-HT_7 receptors in some studies (Wood, Chaubey et al. 2000). In Chapter 4 of this thesis evidence is provided supporting a 5-HT_7 receptor-mediated enhancement of I_h in FMs. As agonist efficacy is likely to reflect both characteristics of the tissue (e.g. receptor number, coupling mechanisms) and drug-receptor interactions the former may explain the lack of effect of 8-OH-DPAT on I_h in FMs. These observations are consistent with previous findings demonstrating a lack of any post-synaptic actions of 8-OH-DPAT (Larkman and Kelly 1997).

The pharmacology of the inhibitory effect of 5-HT on glutamate release was verified using subtype selective antagonists. Isamoltane is an antagonist at 5-HT_{1B} receptors and was found to block the inhibition of EPSC amplitude by 5-HT. Isamoltane does show some affinity for 5-HT_{1A} receptors (IC_{50} = 1070 nM verses 39 nM for 5-HT_{1B} receptors), however, it is unlikely that 5-HT_{1A} receptors were significantly blocked at the concentration applied in these experiments (1 μM) (Wood, Chaubey et al. 2000).

The lack of involvement of 5-HT_{1A} receptors was confirmed by the failure of the highly selective 5-HT_{1A} receptor antagonist, WAY 100635, to block the inhibition of EPSC amplitude by 5-HT (Critchley, Childs et al. 1994). A similar inhibition of glutamate release from terminals presynaptic to spinal motoneurones and hypoglossal motoneurones has been demonstrated, although, in the hypoglossal nucleus both 5-HT_{1A} and 5-HT_{1B} receptors are involved (Bouryi and Lewis 2003; Honda, Tanabe et al. 2003).

6.4.3 Synaptic location of 5-HT_{1B} receptors

5-HT_{1B} receptors function as heteroreceptors to modulate glutamate release in several regions including the rat subiculum and the hypoglossal motor nucleus (Bobker and Williams 1989; Boeijinga and Boddeke 1996; Bouryi and Lewis 2003). There are several lines of evidence to support a presynaptic location for 5-HT_{1B} receptors in the FMN. Firstly, 5-HT and CP93129 increased the rate of failure to generate an EPSC at a constant stimulus intensity. Secondly, 5-HT and CP93129 altered the paired pulse ratio. A change in the paired pulse ratio is indicative of a presynaptic mechanism and an increase is associated with a presynaptic inhibition of neurotransmitter release (Stuart and Redman 1991). Thirdly, 5-HT alters the frequency, but not the amplitude, of mini EPSCs. Mini EPSCs represent spontaneous (in the absence of nerve stimulation) neurotransmitter release at synapses across the entire neurone, therefore, it cannot be assumed that these synapses are the same population as those that are evoked by electrical stimulation. However, the decrease in frequency of mini EPSCs supports the data obtained from the evoked EPSCs.

6.4.4 Mechanism of inhibition of release by 5-HT_{1B} receptors

The mechanism underlying the decrease of neurotransmitter release from the presynaptic terminal by 5-HT_{1B} receptor activation remains unknown, largely due to the inaccessibility of recording from presynaptic terminals. An increase in the paired pulse ratio is also observed when the extracellular [Ca^{2+}] is decreased suggesting that neurotransmitter release can be inhibited by decreasing the Ca^{2+} entering the presynaptic terminal following stimulation (Stuart and Redman 1991). A potential mechanism for reducing Ca^{2+} entry into the terminal is by modulation of the channels through which Ca^{2+} enters the neurone. An inhibition of N-type Ca^{2+} channels following activation of G_i proteins has been demonstrated in the chick dorsal root ganglion and as 5-HT_{1B} receptors activate G_i proteins this could also occur in the FMN (Mirotznik, Zheng et al. 2000). Similarly, at the calyx of Held, activation of presynaptic metabotropic glutamate receptors (mGluRs, some of which are coupled to G_i proteins) reduces glutamate release by inhibiting P/Q-type Ca^{2+} channels (Takahashi, Forsythe et al. 1996).

As Ca^{2+} influx into the presynaptic terminal following nerve stimulation is through voltage-dependent Ca^{2+} channels, reducing the depolarisation of the terminal membrane and the subsequent activation of these channels represents an alternative mechanism for modulating transmitter release. An increase in K^+ conductance would result in membrane hyperpolarisation and a decrease in membrane depolarisation following action potential innervation of the terminal. Subsequently the reduced Ca^{2+} entry into the terminal would result in a lower release probability of vesicles and an inhibition of synaptic transmission. 5-HT_1 receptor activation leads to G protein βγ subunit (Gβγ) which has been shown to activate K^+ conductances in the

hippocampus (Andrade, Malenka et al. 1986; Andrade and Nicoll 1987; Colino and Halliwell 1987). Activation of muscarinic acetylcholine receptor from the heart (M_2 receptors that are coupled to G_i proteins), results in the Gβγ subunit activating G protein coupled inwardly rectifying K^+ (GIRK) channels (Logothetis, Kurachi et al. 1987; Reuveny, Slesinger et al. 1994).

A third proposed mechanism for modulating presynaptic release occurs downstream of Ca^{2+} influx into the nerve terminal (Blackmer, Larsen et al. 2001). Modulation of the proteins involved in the fusion of vesicles with the plasma membrane (SNARE proteins, (Li and Chin 2003)) and could potentially reduce vesicle release (Blackmer, Larsen et al. 2001). This modulation is downstream of Ca^{2+} entry into the terminal and was first demonstrated in the frog neuromuscular junction where activation of adenosine receptors reduces the affinity of the fusion machinery for Ca^{2+} (on which it is dependent) (Silinsky 1984; Silinsky and Solsona 1992). At the frog neuromuscular junction this inhibition of acetylcholine release is dependent on adenylate cyclase activity, however, at the lamprey reticulospinal-motoneurone synapse it appears that the Gβγ subunit can bind directly to the fusion machinery to reduce neurotransmitter release (Silinsky 1984; Silinsky and Solsona 1992; Blackmer, Larsen et al. 2001). The mechanism mediating the inhibition of glutamate release in the FMN is not yet known, however, whether or not this effect is dependent on Ca^{2+} influx into the terminal or an effect downstream of this could be investigated using Ca^{2+} imaging.

6.5 Concluding statement

Chapters 3 and 4 of this thesis have reported the excitatory effects of 5-HT on neonatal rat FMs. This chapter has focused on the inhibitory actions of 5-HT on synaptic transmission and has determined that release of glutamatergic vesicles (as described in Chapter 4) is inhibited by a presynaptic activation of 5-HT_{1B} receptors. These multiple actions of 5-HT in the facial nucleus may provide a mechanism by which 5-HT exerts fine control over motor output.

Chapter 7 General Discussion

7.1 Thesis summary

This thesis has investigated the pre- and post-synaptic mechanisms controlling neonatal rat FM excitability. An enhancement of I_h and an inhibition of gK_{Leak} have been confirmed as the mechanisms underlying the 5-HT-induced excitation of FMs previously observed (VanderMaelen and Aghajanian 1980; Vandermaelen and Aghajanian 1982; Larkman, Penington et al. 1989). The NA-induced excitation was also shown to be mediated by an inhibition of gK_{Leak}. The molecular identity of the channel underlying gK_{Leak} was previously unknown, thus making the physiological significance of its modulation unclear. This thesis provides evidence to support a TASK-1/TASK-3 heteromeric channel identity. This is consistent with previous studies demonstrating that members of the K_{2P} channel family provide leak currents in a variety of neurones and can be inhibited via G protein-coupled receptor activation (Goldstein, Bockenhauer et al. 2001; Patel and Honore 2001).

Identifying the different receptor subtypes mediating these effects of 5-HT and NA was crucial for the understanding of how the agonists exert their different actions in FMs. The mechanism by which 5-HT-receptor activation enhanced I_h was previously determined as a direct action of cAMP on the channel (Larkman and Kelly 1997). Here it has been established that 5-HT_7 receptor activation mediates this enhancement of I_h.

The receptor subtypes that mediate the 5-HT- and NA-induced inhibition of gK_{Leak} have been identified as 5-HT_{2A} receptors and α_1-adrenoceptors, although an

involvement of 5-HT_{2C} receptors cannot be completely ruled out by the findings presented here. Both 5-HT_{2A} receptors and α_1-adrenoceptors are coupled to G_q proteins, activating the PLC pathway. Previous studies have demonstrated that altering the downstream messengers of this pathway ($[Ca^{2+}]_i$ and PKC activation) has no effect on gK_{Leak} (Larkman 2003). It has recently emerged that PIP_2 in the membrane stabilizes a variety of channels (including TASK channels) and its hydrolysis by PLC leads channel closure (Czirjak, Petheo et al. 2001; Chemin, Girard et al. 2003; Lopes, Rohacs et al. 2005). This mechanism for the inhibition of gK_{Leak} in FMs was investigated. PLC-β1 was detected in the mouse FMN and a functional role for this enzyme in the NA-induced current was observed in PLC-$\beta1^{-/-}$ mice, however, the 5-HT-induced current did not appear to be affected by the lack of PLC-β1. An attempt to determine whether alternative isoforms of the enzyme mediated the 5-HT-induced inhibition of gK_{Leak} was made using the non-selective PLC inhibitor, U73122, however no conclusive results were obtained. This suggested that either the inhibitor did not reach its intracellular site of action within the experimental time period or that this action of 5-HT does not involve PLC activity. In the latter respect it is pertinent that a recent report suggests TASK channels can be inhibited by a direct action of $G\alpha_q$ (Chen and Talley 2006).

The nature of the fast excitatory synaptic transmission that controls action potential firing in FMs was previously uncharacterised. In order to further understand synaptic integration in FMs the neurotransmitter phenotype and the receptor subtypes activated were determined. Glutamatergic EPSCs and EPSPs were evoked in FMs by stimulating close to the dendrites of the recorded FM. A contribution of NMDA and non-NMDA (AMPA/kainate) glutamate receptors was identified using selective

antagonists. In addition, GluR2 and NR2B subunit containing glutamate receptors were detected at the synapse tested. Protein for other glutamate receptor subunits have been detected in FMs however, their functional contributions could not be assessed due to the lack of selective ligands (Martin, Blackstone et al. 1993; Sato, Kiyama et al. 1993; Nishi, Hinds et al. 2001).

It was also determined that by using a minimal stimulation protocol single synapses could be activated in FMs. At these putative single synapses fluctuations in amplitude were observed providing evidence that supports the controversial theory of quantal release at single central synapses (Sastry and Bhagavatula 1996; Auger and Marty 2000; Stevens 2003).

Finally the effect of 5-HT on this glutamatergic synaptic transmission was assessed. Unlike the excitatory postsynaptic actions of 5-HT it was determined that 5-HT has an inhibitory effect on glutamate release from the presynaptic terminal and that this action was mediated by activation of presynaptic 5-HT_{1B} receptors.

7.2 Possible functional implications of pH-sensitive gK_{Leak}

Whether the pH-sensitivity of gK_{Leak} is functionally important for FMs is not clear. Changes in external pH are known to occur during periods of ischaemia and hypoxia but functionally significant physiological changes are less apparent. A small change in external pH may be sufficient to alter the properties of gK_{Leak} however the integrated response of the motoneuronal membrane is likely to involve additional effects on other conductances. Experiments performed in the absence ZD-7288 indicated that changes in external pH across the range pH 6 to 8 also altered I_h (not reported here). The overall change in FM membrane conductance thus reflects the

integration of at least these two components. Nevertheless, modulation of gK_{Leak} by endogenous neurotransmitters, particularly NA and 5-HT, indicates an important role in the priming and maintenance of FM membrane excitability during waking and states of sensory arousal.

7.3 TASK-1 knock out mice

Mice lacking TASK-1 have been generated and were found to show little behavioural differences to their littermate controls except from impaired motor coordination (Aller, Veale et al. 2005). This was reported to be due to the lack of TASK-1 in the cerebellar granule neurones which play a key role in motor coordination (Aller, Veale et al. 2005). The resting membrane excitability of the CGNs from the knock out mice was not significantly different from their littermate controls and the leak current was found to be sensitive to Zn^{+} and ruthenium red suggesting that the absence of TASK-1 was compensated for by homomeric TASK-3 channels (Czirjak and Enyedi 2003; Aller, Veale et al. 2005). It is noteworthy that this shift to a homomeric TASK-3 population appears to affect motor coordination in the knock out mice, demonstrating the importance of the TASK-1 channel for normal CGN function (Aller, Veale et al. 2005). It would be of interest to investigate the sensitivity of the FM gK_{Leak} in these mice to assess whether the proposed heteromeric TASK-1/TASK-3 population is also replaced by homomeric TASK-3 channels. The lack of a deficiency in motor function suggests that motoneurone excitability is not significantly impaired in the TASK-1 knock out mice, this is consistent with TASK-1 homomers not playing a dominant role in motoneurone excitability (Aller, Veale et al. 2005). Taken together with the lack of sensitivity to ruthenium red, these findings support a TASK-1/TASK-3 heteromeric identity for

the gK_{Leak} in FMs. The generation of a double TASK-1 and TASK-3 knock out mice would further allow the role of gK_{Leak} in the contribution to the resting membrane potential and its role in synaptic integration in FMs to be further assessed.

7.3 Role of I_h in FMs

7.3.1 Functions of I_h

Pacemaker currents were first identified in the sino-atrial node cells in the heart during the late 1970s (Noma and Irisawa 1976). This current was termed I_f ('funny') due to its apparently unique slow activation in response to hyperpolarisation. In the heart, I_h is involved in rhythmic activity by determining the time which elapses between action potentials in cardiac cells (Kaupp and Seifert 2001). In the early 1980s neuronal pacemaker currents were identified in rod photoreceptors in the eye and termed I_h ('hyperpolarisation-activated') (Attwell and Wilson 1980). Evidence for a similar current in central neurones was obtained from hippocampal pyramidal neurones and was termed I_q ('queer') due to its strange electrophysiological behaviour (Halliwell and Adams 1982). The preferred term in the central nervous system is I_h.

I_h contributes to a pacemaker current in many central neurones and this action particularly well documented for thalamocortical relay neruones (Pape and McCormick 1989; Luthi and McCormick 1998; Luthi and McCormick 1998). Following an action potential the neuronal membrane hyperpolarises, activating I_h which provides a depolarising inward current (Pape and McCormick 1989; Robinson and Siegelbaum 2003). As the membrane depolarises (due to I_h activity) and becomes closer to the threshold for action potential firing, I_h inactivates (Pape and

McCormick 1989; Robinson and Siegelbaum 2003). Therefore the kinetics of I_h activation and inactivation determines the time that elapses between action potentials. Mice lacking the HCN2 subunit suffer from spontaneous absence seizures supporting a pacemaker function of I_h (Ludwig, Budde et al. 2003).

In neurones that do not require an integral pacemaker, I_h can contribute to the resting membrane potential and input resistance. Resting membrane potentials of neurons are typically between -50 mV to -100 mV and I_h is active within this range. As I_h does not inactivate at hyperpolarised potentials, the sustained depolarising current mediated by I_h helps set the resting membrane potential depolarised to the K^+ equilibrium potential (Pape 1996). This is supported by the hyperpolarising shift in the resting membrane potential observed in thalamocortical relay neurones in the HCN2 deficient mice (Ludwig, Budde et al. 2003). As FMs are not spontaneously active it is likely that contributing to the resting membrane potential is a primary role for I_h in these neurones.

An additional action of I_h is in the integration of synaptic inputs. Dendrites were traditionally thought to act as passive cables and in such systems synaptic potentials received in the dendritic network of a neurone would be subject to filtering as they travel to the soma (Whitehead and Rosenberg 1993). Thus the generation of an action potential at the cell soma would be dependent on the location of synaptic inputs in the dendrites and temporal summation of synaptic potentials. Ion channels can confer active properties to the dendritic membrane and the density of I_h has been found to increase in the distal dendrites relative to distance from the soma of neocortical and CA1 hippocampal pyramidal neurones (Magee 1998; Cook and

Johnston 1999; Williams and Stuart 2000; Gulledge 2005). In these neurones I_h removes the location dependence of synaptic inputs and normalises temporal summation (Magee 1999; Williams and Stuart 2000). The potential role for I_h in the integration of synaptic inputs in FMs is discussed further in Section 7.7.1.

7.4 Effect of 5-HT in FMN

7.4.1 Multiple 5-HT receptors in FMN

5-HT exerts several different effects in the CNS due to the diversity of 5-HT receptors and from the findings of this thesis it has become apparent that several subtypes of 5-HT receptors are present in the neonatal rat FMN (summarised in Table 7.1) (IUPHAR 2000).

Receptor subtype	Mechanism	Synaptic location	Effect on FM
5-HT$_7$	Enhances I_h	Postsynaptic	Excitatory (membrane depolarisation)
5-HT$_2$	Inhibits gK_{Leak} (TASK 1/TASK 3 channels)	Postsynaptic	Excitatory (membrane depolarisation)
5-HT$_{1B}$	Inhibits glutamate release	Presynaptic	Inhibitory (reduced synaptic transmission)

Table 7.1. Summary of actions of 5-HT receptors in FMN.

Previously it has been generally accepted that 5-HT has an excitatory action in the FMN (VanderMaelen and Aghajanian 1980; Vandermaelen and Aghajanian 1982; Larkman, Penington et al. 1989; Larkman and Kelly 1992). However, the findings presented in this thesis suggest that if 5-HT is released globally throughout the facial

nucleus that preventing glutamate release at the synapse may be dominant over the increase in post-synaptic membrane excitability and therefore 5-HT would have a predominately negative action.

7.4.2 Role of 5-HT, arousal states and motor activity

The activity of mammalian 5-HT neurones show correlations with arousal state (Jacobs and Fornal 1999). The 5-HT neurone discharge activity was found to be slow and regular during quiet waking states and increased during the aroused state or in response to sensory-stimuli (Jacobs and Fornal 1999). As animals enter into the sleep state the activity of 5-HT neurones declines and can be almost completely absent from animals in a deep, REM sleep (Jacobs and Fornal 1999). These correlations were originally observed for 5-HT neurones of the dorsal raphé nucleus of the freely moving cat but have also been seen other mammalian species and in other groups of 5-HT neurones, including some of those that innervate the facial nucleus (the raphé magnus, obscurus and pallidus nuclei) (Jacobs and Fornal 1991; Jacobs and Fornal 1999).

The firing rates of 5-HT neurones also show strong positive correlations with tonic motor activity (Jacobs and Fornal 1997). It has been proposed that the 5-HT system facilitates motor activity and when active the processing of sensory information and the autonomic and endocrine systems are inhibited (Jacobs and Fornal 1999). When the 5-HT system is inactivated motor function is inhibited and sensory information processing is restored (Jacobs and Fornal 1999). Of particular interest is the correlation between the increases in the activity of 5-HT neurones in the dorsal raphé

nucleus and repetitive oral-buccal motor activity involving muscles innervated by FMs (chewing, biting, and grooming) (Jacobs and Fornal 1997).

This positive correlation between the activity of 5-HT neurones and motor activity argues against a predominately inhibitory action of 5-HT in the FMN. It is therefore anticipated that the 5-HT receptors present in the facial nucleus are not activated equally.

7.4.3 Possible mechanisms for differential activation of 5-HT receptors

One possible mechanism by which the excitatory effect dominates over the inhibitory action of 5-HT is that rather than 5-HT being globally released within the nucleus it is focally released onto different sections of the FM. Thus the excitatory effects would be manifested by 5-HT being released onto dendritic regions downstream of site where EPSPs are generated. 5-HT released at the synapse would exert the inhibitory actions of 5-HT, through activation of the 5-HT_{1B} receptors. This theory could be tested experimentally using the recording protocols described in Chapter 6 and instead of applying 5-HT through the superfusing ASCF it could be focally applied using micropipettes (via pressure ejection).

An alternative hypothesis is that 5-HT is globally released in the facial nucleus and receptor affinities control the dominating action of 5-HT. Thus, the receptors that mediate the excitatory actions of 5-HT would be activated by low concentrations of 5-HT and if an inhibitory effect was required the amount of 5-HT released would be increased, eventually activating the lower affinity, inhibitory 5-HT_{1B} receptors.

5-HT receptors bind 5-HT with affinities within the nanomolar range and 5-HT_1 receptors bind 5-HT with a high affinity relative to 5-HT_2 receptors (an example

study determines the K_i for displacement of LSD as 3.5 ± 0.55 nM and 17 ± 2.9 nM for 5-HT_1 and 5-HT_2 binding site, respectively) (Peroutka and Snyder 1979). The 5-HT_7 receptor has also been found to show high affinity for 5-HT (K_d = 1 nM in CHO cells) (Ruat, Traiffort et al. 1993).

Since the 5-HT_2 receptors appear to show the lowest affinity for 5-HT a higher concentration would be required to activate them than for the activation of the inhibitory 5-HT_{1B} receptors, thus the inhibitory effect would be dominant. It is also apparent that the range of receptor affinities is not that large, therefore, it is unlikely that this is the controlling factor in determining the overall effect of 5-HT on FM excitability.

7.4.4 Functional significance of the inhibitory effects of 5-HT

The functional significance of the 5-HT-induced inhibition of glutamate release reported here is unclear (Jacobs and Fornal 1991; Jacobs and Fornal 1999). In the hypoglossal nucleus activation of 5-HT_{1A} and 5-HT_{1B} receptors mediate a similar inhibition of glutamate release suggesting that this may be a common mechanism in the control of motoneurone activity (Bouryi and Lewis 2003). It may be that the 5-HT released at the synaptic cleft is from neurones whose cell somas are located in a different raphé nucleus to those which release 5-HT onto the postsynaptic membrane and exert its excitatory effects. This may particularly significant if the same group of 5-HT neurones innervate opposing muscles, thus when the 5-HT neurone activity is increased some motoneurones would be activated whereas synaptic transmission onto the other group of motoneurones would be prevented.

7.4.5 5-HT projections into the facial nucleus

The FMN contains the highest density of 5-HT nerve terminals of all the cranial nerve nuclei (Takeuchi, Kojima et al. 1983; Senba 1985). The origin of these projections has been investigated using a combination of immunohistochemistry for 5-HT and retrograde labelling with Fluro-Gold injection into the FMN (Li, Takada et al. 1993). The majority of 5-HT neurones projecting to the FMN were observed in the nucleus raphé magnus, obscurus and pallidus with some in the dorsal raphé and the gigantocellular reticular pars alpha (Li, Takada et al. 1993). However, only small numbers of neurones were identified by this study and most likely under-represents the serotonergic projections to the FMN. The available information regarding the origin of 5-HT inputs into the FMN is currently not substantial enough to address the issue of whether the same FM is innervated by 5-HT neurones from different raphé nuclei.

7.5 Effect of NA in FMN

7.5.1 Multiple actions of NA in FMN

NA has been shown to excite FMs by an inhibition of gK_{Leak}, however, unlike 5-HT NA does not appear to enhance I_h. The functional significance of this difference in action of the two transmitters is not yet apparent.

The excitatory action of NA in FMs is mediated by an activation of α_1-adrenoceptors. Whether NA also has an inhibitory action in the facial nucleus has not yet been addressed. The inhibitory effects of 5-HT_{1B} receptor activation appear to be a result of receptor coupling to G_i proteins. Members of the α_2-adrenoceptor family also

couple to G_i proteins and have been shown to modulate K^+ and Ca^{2+} channels, a potential mechanism for the inhibition of glutamate release (Docherty 1998; IUPHAR 2000). A role for α_2-adrenoceptors in inhibiting glutamate release in the facial nucleus could be examined using the experimental paradigm described in Section 6.2.4 and the α_2-adrenoceptor antagonist, RX 821002 (Diez-Alarcia, Pilar-Cuellar et al. 2006). However, as a positive correlation between motor behaviour and NA neurone activity has been observed (see Section 7.5.2) it is likely that if there are inhibitory NA receptors in the FMN they would not be activated with equal efficacy as the excitatory α_1-adrenoceptors (as hypothesized for the multiple effects of 5-HT).

7.5.2 NA, arousal states and motor activity

Similar to the activity pattern of 5-HT neurones, NA neurones (located in the locus coeruleus) show regular slow firing activity in quiet waking animals, increased activity in behaving animals and reduced firing during deep sleep periods (Aston-Jones and Bloom 1981). NA has also been shown to increase motor activity, although the effect is not as well documented as that of 5-HT (Geyer, Segal et al. 1972 617).

7.6 Synaptic integration in FMN

7.6.1 Role of I_h

Whether action potentials are generated by passive summation of EPSPs or integration of synaptic inputs in FMs is not yet known. However, I_h is involved in the integration of synaptic inputs in neocortical and hippocampal pyramidal neurones

and the presence of this current in FMs suggests that some integration may occur (Magee 1999; Williams and Stuart 2000). In these neurones it has been shown that the I_h is expressed more highly in the distal dendrites that those proximal to the cell soma and this increased I_h removes the location dependence of synaptic input and normalises temporal summation (Magee 1998; Cook and Johnston 1999; Magee 1999; Williams and Stuart 2000; Gulledge 2005). It would be of value to determine whether FMs also show this distribution of I_h which could be assessed by including a low concentration of ZD-7288 (1–10 µM) in the intracellular recording solution (without previously incubating the slice). The time required for the block I_h to occur would be indicative of its expression pattern due to the time it takes for ZD-7288 to diffuse to the intracellular region of the channel where it exerts its effect (Shin, Rothberg et al. 2001). An alternative and more quantitative method for assessing the distribution of I_h across the dendritic membrane would be to use the immunohistochemical techniques utilised in this thesis (Section 2.8 and Section 4.3.1) and the commercially available antibodies to the HCN channel subunits.

Accurate studies examining the effect of I_h on synaptic integration and temporal summation require simultaneous dendritic and somatic recordings in order to compare EPSPs at each of these locations (Williams and Stuart 2000; Larkum, Launey et al 1998; Magee 2000). Making similar dual recordings in FMs would allow synaptic integration in FMs to be examined, although this technique would require addition experimental apparatus to that used for this thesis. If this technique was available it would also be of interest to examine synaptic integration in mice lacking the HCN2 subunit (and the other subunits as the knock-out mice become

available) to assess the contribution of these subunits to I_h in FMs and to investigate whether individual subunits play different roles in the integration of synaptic events.

7.6.2 5-HT modulation and synaptic integration

How the postsynaptic modulatory effects of 5-HT alter synaptic integration is also not yet fully understood. If it is assumed that a role of I_h in FMs is to normalise temporal summation of synaptic inputs and that this occurs due to the increased expression of I_h in the distal dendrites then it can also be assumed that by the 5-HT-mediated enhancement of I_h will also further prevent temporal summation of synaptic inputs. This would result in a more efficient rate of action potential firing for the same number of EPSPs. This is consistent with the correlation between 5-HT neurone activity and motor output.

The inhibition of gK_{Leak} could also potentially play a role in synaptic integration. Inhibition of gK_{Leak} and enhanced I_h results in a membrane depolarisation, therefore the depolarisation required by incoming synaptic inputs to push the membrane above the firing threshold would be decreased. Therefore EPSPs which induce depolarisations that were previously below the threshold for firing would result in an action potential in the presence of 5-HT (and NA for the role of gK_{Leak}).

7.7 Future directions

In addition to the possible experiments described previously in this chapter, future studies are required to further understanding of the neuromodulatory effects of 5-HT and NA. It is anticipated that the next stage on from the work described in this thesis would be to examine any effect of NA on modulating glutamate release. The effect

of 5-HT and NA on EPSPs should also be investigated. The voltage-clamp configuration is useful for investigating the conductances that underlie changes in the membrane potential, however, this is an artificial situation and neurones *in vivo* would be described as being under current-clamp (Neher, Sakmann et al. 1978). Thus evoking EPSPs and applying 5-HT or NA would reveal whether these transmitters alter the shape and/or duration of synaptic events. The receptor subtypes which mediate the various actions of 5-HT and NA have been determined in this thesis and this information can be utilised to examine the contribution of each of these actions to the modulation of FM excitability. By applying the receptor subtype selective agonists and antagonists used in this thesis to FMs in which EPSPs were being evoked the role of each action of 5-HT (and NA if there is multiple actions) could be further understood.

The studies described in this thesis provide a solid groundwork for future studies into how neuromodulation alters FM function. In addition to furthering understanding of neuromodualtion in FMs these findings highlight the multiple actions of 5-HT (and potentially NA) in the central nervous system. Motoneurones are good models for investigating neuromodulation and synaptic integration due to the functional output of their activation being well understood, however, it is anticipated that several (but not necessary all) of the findings from studies on FMs could be extrapolated to other neuronal subtypes and further general understanding of how neurones function.

References

Accili, E. A., C. Proenza, et al. (2002). "From Funny Current to HCN Channels: 20 Years of Excitation." *News Physiol Sci* **17(1)**: 32-37.

Aghajanian, G. K. and G. J. Marek (1997). "Serotonin Induces Excitatory Postsynaptic Potentials in Apical Dendrites of Neocortical Pyramidal Cells." *Neuropharmacology* **36(4-5)**: 589-599.

Aghajanian, G. K. and K. Rasmussen (1989). "Intracellular studies in the facial nucleus illustrating a simple new method for obtaining viable motoneurons in adult rat brain slices." *Synapse* **3(4)**: 331-8.

Alberts, B., A. Johnson, et al. (2002). Molecular Biology of the Cell, Garland Science.

Andrade, R. and R. A. Nicoll (1987). "Pharmacologically distinct actions of serotonin on single pyramidal neurones of the rat hippocampus recorded in vitro." *J Physiol* **394**: 99-124.

Andrade, R., R. C. Malenka, et al. (1986). "A G Protein Couples Serotonin and GABAB Receptors to the Same Channels in Hippocampus." *Science* **234(4781)**: 1261-1265.

Araneda, R. and R. Andrade (1991). "5-Hydroxytryptamine2 and 5-hydroxytryptamine1A receptors mediate opposing responses on membrane excitability in rat association cortex." *Neuroscience* **40(2)**: 399-412.

Arvidsson, L. E., U. Hacksell, et al. (1981). "8-Hydroxy-2-(di-n-propylamino) tetralin, a new centrally acting 5-hydroxytryptamine receptor agonist." *J Med Chem* **24(8)**: 921-3.

Ashmole, I., P. A. Goodwin, et al. (2001). "TASK-5, a novel member of the tandem pore K^+ channel family." *Pflugers Arch* **442(6)**: 828-33.

Auger, C. and A. Marty (2000). "Quantal currents at single-site central synapses." *J Physiol (Lond)* **526(1)**: 3-11.

Barbuti, A., S. Ishii, et al. (2002). "Block of the background K(+) channel TASK-1 contributes to arrhythmogenic effects of platelet-activating factor." *Am J Physiol Heart Circ Physiol* **282(6)**: H2024-30.

Barnes, N. M. and T. Sharp (1999). "A review of central 5-HT receptors and their function." *Neuropharmacology* **38(8)**: 1083-152.

Bayliss, D. A., J. E. Sirois, et al. (2003). "The TASK family: two-pore domain background K^+ channels." *Mol Interv* **3(4)**: 205-19.

Berg, A. P., E. M. Talley, et al. (2004). "Motoneurons express heteromeric TWIK-related acid-sensitive K^+ (TASK) channels containing TASK-1 (KCNK3) and TASK-3 (KCNK9) subunits." *J Neurosci* **24(30)**: 6693-702.

Bian, J., J. Cui, et al. (2001). "HERG K^+ Channel Activity Is Regulated by Changes in Phosphatidyl Inositol 4,5-Bisphosphate." *Circ Res* **89(12)**: 1168-1176.

Bickmeyer, U., M. Heine, et al. (2002). "Differential modulation of I_h by 5-HT receptors in mouse CA1 hippocampal neurons." *Euro J Neuro* **16(2)**: 209-218.

Blackmer, T., E. C. Larsen, et al. (2001). "G Protein beta gamma Subunit-Mediated Presynaptic Inhibition: Regulation of Exocytotic Fusion Downstream of Ca^{2+}." *Science* **292(5515)**: 293-297.

Bleasdale, J. E., G. L. Bundy, et al. (1989). "Inhibition of phospholipase C dependent processes by U-73, 122." *Adv Prostaglandin Thromboxane Leukot Res* **19**: 590-3.

Bobker, D. H. and J. T. Williams (1989). "Serotonin agonists inhibit synaptic potentials in the rat locus ceruleus in vitro via 5-hydroxytryptamine1A and 5-hydroxytryptamine1B receptors." *J Pharmacol Exp Ther* **250(1)**: 37-43.

Bobker, D. H. and J. T. Williams (1989). "Serotonin augments the cationic current Ih in central neurons." *Neuron* **2(6)**: 1535-40.

Boeijinga, P. H. and H. W. Boddeke (1993). "Serotonergic modulation of neurotransmission in the rat subicular cortex in vitro: a role for 5-HT1B receptors." *Naunyn Schmiedebergs Arch Pharmacol* **348(6)**: 553-7.

Boeijinga, P. H. and H. W. Boddeke (1996). "Activation of 5-HT1B receptors suppresses low but not high frequency synaptic transmission in the rat subicular cortex in vitro." *Brain Res* **721(1-2)**: 59-65.

Boess, F. G. and I. L. Martin (1994). "Molecular biology of 5-HT receptors." *Neuropharmacology* **33(3-4)**: 275-317.

Bonhaus, D. W., K. K. Weinhardt, et al. (1997). "RS-102221: A Novel High Affinity and Selective, 5-HT2C Receptor Antagonist." *Neuropharmacology* **36(4-5)**: 621-629.

BoSmith, R. E., I. Briggs, et al. (1993). "Inhibitory actions of ZENECA ZD7288 on whole-cell hyperpolarization activated inward current (If) in guinea-pig dissociated sinoatrial node cells." *Br J Pharmacol* **110(1)**: 343-9.

Bouryi, V. A. and D. I. Lewis (2003). "The modulation by 5-HT of glutamatergic inputs from the raphe pallidus to rat hypoglossal motoneurones, in vitro." *J Physiol* **553(Pt 3)**: 1019-31.

Boyle, W. A. and J. M. Nerbonne (1992). "Two functionally distinct 4-aminopyridine-sensitive outward K^+ currents in rat atrial myocytes." *J Gen Physiol* **100(6)**: 1041-67.

Bruinvels, A. T., B. Landwehrmeyer, et al. (1994). "Localization of 5-HT1B, 5-HT1D[alpha], 5-HT1E and 5-HT1F receptor messenger RNA in rodent and primate brain." *Neuropharmacology* **33(3-4)**: 367-386.

Cardenas, C. G., L. P. Del Mar, et al. (1999). "Serotonergic modulation of hyperpolarization-activated current in acutely isolated rat dorsal root ganglion neurons." *J Physiol* **518(2)**: 507-523.

Chapin, E. M. and R. Andrade (2001). "A 5-HT(7) receptor-mediated depolarization in the anterodorsal thalamus. II. Involvement of the hyperpolarization-activated current I(h)." *J Pharmacol Exp Ther* **297(1)**: 403-9.

Chatterton, J. E., M. Awobuluyi, et al. (2002). "Excitatory glycine receptors containing the NR3 family of NMDA receptor subunits." *Nature* **415(6873)**: 793-8.

Chemin, J., C. Girard, et al. (2003). "Mechanisms underlying excitatory effects of group I metabotropic glutamate receptors via inhibition of 2P domain K^+ channels." *Embo J* **22(20)**: 5403-11.

Chen, S., J. Wang, et al. (2001). "Properties of hyperpolarization-activated pacemaker current defined by coassembly of HCN1 and HCN2 subunits and basal modulation by cyclic nucleotide." *J Gen Physiol* **117(5)**: 491-504.

Chen, X., E. M. Talley, et al. (2006). "Inhibition of a background potassium channel by Gq protein {alpha}-subunits." *Proc Natl Acad Sci* **103(9)**: 3422-3427.

Cho, H., D. Lee, et al. (2005). "Receptor-induced depletion of phosphatidylinositol 4,5-bisphosphate inhibits inwardly rectifying K+ channels in a receptor-specific manner." *Proc Natl Acad Sci* **102(12)**: 4643-4648.

Clarke, C. E., E. L. Veale, et al. (2004). "Selective block of the human 2-P domain potassium channel, TASK-3, and the native leak potassium current, $I_{K(SO)}$, by zinc." *J Physiol* **560(Pt 1)**: 51-62.

Clarke, C. E., Green, P.J., Veale, E.L., Meadows, H.J. & Mathie, A. (2003). "The involvement of residues H98 and E70 in the block of the human two-pore domain potassium channel, TASK-3, by zinc." *J Physiol* **(547P)**: C46.

Clement-Chomienne, O., K. Ishii, et al. (1999). "Identification, cloning and expression of rabbit vascular smooth muscle Kv1.5 and comparison with native delayed rectifier K^+ current." *J Physiol* **515 (Pt 3)**: 653-67.

Colino, A. and J. V. Halliwell (1987). "Differential modulation of three separate K-conductances in hippocampal CA1 neurons by serotonin." *Nature* **328(6125)**: 73-7.

Cook, E. P. and D. Johnston (1999). "Voltage-Dependent Properties of Dendrites That Eliminate Location-Dependent Variability of Synaptic Input." *J Neurophysiol* **81(2)**: 535-543.

Coombs, J. S., J. C. Eccles, et al. (1955). "Excitatory synaptic action in motoneurones." *J Physiol* **130(2)**: 374-95.

Coombs, J. S., J. C. Eccles, et al. (1955). "The specific ionic conductances and the ionic movements across the motoneuronal membrane that produce the inhibitory post-synaptic potential." *J Physiol* **130(2)**: 326-74.

Cornea-Hébert, V., Mustapha Riad, Chun Wu, Sujay K. Singh, Laurent Descarries, (1999). "Cellular and subcellular distribution of the serotonin 5-HT2A receptor in the central nervous system of adult rat." *J Comp Neurol* **409(2)**: 187-209.

Critchley, D. J. P., K. J. Childs, et al. (1994). "Inhibition of 8-OH-DPAT-induced elevation of plasma corticotrophin by the 5-HT1A receptor antagonist WAY100635." *Euro J Pharm* **264(1)**: 95-97.

Curro, F. A. and S. Greenberg (1983). "Characteristics of postsynaptic alpha 1 and alpha 2 adrenergic receptors in canine vascular smooth muscle." *Can J Physiol Pharmacol* **61(8)**: 893-904.

Czirjak, G. and P. Enyedi (2002a). "TASK-3 dominates the background potassium conductance in rat adrenal glomerulosa cells." *Mol Endocrinol* **16(3)**: 621-9.

Czirjak, G. and P. Enyedi (2002b). "Formation of functional heterodimers between the TASK-1 and TASK-3 two-pore domain potassium channel subunits." *J Biol Chem* **277(7)**: 5426-32.

Czirjak, G. and P. Enyedi (2003). "Ruthenium red inhibits TASK-3 potassium channel by interconnecting glutamate 70 of the two subunits." *Mol Pharmacol* **63(3)**: 646-52.

Czirjak, G., G. L. Petheo, et al. (2001). "Inhibition of TASK-1 potassium channel by phospholipase C." *Am J Physiol Cell Physiol* **281(2)**: C700-8.

Czirjak, G., T. Fischer, et al. (2000). "TASK (TWIK-related acid-sensitive K+ channel) is expressed in glomerulosa cells of rat adrenal cortex and inhibited by angiotensin II." *Mol Endocrinol* **14(6)**: 863-74.

Decher, N., M. Maier, et al. (2001). "Characterization of TASK-4, a novel member of the pH-sensitive, two-pore domain potassium channel family." *FEBS Lett* **492(1-2)**: 84-9.

Dingledine, R., K. Borges, et al. (1999). "The glutamate receptor ion channels." *Pharmacol Rev* **51(1)**: 7-61.

Docherty, J. R. (1998). "Subtypes of functional alpha1- and alpha2-adrenoceptors." *Eur J Pharmacol* **361(1)**: 1-15.

Donevan, S. and M. Rogawski (1995). "Intracellular Polyamines Mediate Inward Rectification of Ca^{2+}-Permeable {alpha}-Amino-3-Hydroxy-5-Methyl-4-Isoxazolepropionic Acid Receptors." *Proc Nat Acad Sci* **92(20)**: 9298-9302.

Dunlap, K. and G. D. Fischbach (1978). "Neurotransmitters decrease the calcium component of sensory neurone action potentials." *Nature* **276(5690)**: 837-9.

Dunlap, K. and G. D. Fischbach (1981). "Neurotransmitters decrease the calcium conductance activated by depolarization of embryonic chick sensory neurones." *J Physiol* **317**: 519-35.

Duprat, F., F. Lesage, et al. (1997). "TASK, a human background K+ channel to sense external pH variations near physiological pH." *Embo J* **16(17)**: 5464-71.

Duxon, M. S., T. P. Flanigan, et al. (1997). "Evidence for expression of the 5-hydroxytryptamine-2B receptor protein in the rat central nervous system." *Neuroscience* **76(2)**: 323-9.

Edwards, F. A. and A. Konnerth (1992). "Patch-clamping cells in sliced tissue preparations." *Methods Enzymol* **207**: 208-22.

Edwards, F. A., A. Konnerth, et al. (1989). "A thin slice preparation for patch clamp recordings from neurones of the mammalian central nervous system." *Pflugers Arch* **414(5)**: 600-12.

Firth , T. A., Jones, S. V. (2001). "GTP-binding protein Gq mediates muscarinic-receptor-induced inhibition of the inwardly rectifying potassium channel IRK1 (Kir 2.1)." *Neuropharmacology* **40(3)**: 358-365.

Fonseca, M. I., Y. G. Ni, et al. (2001). "Distribution of serotonin 2A, 2C and 3 receptor mRNA in spinal cord and medulla oblongata." *Mol Brain Res* **89(1-2)**: 11-19.

Friauf, E., Herbert, H. (1985). "Topographic organization of facial motoneurons to individual pinna muscles in rat (*Rattus rattus*) and bat (*Rousettus aegyptiacus*)." *J Comp Neurol* **240(2)**: 161-170.

Gabriel, A., M. Abdallah, et al. (2002). "Localization of the tandem pore domain K^+ channel KCNK5 (TASK-2) in the rat central nervous system." *Brain Res Mol Brain Res* **98(1-2)**: 153-63.

Gamper, N., V. Reznikov, et al. (2004). "Phosphotidylinositol 4,5-Bisphosphate Signals Underlie Receptor-Specific Gq/11-Mediated Modulation of N-Type Ca^{2+} Channels." *J. Neurosci*. **24(48)**: 10980-10992.

Gibson, J. R., A. F. Bartley, et al. (2006). "Role for the subthreshold currents ILeak and IH in the homeostatic control of excitability in neocortical somatostatin-positive inhibitory neurons." *J Neurophysiol* **96(1)**: 420-32.

Goldstein, S. A., D. Bockenhauer, et al. (2001). "Potassium leak channels and the KCNK family of two-P-domain subunits." *Nat Rev Neurosci* **2(3)**: 175-84.

Gonzalez, T., M. Longobardo, et al. (2001). "Effects of bupivacaine and a novel local anesthetic, IQB-9302, on human cardiac K^+ channels." *J Pharmacol Exp Ther* **296(2)**: 573-83.

Gulledge, A., Kampa, BM., Stuart, GJ. (2005). "Synaptic integration in dendritic trees." *J Neurobiol* **64(1)**: 75-90.

Hagan, J. J., G. W. Price, et al. (2000). "Characterization of SB-269970-A, a selective 5-HT(7) receptor antagonist." *Br J Pharmacol* **130(3)**: 539-48.

Han, J., J. Truell, et al. (2002). "Characterization of four types of background potassium channels in rat cerebellar granule neurons." *J Physiol* **542(Pt 2)**: 431-44.

Hannan, A. J., P. C. Kind, et al. (1998). "Phospholipase C-beta1 expression correlates with neuronal differentiation and synaptic plasticity in rat somatosensory cortex." *Neuropharmacology* **37(4-5)**: 593-605.

Harris, N. C. and A. Constanti (1995). "Mechanism of block by ZD 7288 of the hyperpolarization-activated inward rectifying current in guinea pig substantia nigra neurons in vitro." *J Neurophysiol* **74(6)**: 2366-2378.

Heginbotham, L., Z. Lu, et al. (1994). "Mutations in the K^+ channel signature sequence." *Biophys J* **66(4)**: 1061-7.

Herlitze, S., D. E. Garcia, et al. (1996). "Modulation of Ca^{2+} channels by G-protein beta gamma subunits." *Nature* **380(6571)**: 258-62.

Hinrichsen, C. F. L., Watson, Carol D. (1984). "The facial nucleus of the rat: Representation of facial muscles revealed by retrograde transport of horseradish peroxidase." *Anat Rec* **209(3)**: 407-415.

Hodgkin, A. L. and A. F. Huxley (1952). "A quantitative description of membrane current and its application to conduction and excitation in nerve." *J Physiol* **117(4)**: 500-44.

Honda, M., M. Tanabe, et al. (2003). "Serotonergic depression of spinal monosynaptic transmission is mediated by 5-HT1B receptors." *Eur J Pharmacol* **482(1-3)**: 155-61.

Huang, C.-L., S. Feng, et al. (1998). "Direct activation of inward rectifier potassium channels by PIP2 and its stabilization by G[beta][gamma]." *Nature* **391(6669)**: 803-806.

Hughes, B. A., G. Kumar, et al. (2000). "Cloning and functional expression of human retinal kir2.4, a pH-sensitive inwardly rectifying K(+) channel." *Am J Physiol Cell Physiol* **279(3)**: C771-84.

Ikeda, S. R. (1996). "Voltage-dependent modulation of N-type calcium channels by G-protein beta gamma subunits." *Nature* **380(6571)**: 255-8.

IUPHAR (2000). The IUPHAR Compendium of Receptor Characterization and Classification. London, IUPHAR Media.

Julius, D., K. N. Huang, et al. (1990). "The 5HT2 receptor defines a family of structurally distinct but functionally conserved serotonin receptors." *Proc Nat Acad Sci* **87(3)**: 928-932.

Kang, D., J. Han, et al. (2004). "Functional expression of TASK-1/TASK-3 heteromers in cerebellar granule cells." *J Physiol* **554(Pt 1)**: 64-77.

Karschin, C. and A. Karschin (1997). "Ontogeny of gene expression of Kir channel subunits in the rat." *Mol Cell Neurosci* **10(3-4)**: 131-48.

Karschin, C., E. Dissmann, et al. (1996). "IRK(1-3) and GIRK(1-4) inwardly rectifying K^+ channel mRNAs are differentially expressed in the adult rat brain." *J Neurosci* **16(11)**: 3559-70.

Karschin, C., E. Wischmeyer, et al. (2001). "Expression pattern in brain of TASK-1, TASK-3, and a tandem pore domain K(+) channel subunit, TASK-5, associated with the central auditory nervous system." *Mol Cell Neurosci* **18(6)**: 632-48.

Kaupp, U. B. and R. Seifert (2001). "Molecular diversity of pacemaker ion channels." *Annu Rev Physiol* **63**: 235-57.

Kehl, S. J., C. Eduljee, et al. (2002). "Molecular determinants of the inhibition of human Kv1.5 potassium currents by external protons and Zn(2+)." *J Physiol* **541(Pt 1)**: 9-24.

Kim, Y., H. Bang, et al. (2000). "TASK-3, a new member of the tandem pore K(+) channel family." *J Biol Chem* **275(13)**: 9340-7.

Kindler, C. H., M. Paul, et al. (2003). "Amide local anesthetics potently inhibit the human tandem pore domain background K^+ channel TASK-2 (KCNK5)." *J Pharmacol Exp Ther* **306(1)**: 84-92.

Kleckner, N. W. and R. Dingledine (1988). "Requirement for glycine in activation of NMDA-receptors expressed in Xenopus oocytes." *Science* **241(4867)**: 835-7.

Kuno, M. (1971). "Quantum aspects of central and ganglionic synaptic transmission in vertebrates" *Physiol. Rev.* **51(4)**: 647-678.

Kupfermann, I. (1979). "Modulatory actions of neurotransmitters." *Annu Rev Neurosci* **2**: 447-65.

Kursar, J., D. Nelson, et al. (1992). "Molecular cloning, functional expression, and pharmacological characterization of a novel serotonin receptor (5-hydroxytryptamine2F) from rat stomach fundus." *Mol Pharmacol* **42(4)**: 549-557.

Kursar, J., D. Nelson, et al. (1994). "Molecular cloning, functional expression, and mRNA tissue distribution of the human 5-hydroxytryptamine2B receptor." *Mol Pharmacol* **46(2)**: 227-234.

Larkman, P. M. and J. S. Kelly (1992). "Ionic mechanisms mediating 5-hydroxytryptamine- and noradrenaline-evoked depolarization of adult rat facial motoneurones." *J Physiol* **456**: 473-90.

Larkman, P. M. and J. S. Kelly (1997). "Modulation of IH by 5-HT in neonatal rat motoneurones in vitro: mediation through a phosphorylation independent action of cAMP." *Neuropharmacology* **36(4-5)**: 721-33.

Larkman, P. M. and J. S. Kelly (1998). "Characterization of 5-HT-sensitive potassium conductances in neonatal rat facial motoneurones in vitro." *J Physiol* **508 (Pt 1)**: 67-81.

Larkman, P. M. and J. S. Kelly (2001). "Modulation of the hyperpolarisation-activated current, Ih, in rat facial motoneurones in vitro by ZD-7288." *Neuropharmacology* **40(8)**: 1058-72.

Larkman, P. M., J. S. Kelly, et al. (1995). "Adenosine 3':5'-cyclic monophosphate mediates a 5-hydroxytryptamine-induced response in neonatal rat motoneurones." *Pflugers Arch* **430(5)**: 763-9.

Larkman, P. M., N. J. Penington, et al. (1989). "Electrophysiology of adult rat facial motoneurones: the effects of serotonin (5-HT) in a novel in vitro brainstem slice." *J Neurosci Methods* **28(1-2)**: 133-46.

Larkman, P. M. and E. M. Perkins (2005). "A TASK-like pH- and amine-sensitive 'leak' K^+ conductance regulates neonatal rat facial motoneuron excitability *in vitro*." *Eur J Neurosci* **21(3)**: 679-691.

Larkman, P., E. M. Perkins, P. Kind, (2003). Is Phospholipase-C beta-1 necessary for 5-HT- and noradrenaline-mediated modulation of gK^+ Leak in mouse facial motoneurones? *British Neuroscience Association Abstract* **vol 17** (29.01) p96.

Larkum, M. E., T. Launey, A. et al (1998). “Integration of excitatory postsynaptic potentials in dendrites of motoneurons of rat spinal cord slice cultures.” *J Neurophysiol* **80(2)**: 924-935.

Larrabee, M. G. (1995). "Lactate Metabolism and Its Effects on Glucose Metabolism in an Excised Neural Tissue." *J Neurochem* **64(4)**: 1734-1741.

Lauritzen, I., M. Zanzouri, et al. (2003). "K^+-dependent cerebellar granule neuron apoptosis. Role of task leak K^+ channels." *J Biol Chem* **278(34)**: 32068-76.

Lawrence, J. J., Z. M. Grinspan, et al. (2004). "Quantal transmission at mossy fibre targets in the CA3 region of the rat hippocampus." *J Physiol* **554(Pt 1)**: 175-93.

Leonoudakis, D., A. T. Gray, et al. (1998). "An open rectifier potassium channel with two pore domains in tandem cloned from rat cerebellum." *J Neurosci* **18(3)**: 868-77.

Lesage, F. (2003). "Pharmacology of neuronal background potassium channels." *Neuropharmacology* **44(1)**: 1-7.

Lesage, F. and M. Lazdunski (2000). "Molecular and functional properties of two-pore-domain potassium channels." *Am J Physiol Renal Physiol* **279(5)**: F793-801.

Lesage, F., E. Guillemare, et al. (1996). "TWIK-1, a ubiquitous human weakly inward rectifying K^+ channel with a novel structure." *Embo J* **15(5)**: 1004-11.

Li, L. and L.-S. Chin (2003). "The molecular machinery of synaptic vesicle exocytosis." *Cell Mol Life Sci (CMLS)* **60(5)**: 942-960.

Llinas, R. R. (1988). "The intrinsic electrophysiological properties of mammalian neurons: insights into central nervous system function." *Science* **242(4886)**: 1654-64.

Llinas, R. R., C. Nicholson, J. A. Freeman and D. E. Hillman (1968) "Dendritic spikes and their inhibition in alligator Purkinje cell." *Science* **160**, 1132-1135.

Llinas, R. R. and M. Sugimori (1980). "Electrophysiological properties of *in vitro* Purkinje cell dendrites in mammalian cerebellar slices." *J Physiol.* **305**: 197-213.

Logothetis, D. E., Y. Kurachi, et al. (1987). "The [beta][gamma] subunits of GTP-binding proteins activate the muscarinic K^+ channel in heart." *Nature* **325(6102)**: 321-326.

Lopes, C. M. B., T. Rohacs, et al. (2005). "PIP2 hydrolysis underlies agonist-induced inhibition and regulates voltage gating of two-pore domain K^+ channels." J *Physiol (Lond)* **564(1)**: 117-129.

Lopes, C. M., N. Zilberberg, et al. (2001). "Block of Kcnk3 by protons. Evidence that 2-P-domain potassium channel subunits function as homodimers." *J Biol Chem* **276(27)**: 24449-52.

Lopes, C. M., P. G. Gallagher, et al. (2000). "Proton block and voltage gating are potassium-dependent in the cardiac leak channel Kcnk3." *J Biol Chem* **275(22)**: 16969-78.

Lopez-Gimenez, J. F., G. Mengod, et al. (1997). "Selective visualization of rat brain 5-HT2A receptors by autoradiography with [3H]MDL 100,907." *Naunyn Schmiedebergs Arch Pharmacol* **356(4)**: 446-54.

Lovell, P. J., S. M. Bromidge, et al. (2000). "A novel, potent, and selective 5-HT(7) antagonist: (R)-3-(2-(2-(4-methylpiperidin-1-yl)ethyl)pyrrolidine-1-sulfonyl) phen ol (SB-269970)." *J Med Chem* **43(3)**: 342-5.

Ludwig, A., X. Zong, et al. (1998). "A family of hyperpolarization-activated mammalian cation channels." *Nature* **393(6685)**: 587-91.

Macor, J. E., C. A. Burkhart, et al. (1990). "3-(1,2,5,6-Tetrahydropyrid-4-yl)pyrrolo[3,2-b]pyrid-5-one: a potent and selective serotonin (5-HT1B) agonist and rotationally restricted phenolic analogue of 5-methoxy-3-(1,2,5,6-tetrahydropyrid-4-yl)indole." *J Med Chem* **33(8)**: 2087-93.

Magee, J. C. (1998). "Dendritic hyperpolarization-activated currents modify the integrative properties of hippocampal CA1 pyramidal neurons." *J Neurosci* **18(19)**: 7613-24.

Magee, J. C. (1999). "Dendritic lh normalizes temporal summation in hippocampal CA1 neurons." *Nat Neurosci* **2(6)**: 508-14.

Magee, J. C. (2000). "Dendritic integration of excitatory synaptic input." *Nat Rev Neurosci* **1(3)**: 181-90.

Magistretti, P. J. (2005). "Cellular bases of neurometabolic coupling and its relevance for functional brain imaging." *British Neuroscience Assoc, Abstr.* **vol. 18**: P1.

Maingret, F., A. J. Patel, et al. (2001). "The endocannabinoid anandamide is a direct and selective blocker of the background K(+) channel TASK-1." *Embo J* **20(1-2)**: 47-54.

Martin, L. J., C. D. Blackstone, et al. (1993). "AMPA glutamate receptor subunits are differentially distributed in rat brain." *Neuroscience* **53(2)**: 327-58.

Mathie, A. (2007) “Neuronal two-pore-domain potassium channels and their regulation by G protein-coupled receptors.” *J. Physiol.* **578(Pt2)**: 377-85.

Matus-Leibovitch, N., Z. Vogel, et al. (1996). "Chronic morphine administration enhances the expression of Kv1.5 and Kv1.6 voltage-gated K^+ channels in rat spinal cord." *Brain Res Mol Brain Res* **40(2)**: 261-70.

Mayer, M. L., G. L. Westbrook, et al. (1984). "Voltage-dependent block by Mg^{2+} of NMDA responses in spinal cord neurones." *Nature* **309(5965)**: 261-3.

Meadows, H. J. and A. D. Randall (2001). "Functional characterisation of human TASK-3, an acid-sensitive two-pore domain potassium channel." *Neuropharmacology* **40(4)**: 551-9.

Meuth, S. G., T. Budde, et al. (2003). "Contribution of TWIK-related acid-sensitive K^+ channel 1 (TASK1) and TASK3 channels to the control of activity modes in thalamocortical neurons." *J Neurosci* **23(16)**: 6460-9.

Millar, J. A., L. Barratt, et al. (2000). "A functional role for the two-pore domain potassium channel TASK-1 in cerebellar granule neurons." *Proc Natl Acad Sci* **97(7)**: 3614-8.

Mirotznik, R. R., X. Zheng, et al. (2000). "G-Protein Types Involved in Calcium Channel Inhibition at a Presynaptic Nerve Terminal." *J. Neurosci.* **20(20)**: 7614-7621.

Morilak, D. A., S. J. Garlow, et al. (1993). "Immunocytochemical localization and description of neurons expressing serotonin2 receptors in the rat brain." *Neuroscience 54(3)*: 701-717.

Neher, E. (1992). "Correction for liquid junction potentials in patch clamp experiments." *Methods Enzymol* **207**: 123-31.

Neher, E., B. Sakmann, et al. (1978). "The extracellular patch clamp: a method for resolving currents through individual open channels in biological membranes." *Pflugers Arch* **375(2)**: 219-28.

Nerbonne, J. M. (2000). "Molecular basis of functional voltage-gated K^+ channel diversity in the mammalian myocardium." *J Physiol* **525 Pt 2**: 285-98.

Neumaier, J. F., T. J. Sexton, et al. (2001). "Localization of 5-HT7 receptors in rat brain by immunocytochemistry, in situ hybridization, and agonist stimulated cFos expression." *J Chem Neuroanat* **21(1)**: 63-73.

Niemeyer, M. I., L. P. Cid, et al. (2001). "Modulation of the two-pore domain acid-sensitive K^+ channel TASK-2 (KCNK5) by changes in cell volume." *J Biol Chem* **276(46)**: 43166-74.

Nishi, M., H. Hinds, et al. (2001). "Motoneuron-specific expression of NR3B, a novel NMDA-type glutamate receptor subunit that works in a dominant-negative manner." *J Neurosci* **21(23)**: RC185.

North, R. and N. Uchimura (1989). "5-Hydroxytryptamine acts at 5-HT2 receptors to decrease potassium conductance in rat nucleus accumbens neurones." J *Physiol (Lond)* **417(1)**: 1-12.

Notom, T., Shigemoto, R, (2004). "Immunohistochemical localization of I_h channel subunits, HCN1-4, in the rat brain." *J Comp Neurol* **471(3)**: 241-276.

Nowak, L., P. Bregestovski, et al. (1984). "Magnesium gates glutamate-activated channels in mouse central neurones." *Nature* **307(5950)**: 462-5.

Nunnari, J. M., M. G. Repaske, et al. (1987). "Regulation of porcine brain alpha 2-adrenergic receptors by Na^+ ,H^+ and inhibitors of Na^+/H^+ exchange." *J Biol Chem* **262(25)**: 12387-92.

O'Brien, J. A., J. S. Isaacson, et al. (1997). "NMDA and non-NMDA receptors are co-localized at excitatory synapses of rat hypoglossal motoneurons." *Neurosci Lett* **227(1)**: 5-8.

Ogawa, T., A. Sugidachi, et al. (2002). "Pharmacological profiles of R-96544, the active form of a novel 5-HT2A receptor antagonist R-102444." *European Journal of Pharmacology* **457(2-3)**: 107-114.

Olverman, H. J., A. W. Jones, et al. (1984). "L-Glutamate has higher affinity than other amino acids for [3H]-D-AP5 binding sites in rat brain membranes." *Nature* **307(5950)**: 460-462.

Ozawa, S., H. Kamiya, et al. (1998). "Glutamate receptors in the mammalian central nervous system." *Prog Neurobiol* **54(5)**: 581-618.

Pape, H. C. (1996). "Queer current and pacemaker: the hyperpolarization-activated cation current in neurons." *Annu Rev Physiol* **58**: 299-327.

Patel, A. J. and E. Honore (2001). "Properties and modulation of mammalian 2P domain K^+ channels." *Trends Neurosci* **24(6)**: 339-46.

Paxinos, G. (1985). The rat nervous system. Sydney, Academic Press.

Peroutka, S. J. (1985). "Selective labeling of 5-HT1A and 5-HT1B binding sites in bovine brain." *Brain Research 344(1)*: 167-171.

Perrier, J. F., A. Alaburda, et al. (2003). "5-HT1A receptors increase excitability of spinal motoneurons by inhibiting a TASK-1-like K^+ current in the adult turtle." *J Physiol* **548(Pt 2)**: 485-92.

Petralia, R. S., N. Yokotani, et al. (1994). "Light and electron microscope distribution of the NMDA receptor subunit NMDAR1 in the rat nervous system using a selective anti-peptide antibody." *J Neurosci* **14(2)**: 667-96.

Petralia, R. S., Y. X. Wang, et al. (1994). "Histological and ultrastructural localization of the kainate receptor subunits, KA2 and GluR6/7, in the rat nervous system using selective antipeptide antibodies." *J Comp Neurol* **349(1)**: 85-110.

Petralia, R. S., Y. X. Wang, et al. (1994). "The NMDA receptor subunits NR2A and NR2B show histological and ultrastructural localization patterns similar to those of NR1." *J Neurosci* **14(10)**: 6102-20.

Pieribone, V. A., A. P. Nicholas, et al. (1994). "Distribution of alpha 1 adrenoceptors in rat brain revealed by in situ hybridization experiments utilizing subtype-specific probes." *J Neurosci* 14(7): 4252-68.

Pompeiano, M., J. M. Palacios, et al. (1994). "Distribution of the serotonin 5-HT2 receptor family mRNAs: comparison between 5-HT2A and 5-HT2C receptors." *Brain Res Mol Brain Res* **23(1-2)**: 163-78.

Pompeiano, M., J. Palacios, et al. (1992). "Distribution and cellular localization of mRNA coding for 5-HT1A receptor in the rat brain: correlation with receptor binding." *J. Neurosci.* **12(2)**: 440-453.

Purves, D., Fitzpatrick, D., Augustine, G.J., Katz, L.C. LaMantia, A. (2001). Neuroscience. Sunderland, Sinauer Associates Incorporated.

Raastad, M., J. F. Storm, et al. (1992). "Putative Single Quantum and Single Fibre Excitatory Postsynaptic Currents Show Similar Amplitude Range and Variability in Rat Hippocampal Slices." *Eur J Neurosci* **4(1)**: 113-117.

Rae, J., K. Cooper, et al. (1991). "Low access resistance perforated patch recordings using amphotericin B." *J Neurosci Methods* **37(1)**: 15-26.

Rajan, S., E. Wischmeyer, et al. (2000). "TASK-3, a novel tandem pore domain acid-sensitive K^+ channel. An extracellular histiding as pH sensor." *J Biol Chem* **275(22)**: 16650-7.

Rall, W. (1959). "Branching dendritic trees and motoneuron membrane resistivity." *Exp Neurol* **1**: 491-527.

Rall, W., R. E. Burke, et al. (1967). "Dendritic location of synapses and possible mechanisms for the monosynaptic EPSP in motoneurons." *J Neurophysiol* **30(5)**: 1169-1193.

Ranft, A., J. Kurz, et al. (2004). "Isoflurane modulates glutamatergic and GABAergic neurotransmission in the amygdala." *Eur J Neurosci* **20(5)**: 1276-80.

Rasmussen, K. and G. K. Aghajanian (1990). "Serotonin excitation of facial motoneurons: receptor subtype characterization." *Synapse* **5(4)**: 324-32.

Rekling, J. C., G. D. Funk, et al. (2000). "Synaptic control of motoneuronal excitability." *Physiol Rev* **80(2)**: 767-852.

Reuveny, E., P. A. Slesinger, et al. (1994). "Activation of the cloned muscarinic potassium channel by G protein [beta][gamma] subunits." *Nature* **370(6485)**: 143-146.

Reyes, R., F. Duprat, et al. (1998). "Cloning and expression of a novel pH-sensitive two pore domain K^+ channel from human kidney." *J Biol Chem* **273(47)**: 30863-9.

Reynolds, I. and R. Miller (1989). "Ifenprodil is a novel type of N-methyl-D-aspartate receptor antagonist: interaction with polyamines." *Mol Pharmacol* **36(5)**: 758-765.

Robinson, R. B. and S. A. Siegelbaum (2003). "Hyperpolarization-activated Cation Currents: From Molecules to Physiological Function." *Ann Rev Physiol* **65(1)**: 453-480.

Rosenbaum, T. and S. E. Gordon (2004). "Quickening the pace: looking into the heart of HCN channels." *Neuron* **42(2)**: 193-6.

Rothman, S. (1985). "The neurotoxicity of excitatory amino acids is produced by passive chloride influx." *J. Neurosci*. **5(6)**: 1483-1489.

Santoro, B. and G. R. Tibbs (1999). "The HCN gene family: molecular basis of the hyperpolarization-activated pacemaker channels." *Ann N Y Acad Sci* **868**: 741-64.

Santoro, B., D. T. Liu, et al. (1998). "Identification of a Gene Encoding a Hyperpolarization-Activated Pacemaker Channel of Brain." *Cell* **93(5)**: 717-729.

Santoro, B., S. Chen, et al. (2000). "Molecular and Functional Heterogeneity of Hyperpolarization-Activated Pacemaker Channels in the Mouse CNS." *J. Neurosci.* **20(14)**: 5264-5275.

Sastry, B. R. and L. S. Bhagavatula (1996). "Quantal release of transmitter at a central synapse." *Neuroscience* **75(4)**: 987-92.

Sato, K., H. Kiyama, et al. (1993). "The differential expression patterns of messenger RNAs encoding non-N-methyl-D-aspartate glutamate receptor subunits (GluR1-4) in the rat brain." *Neuroscience* **52(3)**: 515-39.

Scheller, M., J. Bufler, et al. (1997). "Isoflurane and sevoflurane interact with the nicotinic acetylcholine receptor channels in micromolar concentrations." *Anesthesiology* **86(1)**: 118-27.

Schorge, S. and D. Colquhoun (2003). "Studies of NMDA Receptor Function and Stoichiometry with Truncated and Tandem Subunits." *J. Neurosci.* **23(4)**: 1151-1158.

Schram, G., P. Melnyk, et al. (2002). "Kir2.4 and Kir2.1 K(+) channel subunits co-assemble: a potential new contributor to inward rectifier current heterogeneity." *J Physiol* **544(Pt 2)**: 337-49.

Schurr, A., C. A. West, et al. (1988). "Lactate-supported synaptic function in the rat hippocampal slice preparation." *Science* **240(4857)**: 1326-8.

Senba, E., Tohyama,M., Shiotani, Y., Kawasaki, Y., Kubo, T., Matsunaga, T., Emson, PC., Steinbusch, HWM. (1985). "Peptidergic and aminergic innervation of the facial nucleus of the rat with special reference to ontogenetic development." *J Comp Neurol* **238(4)**: 429-439.

Sheardown, M. J., E. O. Nielsen, et al. (1990). "2,3-Dihydroxy-6-nitro-7-sulfamoyl-benzo(F)quinoxaline: a neuroprotectant for cerebral ischemia." *Science* **247(4942)**: 571-4.

Sheldon, P., Aghajanian, GK. (1991). "Excitatory responses to serotonin (5-HT) in neurons of the rat piriform cortex: Evidence for mediation by 5-HT_{1C} receptors in pyramidal cells and 5-HT_2 receptors in interneurons." *Synapse* **9(3)**: 208-218.

Shin, K. S., B. S. Rothberg, et al. (2001). "Blocker State Dependence and Trapping in Hyperpolarization-activated Cation Channels: Evidence for an Intracellular Activation Gate." *J. Gen. Physiol.* **117(2)**: 91-102.

Silinsky, E. (1984). "On the mechanism by which adenosine receptor activation inhibits the release of acetylcholine from motor nerve endings." *J Physiol (Lond)* **346(1)**: 243-256.

Silinsky, E. and C. Solsona (1992). "Calcium currents at motor nerve endings: absence of effects of adenosine receptor agonists in the frog." *J Physiol (Lond)* **457(1)**: 315-328.

Simon, W., G. Hapfelmeier, et al. (2001). "Isoflurane blocks synaptic plasticity in the mouse hippocampus." *Anesthesiology* **94(6)**: 1058-65.

Soderling, T. R., S. E. Tan, et al. (1994). "Excitatory interactions between glutamate receptors and protein kinases." *J Neurobiol* **25(3)**: 304-11.

Spencer, W. A. and E. R. Kandel (1961) "Electrophysiology of hippocampal neurones: IV: Fast prepotentials." *J Neurophysiol*. **24**, 272-285.

Steidl, J. V. and A. J. Yool (1999). "Differential sensitivity of voltage-gated potassium channels Kv1.5 and Kv1.2 to acidic pH and molecular identification of pH sensor." *Mol Pharmacol* **55(5)**: 812-20.

Stevens, C. F. (2003). "Neurotransmitter release at central synapses." *Neuron* **40(2)**: 381-8.

Stevens, C. F. and Y. Wang (1995). "Facilitation and depression at single central synapses." *Neuron* **14(4)**: 795-802.

Stuart, G. J. and S. J. Redman (1991). "Mechanisms of presynaptic inhibition studied using paired-pulse facilitation." *Neurosci Letts* **126(2)**: 179-183.

Suh, B.-C. and B. Hille (2002). "Recovery from Muscarinic Modulation of M Current Channels Requires Phosphatidylinositol 4,5-Bisphosphate Synthesis." *Neuron* **35(3)**: 507-520.

Takagi, H. (2000) "Roles of ion channels in EPSP integration at neuronal dendrites." *Neurosci Res*. **37**, 167-171.

Takahashi, T., I. D. Forsythe, et al. (1996). "Presynaptic Calcium Current Modulation by a Metabotropic Glutamate Receptor." *Science* **274(5287)**: 594-597.

Takeuchi, Y., M. Kojima, et al. (1983). "Serotonergic innervation on the motoneurons in the mammalian brainstem. Light and electron microscopic immunohistochemistry." *Anat Embryol (Berl)* **167(3)**: 321-33.

Talley, E. M. and D. A. Bayliss (2002). "Modulation of TASK-1 (Kcnk3) and TASK-3 (Kcnk9) potassium channels: volatile anesthetics and neurotransmitters share a molecular site of action." *J Biol Chem* **277(20)**: 17733-42.

Talley, E. M., G. Solorzano, et al. (2001). "CNS distribution of members of the two-pore-domain (KCNK) potassium channel family." *J Neurosci* **21(19)**: 7491-505.

Talley, E. M., Q. Lei, et al. (2000). "TASK-1, a two-pore domain K^+ channel, is modulated by multiple neurotransmitters in motoneurons." *Neuron* **25(2)**: 399-410.

Tanaka, E. and R. A. North (1993). "Actions of 5-hydroxytryptamine on neurons of the rat cingulate cortex." *J Neurophysiol* **69(5)**: 1749-57.

Tateishi, J. and J. E. Faber (1995). "Inhibition of arteriole alpha 2- but not alpha 1-adrenoceptor constriction by acidosis and hypoxia in vitro." *Am J Physiol* **268(5 Pt 2)**: H2068-76.

Tedford, H. W. and G. W. Zamponi (2006). "Direct G protein modulation of Cav2 calcium channels." *Pharmacol Rev* **58(4)**: 837-62.

Thomas, D. R., P. J. Atkinson, et al (2000). "[(3)H]-SB-269970--A selective antagonist radiligand for 5-HT(7) receptors. *Br J Pharmacol* **130(2)**: 409-417.

Tichelaar, W., M. Safferling, et al. (2004). "The Three-dimensional Structure of an Ionotropic Glutamate Receptor Reveals a Dimer-of-dimers Assembly." *J Mol Biol* **344(2)**: 435-442.

Topert, C., F. Doring, et al. (1998). "Kir2.4: a novel K^+ inward rectifier channel associated with motoneurons of cranial nerve nuclei." *J Neurosci* **18(11)**: 4096-105.

Tremblay, J. P., R. E. Laurie, et al. (1983). "Is the MEPP due to the release of one vesicle or to the simultaneous release of several vesicles at one active zone?" *Brain Res* **287(3)**: 299-314.

Turman JE, L. O., Chandler, SH (2002). "Differential NR2A and NR2B expression between trigeminal neurons during early postnatal development." *Synapse* **44(2)**: 76-85.

Ulens, C. and J. Tytgat (2001). "Functional heteromerization of HCN1 and HCN2 pacemaker channels." *J Biol Chem* **276(9)**: 6069-72.

VanderMaelen, C. P. and G. K. Aghajanian (1980). "Intracellular studies showing modulation of facial motoneurone excitability by serotonin." *Nature* **287(5780)**: 346-7.

Vandermaelen, C. P. and G. K. Aghajanian (1982). "Serotonin-induced depolarization of rat facial motoneurons in vivo: comparison with amino acid transmitters." *Brain Res* **239(1)**: 139-52.

Vega-Saenz de Miera, E., D. H. Lau, et al. (2001). "KT3.2 and KT3.3, two novel human two-pore K(+) channels closely related to TASK-1." *J Neurophysiol* **86(1)**: 130-42.

Volgin, D. V., R. Fay, et al. (2003). "Postnatal development of serotonin 1B, 2 A and 2C receptors in brainstem motoneurons." *Eur J Neurosci* **17(6)**: 1179-88.

Waldmeier, P. C., M. Williams, et al. (1988). "Interactions of isamoltane (CGP 361A), an anxiolytic phenoxypropanolamine derivative, with 5-HT1, receptor

subtypes in the rat brain." *Naunyn Schmiedebergs Arch Pharmacol* **337(6)**: 609-620.

Watkins, C. S. and A. Mathie (1996). "A non-inactivating K^+ current sensitive to muscarinic receptor activation in rat cultured cerebellar granule neurons." *J Physiol* **491 (Pt 2)**: 401-12.

Wenzel, A., J. M. Fritschy, et al. (1997). "NMDA Receptor Heterogeneity During Postnatal Development of the Rat Brain: Differential Expression of the NR2A, NR2B, and NR2C Subunit Proteins." *J Neurochem* **68(2)**: 469-478.

Whitehead, R. R. and J. R. Rosenberg (1993). "On trees as equivalent cables." *Proc Biol Sci* **252(1334)**: 103-8.

Williams, K. (1993). "Ifenprodil discriminates subtypes of the N-methyl-D-aspartate receptor: selectivity and mechanisms at recombinant heteromeric receptors" *Mol Pharmacol* **44(4)**: 851-859.

Williams, S. R. and G. J. Stuart (2000). "Site independence of EPSP time course is mediated by dendritic I(h) in neocortical pyramidal neurons." *J Neurophysiol* **83(5)**: 3177-82.

Wood, M., M. Chaubey, et al. (2000). "Antagonist activity of meta-chlorophenylpiperazine and partial agonist activity of 8-OH-DPAT at the 5-HT(7) receptor." *Eur J Pharmacol* **396(1)**: 1-8.

Wright, D. E., K. B. Seroogy, et al. (1995). "Comparative localization of serotonin1A, 1C, and 2 receptor subtype mRNAs in rat brain." *J Comp Neurol* **351(3)**: 357-73.

Yamaguchi, K., Y. Nakajima, et al. (1990). "Modulation of inwardly rectifying channels by substance P in cholinergic neurones from rat brain in culture." *J Physiol* **426**: 499-520.

Yuste, R. and D. W. Tank (1996). "Dendritic integration in mammalian neurons, a century after Cajal." *Neuron* **16(4)**: 701-16.

Zhang, H., L. C. Craciun, et al. (2003). "PIP2 Activates KCNQ Channels, and Its Hydrolysis Underlies Receptor-Mediated Inhibition of M Currents." *Neuron* **37(6)**: 963-975.

Zucker, R. S. (1989). "Short-term synaptic plasticity." *Annu Rev Neurosci* **12**: 13-31.

Appendix A

Larkman, P. M. and E. M. Perkins (2005). "A TASK-like pH- and amine-sensitive 'leak' K^+ conductance regulates neonatal rat facial motoneuron excitability *in vitro*." Eur J Neurosci 21(3): 679-691.

European Journal of Neuroscience, Vol. 21, pp. 679–691, 2005

A TASK-like pH- and amine-sensitive 'leak' K^+ conductance regulates neonatal rat facial motoneuron excitability *in vitro*

Philip M. Larkman and Emma M. Perkins
Division of Neuroscience, University of Edinburgh, 1 George Square, Edinburgh EH8 9JZ, UK

Keywords: noradrenaline, pH dependence, potassium conductance, TASK channels

Abstract

A 'leak' potassium (K^+) conductance (gK_{Leak}) modulated by amine neurotransmitters is a major determinant of neonatal rat facial motoneuron excitability. Although the molecular identity of gK_{Leak} is unknown, TASK-1 and TASK-3 channel mRNA is found in facial motoneurons. External pH, across the physiological range (pH 6–8), and noradrenaline (NA) modulated a conductance that displayed a relatively linear current/voltage relationship and reversed at the K^+ equilibrium potential, consistent with inhibition of gK_{Leak}. The pH-sensitive current (I_{pH}), was maximal around pH 8, fully inhibited near pH 6 and was described by a modified Hill equation with a pK of 7.1. The NA-induced current (I_{NA}) was occluded at pH 6 and enhanced at pH 7.7. The TASK-1 selective inhibitor anandamide (10 μM), its stable analogue methanandamide (10 μM), the TASK-3 selective inhibitor ruthenium red (10 μM) and Zn^{2+} (100–300 μM) all failed to alter facial motoneuron membrane current or block I_{NA} or I_{pH}. Isoflurane, a volatile anaesthetic that enhances heteromeric TASK-1/TASK-3 currents, increased gK_{Leak}. Ba^{2+}, Cs^+ and Rb^+ blocked I_{NA} and I_{pH} voltage-dependently with maximal block at hyperpolarized potentials. 4-Aminopyridine (4-AP, 4 mM) voltage-independently blocked I_{NA} and I_{pH}. In summary, gK_{Leak} displays some of the properties of a TASK-like conductance. The linearity of gK_{Leak} and an independence of activation on external [K^+] suggests against pH-sensitive inwardly rectifying K^+ channels. Our results argue against principal contributions to gK_{Leak} by homomeric TASK-1 or TASK-3 channels, while the potentiation by isoflurane supports a predominant role for heterodimeric TASK-1/TASK-3 channels.

Introduction

'Leak' K^+ conductances (gK_{Leak}), characterized by no or weak voltage-dependence and fast kinetics, provide a major determinant in regulating excitability of many neuronal types. Inhibition of a gK_{Leak} by both noradrenaline (NA) and serotonin (5-hydroxytryptamine, 5-HT) modulates adult rat facial motoneuron excitability by promoting membrane depolarization and an associated increase in input resistance that markedly affects responses to synaptic input (Larkman & Kelly, 1992). Despite the importance of this conductance for facial motoneuron excitability the identity of the amine-sensitive K^+ channels remains to be established.

It has been widely suggested that members of the twin-pore (2P) domain K^+ channel family provide molecular correlates for physiologically identified 'leak' K^+ conductances (reviewed by Goldstein *et al*., 2001; Patel & Honoré, 2001). In young rat hypoglossal motoneurons and adult turtle spinal motoneurons it has been proposed that members of the TASK (TWIK-related, acid-sensitive, K^+) group of 2P channels underlie an amine-sensitive gK_{Leak} (Talley *et al*., 2000; Perrier *et al*., 2003). The presence of TASK-1 (KCNK3) and TASK-3 (KCNK9) mRNA has been demonstrated in the rat facial motor nucleus, raising the possibility that TASK channels underlie the amine-sensitive gK_{Leak} in facial motoneurons (Talley *et al*., 2000; Karschin *et al*., 2001; Vega-Saenz de Miera *et al*., 2001). Nevertheless, a motoneuron-specific inwardly rectifying K^+ channel, Kir2.4, has also been proposed to underlie the amine-sensitive K^+ current in hypoglossal motoneurons and this may also be expressed by neonatal rat facial motoneurons (Karschin *et al*., 1996; Karschin & Karschin, 1997; Töpert *et al*., 1998).

TASK-1 and TASK-3 channels mediate openly rectifying currents with fast kinetics that can be distinguished by the pH at which they are half-maximally activated (pK) (Duprat *et al*., 1997; Leonoudakis *et al*., 1998; Kim *et al*., 2000; Rajan *et al*., 2000). In addition, the endogenous cannabinoid, anandamide, preferentially blocks TASK-1 channels and the polycationic compound, ruthenium red (RR) selectively blocks TASK-3 channels (Czirják & Enyedi, 2003; Maingret *et al*., 2001). TASK-1 and TASK-3 also appear to form functional heterodimeric channels with emergent properties distinct from the respective homomeric channels (Czirják & Enyedi, 2002a; Talley & Bayliss, 2002; Kang *et al*., 2004). In this respect, acetylcholine inhibits a gK_{Leak} in cultured rat cerebellar granule (CG) neurons with properties similar, but not identical, to TASK-1 (Watkins & Mathie, 1996; Millar *et al*., 2000). Single-channel studies have demonstrated the presence of homomeric TASK-1, homomeric TASK-3 and heteromeric TASK-1/TASK-3 channels in these cells (Han *et al*., 2002; Kang *et al*., 2004).

We have combined pharmacological and biophysical approaches to investigate the identity of the amine-sensitive gK_{Leak} in neonatal rat facial motoneurons. We show that external pH, across the physiological range, modulates a gK_{Leak} with the biophysical and pharmacological properties of the NA-sensitive conductance. This conductance displays

Correspondence: Dr P. M. Larkman, as above.
E-mail: P.Larkman@ed.ac.uk

Received 11 August 2004, revised 8 November 2004, accepted 17 November 2004

doi:10.1111/j.1460-9568.2005.03898.x

some of the biophysical properties of a conductance carried by TASK channels but has a pharmacological profile distinct from either homomeric TASK-1 or homomeric TASK-3 channels. Some of this work has been presented in preliminary form (Larkman & Perkins, 2003).

Materials and methods

Subjects

Wistar rats, 5–16 days old, of either sex, were used for slice electrophysiology experiments. Dissociated CG cell cultures were prepared from 7-day-old Wistar rats. All procedures were approved under the UK Animals (Scientific Procedures) Act 1986.

Slice preparation

Slice preparation and recording methods were similar to those described previously (Larkman & Kelly, 1998). Rats were decapitated without anaesthesia and the hindbrain was rapidly isolated and placed in ice-cold (~4 °C), sucrose-containing artificial cerebrospinal fluid (ACSF) of the following composition (mM): 57 NaCl, 114 sucrose, 3 KCl, 1 $CaCl_2$, 5 $MgCl_2$, 1.25 NaH_2PO_4, 26 $NaHCO_3$, 11 D-glucose and 4 lactate. pH was 7.4 when continuously bubbled with a 95% oxygen, 5% carbon dioxide gas mixture. After mounting the brainstem on the cutting stage of a tissue slicer (DTK-1000, Dosaka Co., Kyoto, Japan) slices (~120 μm thick) were cut and subsequently incubated at 30 °C for 60 min in a total volume of 50 mL ACSF. During this time the sucrose-containing ACSF was slowly exchanged, at a rate of approximately 1 mL/min, with standard ACSF containing (mM): 114 NaCl, 3 KCl, 2 $CaCl_2$, 1 $MgCl_2$, 1.25 NaH_2PO_4, 26 $NaHCO_3$ and 11 D-glucose; pH was 7.4 after bubbling with 95% O_2/5% CO_2. Prior to recording, slices were maintained at room temperature (~23 °C) in standard ACSF. To inhibit the hyperpolarization-activated current, I_h, ZD-7288 (5–10 μM) was added to the maintenance chamber at least 30 min prior to recording.

Cerebellar granule cell cultures

Cerebellar granule cells were seeded on glass cover-slips coated with poly-D-lysine (15 μg/mL) at a density of 7.5×10^5 cells/cm^2 and cultured in MEM without Ca^{2+} and Mg^{2+} (Gibco, Invitrogen, Paisley, UK) supplemented with 10% fetal calf serum (Gibco, Invitrogen), 9.2 mM glucose, 0.56 mM glutamine, 5.2 mM KCl and 1% penicillin–streptomycin. Cytosine-arabinoside (10 μM) was added to the culture medium after 24 h to prevent growth of glial cells. Electrophysiological recordings were attempted between 8 and 14 days *in vitro* (DIV).

Electrophysiology

Individual brainstem slices or cover-slips bearing cultured granule cells were transferred to a recording chamber and continuously perfused (3–5 mL/min) with ACSF. Neurons were visualized using a water immersion objective (40×, Carl Zeiss Ltd, Welwyn Garden City, UK) and Nomarski differential interference contrast optics. Facial motoneurons were cleared of debris and connective tissue prior to introduction of a recording pipette into the chamber. Recording pipettes were made from thin-walled borosilicate glass capillaries (GC150TF, Harvard Apparatus Ltd, Edenbridge, UK) using a patch-pipette puller (Narishige PP-83, Intracel, Royston, UK). The patch-pipette was coated with sylgard to reduce capacitance. The pipette solution contained (mM): 122.5 K gluconate, 17.5 KCl, 9 NaCl, 1 $MgCl_2$, 0.2 EGTA, 10 Hepes, 0.3 GTP (Na^+ salt) and 3 ATP (Mg^{2+} salt), neutralized to pH 7.3 with KOH (4 mM). Occasionally diluting this solution to 90% improved the maintenance of cell condition. Even though block of I_h by ZD-7288 is essentially irreversible over the time required for whole-cell recording (Larkman & Kelly, 2001), ZD-7288 (5–10 μM) was included in the pipette solution during whole-cell recordings to maintain an effective blocking concentration at its intracellular site of action (Shin *et al*., 2001). Perforated-patch recordings from cultured CG cells were made after including amphotericin B (250 μg/mL) in the pipette solution. Membrane currents were recorded with a patch-clamp amplifier (EPC7B, List-Medical, Darmstadt, Germany) filtered at 10 kHz and stored using a digital audio tape recorder (Biologic DTR-1404, Intracel). Series resistance (whole-cell recording, range 14–25 MΩ; perforated-patch recording, range 30–60 MΩ) was monitored with the current response to a repetitive voltage step (−10 mV, 10 ms) and was compensated by up to 70%. Motoneuronal conductance was measured using linear regression across the linear part of the *I/V* plot (−60 to −80 mV) obtained using either voltage step pulses of varying amplitude or ramp pulses (−50 to +50 mV from the holding potential, 2.4 s duration). Cerebellar granule cells were voltage-clamped at −20 mV and conductance was measured by ramping to −120 mV over 900 ms. Off-line analysis was performed using a CED1401+ interface (Cambridge Electronic Design Ltd, Cambridge, UK), personal computer and Signal or Patch and Voltage-Clamp software (Cambridge Electronic Design Ltd). Membrane current responses to voltage steps were digitized at 1–3 kHz while those evoked by voltage ramps were digitized at 0.2–1 kHz. All recorded potentials using standard pipette solutions were corrected for a junction potential of ~8 mV.

Recordings from CG neurons and those in slices involving changes in external pH were made in a modified ACSF containing (mM): 126 NaCl, 3 KCl, 2 $CaCl_2$, 1 $MgCl_2$, 1.25 NaH_2PO_4, 11 D-glucose and 10 Hepes continuously bubbled with 100% O_2. pH was adjusted by titration with NaOH and checked after each recording. Tetrodotoxin (TTX; 0.3 μM) was routinely included in all external recording solutions to block voltage-gated Na^+ channels. Changes in the external K^+ concentration were compensated for by equimolar alterations in the external Na^+ concentration. When Rb^+ was included in the ACSF it replaced equimolar K^+. Drugs were bath-applied in the ACSF unless otherwise stated. To prevent precipitation of Zn^{2+} the ACSF did not contain NaH_2PO_4.

External solutions containing isoflurane were prepared as previously reported (Simon *et al*., 2001; Ranft *et al*., 2004). Briefly, a saturated solution of isoflurane (15 mM; Scheller *et al*., 1997) was prepared by adding an excess of anaesthetic to ACSF in a sealed glass bottle and stirring for 3 h at room temperature. Simon *et al*. (2001) found that dilutions between 1 : 30 and 1 : 7.5 of this stock solution resulted in a final aqueous concentration of 0.2–0.3 mM after bubbling with oxygen and delivery to the recording chamber. We routinely used a 1 : 10 dilution in our experiments.

Data analysis

Single exponential fits to the activation and deactivation of subtracted NA-sensitive current traces were performed using Signal software (v2.0, Cambridge Electronic Design) according to the equation

$$I_t = A + Be^{-t/\tau} \quad (1)$$

where I_t is current amplitude at time t, A and B are constants and τ is the time constant.

Chord conductance was obtained by dividing the current by the electromotive force ($V - V_{rev}$) where V is the membrane potential and V_{rev} the reversal potential. The resulting values could be described by a Boltzmann function of the form

$$g/g_{max} = 1/1 + \exp[(V - V_{0.5})/k], \quad (2)$$

where g_{max} is the maximum conductance, V is the membrane potential, $V_{0.5}$ the potential for half maximal activation and k is a slope constant.

The pH-sensitivity of facial motoneuron membrane current could be described by a modified (four-parameter logistic) Hill equation

$$y = y_{min} + (y_{max} - y_{min})/[1 + (pH/pK)^b] \quad (3)$$

where y is the holding current or input conductance, y_{max} the maximum response, y_{min} the minimum response and $b = -(b' * pK)/0.434$ where b' is the Hill coefficient expressed as a function of H^+ concentration.

The dose–response relationship for phenylephrine could be described by the equation

$$y = y_{min} + (y_{max} - y_{min})/[1 + 10^{(\log EC50 - X) * nH}] \quad (4)$$

where y is the normalized response amplitude, y_{max} the maximum response, y_{min} the minimum response, X is the phenylephrine (PE) concentration and nH is the Hill coefficient. Fitting was performed using Graphpad Prism™ software.

Drugs

4-Aminopyridine (4-AP), 5-hydroxytryptamine creatinine sulphate, amphotericin B, barium chloride, bupivacaine, caesium chloride, NA (arterenol bitartrate), PE hydrochloride, rubidium chloride, RR, tetraethylammonium (TEA) chloride, and zinc chloride were all obtained from Sigma-Aldrich Co. Ltd (Gillingham, Dorset, UK) Anandamide, arachidonyltrifluoromethyl ketone (ATFK), methanandamide, propranolol hydrochloride, prazosin hydrochloride, TTX, WB 4101 [2-(2,6-dimethoxyphenoxyethyl)aminoethyl-1,4-benzodioxane hydrochloride] and ZD-7288 [4-(*n*-ethyl-*n*-phenylamino)-1,2-dimethyl-6-(methylamino) pyrimidinium chloride] were from Tocris Cookson (Bristol, UK). Isoflurane was obtained from Abbott Laboratories Ltd (Maidenhead, UK).

Results

External pH modulates a gK_{Leak} in facial motoneurons

Identification of mRNA for subunits belonging to the TASK and Kir2 families in the rat facial motor nucleus and the knowledge that channels containing these subunits are sensitive to changes in external pH prompted us to investigate the functional expression of pH-sensitive K^+ channels in neonatal rat facial motoneurons (Töpert *et al*., 1998; Talley *et al*., 2000, 2001). We evaluated the effects of changing the external pH on the resting membrane conductance under voltage-clamp conditions in the presence of ZD-7288 to prevent contamination by pH-sensitive I_h. Figure 1A illustrates current–voltage (I/V) plots obtained in pH 8, 7 and 6 ACSF in the same facial motoneuron. The I/V plots indicate that at a holding potential of −60 mV increasing the external [H^+] induced an inward current associated with a decrease in membrane conductance. The current induced by changing external pH (I_{pH}), obtained by subtracting I/V plots obtained in each condition, reversed close to the predicted E_K, supporting the idea that at potentials depolarized to the K^+ equilibrium potential (E_K) the net inward current reflects the inhibition, by external protons, of a resting outward K^+ current. I_{pH} appeared linear over the voltage range −40 to −90 mV; however, some rectification was seen outwith this voltage range (Figs 1B, 5B, and 9B and C). These properties are characteristic of a pH-sensitive gK_{Leak}.

Results summarized from a population of facial motoneurons, voltage-clamped at −60 mV, indicate that switching from a standard physiological external pH of 7.4 to pH 6 induced an inward current of

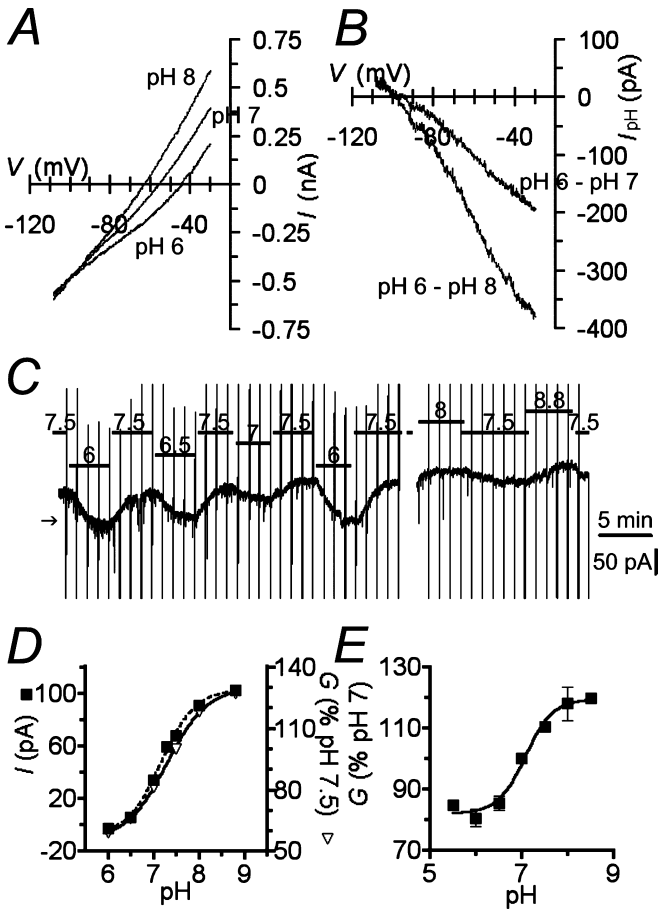

FIG. 1. Altering external pH around the physiological range modulates a leak K^+ conductance in facial motoneurons. (A) I/V relationships obtained using voltage ramp commands from a facial motoneuron superfused with pH 6, pH 7 and pH 8 ACSF. Conductance decreases with increasing H^+ concentration. (B) Subtraction of the plots shown in A indicates that altering external pH modulates a leak K^+ conductance. (C) Chart recording showing the effects of varying the pH of the ACSF on membrane current of a different facial motoneuron voltage clamped at −60 mV. The horizontal bars indicate the external pH and duration of application. Vertical deflections represent current responses to voltage commands not illustrated in this figure. The ACSF contained 3 mM K^+ and the horizontal arrow indicates the zero current level. (D) Plots of membrane current (left abscissa) and changes in membrane conductance, normalized to the conductance at pH 7.5 (right abscissa), at different external pH taken from the facial motoneuron illustrated in C above. Conductance measurements were obtained by linear regression of the I/V relationship between −60 and −80 mV. The sensitivity of changes in membrane current and conductance to external pH could be described by a four-parameter logistic function (eqn 3, Methods). pK values of 7.2 and 7.3 and Hill slopes of 1.2 and 1 were obtained for current and conductance changes, respectively. (E) Averaged data (SEM, $n = 8$) showing the pH sensitivity of changes in membrane conductance normalized to the conductance at pH 7. The relationship could be described by eqn 3 with a pK value of 7.1 ± 0.1 and a Hill slope of 1.5 ± 0.4 ($R^2 = 0.9874$).

−46 ± 6 pA associated with a decrease in membrane conductance from 7.13 ± 0.77 nS to 5.29 ± 0.55 nS ($n = 12$; mean ± SEM). Under the same conditions, switching from pH 7.4 to pH 8 resulted in an outward current (22 ± 8 pA) and a conductance increase to 9.2 ± 1.5 nS ($n = 4$; membrane conductance at pH 7.4 for the same facial motoneurons was 8.3 ± 1.6 nS). Irrespective of the inward or outward nature of the change in membrane current the reversal potential (V_{pH}) was close to the predicted E_K (pH 7.4–6, $V_{pH} = -93 \pm 1.4$ mV; pH 7.4–8, $V_{pH} = -89 \pm 3$ mV). Altering the external K^+ concentration ($[K^+]_o$) to 7 mM moved the V_{pH} to −66 ± 1.3 mV ($n = 7$), in close agreement with the change predicted by the Nernst equation.

The pH-sensitivity of gK_{Leak} was investigated further. Figure 1C shows a representative chart record of membrane current from a facial motoneuron voltage clamped at −60 mV to which ACSF of varying pH was applied. The time required for the pH-induced current changes to reach a steady state varied from 2 to 5 min. We attribute this to the depth of the recorded facial motoneuron in the slice, the relatively slow exchange of ACSF in the recording chamber and the H^+ buffering capacity of the slice. The amplitude of I_{pH} and the change in conductance over a range of external pH could be described by a modified Hill equation (see eqn 3) (Fig. 1D and E). As illustrated in Fig. 1D (for the facial motoneuron shown in Fig. 1C) measuring either parameter gave closely similar values for pH-sensitivity. Data taken from eight facial motoneurons, each of which was exposed to at least four changes in external pH, indicated a fit of the pH-evoked conductance with a pK value of 7.1 ± 0.1 and a Hill slope of 1.5 ± 0.4 (± SEM, $R^2 = 0.9874$). The pH-sensitive K^+ conductance was maximal at pH 8.2 and no further decrease in conductance was seen below pH 6. These data indicate that at physiological pH (∼ 7.4) the resting pH-sensitive gK_{Leak} is approximately 70% of its maximal level.

NA inhibits a gK_{Leak} in neonatal rat facial motoneurons

The biophysical properties of the pH-sensitive gK_{Leak} closely resemble those previously described for the 5-HT-sensitive gK_{Leak} in neonatal rat facial motoneurons (Larkman & Kelly, 1998). NA had also been shown to inhibit a similar conductance in adult rat facial motoneurons (Larkman & Kelly, 1992). Bath-application of NA also induced an inward current in neonatal rat facial motoneurons voltage-clamped at −60 mV in standard ACSF containing 3 mM K^+ (Fig. 2A, inset). ZD-7288 (5–10 μM) was again used to block I_h in these experiments. The NA-induced inward current was unaffected by external TTX (0.3 μM) or zero Ca^{2+}, 5 mM Mg^{2+} ACSF. *I/V* relationships indicated that the inward current was associated with a decrease in membrane conductance (Fig. 2A). In a representative sample of facial motoneurons, NA (10 μM) induced an inward current of −58 ± 7 pA ($n = 19$) associated with a conductance decrease from 9.4 ± 0.8 nS to 7.3 ± 0.7 nS. As seen for I_{pH}, the NA-induced current (I_{NA}) appeared linear over the voltage range −40 to −90 mV; however, some rectification was seen outwith these voltages (Figs 2B, 4B, 5C–E, 7A and B, and 8A and B). I_{NA} reversed at −96 ± 3 mV ($n = 19$), −70 ± 2 mV ($n = 16$) and −61 ± 2 mV ($n = 14$) when the ACSF contained 3, 7 or 12 mM K^+, respectively, in agreement with predictions for the E_K obtained from the Nernst equation (Fig. 2B). These properties suggest that NA inhibits a gK^+ with properties very similar to the pH-sensitive gK_{Leak}. Subtracted current records (Fig. 2C) indicated that the NA-sensitive gK_{Leak} displayed rapid, voltage-independent, activation and deactivation kinetics. Subtracted currents obtained after stepping from −60 mV to −40 mV displayed activation and deactivation time constants of 9 ± 1.6 ms ($n = 7$) and 6.6 ± 0.3 ms ($n = 8$), respectively. Stepping to −90 mV from −60 mV revealed activation and deactivation time constants of 6.9 ± 1.1 ms and 8.5 ± 0.7 ms ($n = 8$), respectively.

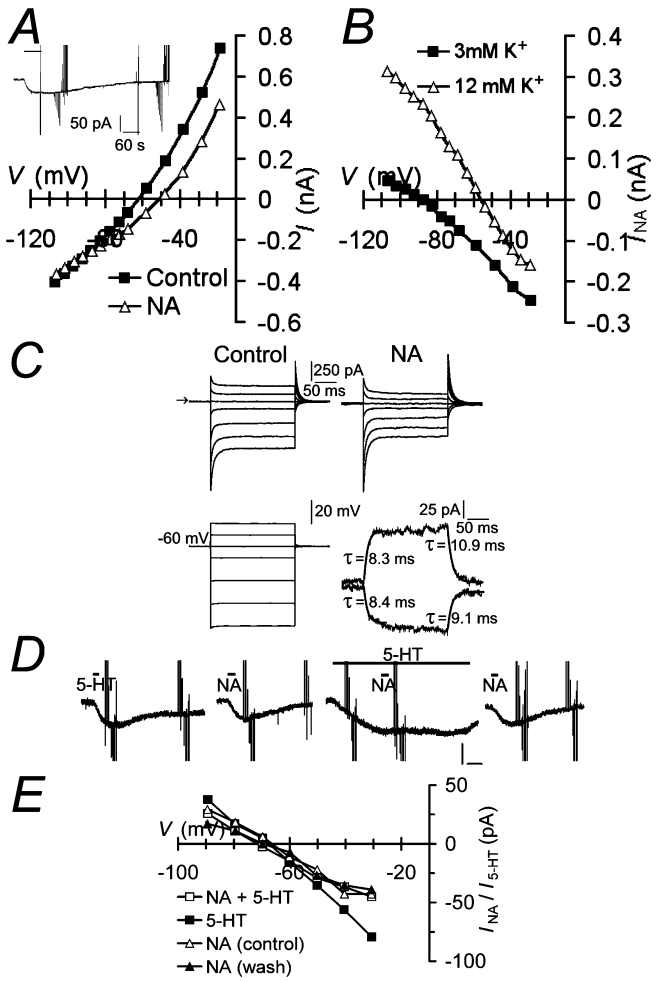

FIG. 2. Noradrenaline inhibits a leak K^+ conductance in neonatal rat facial motoneurons. (A) *I/V* relationships obtained from a facial motoneuron voltage-clamped at −60 mV in the presence (open triangles) and absence (filled squares) of NA (10 μM). Inset: the inward current evoked by bath-application of NA (duration indicated by horizontal bar) to the same facial motoneuron. Vertical deflections are attenuated current responses to voltage step and ramp commands (data not shown). (B) Plots of NA-induced current (I_{NA}) in ACSF containing 3 and 12 mM K^+. I_{NA} shows a small degree of open rectification, more prominent at negative potentials, and reverses at the predicted E_{K+}. (C) Superimposed expanded current responses to voltage step commands of variable amplitude (lower left) before (control) and during (NA) application of NA (10 μM). ACSF contained 7 mM K^+ and the horizontal arrow indicates the zero current level. Traces in C (bottom right) are subtracted records of I_{NA} in response to −30 mV (upper trace) and +20 mV (lower trace) voltage steps. Single exponential curves with the time constants (τ) indicated (eqn 1, Methods) have been superimposed on the activation and deactivation phases of the currents. (D) Chart records of membrane current from another facial motoneuron voltage clamped at −60 mV showing the NA-induced inward current is occluded by the 5-HT-induced inward current. (E) Plots of NA- and 5-HT-induced current (from the records shown in D) share the same biophysical properties and occlude over the whole voltage range tested. Maximal concentrations of bath applied 5-HT (10 μM) and NA (10 μM) were used. Calibration bars in D are 50 pA and 60 s.

Application of a maximal concentration of NA (10 μM) or the α_1-adrenergic receptor agonist PE (30 μM), in the continued presence of a maximal concentration of 5-HT (10 μM) failed to induce any further inward current (Fig. 2D and E), suggesting that the two transmitters act on a shared population of leak K^+ channels. 5-HT

(10 μM), PE (30 μM) or NA (10 μM) applied alone induced inward currents of −45 ± 4 pA ($n = 5$), −45 ± 5 pA ($n = 2$) and −34 ± 2 pA ($n = 3$), respectively ($V_h = -50$ mV, $[K^+]_o = 7$ mM). Co-application of either 5-HT and PE or 5-HT and NA induced inward currents of −43 ± 3 pA and −47 ± 8 pA, respectively. The transmitter-induced current over the range of voltage −30 to −90 mV possessed the same properties whether 5-HT or NA were applied together or separately (Fig. 2E).

NA and changes in external pH modulate the same gK_{Leak}

If NA and external pH (and 5-HT) alter facial motoneuron excitability by modulating the same gK_{Leak}, the effects of lowering external pH and transmitter application should occlude. The NA-induced inward current was examined in conditions designed to inhibit (pH 6.5) and activate (pH 7.7) I_{pH} (Fig. 3A). When external pH was increased to 7.7, a maximal concentration of NA (10 μM) induced a robust inward current of −109 ± 19 pA ($n = 5$). Lowering external pH to 6.5 led to a dramatic reduction in I_{NA} to −34 ± 9 pA in the same facial motoneurons. In the example shown in Fig. 3A the response to NA was almost completely occluded when the external pH was 6.5. Figure 3B shows that at pH 6.5, I_{NA} was occluded over the whole voltage range examined while at pH 7.7 the amplitude and the properties of I_{NA} were almost identical to those of the current induced by switching the external pH from 7.7 to 6.5. This supports the idea that both external pH and NA modulate the same gK_{Leak} and that both have an equivalent maximal level of inhibition.

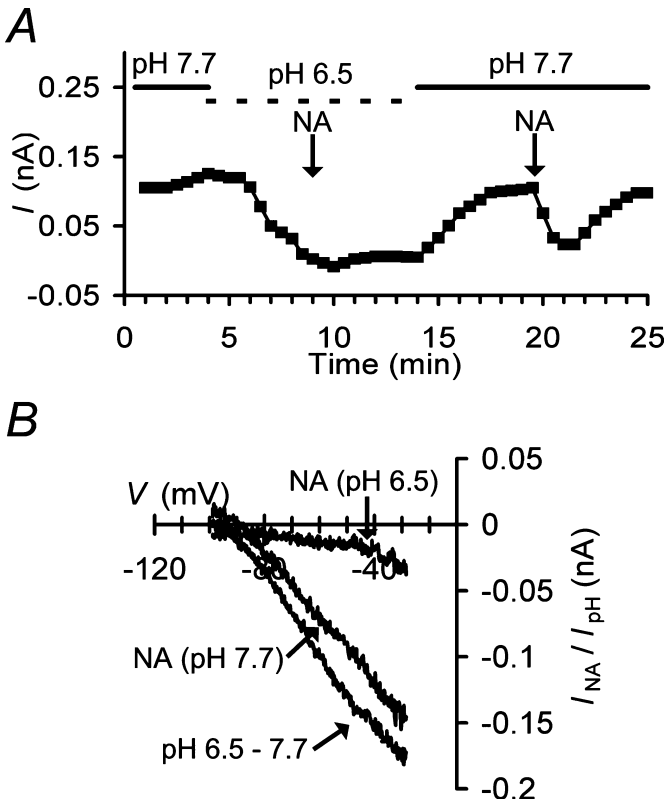

FIG. 3. Inhibition of the leak K^+ conductance by lowering external pH occludes the effects of NA. (A) Plot of membrane current against time for a facial motoneuron voltage-clamped at −60 mV. Solid and dashed horizontal bars indicate the times when the slice was superfused with pH 7.7 and pH 6.5 ACSF, respectively. Arrows indicate points at which NA (10 μM, 15 s) was added to the ACSF. Note the almost complete occlusion of the NA-induced inward current in pH 6.5 ACSF. (B) Plots of the current induced by switching from pH 7.7 to pH 6.5 ACSF and the NA-induced current in both conditions. Data in A and B are from the same facial motoneuron. Occlusion of the NA-induced current by pH 6.5 ACSF was independent of membrane potential.

Lowering external pH has been shown to alter agonist receptor interactions for some adrenoceptors. It was therefore important to confirm the identity of the adrenoceptor mediating these actions in neonatal rat facial motoneurons. PE mimicked the ability of NA to inhibit gK_{Leak} with an EC_{50} of ∼1 μM ($n = 12$, Fig. 4A–C). The β-adrenergic receptor agonist isoproterenol (5–100 μM) had no effect on gK_{Leak} ($n = 3$). NA- and PE-induced inhibition of gK_{Leak} could be abolished by bath-application of the α_1-adrenergic receptor antagonists prazosin (0.5–1 μM, $n = 5$) or WB-4101 (10 μM, $n = 2$) (Fig. 4A and B). Modulation of gK_{Leak} by NA and PE was not blocked by the β-adrenergic receptor antagonist propranolol (10 μM; $n = 3$, Fig. 4D).

The effects of TASK channel blockers on the pH- and NA-sensitive gK_{Leak}

The pH-sensitivity of gK_{Leak} suggested to us that TASK channels might contribute to this conductance. The pharmacological properties of facial motoneuron gK_{Leak} are summarized in Table 1. Low micromolar concentrations of the endogenous cannabinoid anandamide block homomeric human TASK-1 channels (Maingret *et al.*, 2001). Homomeric TASK-3 channels are blocked by higher concentrations of anandamide. Bath-application of anandamide (10–20 μM) had no effect on facial motoneuron resting membrane conductance at the holding potential (−50 mV) in pH 7.4 ACSF ($n = 4$) or on the decrease in gK_{Leak} induced either by NA (10 μM) or lowering the external pH from 7.4 to 6 (Fig. 5A). I_{NA} at a holding potential of −50 mV (3 mM $[K^+]_o$) was −53 ± 3 pA in the absence of anandamide compared with −52 ± 3 pA in its presence ($n = 3$).

It has been reported that anandamide may be metabolically degraded in certain *in vitro* conditions and that this can be prevented by ATFK (Barbuti *et al.*, 2002). When applied alone for up to 20 min, ATFK (10 μM) had no effect on the pH- or NA-induced currents ($n = 2$). Subsequent co-application of anandamide (10 μM) again failed to induce a membrane current or affect the currents induced by application of NA or lowering pH. Methanandamide is a metabolically stable analogue of anandamide that has also been shown to inhibit TASK-1 channels (Maingret *et al.*, 2001). Methanandamide (20 μM) also failed to have any effect on the resting membrane current and failed to inhibit the NA-induced response ($n = 4$, Fig. 5B).

Homomeric TASK-3, but not TASK-1, channels are inhibited by RR (Czirják & Enyedi, 2003). Application of RR (10 μM) to facial motoneurons had no effect on holding current at −50 mV ($n = 4$). Co-application of NA (10 μM) in the presence of RR (10 μM) induced an inward current indistinguishable from the control response obtained in the absence of the TASK-3 blocker (Fig. 5C). Thus, inward I_{NA} at a holding potential of −50 mV (3 mM $[K^+]_o$) was −50 ± 8 pA in the absence of RR compared with −59 ± 6 pA in its presence ($n = 4$). The V_{NA} was also unaffected by the presence of RR.

Actions of ruthenium red and methanandamide on cultured cerebellar granule cells

The absence of any effects of anandamide, methanandamide, and RR on facial motoneurons prompted us to examine the activity of our drugs. We therefore tested the ability of RR and methanandamide to inhibit putative TASK channel-mediated currents in cultured rat CG cells (Maingret *et al.*, 2001; Han *et al.*, 2002; Kang *et al.*, 2004).

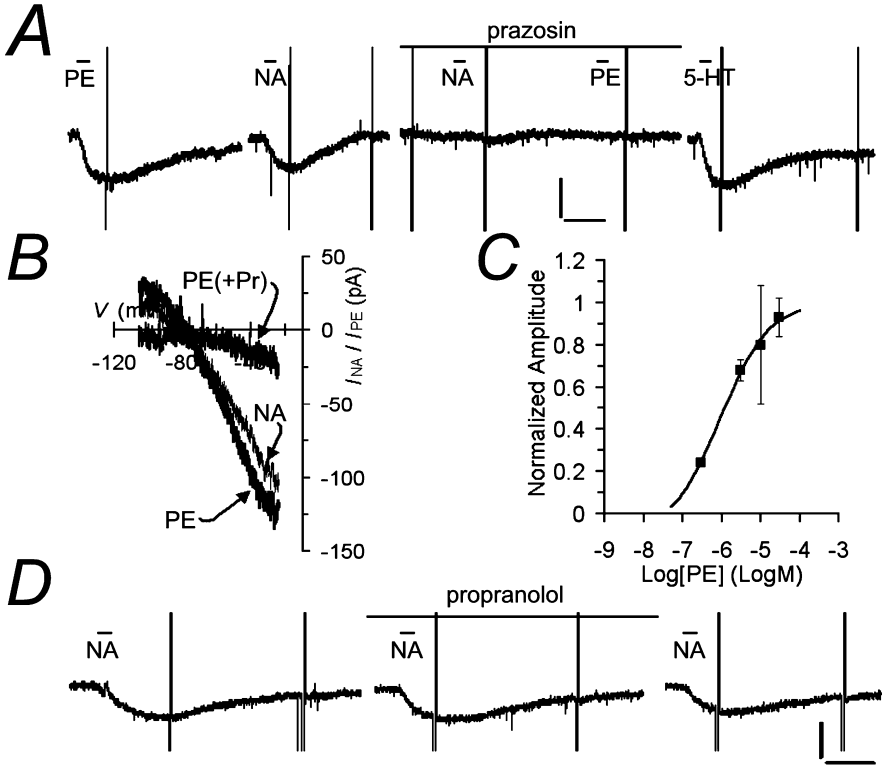

FIG. 4. Noradrenaline, acting through a α_1 receptor, inhibits the same leak K^+ conductance as 5-HT. (A) Chart records of membrane current from a facial motoneuron voltage-clamped at −60 mV showing that the inward currents evoked by bath-application of phenylephrine (PE, 30 μM) and NA (5 μM) were inhibited by the α_1 receptor antagonist, prazosin (0.5 μM). The response to 5-HT (10 μM) was unaffected by this antagonist. (B) The NA- and PE-induced currents, obtained by subtraction of current responses to voltage ramps, share the same biophysical properties and are blocked over the whole voltage range by prazosin. (C) Dose–response curve for PE. Response amplitude was normalized to the response to 5-HT (10 μM). Data points represent mean ± SEM for five different facial motoneurons. The solid line represents a fit of the data to eqn 4 (Methods) with an EC_{50} of 1 μM and a Hill slope of 0.71. (D) Chart records of membrane current from a facial motoneuron voltage-clamped at −60 mV showing a lack of effect of the β-adrenergic receptor antagonist, propranolol (10 μM), on the currents induced by NA (5 μM). Calibration bars in A and D are 50 pA and 60 s.

TABLE 1. Comparative pharmacology of TASK channels and rat facial motoneuron gK_{Leak}

	TASK-1	TASK-3	TASK-1/TASK-3	Rat FM gK_{Leak}
pK[1]	∼ 7.5 (r)	∼ 6.8 (r)	∼ 7.3 (r)	∼ 7.1
Isoflurane (0.3 mM)[1]	No effect (r)	∼ +80% (r)	∼ +50% (r)	∼ +55%
Methanandamide (10 μM)[1]	∼ −85% (r)	∼ −64% (r)	∼ −55% (r)	No effect
Ruthenium red (5 μM)[3]	No effect (r)	∼ – 85% (r)	No effect (r)	No effect (10 μM)
Zn^{2+} (100 μM)[2,7,8]	∼ −40% (r)	No effect (r)	No data	No effect (r)
	No effect (h)	∼ −70% (h)	∼ −20% (h)	
Bupivacaine (100 μM)[7,8]	∼ −60% (r)	∼ −50% (r)	No data	∼ −30%
Ba^{2+} [7,9]	IC_{50} ∼400 μM (r)	IC_{50} ∼300 μM (r)	No data	∼ −90% (500 μM)
Cs^+ [4,7,10]	∼ −30% (100 μM, r)	∼ −75% (3 mM, r)	No data	No effect (300 μM)
		No effect (10 mM, h)		∼ −85% (1 mM)
4-AP[5,8]	∼ −15% (10 mM, r)	No data	No data	∼ −60% (4 mM)
TEA[5,6,7,8]	∼ −30% (100 mM, r)	No effect (1 mM, r)	No data	No effect (30 mM)

Values indicated are percentage current increase (+) or decrease (–) in the presence of the drug indicated, except for the sensitivity of TASK-1 and TASK-3 homomers to Ba^{2+} for which the IC_{50} is given. Values for Ba^{2+} and Cs^+ reflect optimal voltage-dependent blocker sensitivity. Species is either rat (r) or human (h). Where non-uniform drug concentrations are compared the concentrations are given in parentheses in the table. Data for TASK-1/TASK-3 heterodimer refers to concatenated TASK-1/TASK-3 construct. Data taken from [1]Berg *et al.* (2004), [2]Clarke *et al.* (2004), [3]Czirják & Enyedi (2002a), [4]Czirják & Enyedi (2002b), [5]Czirják *et al.* (2000), [6]Duprat *et al.* (1997), [7]Kim *et al.* (2000), [8]Leonoudakis *et al.* (1998), [9]Lopes *et al.* (2001) and [10]Meadows & Randall (2001).

Lowering pH to 6 from 7.4 induced an inward current in CG cells with characteristics of a TASK-mediated leak K^+ conductance (insets to Fig. 5B and C). RR (10 μM) also induced an inward current that was 53 ± 2% ($n = 3$) of the amplitude of tha induced at pH 6. The actions of RR partially occluded the current induced at pH 6. Bath-application of methanandamide (20 μM) had a smaller effect on CG cells, inducing an inward current with characteristics of gK_{Leak} that was 18% of the current induced at pH 6 (inset Fig. 5D). These actions are consistent with reported effects of RR and methanandamide on TASK-1 and TASK-3 channels in cultured CG neurons (Maingret *et al.*, 2001; Han *et al.*, 2002; Lauritzen *et al.*, 2003; Kang *et al.*, 2004). The insensitivity to anandamide of facial motoneuron gK_{Leak} should not be

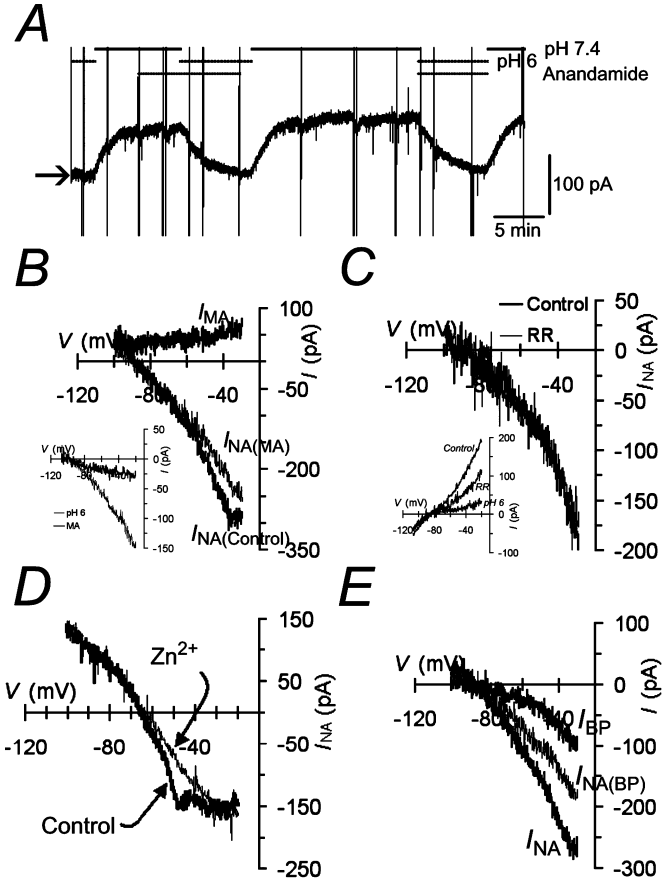

FIG. 5. Homomeric TASK-1 and TASK-3 channel blockers have no effect on the NA- and pH-sensitive leak K^+ conductance. (A) A chart recording showing membrane current against time for a facial motoneuron voltage-clamped at −50 mV. Horizontal bars indicate the times when the slice was superfused with pH 7.4 ACSF, pH 6 ACSF and anandamide (10 μM). The horizontal arrow indicates the zero current level. Vertical deflections are attenuated current responses to ramp voltage commands (data not shown) used to generate *I/V* data. Anandamide failed to alter membrane current in pH 7.4 ACSF and had no effect on the amplitude or time course of the inward current induced by perfusion with pH 6 ACSF. (B) Plots of the methanandamide (20 μM)-induced current (I_{MA}) and the NA-induced current in the absence ($I_{NA(Control)}$) and presence ($I_{NA(MA)}$) of methanandamide. Methanandamide does not inhibit gK_{Leak} or I_{NA}. Inset: the currents induced by methanandamide (10 μM) and pH 6 ACSF in a cultured rat cerebellar granule cell. (C) Plots of I_{NA} in the presence and absence of ruthenium red (10 μM). Note that the currents superimpose, indicating a lack of effect of ruthenium red. Inset: *I/V* plots from a cultured rat cerebellar granule cell indicating that ruthenium red (10 μM) and pH 6 ACSF both significantly inhibit a gK_{Leak} in these neurons. (D) Zn^{2+} (300 μM) fails to block the actions of NA on facial motoneuron gK_{Leak} but does abolish an inflection attributable to enhanced gCa^{2+}. (E) Plots of the current induced by bupivacaine (I_{BP}, 50 μM), NA (I_{NA} 10 μM) and NA in the presence of bupivacaine ($I_{NA(BP)}$). ACSF contained 3 mM K^+ in A, B, C and E and 7 mM K^+ in D.

overstated. A recent report suggests that unlike human TASK-1 and TASK-3 channels the rat homologues are not particularly sensitive to low concentrations of anandamide and that higher concentrations fail to discriminate the two channel types (Berg *et al*., 2004).

The effects of Zn^{2+} and bupivacaine on the pH- and NA-sensitive gK_{Leak}

Homomeric human (h)TASK-1 channels, expressed in cell lines, display little sensitivity to Zn^{2+} (100 μM) whereas homomeric hTASK-3 channels are substantially (~70%) blocked at this concentration (Leonoudakis *et al*., 1998; Clarke *et al*., 2003, 2004). Bath-application of Zn^{2+} (100–300 μM) did not significantly affect facial motoneuron membrane current (+3 ± 1.7 pA at −60 mV) or membrane slope conductance (5 ± 0.5 to 5.5 ± 0.5 nS in the presence of Zn^{2+} over the range −90 to −60 mV, $n = 5$) in pH 7.4 ACSF. In the same facial motoneurons, superfusion with pH 6 ACSF induced an inward current of −49 ± 11 pA and decreased membrane conductance to 3.6 ± 0.7 nS. I_{pH} obtained by changing external pH from 6 to 7.7 was unaffected by the presence of Zn^{2+}. Consistent with its lack of effect on I_{pH}, Zn^{2+} (100–300 μM) also failed to alter I_{NA} (Fig. 5D). Thus, inward I_{NA} at the holding potential (−52 mV, 7 mM $[K^+]_o$) was −51 ± 20 pA ($n = 2$) and outward I_{NA} at −102 mV was 92 ± 28 pA ($n = 3$). These values compared with −44 ± 13 pA and 88 ± 29 pA at −52 mV and −102 mV, respectively, in the presence of Zn^{2+} (300 μM). Despite this lack of effect on gK_{Leak}, Zn^{2+} did inhibit a small enhancement of gCa^{2+} seen in some facial motoneurons (Fig. 5D).

The local anaesthetic bupivacaine has been shown to block non-selectively TASK-1 and TASK-3 channels with IC_{50} values of about 100 μM (Leonoudakis *et al*., 1998; Kim *et al*., 2000). Bupivacaine (100 μM) induced an inward current in four facial motoneurons tested but in two further motoneurons bupivacaine (50 μM) failed to alter membrane current. At a holding potential of −50 mV (3 mM $[K^+]_o$) bupivacaine (100 μM) induced a current of −49 ± 12 pA ($n = 4$), which reversed at −87 ± 3 mV and displayed the linear *I/V* relationship characteristic of inhibition of gK_{Leak} (Fig. 5E). The NA-induced inward current was partially and reversibly occluded by bupivacaine. Thus, NA (10 μM) induced a current of −137 ± 33 pA and −94 ± 22 pA in the absence and presence of bupivacaine, respectively, representing occlusion by 29 ± 8%.

The effects of isoflurane on gK_{Leak}

In a recent study of rat TASK channels the volatile anaesthetic isoflurane inhibited homomeric TASK-1 current but enhanced current carried by homomeric TASK-3 and heteromeric TASK-1/TASK-3 channels (Berg *et al*., 2004). This enhancement was seen even when the current was optimally activated by external pH. We investigated the effects of isoflurane on facial motoneuron gK_{Leak} when the conductance was optimally activated by an external solution of pH 8. Bath-application of isoflurane (see Methods for solution preparation) increased gK_{Leak} in four out of five facial motoneurons tested ($V_{rev} = -63 \pm 2$ mV in ACSF containing 7 mM K^+, Fig. 6A and B). Expressed as a percentage of the maximal pH-sensitive current at −100 mV, obtained by exposing each facial motoneuron sequentially to ACSF of pH 8 and pH 6, isoflurane enhanced the pH-sensitive current by 55 ± 6% ($n = 4$). It is noteworthy that in the remaining facial motoneuron isoflurane reversibly and reproducibly inhibited gK_{Leak}.

The effects of Ba^{2+}, Cs^+ and Rb^+ on gK_{Leak}

Block by external Ba^{2+}, Cs^+ and Rb^+ is a characteristic of inwardly rectifying K^+ channels and the effects of these ions on TASK channels are subtype dependent. Ba^{2+} (at concentrations of 0.5–2 mM) substantially blocks I_{NA} at hyperpolarized potentials, where current flow through gK_{Leak} is inward, but has a much more limited effect at depolarized potentials where current flow is outward. Thus, at −117 mV and −40 mV in the absence of Ba^{2+}, I_{NA} was 139 ± 81 pA and −74 ± 12 pA whereas in its presence these values were 16 ± 14 pA and −47 ± 4 pA, reflecting 10 ± 6% and 75 ± 9%

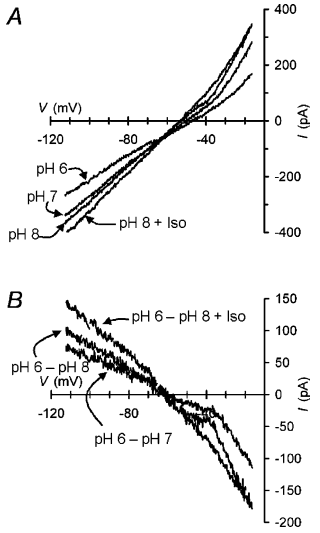

FIG. 6. Isoflurane enhances the pH-sensitive leak K^+ conductance. (A) *I/V* relationships obtained using voltage ramp commands from a facial motoneuron superfused with pH 6, pH 7, pH 8 and pH 8 with isoflurane (concentration as indicated in Methods) ACSF. Isoflurane (Iso) increases gK_{Leak} even when the conductance is optimally activated by pH 8 ACSF. (B) Subtraction of the plots shown in A indicating greater activation of the pH-sensitive gK_{Leak} in the presence of isoflurane (pH 6 – pH 8 + Iso) than in its absence (pH 6 – pH 8).

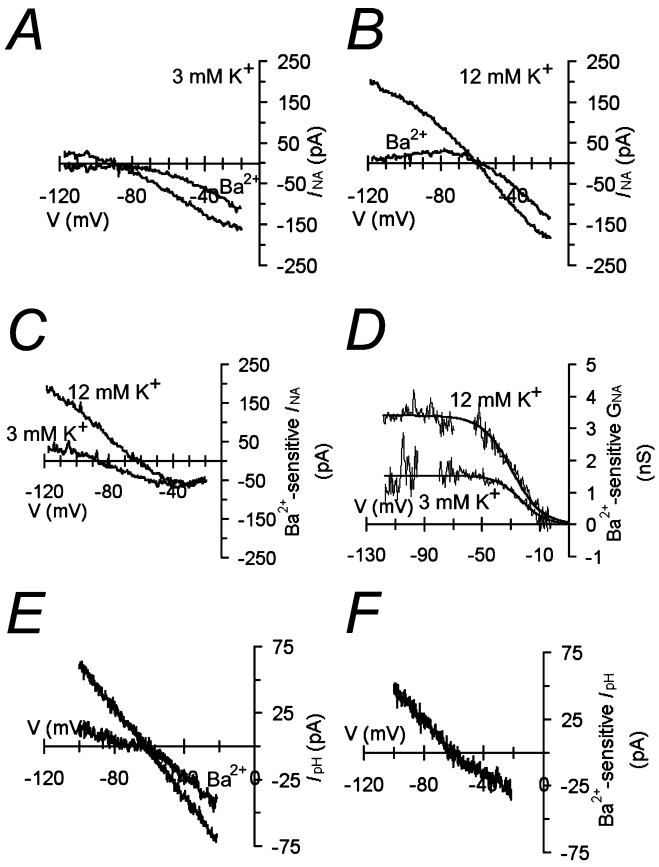

FIG. 7. Ba^{2+} ions voltage-dependently block the NA- and pH-sensitive leak K^+ conductance. (A and B) Plots of NA-induced current at different voltages obtained in the absence and presence of Ba^{2+} (2 mM) in ACSF containing 3 mM (A) and 12 mM (B) K^+. Note the voltage dependence of the Ba^{2+} block. (C) Plots of the Ba^{2+}-sensitive component of the NA-induced current (I_{NA}) obtained by subtraction of plots shown in A and B. (D) Plots of the chord conductance (G) of the Ba^{2+}-sensitive component of the NA-induced current (I_{NA}) (obtained as described in Methods) against voltage. Curve fitting was performed using eqn 2 (Methods). $V_{0.5}$ were −23 mV and −29 mV and the slopes were −8.5 mV and −10.2 mV in 3 and 12 mM K^+ ACSF, respectively. Gaps were introduced into the traces because of a large increase in signal noise as the membrane potential approached the V_{NA}. (E) Plots of current induced by switching from pH 7.7 to pH 6.5 ACSF at different voltages obtained in the absence and presence of Ba^{2+} (1 mM). ACSF contained 7 mM K^+. Note again the voltage dependence of the Ba^{2+} block. (F) Plot of the Ba^{2+}-sensitive component of I_{pH} obtained by subtraction of plots shown in E.

of control values, respectively ($n = 4$) (Fig. 7A and B). We had previously suggested that because the Ba^{2+}-sensitive component of $I_{5\text{-}HT}$ (Larkman & Kelly, 1998) and now I_{NA} displayed inward rectification the actions of Ba^{2+} might represent modulation of an inwardly rectifying K^+ conductance (gK_{ir}) (Fig. 7C). However, fitting a Boltzmann function to the chord conductance of the Ba^{2+}-sensitive component of I_{NA} obtained in different $[K^+]_o$ indicated that the $V_{0.5}$ of activation was relatively independent of $[K^+]_o$, and hence the E_K (Fig. 7D, $[K^+]_o = 3$ mM, $V_{0.5} = -23$ mV, slope = −8.5 mV; $[K^+]_o = 12$ mM, $V_{0.5} = -29$ mV, slope = −10.2 mV), suggesting properties distinct from gK_{ir}.

The effect of Ba^{2+} on facial motoneuron membrane conductance does, however, appear to result from inhibition of both gK_{Leak} and gK_{ir}. At pH 6, where I_{pH} is maximally inhibited, Ba^{2+} inhibited an inwardly rectifying component of membrane current that reversed at the predicted E_K (data not shown). When external pH was raised to 7.7 the Ba^{2+}-sensitive current was increased preferentially at hyperpolarized potentials. Figure 7E indicates the properties of I_{pH} obtained by changing the external pH from 6 to 7.7 in the absence and presence of Ba^{2+}. As for I_{NA}, Ba^{2+} displays a preferential block of I_{pH} at hyperpolarized potentials such that the Ba^{2+}-sensitive I_{pH} showed similar voltage dependence to that of Ba^{2+}-sensitive I_{NA} (Fig. 6F). At −90 mV Ba^{2+} (1 mM) inhibited I_{pH} by 84 ± 20% while at −30 mV inhibition was 13 ± 15% ($n = 3$, 7 mM $[K^+]_o$, $V_{pH} = -66 \pm 1$ mV).

Cs^+ (1 mM) induced an outward current of 181 ± 17 pA at −102 mV without significantly altering the holding current at −52 mV (10 ± 3 pA, $n = 2$, pH = 7.4, 7 mM $[K^+]_o$). At this concentration Cs^+ significantly reduced I_{NA} at −102 mV to 15 ± 3% of control but had less effect at the holding potential (79 ± 8% of control I_{NA}) (Fig. 8A). The V_{NA} was −67 ± 1 mV and −67 ± 2 mV in the absence and presence of Cs^+, respectively. These effects were also observed in 5 mM Cs^+ ($n = 2$). Cs^+ (300 μM) had a smaller effect on membrane current at −102 mV, reducing it by 69 ± 2 pA again without a significant effect at the holding potential (−8 ± 5 pA, $n = 2$). This concentration of Cs^+ failed to alter I_{NA} or I_{pH} at any potential (Fig. 8B) suggesting at least partial inhibition of gK_{ir} but not the pH- and NA-sensitive gK_{Leak}.

The block of TASK conductances by Ba^{2+} but not Cs^+ displays a time dependence (Czirják *et al.*, 2001; Czirják & Enyedi, 2002b). Subtracted current records of Ba^{2+}- and Cs^+-sensitive gK_{Leak} in facial motoneurons evoked by voltage steps to −100 mV were indistinguishable in terms of the kinetics of block by either ion, both showing rapid current block (data not shown).

Low permeability to Rb^+ is a characteristic of some inwardly rectifying K^+ channels while several members of the TASK family show considerable Rb^+ permeability (Lopes *et al.*, 2000). Rb^+ voltage-dependently blocked facial motoneuron I_{NA} in a manner similar to that seen for Ba^{2+} and Cs^+ (Fig. 8C). At −50 mV, NA (10 μM) induced an inward current of −33 ± 5 pA ($n = 6$) in ACSF containing 7 mM K^+ and −23 ± 6 pA when this was replaced with 7 mM Rb^+ (77 ± 14% of

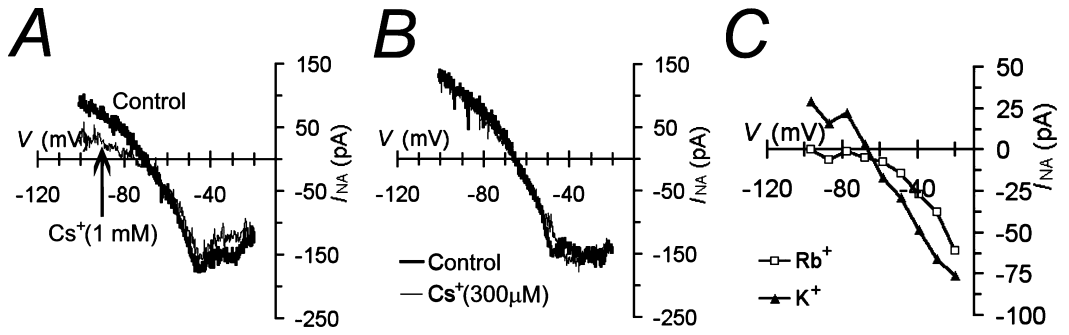

FIG. 8. Cs^+ and Rb^+ ions voltage-dependently block the NA-induced current. (A and B) Plots of NA-induced current in the presence and absence of 1 mM (A) or 300 μM (B) Cs^+. Note that Control and Cs^+ plots in B superimpose, indicating that 1 mM but not 300 μM Cs^+ blocks I_{NA} preferentially at hyperpolarized potentials. (C) Plots of NA-induced current in 7 mM K^+- or 7 mM Rb^+-containing ACSF. Rb^+ voltage-dependently blocks I_{NA}. Records in A and B were from the same facial motoneuron and were obtained in ACSF containing 7 mM K^+.

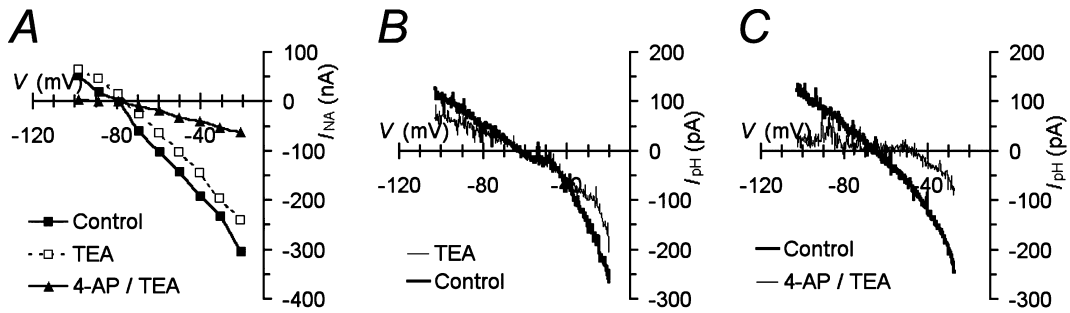

FIG. 9. 4-Aminopyridine (4-AP), but not tetraethylammonium (TEA) blocks NA- and pH-sensitive currents in facial motoneurons. (A) Plots of NA-induced current in the presence of TEA (30 mM, open squares), TEA and 4-AP (4 mM, filled triangles) and under control conditions with neither drug present (filled squares). The block observed in the presence of 4-AP showed little voltage dependence. ACSF contained 3 mM K^+. (B and C) Plots showing the current induced by changing from pH 7.5 to pH 6.5 ACSF is blocked by 4-AP (4 mM, B) but not by TEA (30 mM, C). ACSF contained 7 mM K^+.

control). At −100 mV, I_{NA} was +51 ± 18 pA and −3 ± 11 pA in K^+- and Rb^+-containing ACSF, respectively, reflecting a reduction to −3 ± 11% of the control amplitude. Replacement of external K^+ with Rb^+ also voltage-dependently inhibited $I_{5\text{-HT}}$ in facial motoneurons (Larkman & Kelly, 1998).

The effects of TEA and 4-AP on gK_{Leak}

We have previously characterized the sensitivity of $I_{5\text{-HT}}$ to the K^+ channel blockers TEA and 4-AP (Larkman & Kelly, 1998). As can be seen in Fig. 9 these channel blockers have closely similar actions on I_{NA} and I_{pH}. TEA (30 mM) added to either 3 or 12 mM K^+ ACSF had no significant effect on I_{NA} over the potential range tested ($n = 7$, Fig. 9A). The addition of 4-AP (4 mM) did, however, inhibit I_{NA} over the whole voltage range without altering the V_{NA} ($n = 3$, Fig. 9A). Thus, at −100 mV, 4-AP reduced I_{NA} to 37 ± 22% of the control amplitude while at −40 mV I_{NA} was 31 ± 14% of the control level. We next evaluated the effects of TEA and 4-AP on I_{pH} evoked by switching from ACSF of pH 7.5 to pH 6.5. I_{pH} was also unaffected by TEA (30 mM) but could be inhibited by 4-AP at concentrations equivalent to those required to block I_{NA} ($n = 3$, Fig. 9B and C). At −100 mV and −40 mV, in the presence of TEA, I_{pH} was 86 ± 14% and 103 ± 3% of the control amplitudes, respectively, while addition of 4-AP (4 mM) to the ACSF reduced these values to 19 ± 11% and 32 ± 8%, respectively.

Discussion

Amine neurotransmitters and external pH modulate the same gK_{Leak}

Our results characterize a pH-sensitive gK_{Leak} that contributes to the resting membrane conductance of neonatal rat facial motoneurons. NA also inhibits a gK_{Leak} in neonatal rat facial motoneurons, as seen previously in the adult rat, and several lines of evidence support the idea that this is the pH-sensitive conductance. First, NA and lowering external pH below the normal physiological level (pH 7.4) inhibited a current that displayed rapid kinetics, a small amount of rectification over the potential range −120 to −40 mV and a reversal potential at the predicted E_K. Secondly, lowering external pH occluded the actions of NA. Responses to NA were also occluded by 5-HT-induced inhibition of gK_{Leak}. Maximal concentrations of NA decreased membrane conductance to a level very close to the maximum level of inhibition obtained by lowering external pH. Thirdly, raising the external pH above pH 7.4 induced an outward current associated with an increase in membrane conductance and under these conditions the amplitude of the inward current induced by NA was increased. Finally, the pH- and NA-sensitive gK_{Leak} displayed a common pharmacology to a wide range of K^+ channel blockers. In combination, these results support a common target of modulation.

One possible explanation for the occlusion of the NA-mediated response by low external pH is a change in protein structure that disrupts agonist–receptor interactions. Reports suggest α_2- but not α_1-adreno-

ceptors display alterations in functional responses associated with changes in agonist binding affinity over the pH range 6–8 (Curro & Greenberg, 1983; Nunnari *et al*., 1987; Tateishi & Faber, 1995). Our studies indicate an α_1-adrenoceptor mediates inhibition of gK_{Leak} in facial motoneurons. This is consistent with ligand-binding and *in situ* hybridization data showing α_1-adrenoceptor mRNA and protein expression in all cranial motor nuclei (Pieribone *et al*., 1994). It is therefore unlikely that occlusion of the NA-mediated modulation of gK_{Leak} by low external pH is due to altered agonist–receptor interactions.

pH-sensitivity of the amine-sensitive gK_{Leak}

The presence of mRNA for the pH-sensitive K^+ channels TASK-1 and TASK-3 in the facial motor nucleus makes these channels potential candidates for gK_{Leak} (Talley *et al*., 2000; Karschin *et al*., 2001). TASK-1 and TASK-3 channels mediate openly rectifying, non-inactivating, whole-cell currents similar to the pH- and NA-sensitive gK_{Leak} in facial motoneurons (Duprat *et al*., 1997; Leonoudakis *et al*., 1998; Kim *et al*., 2000; Rajan *et al*., 2000; Talley *et al*., 2000; Vega-Saenz de Miera *et al*., 2001). Activation and inactivation are described as 'instantaneous'. For example, TASK-3 channels expressed in *Xenopus* oocytes displayed time constants of around 4 ms, not very dissimilar from the values of 8–9 ms described here (Rajan *et al*., 2000). The sensitivity of TASK-1 channels to external pH lies across the physiological range with a pK of about 7.3–7.5 (Duprat *et al*., 1997; Talley *et al*., 2000). The pK for TASK-3 channels is approximately one pH unit lower in the range 6–6.7 (Kim *et al*., 2000; Rajan *et al*., 2000; Vega-Saenz de Miera *et al*., 2001) such that at physiological pH a TASK-3-mediated conductance should be maximally activated. The pH-sensitive gK_{Leak} of facial motoneurons has a pK close to 7.1, between the published ranges for either homomeric channel. At pH 7.4 it is activated to approximately 70% of its maximal level, suggesting against a homomeric TASK-3 identity. The pH-sensitivity of facial motoneuron gK_{Leak} was determined in physiological external $[K^+]$ (3 mM) so the pK cannot be attributed to a previously described effect of high external $[K^+]$ on TASK-1 channels (Lopes *et al*., 2000, 2001).

Interestingly, human Kir2.4 is inhibited by external H^+ over the range pH 6–8 with a pK of 7.1 (Karschin *et al*., 1996; Töpert *et al*., 1998; Hughes *et al*., 2000). Kir2.4 mRNA, along with mRNA for Kir2.1 and Kir2.2, is expressed in some neonatal rat facial motoneurons. As such, determining pH-sensitivity alone may not be sufficient to distinguish TASK and Kir2 channel types (Karschin & Karschin, 1997; Töpert *et al*., 1998). It has, however, been suggested that rat Kir2.4 channels are only slightly pH-sensitive (unpublished observations in Talley *et al*., 2000).

Pharmacology of the amine-sensitive gK_{Leak}

The lack of effect of methanandamide or anandamide, with or without pre-application of the metabolic inhibitor ATFK, suggests against a TASK-1 identity for facial motoneuron gK_{Leak}, though as noted earlier the potency of these ligands against rat TASK-1 channels is lower than for human TASK-1 (Berg *et al*., 2004). Equally, the inability of RR to block gK_{Leak} suggests against a TASK-3 identity. The expected effects of these ligands observed in cultured CG cells indicate that our negative results cannot be attributed to factors that might affect the activity of these drugs or their delivery to our slices. Recently, Zn^{2+} has been used to discriminate between human TASK-1 and TASK-3 channels (Clarke *et al*., 2003). Human TASK-1 is unaffected by Zn^{2+} (100 μM) whereas the same concentration blocks hTASK-3 by greater than 70% (IC_{50} = ~20 μM). While the insensitivity of the pH- and NA-sensitive gK_{Leak} to Zn^{2+} also argues against a TASK-3 channel identity there is a suggestion that rat TASK-3 channels are insensitive to Zn^{2+} (100 μM) (Leonoudakis *et al*., 1998; Kim *et al*., 2000). Recently, however, the gK_{Leak} in rat CG neurons has been shown to be substantially blocked by Zn^{2+} (100 μM) (Clarke *et al*., 2004).

It is of interest that the local anaesthetic bupivacaine inhibited a conductance that shared the properties of gK_{Leak} and at least partially occluded the actions of NA in some facial motoneurons. Bupivacaine inhibits both TASK-1 and TASK-3 channels with roughly equivalent potency (Leonoudakis *et al*., 1998; Kim *et al*., 2000) and its ability to block a pH-sensitive gK_{Leak} in thalamocortical neurons appears sufficient to ascribe this a TASK channel-mediated conductance (Meuth *et al*., 2003). Nevertheless, bupivacaine also has actions on other channels including some voltage-gated K^+ channels (González *et al*., 2001). Thus, while the current blocked by bupivacaine in facial motoneurons is consistent with a TASK-like gK_{Leak}, the additional block of other K^+ channels may also contribute to the overall effect of this drug.

Rb^+ voltage-dependently blocks the NA- and pH-sensitive gK_{Leak} in facial motoneurons; however, the Rb^+ permeability of TASK-1 channels is equivalent to that of K^+, although with a lower relative conductance (Lopes *et al*., 2000). This suggests that if TASK-1 channels underlie gK_{Leak}, Rb^+ might be expected at least partially to support this conductance. Cs^+ (100 μM) partially blocks (~30%) inward TASK-1 currents while inward and outward TASK-3 currents are much less sensitive to Cs^+ (up to 10 mM) (Duprat *et al*., 1997; Rajan *et al*., 2000; Meadows & Randall, 2001; Czirják & Enyedi, 2002b). Block of facial motoneuron gK_{Leak} by Cs^+ again suggests against TASK-3 channels, although the sensitivity and voltage-dependent block also differ from TASK-1 channels

Ba^{2+} blocks a significantly greater amount of inward current than outward current through TASK-1 and TASK-3 channels (Czirják *et al*., 2000; Kim *et al*., 2000; Lopes *et al*., 2000, 2001; Millar *et al*., 2000; Rajan *et al*., 2000; Vega-Saenz de Miera *et al*., 2001). The IC_{50} for Ba^{2+} against inward guinea-pig TASK-3 currents is about 300 μM while against outward current it is greater than 5 mM (Rajan *et al*., 2000). Reported IC_{50} values of around 3 mM for rat and human TASK-3 almost certainly reflect measurements made against outward current (Kim *et al*., 2000; Vega-Saenz de Miera *et al*., 2001). Ba^{2+} blocks rat TASK-1 channels with an IC_{50} of around 400 μM and this is both voltage- and pH-dependent, block decreasing with increasing $[H^+]_o$ (Lopes *et al*., 2001). The effects of Ba^{2+} on facial motoneuron gK_{Leak} reported both here and earlier (Larkman & Kelly, 1998) are consistent with a voltage-dependent block at micromolar concentrations that clearly does not discriminate homomeric TASK-1 and TASK-3 channels. The explanation for the absence of any time dependence to the block of gK_{Leak} by Ba^{2+} is not clear, although our experiments were performed in relatively low external $[K^+]$ compared with the studies of TASK channels (Czirják *et al*., 2001; Czirják & Enyedi, 2002b).

Kir channels, including members of the Kir2 family, display distinct sensitivities to Cs^+ and Ba^{2+}. Block of Kir2.4 by Cs^+ is voltage sensitive with an IC_{50} of about 100 μM at −100 mV and 1 mM at −60 mV (Hughes *et al*., 2000). Cs^+ (300 μM) blocked a gK_{ir} in facial motoneurons but at this concentration had no effect on either I_{NA} or I_{pH} even at hyperpolarized potentials. Ba^{2+} blocks Kir2.4 (IC_{50} of between 100 and 300 μM) with potency similar to that described for the amine-sensitive gK_{Leak} in facial motoneurons; however, block of Kir2.4 is relatively voltage-insensitive (Larkman & Kelly, 1998; Hughes *et al*., 2000; Liu *et al*., 2001; Schram *et al*., 2002). Ba^{2+} also blocked a gK_{ir} when the pH- and amine-sensitive gK_{Leak} was fully inhibited by pH 6 ACSF. These results support the presence of a gK_{ir}

in facial motoneurons that is distinct from the pH- and amine-sensitive gK_{Leak}.

Possible identities of facial motoneuron gK_{Leak}: TASK-1/TASK-3 heterodimers

Although our results suggest against homomeric TASK-1 or TASK-3 channels, evidence indicates TASK-1 and TASK-3 interact to form functional heterodimeric channels (Czirják & Enyedi, 2002a; Talley & Bayliss, 2002). Could facial motoneuron gK_{Leak} be accounted for by heteromeric TASK-1/TASK-3 channels? The pharmacologies of homomeric TASK-1, homomeric TASK-3 and heteromeric TASK-1/TASK-3 currents expressed in various systems and facial motoneuron gK_{Leak} are compared in Table 1. It has been suggested that heterodimer formation may be a favoured process when both TASK-1 and TASK-3 subunits are present, although recent studies on cultured CG cells indicate both homomeric and heteromeric channels can also coexist in the same cell (Czirják & Enyedi, 2002a; Kang *et al*., 2004). It has recently been observed that isoflurane enhances current carried by heteromeric TASK-1/TASK-3 and homomeric TASK-3 channels while inhibiting homomeric TASK-1 channels (Berg *et al*., 2004). Isoflurane enhances facial motoneuron gK_{Leak} while RR, the TASK-3 blocker, has no effect. Heteromeric TASK-1/TASK-3 channels are insensitive to RR because the channel subunits must provide symmetrical interaction sites for potency (Czirják & Enyedi, 2002a; Kang *et al*., 2004). These results are consistent with the suggestion that heteromeric channels could account for facial motoneuron gK_{Leak}.

The pK for heteromeric channels lies between the values for homomeric TASK-1 and TASK-3 channels but is nearer that of TASK-1 (Czirják & Enyedi, 2002a; Talley & Bayliss, 2002). The pK for facial motoneuron gK_{Leak} is also consistent with a heteromeric channel. The pH-sensitivity of individual facial motoneurons did not differ significantly from the population average, suggesting a single population of pH-sensitive K^+ channels predominates in these cells. Nevertheless, the observation in one facial motoneuron that isoflurane inhibited gK_{Leak}, consistent with a TASK-1 channel identity (Berg *et al*., 2004), suggests gK_{Leak} may display some heterogeneity within the facial motoneuron population.

Further evidence in favour of a heteromeric identity for facial motoneuron gK_{Leak} is the observation that heteromeric channels share the Zn^{2+} insensitivity of TASK-1 homomers (Clarke *et al*., 2004). The insensitivity of gK_{Leak} to anandamide should be assessed in light of the evidence that rat homomeric TASK-1 and TASK-3 channels expressed in HEK 293 cells show lower sensitivity to anandamide and methanandamide relative to human channels (Berg *et al*., 2004). In addition, these compounds show little selectivity between different rat channels. Anandamide (10 μM) blocks between 60 and 80% of the current flowing through homomeric channels and ~50% flowing through heteromeric channels. This latter observation is clearly at odds with the suggestion that a heteromeric channel mediates gK_{Leak} in facial motoneurons. However, distinct cellular environments may promote differences between endogenous channels and those expressed in cell lines. The sensitivity of the TASK-1/TASK-3 heterodimer to bupivacaine and 4-AP is unknown. The lack of effect of the selective blockers of the homomeric channels precludes any quantification of the relative contributions of channel isoforms within individual facial motoneurons similar to that performed elsewhere (Berg *et al*., 2004).

The gK_{Leak} in facial motoneurons displays properties of an amine-sensitive gK_{Leak} described in neonatal rat hypoglossal motoneurons (Talley *et al*., 2000). First described as TASK-1, hypoglossal motoneuron gK_{Leak} displays pharmacological differences to the cloned rat TASK-1 channel and is also enhanced by isoflurane, leading to the suggestion that it may be a heteromeric channel (Talley *et al*., 2000; Talley & Bayliss, 2002; Berg *et al*., 2004). It is of interest that the anandamide sensitivity of this gK_{Leak} has not been described (Berg *et al*., 2004).

Could other 2P K^+ channels underlie facial motoneuron gK_{Leak}? A recent study indicates protein for TASK-2 is found in the facial motor nucleus (Gabriel *et al*., 2002). TASK-2 gives rise to outwardly rectifying currents with a pK around 7.8, suggesting activation at physiological pH. Outward current through TASK-2 channels is relatively insensitive to Ba^{2+} and Cs^+ and permeability to Rb^+ is less than for K^+, unlike TASK-1 (Reyes *et al*., 1998; Niemeyer *et al*., 2001; Talley *et al*., 2001). TASK-2 is also blocked by bupivacaine (Kindler *et al*., 2003). Nevertheless, alone this conductance could not account for the whole range of pH sensitivity or linearity of the gK_{Leak}. The CNS distribution of TASK-4 channels has not been established, but they are activated by alkaline pH, show little activation at pH 7.5 and have slow activation kinetics which distinguish them from gK_{Leak} in facial motoneurons (Decher *et al*., 2001). TASK-5 channels, either in homomeric or heteromeric (with TASK-1) combinations, have so far eluded functional characterization, but nevertheless mRNA does not appear to be present in facial motoneurons (Ashmole *et al*., 2001; Karschin *et al*., 2001).

Inwardly rectifying and voltage-gated K^+ channels

The absence of inward rectification in gK_{Leak} might be expected to preclude the involvement of Kir2.4 (and other Kir) channels. Nevertheless, block of the amine-sensitive gK_{Leak} by Ba^{2+} generates an inwardly rectifying I/V relationship. This could represent either the voltage-dependent block of a single conductance or the block of an inwardly rectifying conductance that contributes to the overall properties of the gK_{Leak}. A characteristic of gK_{ir} is that the $V_{0.5}$ shifts with $[K^+]_o$, suggesting that the driving force on K^+ determines activation rather than voltage alone (Yamaguchi *et al*., 1990). Examination of the Ba^{2+}-sensitive component of gK_{Leak} in facial motoneurons indicated that $V_{0.5}$ was relatively independent of $[K^+]_o$, suggesting a predominantly voltage-dependent block, distinct from the properties of Kir channels. Nevertheless, it is a possibility that Kir2 heterotetramers in association with accessory β subunits show emergent properties distinct from homomeric channels (Schram *et al*., 2002).

The NA- and pH-sensitive gK_{Leak} in facial motoneurons is blocked by 4-AP (4 mM) but not by TEA (30 mM). TASK-1 and TASK-3 channels are reported to be insensitive to both 4-AP and TEA (Duprat *et al*., 1997; Leonoudakis *et al*., 1998; Czirják *et al*., 2000; Kim *et al*., 2000; Lopes *et al*., 2000; Meadows & Randall, 2001; Vega-Saenz de Miera *et al*., 2001). We have previously shown that 4-AP blocks fast and slow transient outward K^+ currents in facial motoneurons although neither appears to contribute to the amine-sensitive gK_{Leak} (Larkman & Kelly, 1998). Rapidly activating, slowly inactivating, 4-AP-sensitive, voltage-gated K^+ conductances have been characterized in cardiac muscle (Boyle & Nerbonne, 1992). In particular, Kv1.5 has been suggested to contribute a sustained current at depolarized membrane potentials (reviewed by Nerbonne, 2000). Kv1.5 channels are blocked by 4-AP, relatively TEA-insensitive, inhibited by acidosis, blocked by bupivacaine (EC_{50} ~10 μM) and while being sensitive to Zn^{2+} the EC_{50} is close to 800 μM (Clémente-Chomienne *et al*., 1999; Steidl & Yool, 1999; González *et al*., 2001; Kehl *et al*., 2002). The presence of Kv1.5 protein in facial motoneurons is unknown, although it is present in motoneurons at all levels of the spinal cord (Matus-Leibovitch *et al*., 1996). Nevertheless, a pK around 6.2 and a restricted

voltage range for sustained current between at best −60 and 0 mV both suggest that alone these channels may not be sufficient to explain the properties of facial motoneuron gK_{Leak}.

Possible functional implications of pH-sensitive gK_{Leak}

Whether the pH-sensitivity of gK_{Leak} is functionally important for facial motoneurons is not clear. Changes in external pH are known to occur during periods of ischaemia and hypoxia but functionally significant physiological changes are less apparent. A small change in external pH may be sufficient to alter the properties of gK_{Leak}; however, the integrated response of the motoneuronal membrane is likely to involve additional effects on other conductances. Experiments performed in the absence of ZD-7288 indicated that changes in external pH across the range pH 6–8 also altered I_h (our unpublished observations). The overall change in facial motoneuron membrane conductance thus reflects the integration of at least these two components. Nevertheless, modulation of gK_{Leak} by endogenous neurotransmitters, particularly NA and 5-HT, indicates an important role in the priming and maintenance of facial motoneuron membrane excitability during waking and states of sensory arousal. Inhibition of facial motoneuron gK_{Leak} by NA involves activation of α_1 adrenoceptors and it has been previously shown that 5-HT_2 receptors mediate similar actions of 5-HT (Larkman & Kelly, 1992). Both receptor subtypes couple through G_q proteins to phospholipase C-mediated hydrolysis of phosphatidyl-4,5-inositol-bisphosphate (PIP_2). Consistent with this, G_q-coupled muscarinic M_1 and group 1 metabotropic glutamate receptors, but not G_i-coupled muscarinic M_2 receptors, inhibit co-expressed human TASK-1 and TASK-3 channels through a PIP_2 hydrolysis-dependent pathway (Czirják *et al*., 2001; Chemin *et al*., 2003).

Conclusion

While mRNA for TASK-1 and TASK-3 K^+ channel subunits is expressed in the facial motor nucleus and the biophysical properties and pH-sensitivity of gK_{Leak} are reminiscent of TASK channel-mediated conductances, the pharmacology of facial motoneuron gK_{Leak} does not clearly define it as being mediated by homomeric TASK-1 or TASK-3 channels. Heteromeric TASK channels with emergent properties could underlie this conductance, a suggestion reinforced by the enhancement of gK_{Leak} by isoflurane. While the detection of TASK channel protein in facial motoneurons has proved elusive, recent studies indicate TASK-1-like immunoreactivity in rat facial motoneurons (Kindler *et al*., 2000; Kanjhan *et al*., 2004).

Acknowledgements

This work was supported by an award under the EC Framework 5 programme (QLG3-CT-2002–00809) to P.M.L. E.M.P. was supported by a MRC PhD studentship.

Abbreviations

4-AP, 4-aminopyridine; 5-HT, 5-hydroxytryptamine; ACSF, artificial cerebrospinal fluid; ATFK, arachidonyltrifluoromethyl ketone; CG, cerebellar granule (neuron); E_K, potassium equilibrium potential; gK_{ir}, inwardly rectifying potassium conductance; gK_{Leak}, 'leak' potassium conductance; $[H^+]_o$, external proton concentration; I_{NA}, noradrenaline-induced current; I_{pH}, pH-sensitive current; $[K^+]_o$, external potassium concentration; NA, noradrenaline; PE, phenylephrine; pK, pH for half maximal activation; RR, ruthenium red; TASK, TWIK-related acid-sensitive potassium channel; TEA, tetraethylammonium; TTX, tetrodotoxin; TWIK, tandem-pore weakly inwardly rectifying potassium channel; $V_{0.5}$, potential for half maximal activation; V_h, holding potential; V_{pH}, reversal potential for the pH-sensitive current.

References

Ashmole, I., Goodwin, P.A. & Stanfield, P.R. (2001) TASK-5, a novel member of the tandem pore K^+ channel family. *Eur. J. Physiol.*, **442**, 828–833.

Barbuti, A., Ishii, S., Shimizu, T., Robinson, R.B. & Feinmark, S.J. (2002) Block of the background K^+ channel TASK-1 contributes to arrhythmogenic effects of platelet-activating factor. *Am. J. Physiol.*, **282**, H2024–H2030.

Berg, A.P., Talley, E.M., Manger, J.P. & Bayliss, D.A. (2004) Motoneurons express heteromeric TWIK-related acid-sensitive (TASK) channels containing TASK-1 (KCNK3) and TASK-3 (KCNK9) subunits. *J. Neurosci.*, **24**, 6693–6702.

Boyle, W.A. & Nerbonne, J.M. (1992) Two functionally distinct 4-aminopyridine-sensitive outward K^+ currents in rat atrial myocytes. *J. Gen. Physiol.*, **100**, 1041–1067.

Chemin, J., Girard, C., Duprat, F., Lesage, F., Romey, G. & Lazdunski, M. (2003) Mechanisms underlying excitatory effects of group I metabotropic glutamate receptors via inhibition of 2P domain K^+ channels. *EMBO J.*, **22**, 5403–5411.

Clarke, C.E., Green, P.J., Veale, E.L., Meadows, H.J. & Mathie, A. (2003) The involvement of residues H98 and E70 in the block of the human two-pore domain potassium channel, TASK-3, by zinc. *J. Physiol. (Lond.)*, **547P**, C46.

Clarke, C.E., Veale, E.L., Green, P.J., Meadows, H.J. & Mathie, A. (2004) Selective block of the human 2-P domain potassium channel, TASK-3, and the native leak potassium current, IK_{SO}, by zinc. *J. Physiol. (Lond.)*, **560**, 51–62.

Clémente-Chomienne, O., Ishii, K., Walsh, M.P. & Cole, W.C. (1999) Identification, cloning and expression of rabbit vascular smooth muscle Kv1.5 and comparison with native delayed rectifier K^+ current. *J. Physiol. (Lond.)*, **515**, 653–667.

Curro, F.A. & Greenberg, S. (1983) Characteristics of postsynaptic α_1 and α_2 adrenergic receptors in canine vascular smooth muscle. *Can. J. Physiol. Pharmacol.*, **61**, 893–904.

Czirják, G. & Enyedi, P. (2002a) Formation of functional heterodimers between the TASK-1 and TASK-3 two-pore domain potassium channel subunits. *J. Biol. Chem.*, **277**, 5426–5432.

Czirják, G. & Enyedi, P. (2002b) TASK-3 dominates the background potassium conductance in rat adrenal glomerulosa cells. *Mol. Endocrinol.*, **16**, 621–629.

Czirják, G. & Enyedi, P. (2003) Ruthenium red inhibits TASK-3 potassium channel by interconnecting glutamate 70 of the two subunits. *Mol. Pharmacol.*, **63**, 646–652.

Czirják, G., Fischer, T., Spat, A., Lesage, F. & Enyedi, P. (2000) TASK (TWIK-related acid-sensitive K^+ channel) is expressed in glomerulosa cells of rat adrenal cortex and is inhibited by angiotensin II. *Mol. Endocrinol.*, **14**, 863–874.

Czirják, G., Petheo, G.L., Spät, A. & Enyedi, P. (2001) Inhibition of TASK-1 potassium channel by phospholipase C. *Am. J. Physiol.*, **281**, C700–C708.

Decher, N., Maier, M., Dittrich, W., Gassenhuber, J., Bruggemann, A., Busch, A.E. & Steinmeyer, K. (2001) Characterization of TASK-4, a novel member of the pH-sensitive, two-pore domain potassium channel family. *FEBS Lett.*, **492**, 84–89.

Duprat, F., Lesage, F., Fink, M., Reyes, R., Heurteaux, C. & Lazdunski, M. (1997) TASK, a human background K^+ channel to sense external pH variations near physiological pH. *EMBO J.*, **16**, 5464–5471.

Gabriel, A., Abdallah, M., Yost, C.S., Winegar, B.D. & Kindler, C.H. (2002) Localization of the tandem pore domain K^+ channel KCNK5 (TASK-2) in the rat central nervous system. *Mol. Brain Res.*, **98**, 153–163.

Goldstein, S.A.N., Bockenhauer, D., O'Kelly, I. & Zilberberg, N. (2001) Potassium leak channels and the KCNK family of two-P-domain subunits. *Nat. Rev. Neurosci.*, **2**, 175–184.

González, T., Longobardo, M., Caballero, R., Delpón, E., Tamargo, J. & Valenzuela, C. (2001) Effects of bupivacaine and a novel local anaesthetic, IBQ-9302, on human cardiac K^+ channels. *J. Pharm. Exp. Therap.*, **296**, 573–583.

Han, J., Truell, J., Gnatenco, C. & Kim, D. (2002) Characterization of four types of background potassium channels in rat cerebellar granule neurons. *J. Physiol. (Lond.)*, **542**, 431–444.

Hughes, B.A., Kumar, G., Yuan, Y., Swaminathan, A., Yan, D., Sharma, A., Plumley, L., Yang-Feng, T.L. & Swaroop, A. (2000) Cloning and functional expression of human retinal Kir2.4, a pH-sensitive inwardly rectifying K^+ channel. *Am. J. Physiol.*, **279**, C771–C784.

Kang, D., Han, J., Talley, E.M., Bayliss, D.A. & Kim, D. (2004) Functional expression of TASK-1/TASK-3 heteromers in cerebellar granule cells. *J. Physiol. (Lond.)*, **554**, 64–77.

Kanjhan, R., Anselme, A.M., Noakes, P.G. & Bellingham, M.C. (2004) Postnatal changes in TASK-1 and TREK-1 expression in rat brain stem and cerebellum. *Neuroreport*, **15**, 1321–1324.

Karschin, C., Dißmann, E., Stühmer, W. & Karschin, A. (1996) IRK (1–3) and GIRK (1–4) inwardly rectifying K^+ channel mRNAs are differentially expressed in adult rat brain. *J. Neurosci.*, **16**, 3559–3570.

Karschin, C. & Karschin, A. (1997) Ontogeny of gene expression of Kir channel subunits in the rat. *Mol. Cell. Neurosci.*, **10**, 131–148.

Karschin, C., Wischmeyer, E., Preisig-Muller, R., Rajan, S., Derst, C., Grzeschik, K.-H., Daut, J. & Karschin, A. (2001) Expression pattern in brain of TASK-1, TASK-3, and a tandem pore domain K^+ channel subunit, TASK-5, associated with the central auditory nervous system. *Mol. Cell. Neurosci.*, **18**, 632–648.

Kehl, S.J., Eduljee, C., Kwan, D.C.H., Zhang, S. & Fedida, D. (2002) Molecular determinants of the inhibition of human Kv1.5 potassium currents by external protons and Zn^{2+}. *J. Physiol. (Lond.)*, **541**, 9–24.

Kim, Y., Bang, H. & Kim, D. (2000) TASK-3, a new member of the tandem pore K^+ channel family. *J. Biol. Chem.*, **275**, 9340–9347.

Kindler, C.H., Paul, M., Zou, H., Liu, C., Winegar, B.D., Gray, A.T. & Yost, C.S. (2003) Amide local anaesthetics potently inhibit the human tandem pore domain background K^+ channel TASK-2 (KCNK5). *J. Pharm. Exp. Therap.*, **306**, 84–92.

Kindler, C.H., Pietruck, C., Yost, C.S., Sampson, E.R. & Gray, A.T. (2000) Localization of the tandem pore domain K^+ channel TASK-1 in the rat central nervous system. *Mol. Brain. Res.*, **80**, 99–108.

Larkman, P.M. & Kelly, J.S. (1992) Ionic mechanisms mediating 5-hydroxytryptamine- and noradrenaline-evoked depolarization of adult rat facial motoneurons. *J. Physiol. (Lond.)*, **456**, 473–490.

Larkman, P.M. & Kelly, J.S. (1998) Characterization of 5-HT-sensitive potassium conductances in neonatal rat facial motoneurons in vitro. *J. Physiol. (Lond.)*, **508**, 67–81.

Larkman, P.M. & Kelly, J.S. (2001) Modulation of the hyperpolarisation-activated current, I_h, in rat facial motoneurons *in vitro* by ZD-7288. *Neuropharmacology*, **40**, 1058–1072.

Larkman, P.M. & Perkins, E.M. (2003) Noradrenaline-mediated inhibition of TASK-like channels in neonatal rat facial motoneurons *in vitro*. *J. Physiol. (Lond.)*, **552P**, C78.

Lauritzen, I., Zanzouri, M., Honoré, E., Duprat, F., Ehrengruber, M.U., Ladzunski, M. & Patel, A.J. (2003) K^+-dependent cerebellar granule neuron apoptosis. *J. Biol. Chem.*, **278**, 32068–32076.

Leonoudakis, D., Gray, A.T., Winegar, B.D., Kindler, C.H., Harada, M., Taylor, D.M., Chavez, R.A., Forsayeth, J.R. & Yost, C.S. (1998) An open rectifier potassium channel with two pore domains in tandem cloned from rat cerebellum. *J. Neurosci.*, **18**, 868–877.

Liu, G.X., Derst, C., Schlichthörl, G., Heinen, S., Seebohm, G., Brüggemann, A., Kummer, W., Veh, R.W., Daut, J. & Preisig-Müller, R. (2001) Comparison of cloned Kir2 channels with native inward rectifier channels from guinea-pig cardiomyocytes. *J. Physiol. (Lond.)*, **532**, 115–126.

Lopes, C.M.B., Gallagher, P.G., Buck, M.E., Butler, M.H. & Goldstein, S.A.N. (2000) Proton block and voltage gating are potassium-dependent in the cardiac leak channel Kcnk3. *J. Biol. Chem.*, **275**, 16969–16978.

Lopes, C.M.B., Zilberberg, N. & Goldstein, S.A.N. (2001) Block of Kcnk3 by protons: evidence that 2-P-domain potassium channel subunits function as homodimers. *J. Biol. Chem.*, **276**, 24449–24452.

Maingret, F., Patel, A.J., Lazdunski, M. & Honoré, E. (2001) The endocannabinoid anandamide is a direct and selective blocker of the background K^+ channel TASK-1. *EMBO J.*, **20**, 47–54.

Matus-Leibovitch, N., Vogel, Z., Ezra-Macabee, V., Etkin, S., Nevo, I. & Attali, B. (1996) Chronic morphine administration enhances the expression of Kv1.5 and Kv1.6 voltage-gated K^+ channels in rat spinal cord. *Mol. Brain Res.*, **40**, 261–270.

Meadows, H.J. & Randall, A.D. (2001) Functional characterisation of human TASK-3, an acid-sensitive two-pore domain potassium channel. *Neuropharmacology*, **40**, 551–559.

Meuth, S.G., Budde, T., Kanyshkova, T., Broicher, T., Munsch, T. & Pape, H.-C. (2003) Contribution of TWIK-related acid-sensitive K^+ channel 1 (TASK1) and TASK3 channels to the control of activity modes in thalamocortical neurons. *J. Neurosci.*, **23**, 6460–6469.

Millar, J.A., Barratt, L., Southan, A.P., Page, K.M., Fyffe, R.E.W., Robertson, B. & Mathie, A. (2000) A functional role for the two-pore domain potassium channel TASK-1 in cerebellar granule neurons. *Proc. Natl Acad. Sci. USA*, **97**, 3614–3618.

Nerbonne, J.M. (2000) Molecular basis of functional voltage-gated K^+ channel diversity in the mammalian myocardium. *J. Physiol. (Lond.)*, **525**, 285–298.

Niemeyer, M.I., Cid, L.P., Barros, L.F. & Sepúlveda, F.V. (2001) Modulation of the two-pore domain acid-sensitive K^+ channels TASK-2 (KCNK5) by changes in cell volume. *J. Biol. Chem.*, **276**, 43166–43174.

Nunnari, J.M., Repaske, M.G., Brandon, S., Cragoe,E.J. Jr & Limbird, L.E. (1987) Regulation of porcine brain α_2-adrenergic receptors by Na^+, H^+ and inhibitors of Na^+/H^+ exchange. *J. Biol. Chem.*, **262**, 12387–12392.

Patel, A.J. & Honoré, E. (2001) Properties and modulation of mammalian 2P domain K^+ channels. *Trends Neurosci.*, **24**, 339–346.

Perrier, J.-F., Alaburda, A. & Hounsgaard, J. (2003) 5-HT_{1A} receptors increase excitability of spinal motoneurons by inhibiting a TASK-1-like K^+ current in the adult turtle. *J. Physiol. (Lond.)*, **548**, 485–492.

Pieribone, V.A., Nicholas, A.P., Dagerlind, A. & Hokfelt, T. (1994) Distribution of α_1 adrenoceptors in rat brain revealed by *in situ* hybridization experiments utilizing subtype-specific probes. *J. Neurosci.*, **14**, 4252–4268.

Rajan, S., Wischmeyer, E., Liu, G.X., Preisig-Müller, R., Daut, J., Karschin, A. & Derst, C. (2000) TASK-3, a novel tandem pore domain acid-sensitive K^+ channel. An extracellular histidine as pH sensor. *J. Biol. Chem.*, **275**, 16650–16657.

Ranft, A., Kurz, J., Deuringer, M., Haseneder, R., Dodt, H.U., Zieglgansberger, W., Kochs, E., Eder, M. & Hapfelmeier, G. (2004) Isoflurane modulates glutamatergic and GABAergic neurotransmission in the amygdala. *Eur. J. Neurosci.*, **20**, 1276–1280.

Reyes, R., Duprat, F., Lesage, F., Fink, M., Salinas, M., Farman, N. & Lazdunski, M. (1998) Cloning and expression of a novel pH-sensitive two pore domain K^+ channel from human kidney. *J. Biol. Chem.*, **273**, 30863–30869.

Scheller, M., Bufler, J., Schneck, H., Kochs, E. & Franck, C. (1997) Isoflurane and sevoflurane interact with the nicotinic acetylcholine receptor channels in micromolar concentrations. *Anesthesiology*, **86**, 118–127.

Schram, G., Melnyk, P., Pourrier, M., Wang, Z. & Nattel, S. (2002) Kir2.4 and Kir2.1 K^+ channel subunits co-assemble: a potential new contributor to inward rectifier current heterogeneity. *J. Physiol. (Lond.)*, **544**, 337–349.

Shin, K.S., Rothberg, B.S. & Yellen, G. (2001) Blocker state dependence and trapping in hyperpolarization-activated cation channels: evidence for an intracellular activation gate. *J. Gen. Physiol.*, **117**, 91–101.

Simon, W., Hapfelmeier, G., Kochs, E., Zieglgansberger, W. & Rammes, G. (2001) Isoflurane blocks synaptic plasticity in the mouse hippocampus. *Anesthesiology*, **94**, 1058–1065.

Steidl, J.V. & Yool, A.J. (1999) Differential sensitivity of voltage-gated potassium channels Kv1.5 and Kv1.2 to acidic pH and molecular identification of pH sensor. *Mol. Pharmacol.*, **55**, 812–820.

Talley, E.M. & Bayliss, D.A. (2002) Modulation of TASK-1 (Kcnk3) and TASK-3 (Kcnk9) potassium channels. Volatile anesthetics and neurotransmitters share a molecular site of action. *J. Biol. Chem.*, **277**, 17733–17742.

Talley, E.M., Lei, Q., Sirois, J.E. & Bayliss, D.A. (2000) TASK-1, a two-pore domain K^+ channel, is modulated by multiple neurotransmitters in motoneurons. *Neuron*, **25**, 399–410.

Talley, E.M., Solorzano, G., Lei, Q., Kim, D. & Bayliss, D.A. (2001) CNS distribution of members of the two-pore-domain (KCNK) potassium channel family. *J. Neurosci.*, **21**, 7491–7505.

Tateishi, J. & Faber, J.E. (1995) Inhibition of arteriole α_2- but not α_1-adrenoceptor constriction by acidosis and hypoxia *in vitro*. *Am. J. Physiol.*, **268**, H2068–H2076.

Töpert, C., Döring, F., Wischmeyer, E., Karschin, C., Brockhaus, J., Ballanyi, K., Derst, C. & Karschin, A. (1998) Kir2.4: a novel K^+ inward rectifier channel associated with motoneurons of cranial nerve nuclei. *J. Neurosci.*, **18**, 4096–4105.

Vega-Saenz de Miera, E., Lau, D.H.P., Zhadina, M., Pountney, D., Coetzee, W.A. & Rudy, B. (2001) KT3.2 and KT3.3, two novel human two-pore K^+ channels closely related to TASK-1. *J. Neurophysiol.*, **86**, 130–142.

Watkins, C.S. & Mathie, A. (1996) A non-inactivating K^+ current sensitive to muscarinic receptor activation in rat cultured cerebellar granule neurons. *J. Physiol. (Lond.)*, **491**, 401–412.

Yamaguchi, K., Nakajima, Y., Nakajima, S. & Stanfield, P.R. (1990) Modulation of inwardly rectifying channels by substance P in cholinergic neurones from rat brain in culture. *J. Physiol. (Lond.)*, **426**, 499–520.